All Theses and Dissertations (ETDs)

Summer 9-1-2014

Kinematic Characterization of Left Ventricular Chamber Stiffness and Relaxation

Sina Mossahebi
Washington University in St. Louis

Follow this and additional works at: https://openscholarship.wustl.edu/etd

WASHINGTON UNIVERSITY IN ST. LOUIS

Department of Physics

Dissertation Examination Committee:
Sándor J. Kovács, Chair
Anders E. Carlsson
James G. Miller
Yoram Rudy
Samuel A. Wickline

Kinematic Characterization of Left Ventricular Chamber Stiffness and Relaxation

by

Sina Mossahebi

A dissertation presented to the
Graduate School of Arts and Sciences
of Washington University in St. Louis in
partial fulfillment of the requirements for the degree
of Doctor of Philosophy

August 2014
Saint Louis, Missouri

TABLE OF CONTENTS

LIST OF FIGURES

LIST OF TABLES

Acknowledgements

I would like to express my sincere gratitude to my project advisor, Dr. Sándor Kovács, for his immense guidance, thoughtful criticisms, and ongoing support in addition to his exceptional mentoring throughout my dissertation projects. During the past five years, he has taught me how to express my ideas in a clear and simple manner for the purposes of effectively communicating with others, writing high quality scientific papers, and giving oral presentations.

I would also like to express my deep appreciation for my most influential teacher at the University of Tehran, Dr. Masoud Alimohammadi. Without his inspiration, I would likely not have pursued research in physics and the life sciences.

I am grateful to Drs. James Miller, Anders Carlson, Mark Holland, and Samuel Wickline for their letters of reference in support of my applications, with special thanks to my physics mentors, James Miller and Anders Carlsson, for attending the committee meetings and evaluating my research. Without the assistance of my committee members, the work presented in my dissertation would have not been possible.

I would like to thank the staff of the Cardiac Procedure Center at Barnes Jewish Hospital. Peggy Brown, our expert sonographer, was always positive, kind, and skilled in her practice.

I thank my dissertation committee, Drs. Anders Carlsson, Jim Miller, Yoram Rudy, and Samuel Wickline, for reviewing this work. In addition, the dissertation could not have been complete without the support of the members of the Cardiovascular Biophysics Laboratory. Leonid Shmuylovich and Wei Zhang taught me everything I know about the Cardiovascular Biophysics Laboratory, and it was a joy to collaborate with them. Former members of our lab who have helped me develop ideas and thoughts include Erina Ghosh, Simeng Zhu, and Howard Chen, and I thank them for their contributions to my academic growth.

My acknowledgments would not be complete without recognizing my family and friends for keeping my spirits up. Words fail me to express my indebtedness to my parents, Shahnaz and Mohammad, who deserve a very special mention for their constant encouragement, support, and unconditional love. I am also grateful to my wonderful sister, Sara, and my brother, Pouria, for their love and confidence in me.

Finally, I would like to express my thanks to the Washington University in St. Louis Department of Physics, as well as the Washington University School of Medicine, for providing such an invaluable opportunity, excellent education, and exceptional training to me and all other physics graduate students.

ABSTRACT OF THE DISSERTATION

Kinematic Characterization of Left Ventricular Chamber Stiffness and Relaxation
by

Sina Mossahebi

Doctor of Philosophy in Physics

Washington University in St. Louis, 2014

Professor Sándor J. Kovács, Chair

Heart failure is the most common cause of hospitalization today, and diastolic heart failure accounts for 40-50% of cases. Therefore, it is critical to identify diastolic dysfunction at a subclinical stage so that appropriate therapy can be administered before ventricular function is further, and perhaps irreversibly impaired. Basic concepts in physics such as kinematic modeling provide a unique method with which to characterize cardiovascular physiology, specifically diastolic function (DF). The advantage of an approach that is standard in physics, such as the kinematic modeling is its causal formulation that functions in contrast to correlative approaches traditionally utilized in the life sciences.

Our research group has pioneered theoretical and experimental quantitative analysis of DF in humans, using both non-invasive (echocardiography, cardiac MRI) and invasive (simultaneous catheterization-echocardiography) methods. Our group developed and validated the Parametrized Diastolic Filling (PDF) formalism which is motivated by basic physiologic principles (LV is a mechanical suction pump at the mitral valve opening) that obey Newton's Laws. PDF formalism is a kinematic model of filling employing an equation of motion, the solution of which accurately predicts all E-wave contours in accordance with the rules of damped harmonic oscillatory motion. The equation's lumped parameters—ventricular stiffness, ventricular

viscoelasticity/relaxation and ventricular load—are obtained by solving the 'inverse problem'. The parameters' physiologic significance and clinical utility have been repeatedly demonstrated in multiple clinical settings.

In this work we apply our kinematic modeling approach to better understand how the heart works as it fills in order to advance the relationship between physiology and mathematical modeling. Through the use of this modeling, we thereby define and validate novel, causal indexes of diastolic function such as early rapid filling energy, diastatic stiffness, and relaxation and stiffness components of E-wave deceleration time.

Chapter 1: Introduction

1.1 Cardiac Anatomy, Function, and Hemodynamics

1.1.1 <u>Cardiac Anatomy</u>

The mammalian heart is a four-chambered structure, consisting of two pumps in series: a "right heart", consisting of right atrium and right ventricle, that pumps venous blood to the pulmonary circulation, and a "left heart", consisting of left atrium and left ventricle, which pumps oxygenated blood from the lungs to the periphery at a relatively high pressure. The four heart chambers are enclosed by a thin, fibrous membrane called the pericardial sac. The right atrium receives blood from the systemic circulation through the large veins (the inferior and superior vena cava), while the left atrium receives oxygenated blood from the lungs through four pulmonary veins. The right ventricle ejects blood into the lungs through the pulmonary valve, and the left ventricle ejects blood to the periphery through the aorta. Figure 1.1 illustrates the four-chambered human heart and associated vasculature.
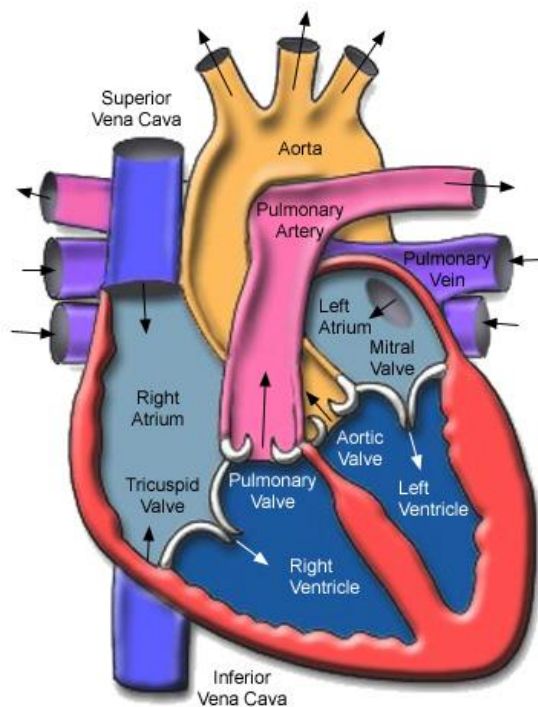
Figure 1.1 Schematic of the four-chambered heart and its associated vasculature.

The four chambers of the heart, the right and left atrium and right and left ventricles, are shown. The papillary muscles and chordae tendineae, which connect the mitral and tricuspid valves to the ventricular walls, are not shown. See text for details.

2

1.1.2   The Constant-Volume Attribute of the Heart

The atria, ventricles, and portions of the inflow and outflow tracts reside within the confines of the fibrous, inelastic pericardial sack. It was initially demonstrated in dogs that the total pericardial volume remains constant within about 5% using the dynamic spatial reconstructor, a modified X-ray machine (26). Later it was demonstrated (in dogs) that the total volume of the left and right sides of the heart remained essentially constant over the cardiac cycle as well (24). Further, an MRI study in humans has shown that the total volume of the contents in the pericardial sack remains constant within 5% throughout the cardiac cycle as in dogs (7, 23, 25, 26, 67). This attribute dictates that the ventricles and atria empty and fill in a reciprocating manner to maintain a constant total heart volume.

Since this dissertation focuses on the function of the left side of the heart, the rest of the background on cardiac anatomy and function will be devoted to the left atrium, left ventricle, and associated vessels.

1.1.3 Left Heart

Oxygenated blood returning from the lungs enters the left atrium via four pulmonary veins. This blood passes from the left atrium into the left ventricle via the mitral (bicuspid) valve, which consists of two leaflets attached to a ring of fibrous tissue called the mitral annulus. The position of the mitral annulus denotes the base of the left ventricle, while the inferior tip of the ventricle denotes the apex (Figure 1.2).

The left ventricle, whose shape has been likened to a half prolate ellipsoid, generates pressures high enough (80mmHg-120mmHg) to overcome arterial resistance and perfuse the body. The ventricular wall is composed of helically-oriented muscle fibers such that the fiber orientation varies smoothly from more longitudinally-directed near the inner layer (endocardium) to circumferential in the middle of the wall, then back to more longitudinally-directed at the outer layer (epicardium). The range of fiber angles from endocardium to epicardium encompasses approximately 120 degrees in humans (19). The left ventricle pumps blood to the aorta via the left ventricular outflow tract and through the aortic valve.
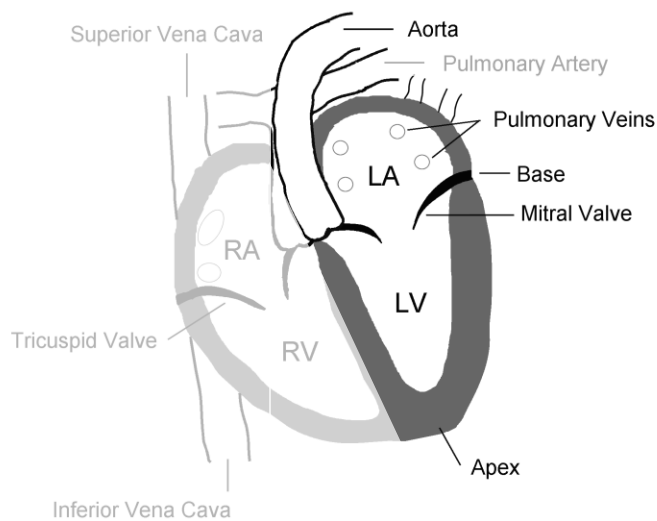
Figure 1.2 Schematic of the left heart and its associated vasculature.

The base, apex, and two chambers of the left heart, the left atrium and ventricle, are shown. See text for details. LA, left atrium; LV, left ventricle.

1.1.4 Molecular and Cellular Components of the Myocardium

While the scope of this thesis relates to functioning of the heart at the organ level, it is worthwhile to review cardiac structure and function at the cellular level in order to understand how functioning at the organ level is governed.

The ventricular myocardium is composed of cardiomyocytes surrounded by an extracellular matrix, which consist primarily of collagen and elastin fibers (65). These fibers are synthesized by fibroblasts and contribute to the mechanical properties of the myocardium. The primary functional units within cardiomyocytes are sarcomeres (2.2 microns in length when relaxed), which consist of overlapping thick (myosin) and thin (actin) filaments (Figure 1.3) and are aligned in a hexagonal packing arrangement in the cross- sectional view.
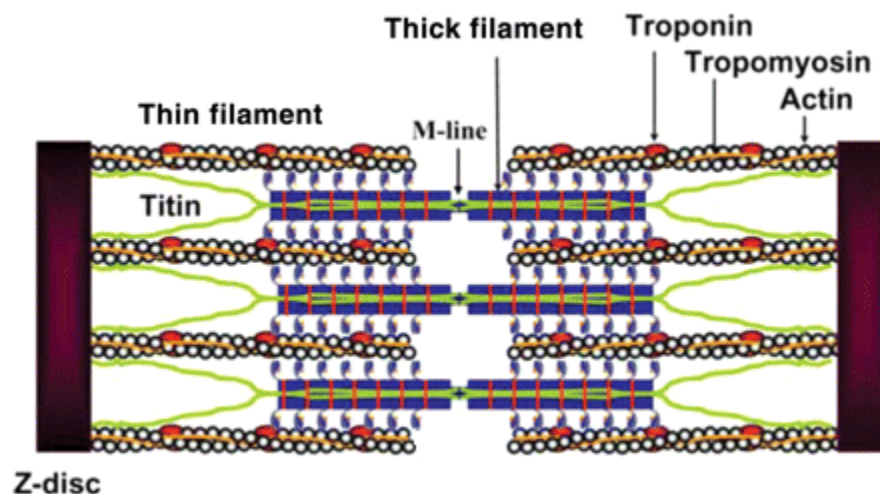
Figure 1.3 Schematic of the components of a sarcomere.

Calcium binding to troponin allows the heads of the thick filament (myosin) crossbridges to bind to the thin filaments and generate the power stroke, shortening the sarcomere. Lengthening occurs upon calcium unbinding and detachment of the myosin crossbridges from the thin filaments. Elastic recoil of titin (connected to the thick filament) restores the sarcomere to its resting length. See text for details.

Excitation of the cardiomyocytes allows entry of calcium from the extracellular space through various ion channels and stimulates the release of calcium ions from internal stores (sarcoplasmic reticulum). The ions, bind to a protein (troponin) associated with the myosin crossbridges on the thick filaments. This calcium binding allows the crossbridges to bind to the

thin filaments and generate the power stroke, sliding the thin filaments past the thick filaments and thus shortening the sarcomere (35). This process is responsible for systole.

Relaxation begins as calcium becomes unbound from the sarcomeric contractile apparatus and is actively pumped back into its internal stores. This allows the myosin cross-bridges to detach from the thin filaments and the lengthening of the sarcomere to commence. The process is facilitated by a large sarcomeric protein called titin, which connects the thick filaments with the end of the sarcomere (Z-disk) and generates a restoring force during relaxation (22). Titin has been shown to behave as a linear, bi-directional spring within the normal physiologic range of sarcomere lengths (18), which has implications for the modeling approach discussed later in this dissertation. As is true with the extracellular matrix, the mechanical properties of titin can change (via differential expression of its two principal isoforms) with age and disease (38, 54, 74).

1.1.5   <u>Electrical Activation of Cardiovascular Chambers</u>

The global electrical behavior of the heart can be recorded through the electrocardiogram (ECG), where electrical leads are connected to the body in an orientation that is roughly along the primary direction of chamber depolarization. The ECG can provide important information about the patient's heart rhythm, previous heart attack(s), increased thickness of the heart muscle, signs of decreased oxygen delivery to the heart, as well as problems with conduction of the electrical current from one portion of the heart to another. Figure 1.4 shows a schematic diagram of ECG in normal sinus rhythm for one cardiac cycle.

Each electrical signal (depolarization) begins in a group of cells called the sinus node or

sinoatrial (SA) node. The SA node is located in the right atrium. From the SA node, the signal travels through the right and left atria. This causes the atrial depolarization and contraction, which helps move blood into the ventricles (15). The atrial depolarization is seen on the ECG as the positive P-wave deflection.
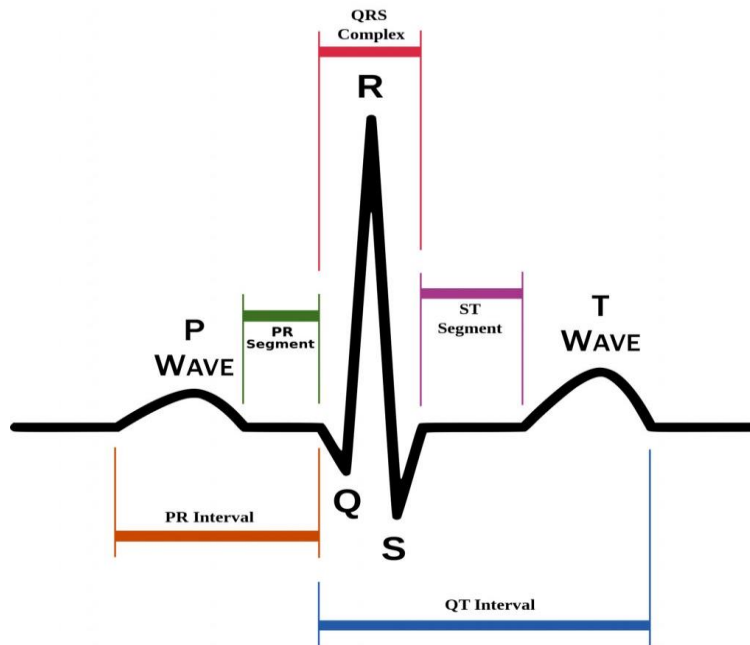
Figure 1.4 Schematic diagram of electrocardiogram
It represents one cardiac cycle in normal sinus rhythm. See text for details.

The electrical signal passes between the atria and ventricles through a group of cells called the atrioventricular (AV) node. The signal slows down as it passes through the AV node. This slowing allows the ventricles enough time to finish filling with blood and also ensures that atrial mechanical contraction and atrioventricular flow is complete before ventricular contraction occurs. On the ECG, this part of the process is the flat line between the end of the P-wave and the beginning of the QRS complex (PR segment). The electrical signal then leaves the AV node and travels along a pathway called the bundle of His. Past the AV node, the depolarization wave splits along the left and right bundles of the conduction system, then Purkinje fibers come off of

the bundles and deliver the depolarization wave to the endocardial (inner wall) ventricular tissue. The signal spreads quickly across the ventricles, causing them to contract and pump blood to the lungs and the rest of body. The ventricular depolarization and onset of contraction is recorded as the QRS complex on the ECG. Following ventricular depolarization the QRS is inscribed while the duration of contraction (systole), is well approximated on the surface ECG by the QT interval. After the T-wave, the tissue relaxes and repolarizes so as to accommodate the filling of the chamber before the next ejection.

1.1.6 Cardiac Cycle

The cardiac cycle includes a period of cardiac muscle relaxation, known as diastole, and a period of contraction, known as systole.

Systole:

Systole is commonly defined (mechanically) as the time interval from mitral valve closure until aortic valve closure, and the process can be divided into two segments, isovolumic contraction and ejection.

1) Isovolumic contraction

The onset of ventricular contraction coincides with the peak of the R-wave of the ECG and the initial vibration of the first heart sound. It is indicated on the left ventricular pressure curve as the earliest rise in ventricular pressure after atrial contraction. The phase between the start of left ventricular systole (mitral valve closure) and the opening of the aortic valve (when

ventricular pressure rises abruptly) is termed isovolumic contraction because left ventricular volume is constant during this brief (50-70 msec) period. During isovolumic contraction, the ventricle develops pressure while its wall manifests twisting of the base and apex in opposite directions such that the ventricle exhibits a net counterclockwise twist when viewed from the base. This torsional motion is due to the differential fiber orientation of myocytes across the LV wall. The early initial rise of left ventricular pressure above left atrial pressure, closes the mitral valve and initiate isovolumic contraction. This phase is marked primarily by the shortening of the ventricle along its long and short axes with some torsional motion as well.

2) *Ejection*

When ventricular pressure has risen above aortic pressure, the aortic valve opens. Opening of the aortic valve marks the end of isovolumic contraction and the onset of the ejection phase. During approximately the first third of the ejection period, left ventricular pressure slightly exceeds aortic pressure and flow accelerates (continues to increase), whereas during the last two thirds of ventricular ejection, the reverse holds true. This reversal of the ventricular-aortic pressure gradient in the presence of continued blood flow from the left ventricle into the aorta (caused by the momentum of the forward blood flow) is the result of potential energy stored in the stretched arterial walls, which produces a deceleration of blood flow into the aorta. During ventricular systole, the septum and the free wall of the left ventricle become thicker and move closer to each other. Figure 1.5 (The Wigger's Diagram) displays the phases of the cardiac cycle and its associated left atrial, left ventricular, and aortic pressures.
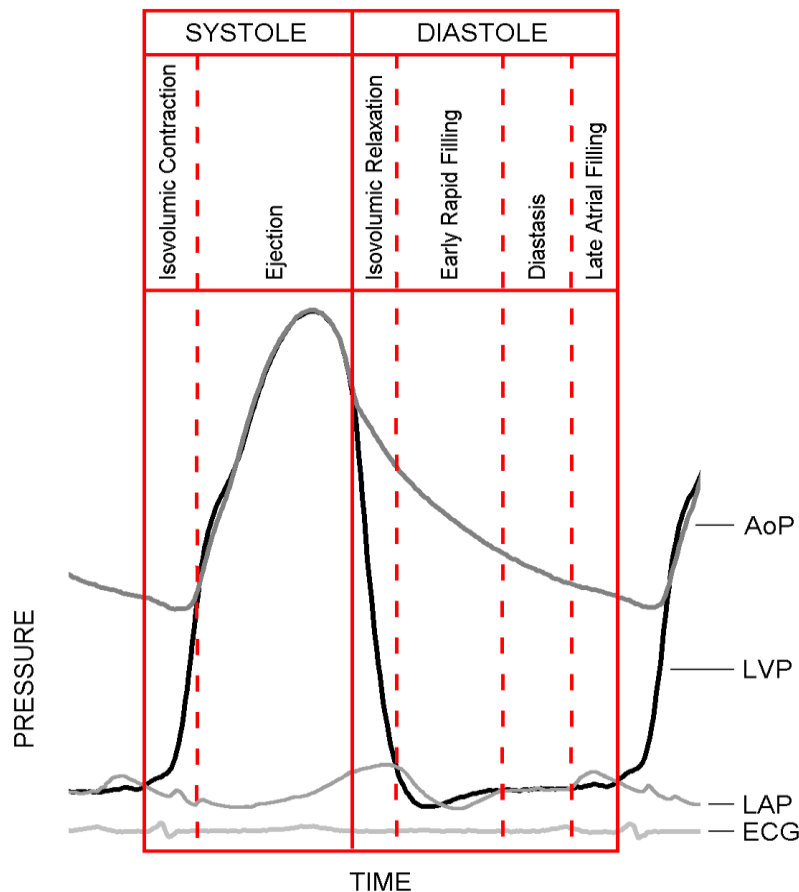
Figure 1.5 Wigger's Diagram.

Wigger's Diagram exhibiting the systolic and diastolic phases of the cardiac cycle.

Actual aortic (AoP) and left ventricular pressure (LVP) are plotted, along with the electrocardiogram (ECG). The left atrial pressure (LAP) plot does not consist of actual data, but was drawn in to illustrate its qualitative relationship to LVP during the cardiac cycle, especially filling. Systole begins with a rapid rise in LVP during isovolumic contraction. Once LVP exceeds AoP, ejection begins. Diastole begins with isovolumic relaxation, which marks the end of ejection, and is initiated with a fall in LVP below AoP. Early rapid filling begins as LVP falls below LAP and ends at diastasis when these pressures equilibrate. Notably, the initial portion of early rapid filling in which LAP exceeds LVP is driven by ventricular suction, while the latter portion in which LVP exceeds LAP is driven by inertial forces. Late atrial filling marks the end of diastasis and is marked by a transient rise in LAP that further distends (pressurizes) the ventricle. Late atrial filling (and diastole) terminates upon ventricular (isovolumic) contraction as seen by the initiation of the QRS complex on the ECG.

10

Diastole:

Once ejection ends as ventricular pressure falls below aortic pressure, (mechanical) diastole is commonly considered to have begun. Diastole is defined (mechanically) as the time interval from aortic valve closure until mitral valve closure. This entire phase can also be further divided into two main segments: isovolumic relaxation and diastolic filling.

1) *Isovolumic relaxation*

The phase between the aortic valve closure and mitral valve opening, termed isovolumic relaxation (50-70 msec), is characterized by a rapid fall in left ventricular pressure without a change in left ventricular volume. The decay in left ventricular pressure is due crossbridge detachment and calcium sequestration within myocytes. Because of the helical fiber orientation of the LV wall it is also accompanied by clockwise (when viewed from the base) untwisting of the ventricle while both aortic and mitral valves are closed.

2) *Filling*

Isovolumic relaxation ends and filling begins once left ventricular pressure falls below left atrial pressure, re-establishing the atrioventricular pressure gradient and opening the mitral valve. Diastolic filling itself can also be subdivided into phases: early rapid filling, diastasis, and late atrial filling.

Early rapid filling

The major part of the ventricular filling occurs immediately on opening of the mitral valve, when the left ventricle abruptly sucks in the blood that returned to the atria during the previous ventricular systole. This period of ventricular filling is called early rapid filling. The

rapid filling phase starts with the decrease in left ventricular pressure below left atrial pressure, resulting in the opening of the mitral valve. The rapid flow of blood from atria to relaxing ventricles produces a decrease in atrial and ventricular pressures and a rapid increase in ventricular volume.

Diastasis

The rapid filling phase is followed by a phase called diastasis. During diastasis, left ventricular and left atrial pressures are equal, therefore the pressure gradient across the mitral valve is zero (14), and the resultant forces generated by and acting on the ventricle are balanced (but not zero) (58). No atrioventricular blood flow (10, 14, 40) or tissue motion is present (57, 70), the atrium and ventricle are both relaxed, and pressure remains constant ($dP/dt \cong 0$). Accordingly, diastasis comprises the static equilibrium state of the passive LV (41, 79).

Late atrial filling

The onset of late atrial filling (atrial systole) occurs soon after the beginning of the P-wave of the ECG (atrial depolarization) and the transfer of blood from atrium to ventricle made by contraction of the left atrium. Atrial contraction is responsible for the small increases in atrial ventricular pressures as well as in ventricular volume. Throughout left ventricular diastole, atrial pressure barely exceeds ventricular pressure, indicating a low-resistance pathway across the open mitral valve during ventricular filling. Atrial contraction can force blood into the pulmonary veins because there are no valves at the junctions of the pulmonary veins and left atrium. Therefore, little blood is pumped back into the pulmonary veins during the atrial contraction. Filling ends and isovolumic contraction begins upon electromechanical activation of the ventricle and closure of the mitral valve, as marked by the R-wave on the electrocardiogram (ECG).

This dissertation will focus on diastolic function. As a result, more detail about the background of diastole is provided below.

1.1.7   <u>The Physiology of Diastole</u>

The onset of mechanical diastole is classically defined as the closure of the aortic valve, although there is evidence that ventricular relaxation begins substantially earlier, likely during ejection (13, 68). Once left ventricular pressure falls below aortic pressure, the aortic valve closes and isovolumic relaxation begins. At this point, the mitral valve is also closed, because left ventricular pressure exceeds left atrial pressure. During isovolumic relaxation, left ventricular pressure falls due to relaxation of the left ventricular myofibers, which is achieved by crossbridge uncoupling and calcium sequestration. This change is accompanied by a release in the torsion stored during previous systole in the intracellular (titin) and extracellular (collagen, elastin) compartments of the myocardium via untwisting. Importantly, chamber volume is constant during isovolumic relaxation, although the ventricle may exhibit a change in shape via slight motion along its long and short axes and displacement of the closed mitral valve leaflets. The pressure decay during isovolumic relaxation beyond peak negative dP/dt is commonly approximated with an exponential (76).

As the left ventricle continues to relax, left ventricular pressure eventually falls below left atrial pressure. This pressure crossover results in the opening of the mitral valve and the onset of early rapid filling. Notably, early rapid filling is initiated by ventricular suction (8, 32, 33, 65), as the left ventricular volume increases while its pressure (initially) continues to decrease due to relaxation of the ventricular myocytes, or dP/dV<0. As a result, the ventricle works as a suction

pump during the beginning of early rapid filling (32, 36, 37, 79). This suction-initiated filling process can also be understood as the walls of the left ventricle springing apart faster than blood can enter from the left atrium. As blood enters the left ventricle, the chamber expands to accommodate it both along the long-axis, via displacement of the mitral annulus toward the left atrium, and along the short-axis, via wall thinning and a relatively small outward displacement of the epicardial/pericardial border (75). It is important to note that long-axis excursion of the mitral annulus and wall thinning along the short-axis are coupled due to the (near) incompressibility of the myocardium; since myocardial tissue volume is conserved, lengthening of the ventricle must be accompanied by a simultaneous thinning of its walls. The negative atrioventricular pressure gradient (LVP<LAP) accelerates the blood across the mitral valve until minimum LVP is attained. As the blood continues to fill the ventricle and LV relaxation terminates, the suction-driven phase of early rapid filling ends and the remainder of early rapid filling through passive expansion of the left ventricle. During this period, LV pressure and volume both increase (dP/dV>0). Once atrial pressure falls below ventricular pressure (LVP>LAP), the rate of filling decelerates and flow continues primarily due to inertial effects.

The end of early filling is marked by an equilibration of atrial and ventricular pressures and thus signifies the beginning of diastasis, a period during which no net blood flow or wall motion occurs. All forces on the ventricle are balanced (but not zero) (79). However, it should be noted that the duration of diastasis is highly dependent on heart rate and that diastasis is absent when the heart rate is typically above 80 bpm (11).

At sufficiently low heart rates, diastasis ends upon the onset of the ECG P-wave, which initiates atrial contraction as well as the second diastolic filling phase, late atrial filling. Whereas early rapid filling is driven by ventricular relaxation/recoil, late atrial filling is driven entirely by

atrial contraction (when the ventricle is completely passive), which re-establishes the atrioventricular pressure gradient (LAP>LVP) and drives blood through the mitral valve into the ventricle. Atrial filling is generally of lower magnitude and shorter duration than early filling in normal hearts, but its contribution to diastolic filling tends to increase with dysfunction and aging. Late atrial filling ends at the ECG R-wave when the ventricle starts to contract. Ventricular contraction increases the LV pressure above the atrial pressure to close the mitral valve, and the isovolumic contraction phase of the next cardiac cycle starts. Figure 1.5 (shown above) displays the phases of the cardiac cycle and the associated left atrial, left ventricular, and aortic pressures.

While early rapid filling and its flow profile are governed largely by intrinsic left ventricular function, they are also influenced by loading effects. Loading effects can be grouped into preload and afterload. Preload effectively refers to the extent to which the ventricular chamber is distended during filling and is determined by the amount of blood with which the ventricle fills. Unless the ventricle is dilated and failing, increased filling volume will stretch the contractile elements within the cardiomyocytes further, resulting in increased force (pressure) generation during the next systole, according to Starling's Law (5). Left ventricular end-diastolic volume (LVEDV) and pressure (LVEDP) are common invasive surrogates of preload (5). Afterload refers to the force, or pressure, that the left ventricle contracts against during systole, which is often considered to be the mean arterial pressure (5). While not as important a determinant of diastolic function as preload, afterload can influence the extent to which the myocardial contractile elements shorten and twist, which in turn can alter the time course of pressure decline during isovolumic relaxation and early filling via contraction-relaxation coupling. It is important to note that all conventional diastolic function indexes vary with load (9,

27, 34, 43, 60, 69, 72, 77). As a result, the intrinsic DF properties can be confounded or even masked by mere loading conditions.

Two important points which facilitate understanding and modeling of cardiac function must be discussed. First, several investigators have shown that the volume enclosed by the pericardial sac remains nearly constant over the cardiac cycle (7, 20, 26), as outflow from the heart is largely balanced by simultaneous inflow. Second, this near-constant-volume property extends to the left and right sides of the heart individually (26). As a result, ventricular filling and emptying is essentially accompanied by simultaneous atrial filling and emptying. For instance, during left ventricular ejection, the apical displacement of the mitral annulus drives filling of the left atrium via suction of blood from the pulmonary veins. During early and late filling, displacement of the mitral annulus toward the left atrium allows blood to flow from the left atrium into the left ventricle. Thus, atrial and ventricular volumes reciprocate through apically- and atrially-directed motion of the mitral annulus (20). During ventricular filling, this process can be envisioned as a cylinder divided into upper (atrial) and lower (ventricular) chambers (3) in which the flow leaving the upper chamber is equivalent to the flow entering the lower chamber (40). Specifically, the volume swept out by the cross-sectional area of the mitral annulus equals the blood volume passing through the mitral valve.

1.1.8   <u>Characterization of Diastolic Function</u>

Traditionally, studies of cardiac function have relied primarily on the understanding of the pumping ability, or systolic function, of the ventricles. The filling process, or diastolic function (DF), of the ventricles went largely overlooked. Recently, it has become clear that

impairment of proper ventricular filling (diastolic dysfunction) directly increases morbidity and mortality (82). Diastolic dysfunction (DD) is predictor of and a precursor to diastolic heart failure (DHF), a clinical syndrome that has reached epidemic proportions. Advanced DD leads to diastolic heart failure, accounting for up to 40-50% of all heart failure cases in the United States (63, 73).

Given the prevalence of DD in such a large percentage of heart failure patients, there is a strong need for better and more complete understanding of diastolic heart physiology (31, 83), including the functional interactions between atria and ventricles, and four-chambered heart function as a whole. Unfortunately, DF has proven to be quite complex, and unifying models accurately encompassing all of its cardinal aspects have been lacking (55). However, the development of noninvasive imaging modalities have substantially increased the understanding of diastole and have led to the establishment of robust clinical indexes by which DF may be assessed. In particular, recent advances in the fields of echocardiography and cardiac magnetic resonance imaging (MRI) have made them ideal tools for further elucidation of diastolic heart physiology.

Left ventricular chamber stiffness and relaxation parameters are most common indexes in order to characterize DF (81, 83). Conventionally, these parameters have been computed from pressure and volume (P-V) data obtained during cardiac catheterization. Although LV hemodynamics via cardiac catheterization comprises the gold standard for characterizing DF, Doppler echocardiography is the clinically preferred method for global DF characterization by analyzing transmitral blood flow velocity as a function of time during filling (Doppler E-wave). All echo-derived DF indexes are load dependent and have limited sensitivity and specificity. Because of these limitations, the derivation and validation of novel indexes (whose conceptual

basis is derived from a causal and mechanistic characterization of how the heart actually works when it fills) is justified in order to reliably determine presence and severity of DD, and also to more rigorously assess therapeutic response.

Stiffness measures the change of pressure over the change of volume (dP/dV), or in a one-dimensional sense, the change of force over the change in distance (dF/dx). Stiffness can be characterized in several ways. Classically, chamber stiffness determination has required catheterization-based measurement of simultaneous LV pressure and volume. One method is to compute the ratio of LV pressure increase and LV volume increase during atrial contraction in the same heart beat using invasive P-V data (30). Other investigators have used a pressure-volume loop in a single heart beat and fit it with either a straight line or a curve to obtain stiffness. This method may be limited by the fact that the ventricle may not achieve complete relaxation during the early portion of diastole; hence, the P-V relationship may be confounded by incomplete relaxation (28). Other than the single beat approaches described above, multiple heartbeats have been used to construct the P-V relationship. Combining mid to late diastolic filling P-V points from several beats provides a good estimate of stiffness, a method which is especially advantageous in diseased ventricles (61). Another method that is widely used to obtain P-V relationship is to identify the end diastolic points from multiple beats (39, 62) and fit them with an exponential curve to obtain the end diastolic pressure volume relationship (EDPVR). This method remains the gold standard for LV chamber stiffness characterization. Noninvasively, LV stiffness has been shown to be related to the deceleration portion of the early diastolic filling transmitral E-wave (42, 66).

Relaxation is conceptually defined by the level of wall stress relative to diastasis (equilibrium volume). It is quantitated in terms of the rate of pressure decay and its asymptotic

value during diastasis. At a cellular level, relaxation involves the rate of the crossbridge uncoupling from the thin filaments and the rate of calcium ions from the contractile apparatus being pumped back into the sarcoplasmic reticulum (calcium sequestration). This sequestration requires ATP and decreases the Ca^{2+} concentration in the vicinity of the contractile machinery by a factor of 10,000 on timescales of tens of milliseconds, from the millimolar to the micromolar range. In a physical sense, the spatio-temporal process of relaxation modulates how efficiently the potential energy stored during the previous systole can be recovered as motion of tissue, and ultimately as kinetic energy of the blood that enters into the ventricle during the early filling initiated by suction. Relaxation is traditionally measured invasively by the rate of pressure decay during isovolumic relaxation (peak negative dP/dt) and noninvasively as the duration of the isovolumic relaxation time (IVRT = time from AVC to MVO) and from the shape and duration of the deceleration portion of the transmitral E-wave during early diastolic filling (2).

1.2   Data   Acquisition   and   the   Analysis   of Ventricular Function

1.1.1 <u>Acquisition and Analysis of Echocardiographic Data</u>

Echocardiography is currently the preferred non-invasive method for diastolic function assessment due to its portability, ease and speed of use, cost-effectiveness, excellent temporal resolution, and spatial resolution (2). Echocardiography operates on the principle that it receives and processes echoes emitted from a signal source that can provide information on the structure of the heart and position of its walls and valves, as well as the velocity and timing of blood and tissue motion. In the practice of transthoracic echocardiography, the echocardiographic transducer, consisting of arrays of piezoelectric crystals, is positioned on the chest wall during an echocardiographic examination, and its specific position and orientation is adjusted according to the desired view of the heart. An electrical signal causes high-frequency mechanical vibrations to be emitted by the piezoelectric crystals, which subsequently propagate through the chest wall and into the heart. Because the blood-myocardial tissue interface constitutes an acoustic discontinuity, reflection of the ultrasonic pulses from the tissue exceeds reflection from the blood, allowing adequate contrast between the tissue and blood within the heart. The returning ultrasonic echoes are transduced by the piezoelectric crystals, which are then processed by the echocardiography machine to create an image.

A variety of different echocardiographic modalities exist; the choice of which modality to use depends both upon the capabilities of the echocardiography machine and the nature of the physiologic information one wishes to obtain. The earliest clinical application of echocardiographic imaging—M-Mode imaging—consisted of measuring and displaying cardiac

structures along one ultrasonic pulse line over time. Technological advances allowed echocardiographers to send and receive multiple ultrasonic pulses in a variety of beam shapes, thereby allowing for live 2D and 3D imaging during the echocardiographic exam. Perhaps the most common echocardiographic modality is pulsed Doppler echocardiography, in which discrete pulses of sound are emitted along a line of sight at a certain frequency. A sample volume is defined by the sonographer so that the returning signal is restricted to the specific spatial region of interest. The phase shift of the (detected) signal returning from this sample volume is used to determine the velocity of blood (or tissue) motion within the sample volume. Objects moving at higher velocities will produce larger phase shifts, and vice-versa. Finally the reflected signal is processed, and velocities measured at the sample volume are plotted versus time. Blood velocity at the mitral valve, aortic valve, and at the pulmonary veins may be measured using Doppler echo, and with appropriate filtering, tissue velocity at the mitral annular may be also assessed. This dissertation incorporates data acquired from pulsed Doppler echocardiography of transmitral inflow (E- and A-waves) and mitral annular velocity (E'- and A'-waves).

Pulsed Doppler is most routinely used to image the transmitral flow pattern by specifying a sample volume at the tips of the mitral valve leaflets (Figure 1.6). As soon as there is an atrioventricular pressure gradient, the mitral valve opens and the transmitral velocity signal shows the early E-wave velocity contour (14). The negative atrioventricular pressure gradient (LVP<LAP) accelerates the blood across the mitral valve until minimum LVP is attained. Once atrial pressure falls below ventricular pressure (LVP>LAP), the rate of filling decelerates. E-wave deceleration is driven in part by the reversal in atrioventricular pressure gradient, and following the end of the E-wave, a diastatic interval with no pressure change and no or low flow commences. The time-integral of the E-wave, multiplied by an effective mitral valve leaflet cross

sectional area (MVA), represents early diastolic filling volume (6). Diastasis ends with the P-wave and atrial contraction. Atrial contraction results in a positive atrioventricular pressure gradient that accelerates the late diastolic filling transmitral A-wave. Continued ventricular filling from the A-wave increases ventricular pressure, and once the atrioventricular pressure gradient reverses, the A-wave decelerates. The A-wave ends abruptly with R-wave driven ventricular contraction, rapid pressure rise and closure of the mitral valve.
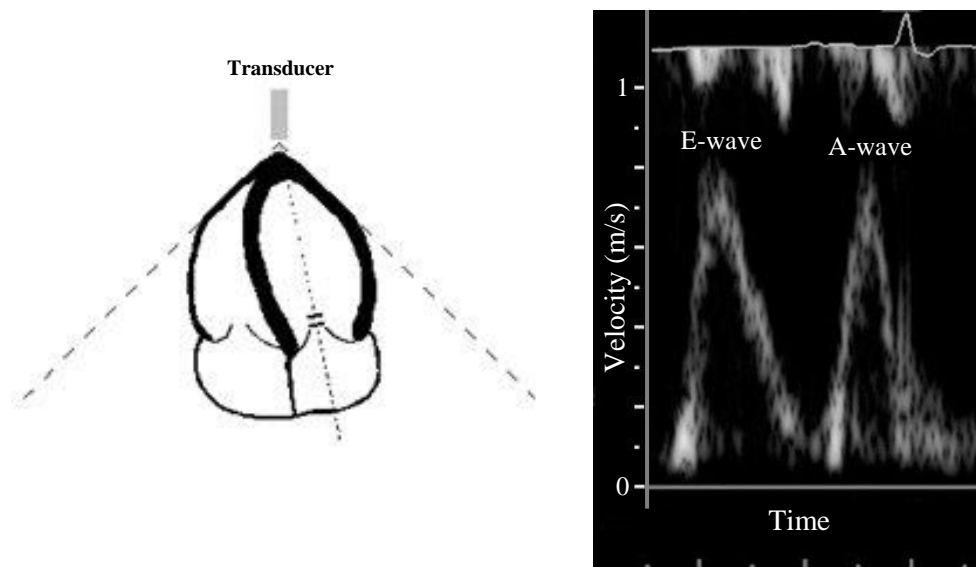
Figure 1.6 Illustration of transmitral flow data acquisition.
Left: Schematic of echocardiographic window showing insonification direction and sample volume position (at tips of mitral valve leaflets) for acquisition of transmitral flow velocity as a function of time using pulsed Doppler echocardiography. Right: Typical transmitral flow profile from pulsed Doppler echocardiography with superimposed ECG as a function of time showing early filling (E) and atrial filling (A) waves. Only the velocity of blood flow within the sample volume is displayed, accounting for the narrow velocity band characterizing the E- and A-waves. Distance between time tick marks on abscissa is 200 ms.

A set of widely used DF parameters can be obtained from the analysis of transmitral E- and A-waves as shown in Figure 1.7. Conventionally, E- and A-waves are approximated as

22

triangles. Clinicians or sonographers simply select the start, peak, and end of each wave, thereby defining the acceleration time (AT), deceleration time (DT), peak velocity (E_{peak}, A_{peak}), the ratio of the E- and A- wave peaks (E/A), and the ratio of the E- and A- wave velocity time integral (E_{VTI}/A_{VTI}). Isovolumic relaxation time (IVRT) is defined as the time between aortic valve closure and mitral valve opening, i.e. the start of the E-wave can also be measured (2). E/A, E_{VTI}/A_{VTI}, DT, and IVRT have been used as relaxation parameters, and all of these properties change with age as DF is impaired (12). It is worth noting that these triangular approximations for waveform shapes and the associated analysis only utilize two or three points of the entire E- and A-waves, and the curvilinear features evident in contour of the waves is ignored.
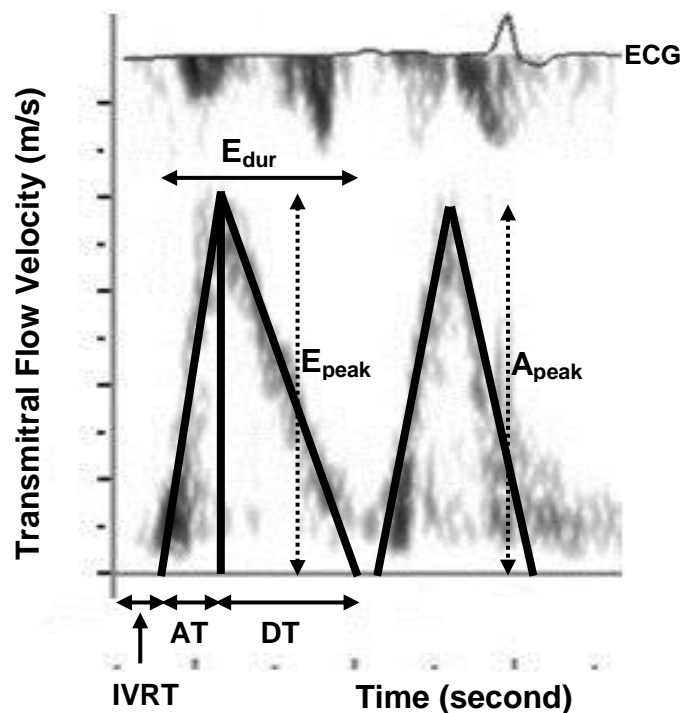
Figure 1.7 Commonly used diastolic function indexes.

Transmitral E- and A-wave obtained using Doppler echocardiography demonstrating commonly used diastolic function indexes. E_{dur}, duration of the E-wave; E_{peak}, A_{peak}, peak velocity of the E- and A-wave, respectively; AT, acceleration time; DT, deceleration time; IVRT, isovolumic relaxation time. See text for details.

Pulsed Doppler echocardiography can be adapted to imaging tissue as well as flow via adjustment of the filter settings in the echocardiography machine such that lower velocity tissue motion is recorded. In Doppler tissue imaging (DTI), the sample volume is generally placed either on the myocardium itself or at the junction between the mitral annulus and myocardium. One of such applications is the characterization of the mitral annular motion (Figure 1.8). The sample volume is usually placed at the medial or lateral aspects of the annulus, and the displacement and velocity of the annulus during diastolic filling (E'- and A'-waves) can be measured and used to characterize diastolic function (17, 59). Mitral annular velocity is shown by two negative E'- and A'-waves during the filling phase.
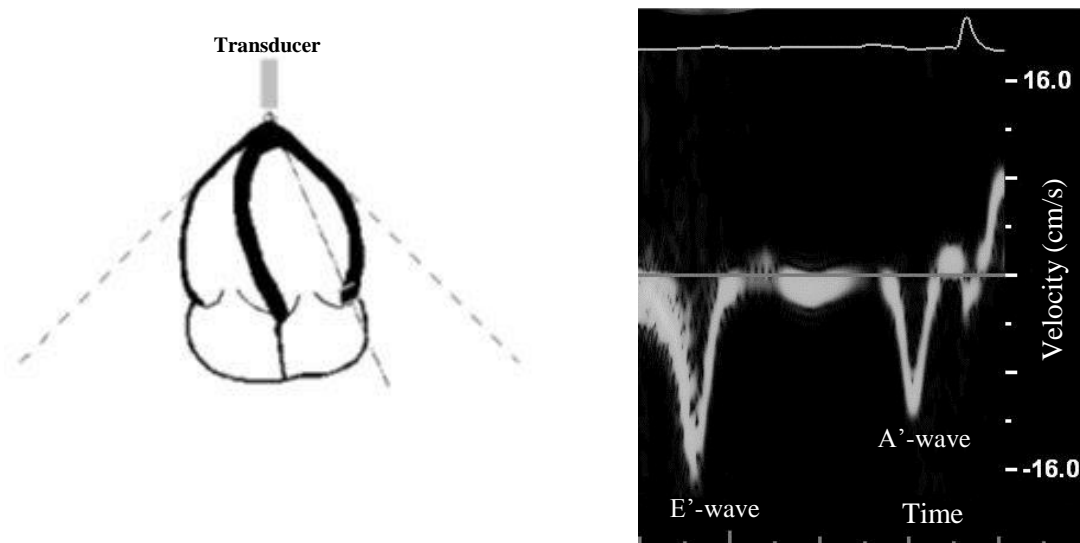
Figure 1.8 Illustration of Doppler Tissue Imaging data acquisition.
Left: Schematic of echocardiographic window showing insonification direction and sample volume position (at lateral aspect of mitral annulus) for acquisition of longitudinal annular motion velocity using Doppler Tissue Imaging (DTI). Right: Typical DTI profile of lateral mitral annulus motion with superimposed ECG as a function of time showing annular deflections corresponding to the early and atrial filling waves (E' and A'-waves, respectively). While the mitral annulus does not move perfectly parallel to the insonification direction (i.e. longitudinally), there is typically just a small angle dependence of annular motion on the insonification direction.

The negative E'-wave represents longitudinal lengthening during early diastole, which is a necessary consequence of longitudinal volume accommodation and conservation of ventricular tissue and chamber volume. As the atrium contracts, the mitral annulus is pulled up; therefore most of the A-wave volume is accommodated longitudinally, and the A'-wave is observed simultaneously with the transmitral A-wave.

1.1.2 <u>Echocardiographic Characterization of Diastolic Function</u>

It has been shown that the maximum velocity of the mitral annulus motion during early filling (E') and its ratio to the maximum transmitral flow velocity (E/E') have been correlated with DF. It has been shown that E/E' is related to the end diastolic pressure (LVEDP), which otherwise relies on invasive measurements (53, 59). Because of the incompressibility of the myocardium and the constant volume attribute of the heart (7), transmitral flow and the motion of the annulus must be coupled (40). DF via E-waves is categorized into 4 patterns in order of worsening diastolic function: normal, delayed relaxation, pseudonormal, and constrictive-restrictive (1) (Figure 1.9).
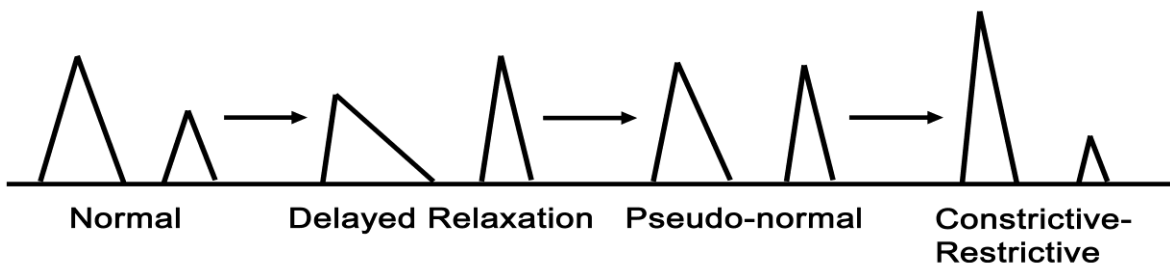
Figure 1.9 Different patterns of diastolic dysfunction (DD)
DD starts from the delayed relaxation pattern where the relaxation function is impaired. The atrium increases the filling pressure to compensate for the reduced pressure gradient during filling and generates a pseudo-normal filling pattern. In late stage DD, the filling pressure and the stiffness of the ventricle are significantly increased. As a result, the LV chamber cannot relax effectively to fill itself with blood and exhibit the constrictive-restrictive pattern. See text for details.

When diastolic function is slightly impaired, a 'delayed relaxation' filling pattern (Grade 1 diastolic dysfunction) may be observed. Delayed relaxation filling pattern is associated with impaired relaxation, without significant increase in (mean) LA pressure. LV diastolic pressure is increased; therefore, the early diastolic pressure gradient is decreased (56). The hallmark of the delayed relaxation pattern is prolonged DT, decreased E and E', and E-wave velocity peak to A-

wave velocity peak (E/A ratio) reversal (from E/A>1 to E/A<1).

In grade 2 diastolic dysfunction (pseudonormal filling) LV relaxation is further impaired and is associated with an increase in LV chamber stiffness such that LA pressure becomes elevated. However, the early diastolic pressure gradient is maintained, resulting in relatively normal E-wave contours and reduced E' (21). While the pseudonormal pattern appears similar to the normal pattern, it may be unmasked clinically by load variation. Indeed preload reduction following a Valsalva maneuver turns a pseudonormal pattern into a delayed relaxation pattern.

With further elevation of chamber stiffness LA pressure becomes significantly elevated (grade 3 or restrictive pattern), E_{peak} increases and E' is further reduced. DT and E_{dur} shorten substantially, resulting in elevation of E/E'.

Deceleration Time of E-wave as a Diastolic Function Index

The deceleration time (DT) of the E-wave based on the triangle approximation is another common DF index. Approximation of the deceleration portion of the E-wave as a cosine function using Newton's Second Law has allowed derivation of a relationship between DT and ventricular stiffness (42). Based on this model, stiffness increases as the inverse of the square of DT. However, recent work from our group has found that approximation of the E-wave deceleration portion as a cosine does not account for the inflection point, resulting in the transition of the velocity contour from concave-down to concave-up (64, 66). This feature of E-wave deceleration is caused by relaxation/viscoelastic effects that were not incorporated in the original cosine model. These relaxation/viscoelastic effects modulate the relationship between DT and stiffness such that increased (i.e. impaired) relaxation/viscoelasticity increases DT at a constant stiffness.

27

1.1.3 <u>Acquisition and Analysis of Hemodynamic Data</u>

Invasive assessment of DF is sometimes used in conjunction with non-invasive assessment. Invasive DF assessment usually involves introducing a catheter into the femoral artery and feeding it in retrograde fashion through the aortic valve into the left ventricle. The piezoelectric pressure sensors near the end of the catheter can measure the pressures in the LV and aorta with high fidelity. LV volume can also be measured by the conductance between different electrodes (result in volts) on the catheter within the ventricle (78). Electrodes along the catheter create an electric field, and the resulting voltage change (and by Ohm's law conductance of the chamber) is measured by receiving electrodes on the catheter. Because conductance and volume to a first approximation have been shown to be linearly related (4), the measurement of conductance changes in the chamber may be used to determine volume changes in real time.

While left ventricular end-diastolic pressure (LVEDP) is the only pressure-based index commonly reported in the clinical setting, the maximum rate of pressure decline (dP/dt_{min}) is often determined as an index of relaxation during isovolumic relaxation. A more standard invasive relaxation index, the time constant of isovolumic relaxation (τ), can be determined by fitting a decaying exponential to the left ventricular pressure data from dP/dt_{min} to the mitral valve opening (76). Alternatively, τ (as well as LVEDP) can be determined from the pressure phase-plane, or the first derivative of left ventricular pressure (dP/dt) plotted as a function of left ventricular pressure itself (phase plane). Assuming an exponential pressure decay following dP/dt_{min}, the slope of the line fit from dP/dt_{min} to mitral valve opening in the phase plane is $-1/\tau$, which yields τ (76). LVEDP and τ are considered "gold-standard" indices of DF because they are determined invasively. However, they are also load-dependent; indeed, LVEDP may be considered a measure of load.

Pressure-Volume Analysis

With the high fidelity pressure and simultaneous volume data, pressure volume loops can be plotted on the P-V plane. The stages of the cardiac cycle may be mapped onto the pressure volume loop as shown in Figure 1.10.
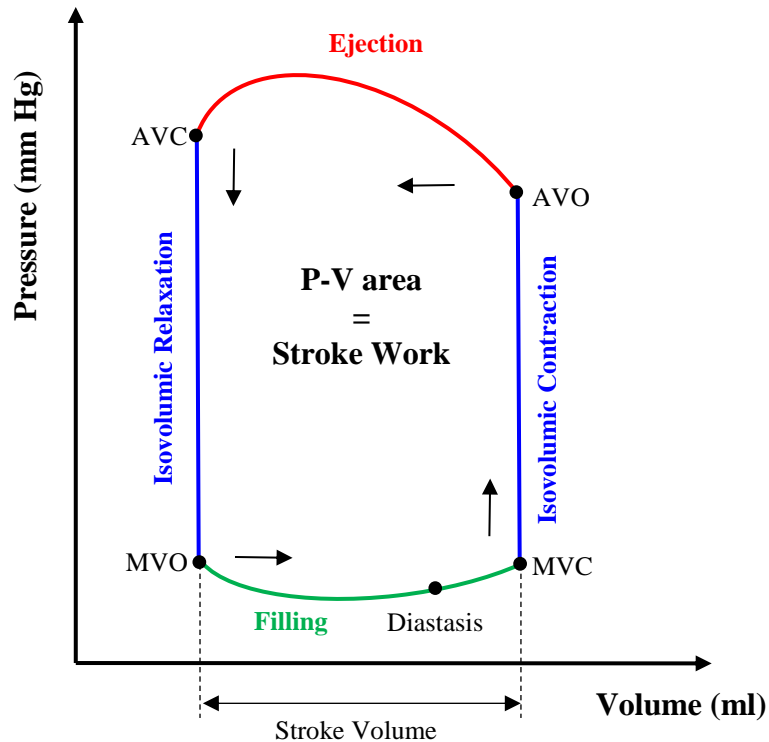
Figure 1.10 Normal pressure-volume loop showing four phases of cardiac cycle.
MVO, mitral valve opening; MVC, mitral valve closure; AVO, aortic valve opening; AVC, aortic valve closure. See text for details.

With the change of load, the position of the loop can change on the P-V plane. Several measurements of physiologic importance can be taken from the PV loops. The area inside the pressure volume loop ($\oint PdV$) for each heart beat defines the external work done by the ventricle (29). Using the stroke work, a mechanical efficiency can be calculated (29). We have

demonstrated that the area under the diastolic filling portion alone is related diastolic recoil energy (51) and details of the relation is presented in more depth in Chapter 3.

Stoke Volume and Ejection Fraction

The difference between end-diastolic and end-systolic volume is the ventricular stroke volume; therefore the width of the pressure volume loop may be used to easily assess changes in ejected volume. The ratio of stroke volume to end diastolic volume defines the ventricular ejection fraction. Ejection fractions below 50% are typically viewed as indicative of systolic dysfunction. Ejection fraction may be determined from conductance catheter volume measurements, but are more routinely determined by contrast ventriculography or by 2D or 3D echocardiography.

End Systolic Pressure Volume Relation and Contractility

Maximum elastance, E_{max}, a validated load independent index of systolic function, is obtained by fitting the PV points that have the highest P/V values (elastance) (close to end systole as shown in Figure 1.11) in different heartbeats at variable loads (71). Maximum elastance represents a load independent index of cardiac muscle contractility so that increases in contractility increase the slope of the end-systolic pressure volume relation. Therefore, it alters the general location of load-varying pressure volume loops.

End Diastolic Pressure Volume Relation and Diastolic Chamber Compliance

The current gold standard for LV passive chamber stiffness is the end diastolic pressure volume relationship (EDPVR). The EDPVR can be obtained by fitting the end diastolic PV points for several beats (multiple beat approach) or fitting several data points within one heart beat (single beat approach) (30) to exponential curves (Equation 1.1) (45) or straight lines (80). The ratio of pressure to volume in an elastic chamber is similar to the ratio of force to displacement in a spring; therefore, the slope of the end-diastolic pressure volume relation defines effective chamber stiffness (inverse of compliance). The exponential equation that is used to fit the PV data is:

$$P = be^{KV} + V_o \qquad\qquad [1.1]$$

From the EDPVR, LV invasive chamber stiffness can be measured in terms of the parameter (K) on the exponential (Equation 1.1) or the slope of the straight line. In patients with heart failure, when ventricular stiffness is significantly increased, the EDPVR shifts upwards and leftwards (as shown in Figure 1.11) (81, 83).
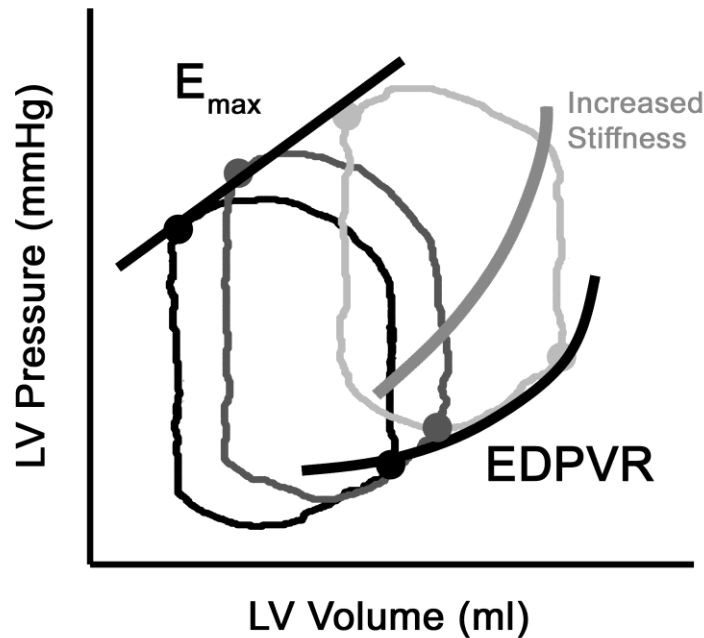
Figure 1.11 Pressure-volume loops of three beats showing loading effects.
End diastolic pressure volume relationship (EDPVR) can be obtained from multiple PV loops, and the slope
of the EDPVR represents chamber stiffness. The slope of the ESPVR, maximum elastance (E_{max}), changes
with changes in contractility. See text for details.

Pressure Analysis

In cardiovascular research, more parameters and indexes are commonly obtained from invasive pressure-volume data. The decay of pressure during isovolumic relaxation has been intensively used. Weiss proposed that the rate of pressure decline as a function of time is proportional to pressure itself. Therefore, the following equation for isovolumic pressure decay was proposed (76):

$$P(t) = (P_o - P_\infty)e^{-t/\tau} + P_\infty \qquad [1.2]$$

where τ is the time constant of isovolumic relaxation, P_o is a constant, and P_∞ is the pressure asymptote.

A prolonged τ (>50ms) reflects a slower pressure decay termed delayed relaxation. Practically, the data from 5ms after the inflection point (-*dP/dt*$_{min}$) until 5ms before mitral valve opening (which is estimated as LVEDP) are utilized in the fit. The original exponential fit was plotted on pressure vs. time axes (Figure 1.12).
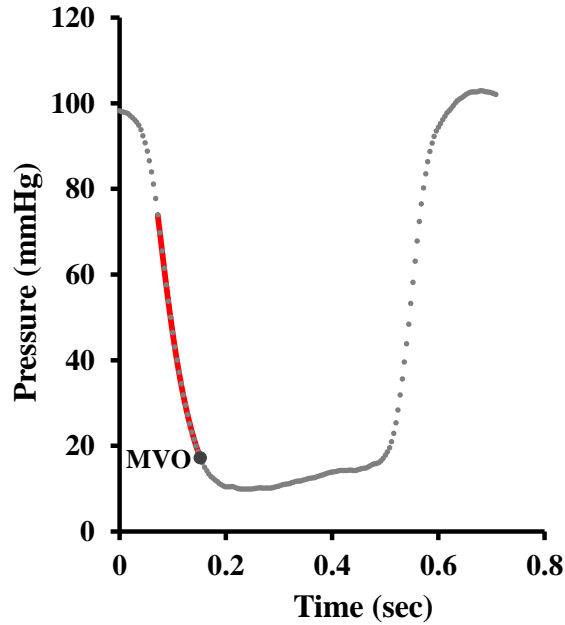
Figure 1.12 The exponential fit to isovolumic relaxation segment.
The original exponential fit (red curve) was plotted on pressure vs. time axes for one cardiac cycle.
See text for details.

Because of existing limitations of the Weiss equation in some cases, the logistic time constant τ$_L$ was proposed (44), where pressure as a function of time obeys a relationship in which the rate of pressure decline is proportional to the square of the pressure. Therefore, the following nonlinear expression for isovolumic pressure decay was proposed (44):

$$P(t) = \frac{P_A}{1 + e^{-t/\tau_L}} + P_B \qquad [1.3]$$

where τ$_L$ is the logistic time constant, P$_A$ is a constant, and P$_B$ is the pressure asymptote.

33

Phase Plane Analysis

A more straightforward and intuitive approach to obtain τ is through pressure phase plane (PPP) (16). PPP is the plot of pressure vs. the time derivative of pressure (dP/dt), as shown in Figure 1.13. All PPP trajectories are inscribed clockwise, and each cardiac cycle is represented by one loop on the PPP. Although time is not explicit on the PPP, several important parameters, including LVEDP, maximum and minimum pressure, *dP/dt$_{max}$*, and *-dP/dt$_{min}$* (shown in Figure 1.13) can be readily measured. On PPP, the Weiss equation gives a straight line during isovolumic relaxation portion. Thus, the isovolumic relaxation time constant τ can be easily measured from the slope ($-1/\tau$) of the fitted straight line from -dP/dt$_{min}$ to MVO. If the PPP IVR portion is curved, the logistic time constant is used to perform the fit (44).
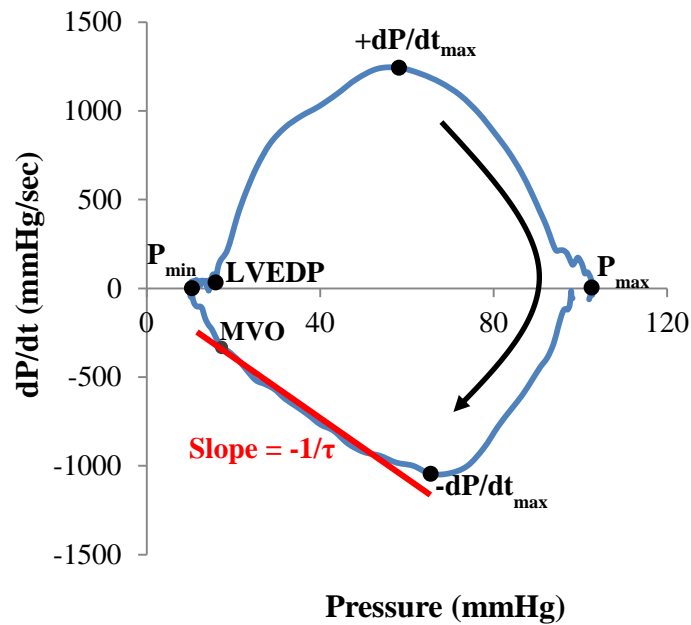
Figure 1.13 Pressure phase plane (pressure vs. dP/dt) for one cardiac cycle.
Peak positive dP/dt, peak pressure, peak negative dP/dt, and minimum pressure define the 4 extrema of the phase plane loop. PPP shows how isovolumic relaxation time constant (τ) can be measured. Each heart cycle is represented as a clockwise cycle on the PPP. Other important measurements (+dP/dt$_{max}$, -dP/dt$_{max}$) are shown. See text for details.

A kinematic model has been derived and validated for isovolumic pressure decay (IVPD) applicable during IVR (12). The 'Chung model' accurately characterizes the wide range of physiologically observed IVPD contours when viewed as pressure phase plane (PPP) trajectories. It was shown that IVPD is governed by the interplay of inertial, stiffness, and relaxation forces (12). The model is discussed in details in the next chapter.

1.3   Thesis Overview

Each chapter comprising this dissertation, with the exception of the Introduction and Method chapters (Chapters 1 and 2), consists of a separate manuscript. These manuscripts have either been already accepted for publication or are currently in review.

In Chapter 3, through joint work with Shmuylovich, the thermodynamics of diastole are investigated. The chapter consists of the investigation of the causal relationship between the Doppler E-wave and the simultaneous ventricular pressure contour. Since both the pressure and the flow measurements are taken during the same mechanical event (early diastolic filling) the features of the pressure and flow contours must be causally related. The external work performed by the LV in one cardiac cycle can be characterized using pressure-volume coordinates where each cycle inscribes a closed loop. The area inside the loop is the external work of the heart per cycle. Rather than looking the entire cycle, the filling function of the heart can be considered by looking at the energy during early filling –from mitral valve opening (MVO) to diastasis. This function can be measured from P and V data obtained during cardiac catheterization. From a thermodynamics perspective, this energy can be computed from the area under the appropriate segment of the pressure-volume (P-V) loop. We also know that the energy of filling can be independently computed from echocardiography by analyzing transmitral blood flow velocity as a function of time during filling (Doppler E-wave). Applying Bernoulli's equation and PDF formalism, we derive an E-wave based expression for the energy associated with early, rapid filling, and find that, in accordance with the first law of thermodynamics, the E-wave derived energy is equivalent to energy calculated from simultaneously acquired pressure-volume data (51).

Chapter 4 builds on the work of Chapter 3. After establishing the energy relation between

non-invasive and invasive methods, we propose to undertake the next logical step in our quest for more complete understanding of the physiology of diastole in terms of thermodynamics, kinematic modeling of diastole and diastasis. Accordingly, we hypothesize that the relaxed (diastatic) stiffness of the LV as an index of DF can be computed directly from E-wave analysis alone using our methods, and we validate it using simultaneous P-V loop data (48).

Chapter 5, in joint work with Shmuylovich is a natural follow-up to Chapter 3. We applied D-PVR to atrial fibrillation (AF) patients and measured chamber stiffness. Measurement of chamber stiffness in NSR (where there is atrial contraction) and in AF via the EDPVR presents a problem because of the lack of atrial contraction in AF. As a result, comparing the EDPVR in AF and normal sinus rhythm is not appropriate. Using the D-PVR inscribed by diastasis, which is present in both AF and NSR, we found that LV stiffness is increased in AF subjects. This result was further supported by other, independent noninvasive stiffness measurements (50).

Chapter 6 concerns of the investigation of the force relationship between two phases of the cardiac cycle—isovolumic relaxation and early rapid filling. We derive the terminal force of isovolumic relaxation using pressure data by applying the kinematic model of isovolumic relaxation (Chung model). From echo data, we use the force equation of simple harmonic oscillator (PDF model). We find a close linear relationship between the terminal force of isovolumic relaxation and the initial force of early rapid filling, in accordance with the prediction stemming from physical argument (49).

Chapter 7 introduces the concept of decomposition of E-wave deceleration time (DT) to its stiffness and relaxation components as well as its derivation. LV chamber stiffness and relaxation parameters are the most common indexes used to characterize diastolic function. E-

37

wave deceleration time (DT) was thought to be determined only by chamber stiffness. However, kinematic modeling of filling has shown that DT is actually an algebraic function of both stiffness (PDF parameter k) and relaxation (PDF parameter c). We hypothesize and validate that kinematic modeling based E-wave analysis accurately predicts the stiffness (DT_s) and relaxation (DT_r) components of DT, such that $DT = DT_s + DT_r$ (47).

Chapter 8 and 9 extend the work of Chapter 7 on the application of decomposition of E-wave DT to its stiffness and relaxation components in normal sinus rhythm (NSR) vs atrial fibrillation (AF) groups and normal filling (NL) vs. pseudonormal filling (PN) groups.

In Chapter 8, the fractionation of DT into relaxation and stiffness components shows that AF has increased stiffness compared to NSR. In addition, a larger percentage of E-wave DT in AF is due to stiffness than to relaxation compared to NSR (46).

In Chapter 9, we show that PDF parameters, and the relaxation and stiffness components of DT could differentiate normal and pseudonormal filling without requiring knowledge of E', We also show that pseudonormal filling had increased stiffness compared to normal filling (52).

1.4   References

1.   **Anderson B**. *Echocardiography: The Normal Examination of Echocardiographic Measurements*. Dutoit: Blackwell Publishing, 2002.

2.   **Appleton CP, Firstenberg MS, Garcia MJ, and Thomas JD**. The echo-Doppler evaluation of left ventricular diastolic function. A current perspective. *Cardiol Clin* 18: 513-546, ix, 2000.

3.   **Arts T, and Reneman RS**. Dynamics of left ventricular wall and mitral valve mechanics--a model study. *J Biomech* 22: 261-271, 1989.

4.   **Baan J, van der Velde ET, de Bruin HG, Smeenk GJ, Koops J, van Dijk AD, Temmerman D, Senden J, and Buis B**. Continuous measurement of left ventricular volume in animals and humans by conductance catheter. *Circulation* 70: 812-823, 1984.

5.   **Berne R, and Levy M**. *Cardiovascular Physiology: Mosby*. 2001.

6.   **Bowman AW, Frihauf PA, and Kovács SJ**. Time-varying effective mitral valve area: prediction and validation using cardiac MRI and Doppler echocardiography in normal subjects. *Am J Physiol Heart Circ Physiol* 287: H1650-1657, 2004.

7.   **Bowman AW, and Kovács SJ**. Assessment and consequences of the constant-volume attribute of the four-chambered heart. *Am J Physiol Heart Circ Physiol* 285: H2027-2033, 2003.

8.   **Brecher GA**. Experimental evidence of ventricular diastolic suction. *Circ Res* 4: 513-518, 1956.

9.   **Choong CY, Herrmann HC, Weyman AE, and Fifer MA**. Preload dependence of Doppler-derived indexes of left ventricular diastolic function in humans. *J Am Coll Cardiol* 10: 800-808, 1987.

10.   **Chung CS, Ajo DM, and Kovács SJ**. Isovolumic pressure-to-early rapid filling decay rate relation: model-based derivation and validation via simultaneous catheterization echocardiography. *J Appl Physiol (1985)* 100: 528-534, 2006.

11.   **Chung CS, Karamanoglu M, and Kovács SJ**. Duration of diastole and its phases as a function of heart rate during supine bicycle exercise. *Am J Physiol Heart Circ Physiol* 287:

H2003-2008, 2004.

12.   **Chung CS, and Kovács SJ**. Physical determinants of left ventricular isovolumic pressure decline: model prediction with in vivo validation. *Am J Physiol Heart Circ Physiol* 294: H1589-1596, 2008.

13.   **Chung CS, and Kovács SJ**. Pressure phase-plane based determination of the onset of left ventricular relaxation. *Cardiovasc Eng* 7: 162-171, 2007.

14.   **Courtois M, Kovács SJ, and Ludbrook PA**. Transmitral pressure-flow velocity relation. Importance of regional pressure gradients in the left ventricle during diastole. *Circulation* 78: 661-671, 1988.

15.   **Dubin D**. *Rapid interpretation of EKG's*. Hong Kong: 2000.

16.   **Eucker SA, Lisauskas JB, Singh J, and Kovács SJ**. Phase plane analysis of left ventricular hemodynamics. *J Appl Physiol (1985)* 90: 2238-2244, 2001.

17.   **Feigenbaum H**. *Echocardiography*. Baltimore: Williams & Wilkins, 1993.

18.   **Granzier HL, and Labeit S**. The giant protein titin: a major player in myocardial mechanics, signaling, and disease. *Circ Res* 94: 284-295, 2004.

19.   **Greenbaum RA, Ho SY, Gibson DG, Becker AE, and Anderson RH**. Left ventricular fibre architecture in man. *Br Heart J* 45: 248-263, 1981.

20.   **Hamilton W, and Rompf H**. Movements of the base of the ventricle and relative constancy of the cardiac volume. *Am J Physiol* 102: 559-565, 1932.

21.   **Hasegawa H, Little WC, Ohno M, Brucks S, Morimoto A, Cheng HJ, and Cheng CP**. Diastolic mitral annular velocity during the development of heart failure. *J Am Coll Cardiol* 41: 1590-1597, 2003.

22.   **Helmes M, Trombitás K, and Granzier H**. Titin develops restoring force in rat cardiac myocytes. *Circ Res* 79: 619-626, 1996.

23.   **Hoffman E, Ehman R, Sinak L, Felmlee J, Chandrasekaran K, Julsrud P, and Ritman E**. Law of constant heart volume in humans: a non-invasive assessment via X-ray, CT, MRI, and echo. *J Am Coll Cardiol* 9: 1987.

24.   **Hoffman E, and Ritman E**. Intracardiac cycle constancy of total heart volume. *Dyn Cardiovasc Im* 1: 199-205, 1987.

25.   **Hoffman EA, and Ritman EL**. Heart-lung interaction: effect on regional lung air content and total heart volume. *Ann Biomed Eng* 15: 241-257, 1987.

26.   **Hoffman EA, and Ritman EL**. Invariant total heart volume in the intact thorax. *Am J Physiol* 249: H883-890, 1985.

27.   **Hurrell DG, Nishimura RA, Ilstrup DM, and Appleton CP**. Utility of preload alteration in assessment of left ventricular filling pressure by Doppler echocardiography: a simultaneous catheterization and Doppler echocardiographic study. *J Am Coll Cardiol* 30: 459-467, 1997.

28.   **Jaber WA, Lam CS, Meyer DM, and Redfield MM**. Revisiting methods for assessing and comparing left ventricular diastolic stiffness: impact of relaxation, external forces, hypertrophy, and comparators. *Am J Physiol Heart Circ Physiol* 293: H2738-2746, 2007.

29.   **Kameyama T, Asanoi H, Ishizaka S, Yamanishi K, Fujita M, and Sasayama S**. Energy conversion efficiency in human left ventricle. *Circulation* 85: 988-996, 1992.

30.   **Kass DA**. Assessment of diastolic dysfunction. Invasive modalities. *Cardiol Clin* 18: 571-586, 2000.

31.   **Kass DA, Bronzwaer JG, and Paulus WJ**. What mechanisms underlie diastolic dysfunction in heart failure? *Circ Res* 94: 1533-1542, 2004.

32.   **Katz LN, and Ackerman W**. The effect of the heart's position on the electrocardiographic appearance of ventricular extrasystoles. *J Clin Invest* 11: 1221-1239, 1932.

33.   **Kennish A, Yellin E, and Frater RW**. Dynamic stiffness profiles in the left ventricle. *J Appl Physiol* 39: 665-671, 1975.

34.   **Kmetzo JJ, Plotnick GD, and Gottdiener JS**. Effect of postural changes and isometric exercise on Doppler-derived measurements of diastolic function in normal subjects. *Chest* 100: 357-363, 1991.

35.   **Kobayashi T, and Solaro RJ**. Calcium, thin filaments, and the integrative biology of cardiac contractility. *Annu Rev Physiol* 67: 39-67, 2005.

36.	**Kovács SJ, Barzilai B, and Pérez JE**. Evaluation of diastolic function with Doppler echocardiography: the PDF formalism. *Am J Physiol* 252: H178-187, 1987.

37.	**Kovács SJ, Meisner JS, and Yellin EL**. Modeling of diastole. *Cardiol Clin* 18: 459-487, 2000.

38.	**Lahmers S, Wu Y, Call DR, Labeit S, and Granzier H**. Developmental control of titin isoform expression and passive stiffness in fetal and neonatal myocardium. *Circ Res* 94: 505-513, 2004.

39.	**Levine BD, Zuckerman JH, and Pawelczyk JA**. Cardiac atrophy after bed-rest deconditioning: a nonneural mechanism for orthostatic intolerance. *Circulation* 96: 517-525, 1997.

40.	**Lisauskas J, Singh J, Courtois M, and Kovács SJ**. The relation of the peak Doppler E-wave to peak mitral annulus velocity ratio to diastolic function. *Ultrasound Med Biol* 27: 499-507, 2001.

41.	**Lisauskas JB, Singh J, Bowman AW, and Kovács SJ**. Chamber properties from transmitral flow: prediction of average and passive left ventricular diastolic stiffness. *J Appl Physiol (1985)* 91: 154-162, 2001.

42.	**Little WC, Ohno M, Kitzman DW, Thomas JD, and Cheng CP**. Determination of left ventricular chamber stiffness from the time for deceleration of early left ventricular filling. *Circulation* 92: 1933-1939, 1995.

43.	**Masuyama T, St Goar FG, Alderman EL, and Popp RL**. Effects of nitroprusside on transmitral flow velocity patterns in extreme heart failure: a combined hemodynamic and Doppler echocardiographic study of varying loading conditions. *J Am Coll Cardiol* 16: 1175-1185, 1990.

44.	**Matsubara H, Takaki M, Yasuhara S, Araki J, and Suga H**. Logistic time constant of isovolumic relaxation pressure-time curve in the canine left ventricle. Better alternative to exponential time constant. *Circulation* 92: 2318-2326, 1995.

45.	**Mirsky I**. Assessment of diastolic function: suggested methods and future considerations. *Circulation* 69: 836-841, 1984.

46.	**Mossahebi S, and Kovács SJ**. Diastolic Function in Normal Sinus Rhythm vs. Chronic

Atrial Fibrillation: Comparison by Fractionation of E-wave Deceleration Time into Stiffness and Relaxation Components. *Journal of Atrial Fibrillation* 6: 13-19, 2014.

47.   **Mossahebi S, and Kovács SJ**. Kinematic Modeling Based Decomposition of Transmitral Flow (Doppler E-wave)   Deceleration Time into Stiffness and Relaxation Components. *Cardiovascular Engineering & Technology* 5: 25-34, 2014.

48.   **Mossahebi S, and Kovács SJ**. Kinematic modeling-based left ventricular diastatic (passive) chamber stiffness determination with in-vivo validation. *Ann Biomed Eng* 40: 987-995, 2012.

49.   **Mossahebi S, and Kovács SJ**. The isovolumic relaxation to early rapid filling relation: kinematic model based prediction with in vivo validation. *Physiol Rep* 2: e00258, 2014.

50.   **Mossahebi S, Shmuylovich L, and Kovács SJ**. The Challenge of Chamber Stiffness Determination in Chronic Atrial Fibrillation vs. Normal Sinus Rhythm: Echocardiographic Prediction with Simultaneous Hemodynamic Validation. *Journal of Atrial Fibrillation* 6: 46-51, 2013.

51.   **Mossahebi S, Shmuylovich L, and Kovács SJ**. The thermodynamics of diastole: kinematic modeling-based derivation of the P-V loop to transmitral flow energy relation with in vivo validation. *Am J Physiol Heart Circ Physiol* 300: H514-521, 2011.

52.   **Mossahebi S, Zhu S, and Kovács SJ**. Fractionating E-wave deceleration time into its stiffness and relaxation components distinguishes pseudonormal from normal filling. 2014 (In Review).

53.   **Nagueh SF, Middleton KJ, Kopelen HA, Zoghbi WA, and Quiñones MA**. Doppler tissue imaging: a noninvasive technique for evaluation of left ventricular relaxation and estimation of filling pressures. *J Am Coll Cardiol* 30: 1527-1533, 1997.

54.   **Neagoe C, Kulke M, del Monte F, Gwathmey JK, de Tombe PP, Hajjar RJ, and Linke WA**. Titin isoform switch in ischemic human heart disease. *Circulation* 106: 1333-1341, 2002.

55.   **Noble D**. Modeling the heart--from genes to cells to the whole organ. *Science* 295: 1678-1682, 2002.

56.   **Ohno M, Cheng CP, and Little WC**. Mechanism of altered patterns of left ventricular

filling during the development of congestive heart failure. *Circulation* 89: 2241-2250, 1994.

57.   **Oki T, Tabata T, Mishiro Y, Yamada H, Abe M, Onose Y, Wakatsuki T, Iuchi A, and Ito S**. Pulsed tissue Doppler imaging of left ventricular systolic and diastolic wall motion velocities to evaluate differences between long and short axes in healthy subjects. *J Am Soc Echocardiogr* 12: 308-313, 1999.

58.   **Omens JH, and Fung YC**. Residual strain in rat left ventricle. *Circ Res* 66: 37-45, 1990.

59.   **Ommen SR, Nishimura RA, Appleton CP, Miller FA, Oh JK, Redfield MM, and Tajik AJ**. Clinical utility of Doppler echocardiography and tissue Doppler imaging in the estimation of left ventricular filling pressures: A comparative simultaneous Doppler-catheterization study. *Circulation* 102: 1788-1794, 2000.

60.   **Paelinck BP, van Eck JW, De Hert SG, and Gillebert TC**. Effects of postural changes on cardiac function in healthy subjects. *Eur J Echocardiogr* 4: 196-201, 2003.

61.   **Pak PH, Maughan L, Baughman KL, and Kass DA**. Marked discordance between dynamic and passive diastolic pressure-volume relations in idiopathic hypertrophic cardiomyopathy. *Circulation* 94: 52-60, 1996.

62.   **Perhonen MA, Zuckerman JH, and Levine BD**. Deterioration of left ventricular chamber performance after bed rest : "cardiovascular deconditioning" or hypovolemia? *Circulation* 103: 1851-1857, 2001.

63.   **Redfield MM, Jacobsen SJ, Burnett JC, Mahoney DW, Bailey KR, and Rodeheffer RJ**. Burden of systolic and diastolic ventricular dysfunction in the community: appreciating the scope of the heart failure epidemic. *JAMA* 289: 194-202, 2003.

64.   **Riordan MM, Chung CS, and Kovács SJ**. Diabetes and diastolic function: stiffness and relaxation from transmitral flow. *Ultrasound Med Biol* 31: 1589-1596, 2005.

65.   **Robinson TF, Factor SM, and Sonnenblick EH**. The heart as a suction pump. *Sci Am* 254: 84-91, 1986.

66.   **Shmuylovich L, and Kovács SJ**. E-wave deceleration time may not provide an accurate determination of LV chamber stiffness if LV relaxation/viscoelasticity is unknown. *Am J Physiol Heart Circ Physiol* 292: H2712-2720, 2007.

67.   **Sinak LJ, Hoffman EA, Schwartz RS, Smith HC, Holmes DR, Bove AA, Robb RA, Harris LD, and Ritman EL**. Three-dimensional cardiac anatomy and function in heart disease in adults: initial results with the dynamic spatial reconstructor. *Mayo Clin Proc* 60: 383-392, 1985.

68.   **Solomon SB, Nikolic SD, Frater RW, and Yellin EL**. Contraction-relaxation coupling: determination of the onset of diastole. *Am J Physiol* 277: H23-27, 1999.

69.   **Stoddard MF, Pearson AC, Kern MJ, Ratcliff J, Mrosek DG, and Labovitz AJ**. Influence of alteration in preload on the pattern of left ventricular diastolic filling as assessed by Doppler echocardiography in humans. *Circulation* 79: 1226-1236, 1989.

70.   **Støylen A, Slørdahl S, Skjelvan GK, Heimdal A, and Skjaerpe T**. Strain rate imaging in normal and reduced diastolic function: comparison with pulsed Doppler tissue imaging of the mitral annulus. *J Am Soc Echocardiogr* 14: 264-274, 2001.

71.   **Suga H, Sagawa K, and Shoukas AA**. Load independence of the instantaneous pressure-volume ratio of the canine left ventricle and effects of epinephrine and heart rate on the ratio. *Circ Res* 32: 314-322, 1973.

72.   **Sztajzel J, Ruedin P, Monin C, Stoermann C, Leski M, Rutishauser W, and Lerch R**. Effect of altered loading conditions during haemodialysis on left ventricular filling pattern. *Eur Heart J* 14: 655-661, 1993.

73.   **Tresch DD, and McGough MF**. Heart failure with normal systolic function: a common disorder in older people. *J Am Geriatr Soc* 43: 1035-1042, 1995.

74.   **Warren CM, Jordan MC, Roos KP, Krzesinski PR, and Greaser ML**. Titin isoform expression in normal and hypertensive myocardium. *Cardiovasc Res* 59: 86-94, 2003.

75.   **Waters EA, Bowman AW, and Kovács SJ**. MRI-determined left ventricular "crescent effect": a consequence of the slight deviation of contents of the pericardial sack from the constant-volume state. *Am J Physiol Heart Circ Physiol* 288: H848-853, 2005.

76.   **Weiss JL, Frederiksen JW, and Weisfeldt ML**. Hemodynamic determinants of the time-course of fall in canine left ventricular pressure. *J Clin Invest* 58: 751-760, 1976.

77.   **Yamamoto K, Masuyama T, Tanouchi J, Uematsu M, Doi Y, Mano T, Hori M, Tada M, and Kamada T**. Peak early diastolic filling velocity may decrease with preload

augmentation: effect of concomitant increase in the rate of left atrial pressure drop in early diastole. *J Am Soc Echocardiogr* 6: 245-254, 1993.

78.   **Yang SS, Bentivoglio L, Maranhao V, and Goldberg H**. *From Cardiac Catheterization Data to Hemodynamic Parameter* Philadelphia: F. A. Davis Company, 1988.

79.   **Zhang W, Chung CS, Shmuylovich L, and Kovács SJ**. Is left ventricular volume during diastasis the real equilibrium volume, and what is its relationship to diastolic suction? *J Appl Physiol (1985)* 105: 1012-1014, 2008.

80.   **Zhang W, and Kovács SJ**. The diastatic pressure-volume relationship is not the same as the end-diastolic pressure-volume relationship. *Am J Physiol Heart Circ Physiol* 294: H2750-2760, 2008.

81.   **Zile MR, Baicu CF, and Gaasch WH**. Diastolic heart failure--abnormalities in active relaxation and passive stiffness of the left ventricle. *N Engl J Med* 350: 1953-1959, 2004.

82.   **Zile MR, and Brutsaert DL**. New concepts in diastolic dysfunction and diastolic heart failure: Part I: diagnosis, prognosis, and measurements of diastolic function. *Circulation* 105: 1387-1393, 2002.

83.   **Zile MR, and Brutsaert DL**. New concepts in diastolic dysfunction and diastolic heart failure: Part II: causal mechanisms and treatment. *Circulation* 105: 1503-1508, 2002.

Chapter 2: Methods

2.1　Methods to Evaluate Diastolic Function

Diastolic dysfunction (DD) is predictor of and a precursor to diastolic heart failure (DHF), a clinical syndrome that has reached epidemic proportions. Critical to the management of this epidemic is the quantitative assessment of diastolic function (DF). Advancement in both invasive and non-invasive data collection methods has made a significant contribution to characterization of DF. Cardiac catheterization, considered the gold standard because of its invasive nature, can be employed to measure continuous pressures and volumes within the heart and vasculature. This pressure and volume data is used to compute different indexes such as: time constant of isovolumic relaxation (τ); the chamber stiffness computed at different time points such as diastasis and end-diastole; the end systolic pressure-volume relationship (ESPVR); the end-diastolic pressure-volume relationship (EDPVR); the maximum elastance; and the arterial elastance. Although left ventricular (LV) hemodynamics via cardiac catheterization comprises the gold standard for characterizing DF, Doppler echocardiography is the clinically preferred non-invasive method. Echocardiography allows real-time measurement of cardiac function with high temporal resolution. Doppler echocardiography is routinely used to measure flow velocity as a function of time into the ventricles during diastole. Numerous indexes have been derived from the amplitudes and durations of these flow patterns and are currently used to characterize DF. Other forms of echocardiography that have proven useful in the assessment of DF include Doppler tissue imaging (DTI), M-mode, strain, strain rate and twist.

Our research group has pioneered theoretical and experimental quantitative analysis of diastolic function in humans, using both non-invasive (echocardiography, cardiac MRI) and invasive (simultaneous catheterization-echocardiography) methods.

2.2 Overview of Cardiovascular Biophysics Laboratory Research Methodology

All the data presented in the following chapters of this thesis was obtained from the Cardiovascular Biophysics Laboratory database. This is a unique database containing simultaneous cardiac catheterization and echocardiography data. The database is the largest of its kind in the world and has been enrolling subjects for several decades. In total, it contains simultaneous echo-cath data from over 500 subjects. Figure 2.1 summarizes the latest version of our method of data acquisition and analysis.

The subsequent sections in this chapter describe the method used to collect echo-cath data and the semi- automated method of processing this data. The last section of this chapter describes mathematical models used to analyze echocardiographic transmitral images and hemodynamic phase planes obtained from cardiac catheterization data.
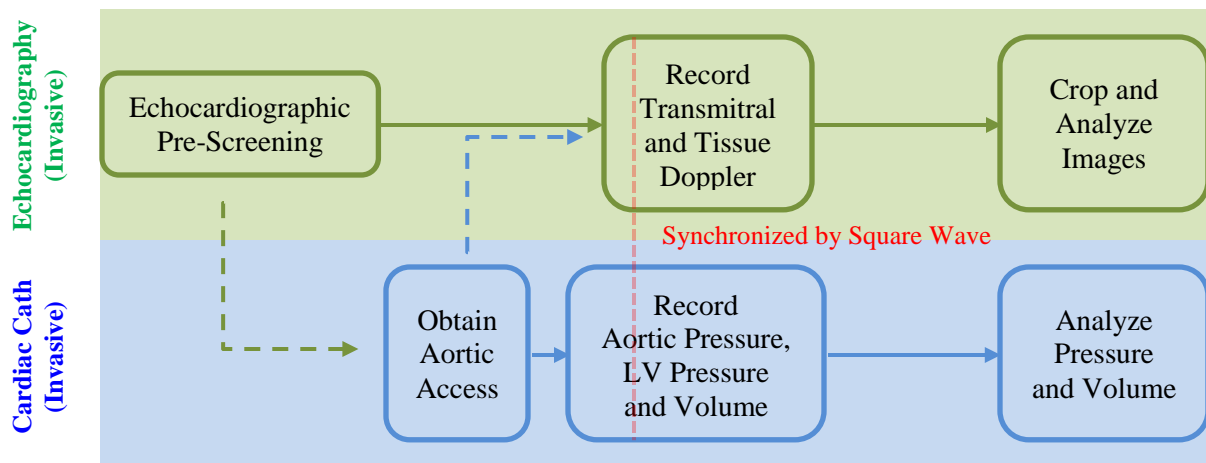
Figure 2.1 General overview of data acquisition and analysis.
See text for details.

2.3 Simultaneous Cardiac Catheterization and Echocardiography

2.3.1 Subject Selection

All subjects in the Cardiovascular Biophysics Laboratory Database had simultaneous echocardiography and cardiac catheterization performed and had been referred by their physicians for elective diagnostic cardiac catheterization to evaluate the possibility of coronary artery disease. The subjects had been recruited to participate in the study. All enrolled subjects were required to meet the following inclusionary criteria: (I) scheduled for elective diagnostic left-heart catheterization, in a fasting, non-sedated state, (II) judged to be clinically stable and (III) willing to participate by giving informed consent in accordance with a study protocol approved by the Washington University Medical Center Human Research Protection Office (HRPO). The database inclusion criteria are: have no pacemaker, absence of any significant valvular abnormalities, absence of wall motion abnormalities or bundle branch block on ECG, and presence of a satisfactory echocardiographic window with clearly identifiable E- and A-waves, except in subjects with AF. The enrolled subject population typically consists of inpatients or same-day catheterization patients encountered in clinical practice. This assures a realistic age, gender, and ethnicity mix characteristic of clinical practice.

2.3.2 Echocardiographic Prescreening

After screening and discussion with Dr. Kovács, subjects have a complete 2D/ echo-Doppler study in accordance with ASE criteria (21) performed prior to arterial access in the

catheterization laboratory. With the patient supine, both short-axis and long-axis views are obtained using a 2.5MHz transducer in a dedicated echo imaging machine (Philips iE33) resident in the catheterization laboratory by our sonographer. Short-axis views are obtained at the level of the mitral and aortic valves in order to visualize both valves. Additional short-axis views are obtained at the mitral leaflet tip and mid-LV in order to estimate LV size. Continuous wave Doppler is used to record aortic outflow and mitral inflow from the apical view for determination of isovolumic relaxation time using a sweep speed of 10 cm/sec. Pulmonary S-and D-waves and transmitral E- and A-waves are recorded in pulsed Doppler mode with sample volumes gated at the pulmonary veins and mitral leaflet tips respectively. For pulsed Doppler imaging, the wall filter is set at 125 Hz or 250 Hz, the baseline is adjusted to take advantage of the full width of the display, and the velocity scale is adjusted to exploit the dynamic range of the output without aliasing. Septal and lateral E'- and A'-waves are recorded in Tissue Doppler mode with sample volumes at the septal and lateral sides of the mitral annulus, respectively. In addition, Color M-Mode imaging is used to obtain diastolic early and late filling interventricular velocity maps.

If the subject has an appropriate echocardiographic window and no aortic valve abnormalities, then the simultaneous high-fidelity catheterization and echocardiography study proceeds. If a poor echo window, bicuspid aortic valve, or significant calcification or stenosis of the aortic valve is observed by echocardiography, then the routine cardiac catheterization study proceeds, but the subject is not enrolled in the simultaneous high-fidelity catheterization and echocardiography portion of the study.

2.3.3   <u>Cardiac Catheterization Procedure</u>

After appropriate sterile skin prep and drape of the patient, local anesthesia (1% xylocaine) is given and percutaneous right or left femoral arterial access is obtained in preparation for the performance of the catheterization by the sponsor, using a valved sheath (6-F, Arrow Inc, Reading, PA). After arterial access and placement of a 64 cm sheath (Arrow Inc, Reading, PA), a 6F micromanometer-tipped pigtail (triple pressure transducer) pressure-volume, conductance catheter (Model 560-1, 560-5, Millar Instruments, Houston, TX) will be directed into the mid-LV in a retrograde fashion across the aortic valve under fluoroscopic control. Prior to insertion, the manometer-tipped catheter is calibrated against "zero" by submersion just below the surface of an NS bath at 37° C, and again after insertion relative to hydrostatic "zero" using the lumen with respect to the mid-thoracic fluid-filled transducer (HP). It is balanced using a transducer control unit (Model TC-510, Millar Instruments, Houston, TX), and pressures are fed to the catheterization laboratory amplifier (Quiton Q-Cath Physiological Recording System) and simultaneously into the input ports of the physiological amplifier of the Doppler imaging system for synchronization (Philips iE33). The LV and AO pressures, LV volume from the conductance catheter, and one ECG channel are also simultaneously recorded on disk in digital format using our multichannel Physiologic Data acquisition system, consisting of a Pentium class computer with 100Mb hard disk, 64Mb RAM and NB-M10-16H digitized board. The sampling rates for up to 8 channels of data are controlled using Leycom Software (Leycom Sigma-5, CardioDynamics, Rjinsburg, The Netherlands). Ventriculography is subsequently performed using a 6F bent, pigtail catheter (Cordis) using 35cc of contrast injected at 11cc/s, and ejection fraction is subsequently determined by planimetry. The image is calibrated for volume using a cm grid placed at the mid-axillary level; the subsequent image analysis of end-systolic and end-diastolic

frames provides a fairly robust measure of end-systolic and end-diastolic volume. The remainder of the catheterization and coronary angiography proceeds in accordance with established clinical practices (27).

2.3.4   <u>Simultaneous Echocardiography Procedure</u>

A schematic representation of the catheterization lab/ data acquisition setup during simultaneous echocardiography-catheterization in cardiac cath lab is shown in Figure 2.2. After completion of a complete 2D-echo Doppler study at the time of procedure initiation, and after the catheter has been advanced into the LV and starts recording pressures and volumes, with the subject supine, a repeat echocardiographic examination is performed. The subjects are imaged using the apical 4 chamber view with the sample volume gated at 1.5 to 5 mm, which is directed between the tips of the mitral valve leaflets and is orthogonal to the MV plane. 30-40 cardiac cycles are then recorded along with the simultaneous LV pressure signal. Continuous wave Doppler is used to record aortic outflow and mitral inflow from the apical view for determination of the IVRT using a sweep speed of 10cm/s. To synchronize the echocardiographic images with pressure waveforms, a fiducial marker in the form of a square wave with at least 1-second long step function with amplitude of 100 mmHg is sent from the catheter transducer box to the pressure signals (distal, middle and proximal pressure channels) in the PC and the echocardiographic imager. In addition, Doppler Tissue Imaging (DTI) of the medial and the lateral mitral annulus is recorded using the DTI method, and 10-15 cardiac cycles are recorded along with the simultaneous LV pressure signal. Images of individual beats are captured in DICOM format from the disk for offline analysis using custom image processing software. The

entire case is also recorded onto VHS tape (Accuson and HP) or burned to DVD (iE33), and the resulting continuous data stream is processed offline. Simultaneous Doppler data and left ventricular pressure and volume via conductance are obtained for a minimum of 40 consecutive beats during quiet respiration.
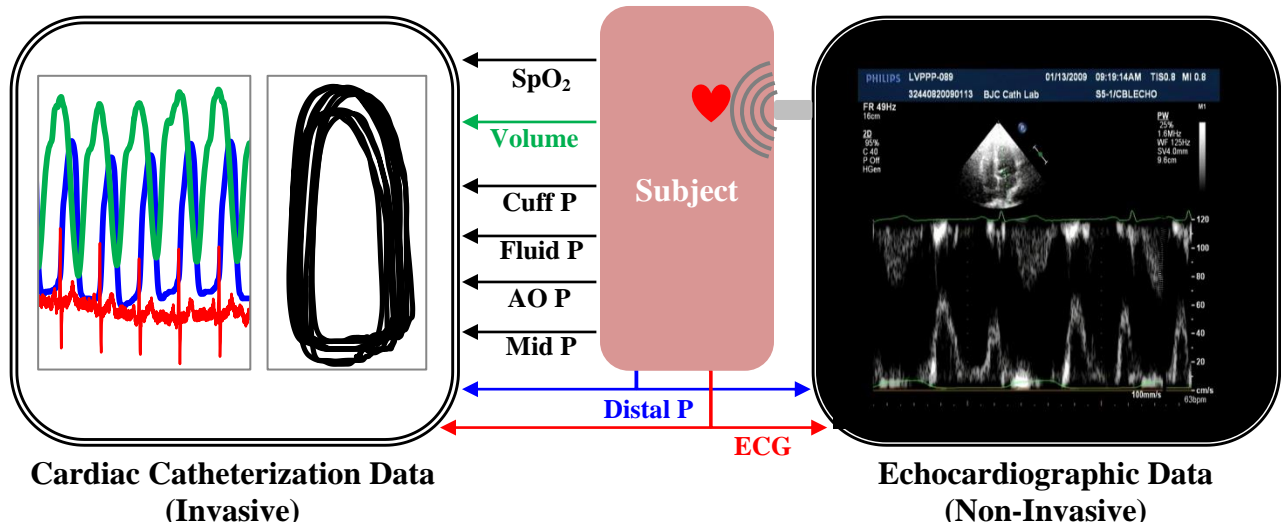
Figure 2.2 Schematic representation of data acquisition setup.

A schematic representation of data acquisition setup in the cardiac catheterization lab for simultaneous catheterization and echocardiography. The customized personal computer (PC) on the left accepts, displays, and stores multiple pressure signals and a conductance volume channel from the catheter. One pressure signal and a split ECG signal are fed to the echocardiographic imager (right) from the PC input for simultaneous display of ECG and pressure on the transmitral velocity display. See text for details.

2.4   Semi-automated Processing of Acquired Data

The hemodynamic data obtained from cardiac catheterization is saved as a compressed ".arj" file. The data is extracted from the compressed format and stored in a tab delimited text file. Echocardiographic data from the prescreening portion is saved on a DVD as DICOM files. Echocardiographic data obtained simultaneously with cardiac catheterization is burned to a DVD and extracted as an .avi file. This section describes the method used to process these data types.

2.4.1   Extracting Pressure-Volume and ECG Data

Square waves are at least 1 second long step functions with an amplitude of 100 mmHg that are introduced into the pressure signals (distal, middle and proximal pressure channels) by the transducer control box for calibration and synchronization purposes. An automated script finds square waves by looking for extended minima in the pressure derivative signal that are flanked by extreme maxima and minima; manual analysis is employed to confirm the start and stop of the automatically discovered square waves. If the square wave amplitudes or absolute values deviate from 0 mmHg and 100 mmHg, then the entire pressure signal is shifted and scaled appropriately.

2.4.2   Processing ECG signal and identifying features

ECG Analysis

The typical hemodynamic signal captured in the catheterization laboratory consists of

simultaneous pressure and ECG signals. To identify cardiac cycles in the hemodynamic data, the simultaneously recorded ECG signal is analyzed. This analysis is done in multiple steps. The first step in data analysis involves the determination of all ECG R-wave peaks. A custom MATLAB code achieves this task by searching for local maxima in the DC filtered ECG signal over successive windows defined by the dominant period (determined by the frequency of the peak in the Fourier power spectrum) in the signal. The other features of the ECG signal—QRS complex, P-wave and the T-wave—were analyzed. The QRST complex is analyzed by applying linear approximations to the upslope and downslope of the R-wave and determining crossover points with the baseline zero voltage level of the DC filtered signal. The first minima preceding and following those crossover points define the Q- and S-waves, respectively. The maximum in the absolute value of the ECG signal between the S-wave and the time at which minimum pressure occurs defines the T-wave peak. Linear approximation of the T-wave upslope and downslope define the start and end of the T-wave, respectively, and the maximum in the absolute value of the ECG signal between the end of the T-wave and the start of the following R-wave defines the P-wave peak. Linear approximation of the upslope and downslope of the P-wave define the approximate start and end of the P-wave. Following automated analysis, manual analysis was performed to adjust any errors due to lack of P-wave or spurious ECG data.

Processing Hemodynamic Data and Analyzing Pressure

The sequence of R-wave peaks which defines successive cardiac cycles is used to analyze pressure data. For each beat the later R-peak defines the beat; for example the 2nd R-peak defines the 1st beat. To avoid errors due to respiratory modulation of the pressure signal, the data is filtered to remove low frequencies (0.15 Hz and below). The maximum and minimum pressures

57

between peak R-waves define the maximum and minimum pressures of the cardiac cycle. To calculate the peak positive dP/dt and peak negative dP/dt, the derivative of pressure is calculated. The same analysis is done on both the LV pressure channels and the aortic pressure channel. The maximum pressure between the later R-wave peak and the minimum pressure defines the LV end-diastolic pressure (LVEDP) of the beat. Usually this is same as the pressure at the R-wave peak, but in cases of 1st degree AV block, left ventricular pressure reaches a maximum, then falls back toward diastatic pressure.

The next step is defining mitral valve opening (MVO) and diastatic pressures. The mitral valve opening pressure is estimated to be the pressure between maximum and minimum pressures which is closest to LVEDP. The diastasis pressure is defined as the pressure at the P-wave peak, when the P-wave is present; otherwise, the LVEDP is used. As an initial guess, the midpoint between the time at the P-wave peak and minimum pressure is assumed to be the start of diastasis. A linear regression of the pressures between the assumed start of diastasis and time of minimum pressure, as well as a linear regression of the pressures between the assumed start of diastasis and the time of P-wave peak, are constructed. The intersection of these linear regressions defines the next guess of the start of diastasis, and this process is repeated until it converges on a single value or a set of repeated values. If the process converges on a loop of values, then the average of those values defines the time at which diastasis starts.

2.4.3 <u>Analysis of the Isovolumic Pressure Decay Contour</u>

Conventional Analysis

The pressure decay during LV isovolumic relaxation has been quantified by different models. The most common parameter for IVR analysis is based on Weiss formulation (26) to define time constant of isovolumic relaxation (τ), which fits the isovolumic pressure contour from peak negative dP/dt to mitral valve opening by an exponential decay model.

The logistic model defines the calculation of the logistic time constant (τ_L), where pressure as a function of time obeys a relationship in which the rate of pressure decline is proportional to the square of the pressure (17). τ_L is extracted from the isovolumic pressure decay contour by applying a Levenberg Marquardt algorithm. This finds the τ_L value that minimizes the error in the pressure phase plane between the measured pressure decay contour and phase plane contour, which is predicted by the following equation and it's time derivative:

$$P(t) = \frac{P_A}{1 + e^{-t/\tau_L}} + P_B \qquad [2.1]$$

where τ_L is the logistic time constant, P_A is a constant, and P_B is the pressure asymptote.

Kinematic Model Based Analysis–Chung Model of Relaxation

In an effort to completely characterize the wide range of physiologically observed IVPD PPP trajectories, a kinematic model was developed in our lab by Chung and Kovács (5). Chung et al. proposed a general model of IVPD governed by the physically intuitive interplay of inertial, stiffness, and relaxation forces, which models the pressure decay during isovolumic relaxation analogous to the motion of a damped simple harmonic oscillator. The equation for this model is given by:

$$\frac{d^2P}{dt^2} + \frac{1}{\mu}\frac{dP}{dt} + E_k(P - P_\infty) = 0 \qquad\qquad [2.2]$$

where μ is a relaxation parameter, E_k is a stiffness parameter, and P_∞ is the pressure asymptote.
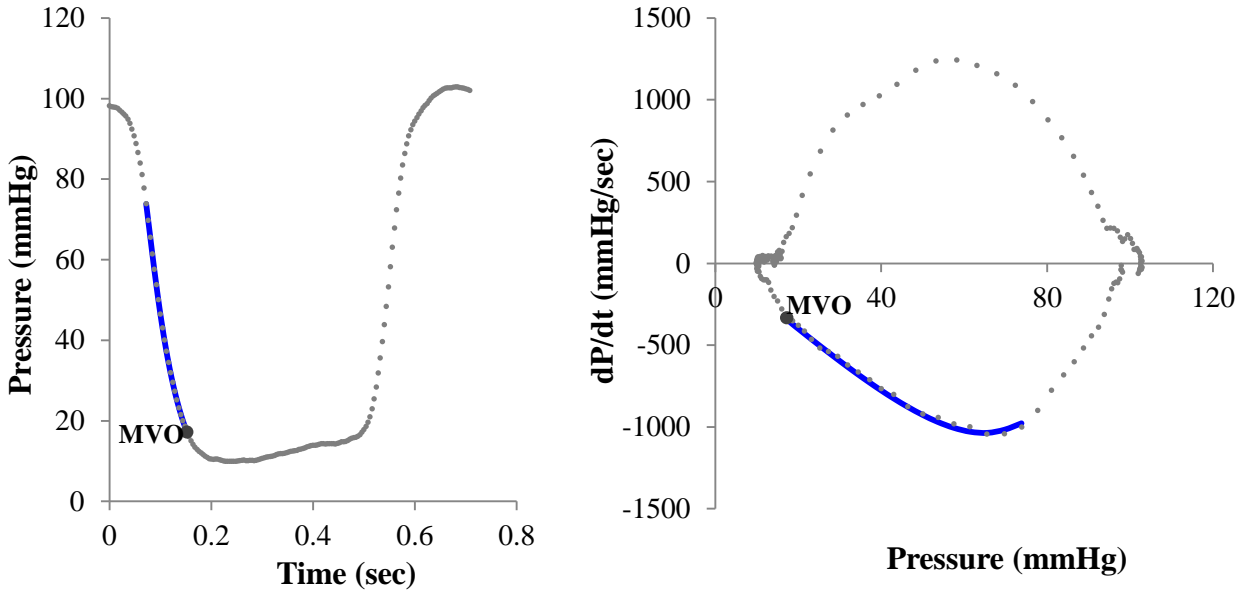
Figure 2.3 Chung model predicted isovolumic pressure decay.

Chung model predicted isovolumic pressure decay up to mitral valve opening (MVO) employing elastic (E_k) and relaxation (μ) parameters. A) Raw data (grey dots) showing pressure vs. time with model fit (solid blue line) superimposed. B) Chung model fit to same data in the pressure phase plane (dP/dt vs. P). Note ability of Chung model to fit curvilinear feature of IVR phase plane segment commencing at pressures greater than that at which negative dP/dt was greatest. See text for details.

The Chung model fits the isovolumic pressure decay contour from before peak negative *dP/dt* till mitral valve opening (Figure 2.3). The Chung model, Equation [2.2], can be solved to yield solutions in two regimes—underdamped and overdamped. When the recoil (E_kP) and relaxation $[(1/\mu)dP/dt]$ terms numerically dominate the inertial term ($d^2P/dt^2 \approx 0$) (24), the solution to Equation [2.2] reduces to the familiar monoexponential solution for IVPD with $\tau = 1/\mu E_k$. As a further benefit of the approach, note that neither the monoexponential (26) nor the logistic parameter-predicted pressure decay (17) can characterize the range of physiologically

encountered IVPD (as it appears in the PPP) and the data before dP/dt_{min}, as shown in Figure 2.3 (5).

2.4.4   <u>Automated Method for Fitting and Parameter Extraction</u>

A custom MATLAB program was written to automatically fit isovolumic pressure decay contour with the kinematic model. Kinematic model parameters (μ, E_k, P_∞) were extracted for each individual beat by applying a Levenberg-Marquardt (LM) algorithm to the pressure and pressure derivative data defined by the extracted isovolumic pressure decays contour. The algorithm requires initial guesses for the kinematic parameters and the $dP(t)/dt$ data over the isovolumic pressure decay contour.

The initial parameters are derived from Equation [2.2]. The start of the fit (t_o) is at the inflection point of dP/dt (i.e. $d^2P/dt^2 = 0$). The Equation [2.2] is evaluated at this time point. It is also evaluated at peak negative dP/dt (where again $d^2P/dt^2 = 0$). Using the two derived expressions, P_∞ can be expressed in terms of pressures and pressure derivatives. By solving Equation [2.2] at $t = t_o$, the expressions for E_k and μ can be evaluated (25).

Beginning with these initial guesses, the Levenberg-Marquardt algorithm minimizes χ^2 by iterating through parameter space, where χ^2 is defined by $\Sigma(\Delta P)/\sigma$, with ΔP defined by the error between model predicted and measured $dP(t)/dt$ along the isovolumic pressure decay contour, and σ defined as the error in measured $dP(t)/dt$. Iteration ends when subsequent χ^2 values change by less than a predetermined threshold value. Upon completion, the root mean square error (RMSE) between model-predicted $dP(t)/dt$ and measured $dP(t)/dt$ is calculated using the LM-determined best fit kinematic parameters.

2.4.5 <u>Extracting Echocardiographic Data</u>

The next step is reading the DICOM images from prescreening echocardiographic data. A custom MATLAB script was written to read the DICOM images, display them, and save the selected images as bitmap files. For each subject, images from different echo views were saved. Continuous transmitral flow data is captured synchronously with the Millar pressure data in the form of a video file. The echo video was synchronized with the hemodynamic data by matching the time point of the square wave start on the video with the time point of square wave on the pressure channel. A time offset is introduced into the video to align the transmitral contours to the pressure signal. With this offset in place, the R-wave peak times are used to determine the corresponding frame number in the video file where the R-wave for that beat occurs. Typically, the frame that comes several frames beyond the R-wave is extracted to ensure no loss of A-wave signal. These frames are extracted programmatically from the video file based on the previously determined R-wave peaks. Using a custom MATLAB program, the user can crop and save selected beats and also do conventional echocardiographic analysis (Figure 2.4).

2.4.6 <u>Transmitral and Tissue Doppler Image Analysis</u>

A custom MATLAB script is used to determine the conventional features of transmitral flow and tissue Doppler. It is also used to crop Doppler E-and A-waves (or E'- and A'-waves) and make it ready for PDF analysis. The details of methods are available at *Journal of Visualized Experiments* (20). Briefly, the program reads-in echo images of a particular view as folders containing bitmap images (Figure 2.4). The interface allows the user to mark the time sampling rate (TSR) and the velocity sampling rate (VSR) for each image as shown on the lower left of

Figure 2.4. TSR and VSR specify the number of pixels in the image which quantify 1s and 1 m/s respectively.

Load and select
echo data

Doppler
echo frame

Set time and
velocity sample rate

Set E- and A-waves
to be analyzed

Physiological
state
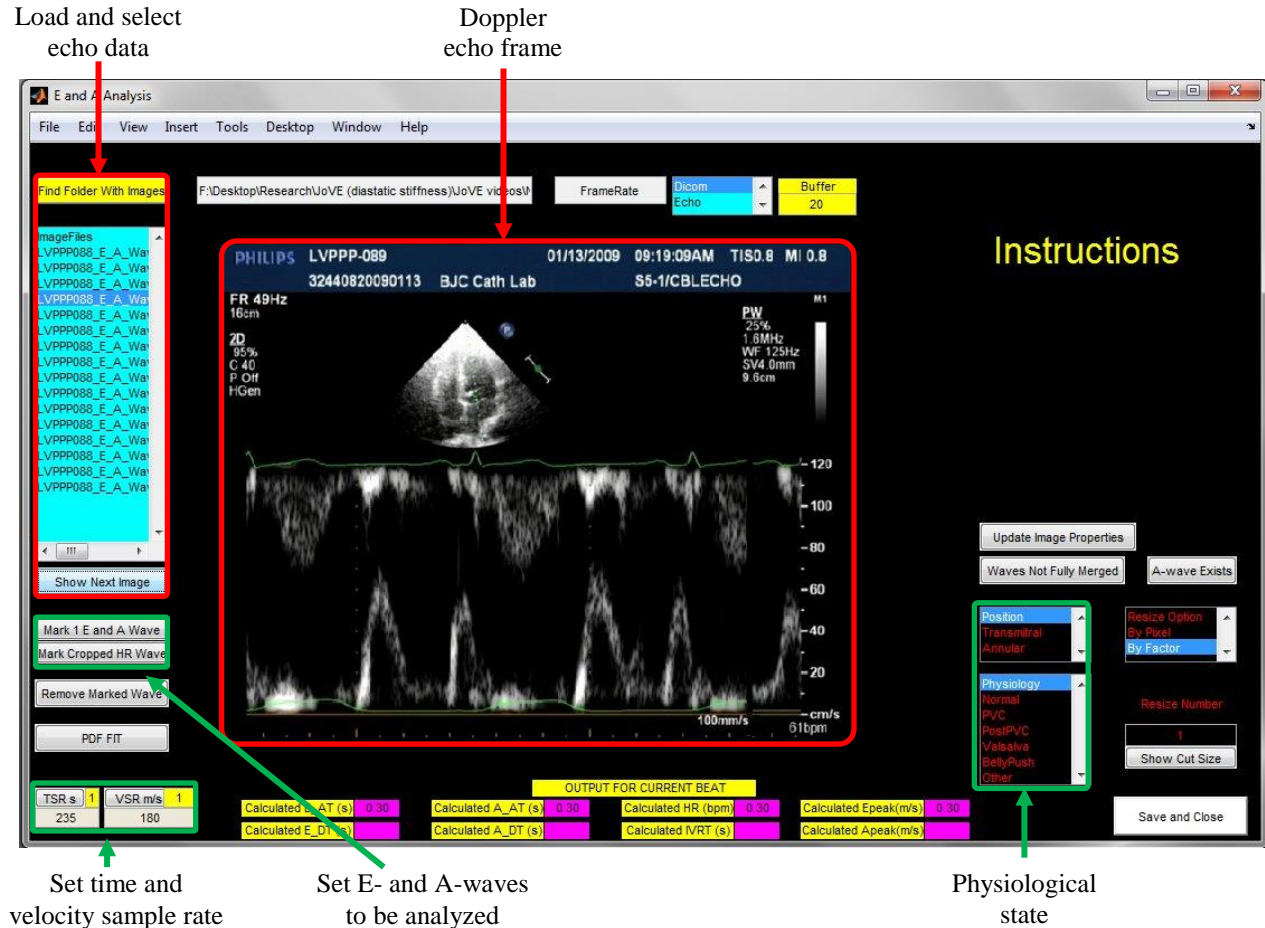
Figure 2.4 Screenshot of a custom MATLAB interface.

A screenshot of a custom MATLAB interface for efficient conventional clinical analysis of Doppler echocardiography transmitral velocity contours. The user must first set the scale of the image by determining the time and velocity sample rates (TSR and VSR). Then, to analyze the image the R-R interval must be determined and the E-wave and A-wave start, peak, and end points must be selected.

The next step is to mark and crop a single E- and A-wave. For this, first the R-R interval enclosing the E- and A-wave is marked manually (blue vertical lines in Figure 2.5). Then, the E-

wave peak is marked, and a straight line connecting the peak to the start and end of the E-wave is used to calculate the acceleration time, deceleration time and duration of the E-wave. The A-wave is marked using a similar procedure. The cropped images are saved as bitmap files along with the extracted parameters, such as peak velocities and durations. These cropped images are used for quantification of kinematic model parameters based on the parametrized diastolic filling (PDF) formalism, which is described in subsequent sections. A similar MATLAB-based user interface is used to read in tissue Doppler images and mark the E'- and A'-waves.
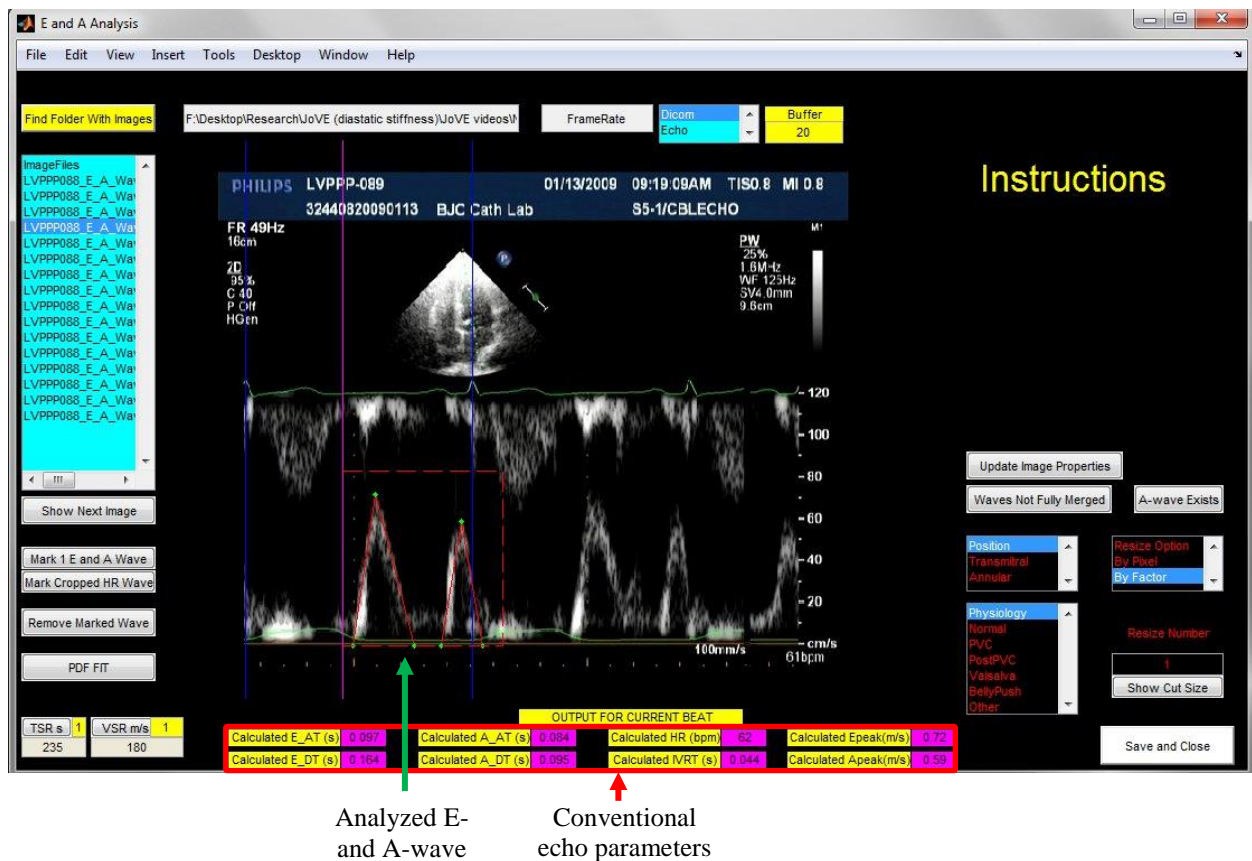
Figure 2.5 Screenshot of a custom MATLAB interface with conventional echo parameters.

A screenshot of a custom MATLAB interface for efficient conventional clinical analysis of Doppler echocardiography transmitral velocity contours. It shows the selected R-R interval (blue lines) and the analyzed E- and A-waves (red dashed lines). The resulting conventional transmitral contour parameters are saved for future use.

64

2.4.7 <u>Kinematic Modeling of Diastolic Filling: Parametrized Diastolic Filling (PDF) Formalism</u>

In an effort to better understand the physiology of normal heart function and its progression to dysfunction, one of the goals of our laboratory has been to elucidate and characterize fundamental properties of normal cardiac function in a dynamic and physical sense. An important advancement in understanding diastolic function was made by Kovács et al. in 1987 (9) based on the perspective that, during diastole, the heart acts as a suction pump. As previously mentioned, LV fills during early filling by acting as a mechanical suction pump that increases LV volume while decreasing the pressure (dP/dV<0 after MVO). This suction pump behavior of the ventricle is powered by the release of potential energy stored in the myocardium (titin, extracellular matrix, etc.) from the previous systole. The atrioventricular pressure gradient across the mitral valve that is established by the recoil of the wall generates ventricular suction which aspirates blood from LA to LV. Kovács et al. (9) proposed that the ventricle at the onset of diastolic filling is essentially analogous to a damped spring released from a loaded (compressed, in this case) state, and transmitral flow (Doppler E-wave) can be characterized by damped simple harmonic oscillator (SHO) motion (Figure 2.6) in terms of elastic, inertial, and damping forces. The equation of motion for a damped SHO is:

$$m\frac{d^2x}{dt^2} + c\frac{dx}{dt} + kx = 0 \qquad [2.3]$$

The first term denotes the inertial force of the oscillator, the second term denotes the damping force (viscous loss), and the third term denotes the elastic force. In Equation [2.3], x is the displacement of the oscillator, and dx/dt is the velocity of the oscillator. The parameters c (g·cm/s) and k (g·cm/s^2) denote the damping constant and spring constant of the system,

respectively. These are lumped parameters in the sense that they incorporate all physiologic contributions to viscous losses and stiffness, respectively. This equation is based on an unforced damped oscillator with an initial displacement x_o. The parameter x_o (cm) accounts for load and represents the initial displacement of the spring prior to motion. It also corresponds to the elastic strain stored in the myocardium and surrounding structures available at mitral valve opening that facilitate mechanical recoil (22). Corresponding to no transmitral flow prior to valve opening, the initial velocity (dx/dt) of the system is zero. The inertial term m (g) is normalized to 1 to enable the computation of c and k per unit mass. An illustration of the model is shown in Figure 2.6.

Oscillator	Solutions	Transmitral Velocity E-wave
$\ddot{x} + c\dot{x} + kx = 0$	**Under-damped** $$v(t) = \frac{kx_o}{\omega} e^{-\frac{ct}{2}} \sin(\omega t)$$ $$\omega = \frac{\sqrt{4k - c^2}}{2}$$	Under-damped $v(t)$
Initial Conditions $x(0) = x_o$ $v(0) = 0$	**Over-damped** $$v(t) = \frac{kx_o}{\beta} e^{-\frac{ct}{2}} \cdot \sinh(\beta t)$$ $$\beta = \frac{\sqrt{c^2 - 4k}}{2}$$	Over-damped $v(t)$ t
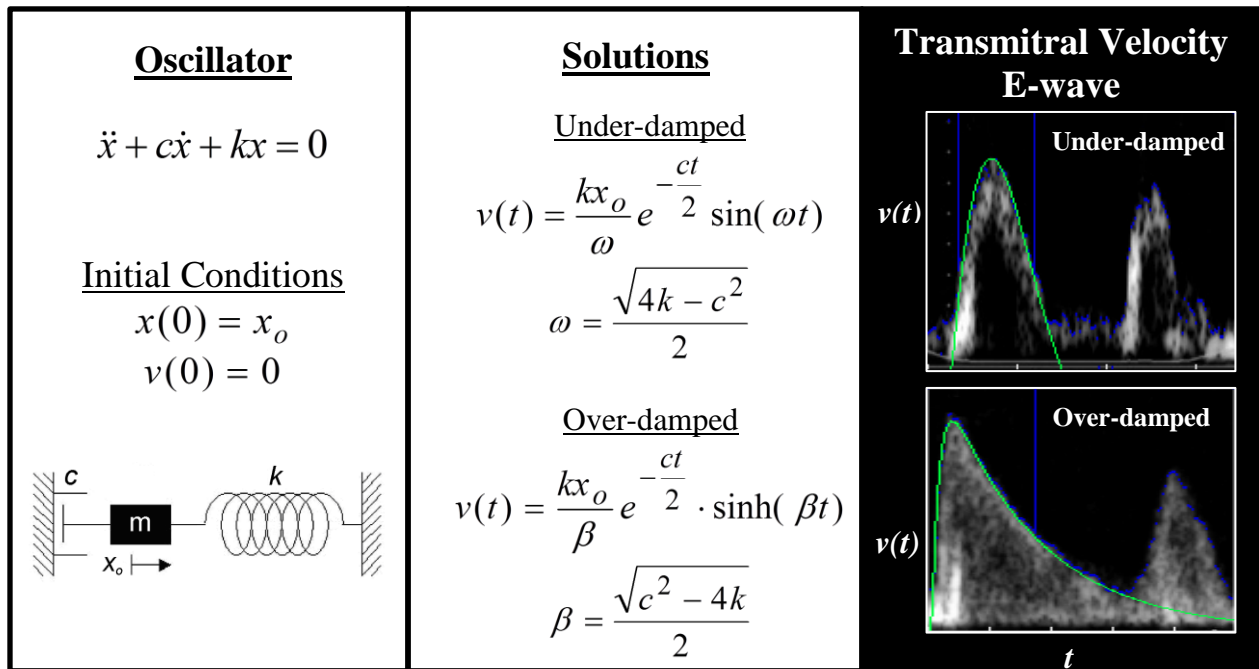
Figure 2.6 PDF model.

Left: Schematic of a damped simple harmonic oscillator, the model upon which the PDF formalism is based. The model consists of a mass m which is released from an initial (compressed) displacement, x_o. The spring constant k represents ventricular stiffness, while the damping constant c quantifies ventricular relaxation/viscoelasticity. Middle: Under-damped and over-damped solutions of damped simple harmonic oscillator with the initial conditions: x(t=0) = x_o (spring is compressed at mitral valve opening) and v(t=0)=0 (initial flow velocity is zero prior to mitral valve opening). Right: The PDF model accurately predicts clinically recorded early rapid filling transmitral flow velocity contours. Both underdamped and overdamped kinematic regimes are observed clinically. See text for details.

Since Equation [2.3] is linear, it is invertible and can be fit to the Doppler E-wave contour using a non-linear least-squares method to yield unique best-fit stiffness and damping parameters (Figure 2.7) (8); in another words for each beat, one can solve the "inverse" problem using a clinical E-wave contour as input and the mathematically unique model parameters (x_o, c and k) as the best-fit determined output.

The solution to the PDF formalism for a particular E-wave, expressed as transmitral flow velocity as a function of time, depends upon the relative values of c and k. The solutions for underdamped, overdamped, and critically damped motion, given the initial conditions of $x(t=0) = x_o$ (spring is compressed at mitral valve opening) and $v(t=0)=dx/dt(t=0) = 0$ (initial flow velocity is zero prior to mitral valve opening) are:

$$v(t) = \frac{kx_o}{\omega} e^{-\alpha t} \sin(\omega t) \qquad [2.4a]$$

for underdamped motion ($c^2 < 4k$),

$$v(t) = \frac{kx_o}{\beta} e^{-\alpha t} \sinh(\beta t) \qquad [2.4b]$$

for overdamped motion ($c^2 > 4k$), and

$$v(t) = kx_o te^{-\alpha t} \qquad [2.4c]$$

for critically damped motion ($c^2 = 4k$).

In these equations, $\omega = \sqrt{4k - c^2}$, $\beta = \sqrt{c^2 - 4k}$, and $\alpha = c/2$.
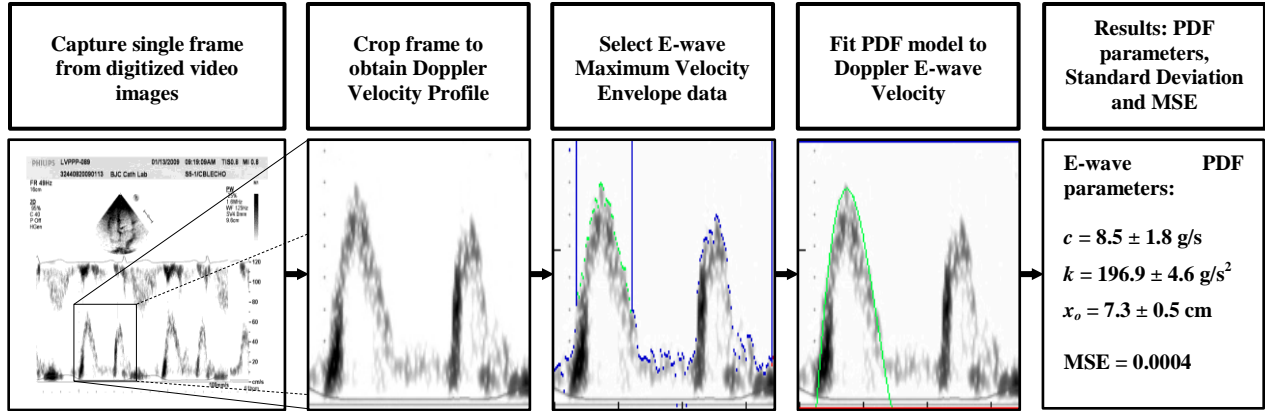
Figure 2.7 Model-based image processing method used to fit the PDF formalism to E- waves. After the E-wave is cropped, the maximum velocity envelope is identified. The best-fit (lumped) parameters c, k, and x_o are generated along with the mean-squared error of the fit (MSE). See text for details.

The PDF formalism predicts that all E-wave shapes obey the SHO equation of motion, and different sets of parameter values account for the different E-wave shapes. This kinematic approach has inherent advantages because of its predictive rather than accommodative nature (13). The PDF formalism has been validated by fitting the E-waves using a model-based imaging processing (MBIP) method, detailed in Figure 2.7. The PDF formalism has not only been shown to closely fit a variety of E-wave contours, but also to generate three unique best-fit parameters with conceptually and experimentally well-established physiologic analogs (7, 11, 12, 15) for each E-wave that allow the estimation of LV stiffness, damping/relaxation, and stored elastic strain on a beat-by-beat basis. In this manner, global LV diastolic function can be characterized accurately in physiologically relevant terms.

Thus E'-wave velocity is characterized by three SHO parameters- k', c', and x_o'. By analogy, the differential equation is:

$$\frac{d^2x}{dt^2} + c'\frac{dx}{dt} + k'x = 0 \qquad [2.5]$$

68

Using analogous initial conditions (initial displacement is x_o' and initial velocity is 0)

gives two solutions—the underdamped and overdamped—which are given below:

$$v'(t) = \frac{k' x_o'}{\omega'} e^{-\alpha' t} \sin(\omega' t) \qquad\qquad [2.6a]$$

for underdamped motion ($c'^2 < 4k'$),

$$v'(t) = \frac{k' x_o'}{\beta'} e^{-\alpha' t} \sinh(\beta' t) \qquad\qquad [2.6b]$$

for overdamped motion ($c'^2 > 4k'$).

In these equations, $\omega' = \sqrt{4k' - c'^2}$, $\beta' = \sqrt{c'^2 - 4k'}$, and $\alpha' = c'/2$.

2.4.8 **Automated Method for PDF Analysis**

The automated fitting of the Doppler E- and A-waves and tissue Doppler E'- and A'-waves is done using a custom LabView program. The cropped images from Section 2.5.6 are loaded onto the program as shown in Figure 2.8. After the E-wave is cropped from original transmitral Doppler recordings, the maximum velocity envelope is traced and fit by the PDF velocity equations (Equation [2.4a], [2.4b], or [2.4c]). In brief, the time points at the beginning and end of the E-wave and the A-wave are selected. These time points are selected so that only the clean (noise free) portion of the flow profile is selected. The user also sets the threshold value so that the selected pixels approximate the transmitral flow profile. The user-selected MVE points are the input to the computer program that automatically fits the PDF model solution for velocity as a function of time using a Levenberg-Marquardt (iterative) algorithm.

69
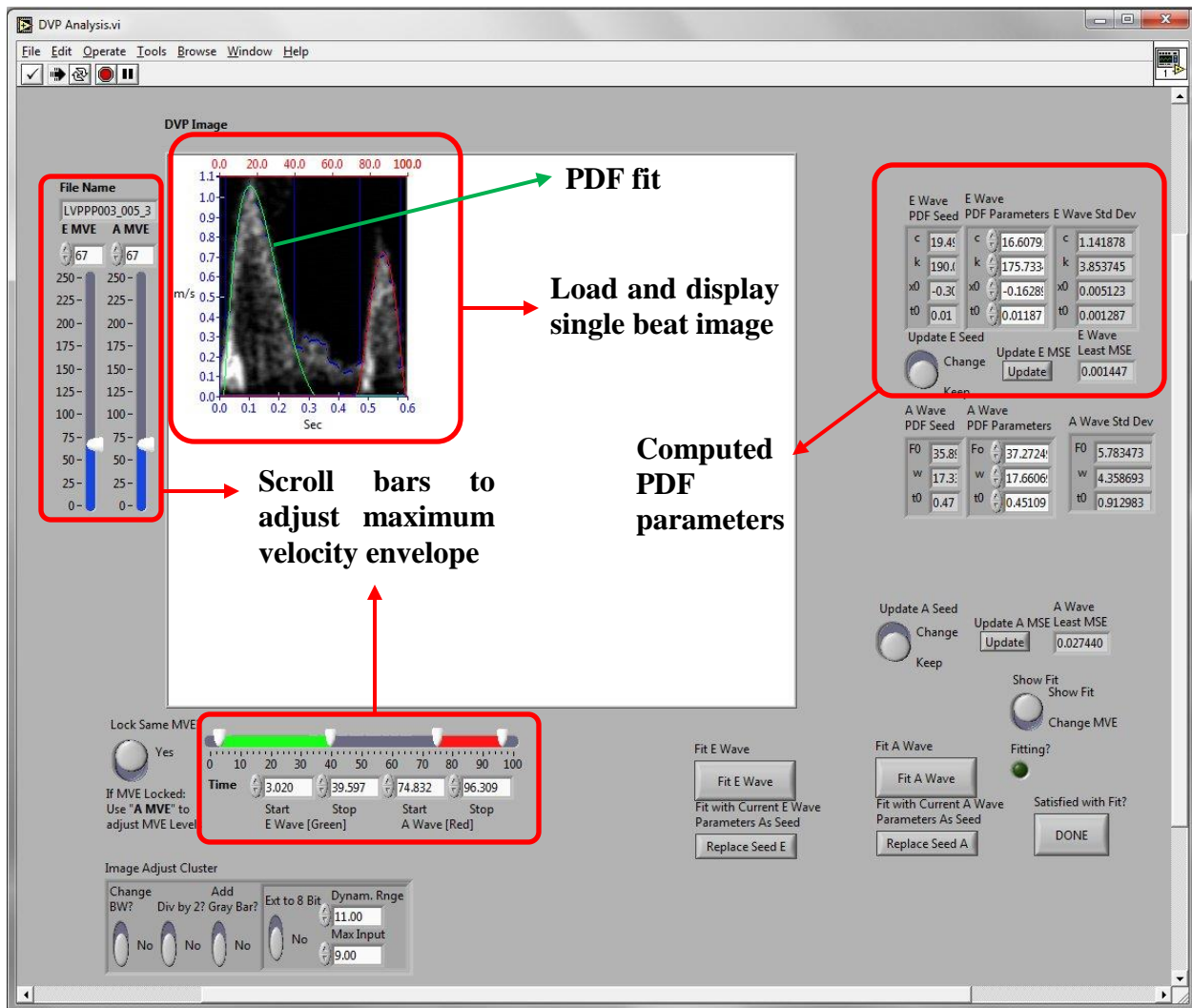
Figure 2.8 A screenshot of a LabView interface for PDF model based image processing.
First the user selects the maximum velocity envelope (MVE) and the start and end of the E-wave. A Levenberg-Marquardt algorithm iterates over parameter space until the mean square error (MSE) between model fit and user defined input data is minimized.

The fit yields a set of mathematically unique E-wave model parameters (x_o, c, and k) together with a goodness of fit measurement (MSE) such that the mean square error between the clinical (input) data (MVE) and the PDF model predicted contour is minimized.

Since the model is linear, a unique set of parameters is obtained for each Doppler E-wave derived MVE used as input. Thus numerically unique k, c and x_o values are generated for each E-wave and k', c' and x_o' for each E'-wave. In the event that the fit is obviously suboptimal when superimposed on the E-wave (or E'-wave) image (i.e. the algorithm attempted to fit noise included in the MVE) the MVE is modified using more/less points, thereby modifying the model predicted contour with consequent modification of PDF parameters to achieve a better fit.

The initial displacement of the oscillator x_o (cm) is linearly related to the E-wave VTI (i.e. related to volumetric preload) (10), the spring constant of the oscillator k (g/s^2) is linearly related to the chamber stiffness (dP/dV) (14), while the oscillator's damping constant or chamber viscoelasticity/relaxation index c (g/s) characterizes the resistance (relaxation/viscosity) and energy loss of the filling process (7, 10). It has been shown that the PDF formalism can successfully fit all the E-waves encountered in clinical practice.

The set of discoveries made using this simple harmonic oscillation paradigm includes: the relationship between isovolumic relaxation feature and early filling E-wave feature; the effect of HR on E- and A-wave characteristics; the determination of the onset of relaxation; physical meaning of the third and fourth heart sound; physiologic significance of the mitral annular oscillation and its characterization; the development of a load independent index of diastolic function, etc. (3, 4, 6, 16, 18, 22-24). Using the PDF parameters, several other kinematic indexes can be derived. The term kx_o is equivalent to the maximum force in the system prior to oscillation. This has been validated as an analog index of the peak pressure gradient across the mitral valve during early filling (1). Parameter $1/2kx_o^2$ is the initial potential energy of the oscillator (19) as discussed in details in Chapter 3. As previously discussed, all conventional diastolic function parameters depend upon load. Using the PDF paradigm, the load independent

index of diastolic function problem has been formulated and solved. In the face of load change, this index remains constant (2, 24). The value of this index differentiates normal subjects from subjects with diastolic dysfunction (24).

In summary, with the kinematic PDF paradigm, filling related diastolic function can be characterized in a physical, causal, and mathematically precise way.

2.5 References

1.   **Bauman L, Chung CS, Karamanoglu M, and Kovács SJ**. The peak atrioventricular pressure gradient to transmitral flow relation: kinematic model prediction with in vivo validation. *J Am Soc Echocardiogr* 17: 839-844, 2004.

2.   **Boskovski MT, Shmuylovich L, and Kovács SJ**. Transmitral flow velocity-contour variation after premature ventricular contractions: a novel test of the load-independent index of diastolic filling. *Ultrasound Med Biol* 34: 1901-1908, 2008.

3.   **Chung CS, Ajo DM, and Kovács SJ**. Isovolumic pressure-to-early rapid filling decay rate relation: model-based derivation and validation via simultaneous catheterization echocardiography. *J Appl Physiol (1985)* 100: 528-534, 2006.

4.   **Chung CS, and Kovács SJ**. Consequences of increasing heart rate on deceleration time, the velocity-time integral, and E/A. *Am J Cardiol* 97: 130-136, 2006.

5.   **Chung CS, and Kovács SJ**. Physical determinants of left ventricular isovolumic pressure decline: model prediction with in vivo validation. *Am J Physiol Heart Circ Physiol* 294: H1589-1596, 2008.

6.   **Chung CS, and Kovács SJ**. Pressure phase-plane based determination of the onset of left ventricular relaxation. *Cardiovasc Eng* 7: 162-171, 2007.

7.   **Dent CL, Bowman AW, Scott MJ, Allen JS, Lisauskas JB, Janif M, Wickline SA, and Kovács SJ**. Echocardiographic characterization of fundamental mechanisms of abnormal diastolic filling in diabetic rats with a parameterized diastolic filling formalism. *J Am Soc Echocardiogr* 14: 1166-1172, 2001.

8.   **Hall AF, and Kovács SJ**. Automated method for characterization of diastolic transmitral Doppler velocity contours: early rapid filling. *Ultrasound Med Biol* 20: 107-116, 1994.

9.   **Kovács SJ, Barzilai B, and Pérez JE**. Evaluation of diastolic function with Doppler echocardiography: the PDF formalism. *Am J Physiol* 252: H178-187, 1987.

10.   **Kovács SJ, Meisner JS, and Yellin EL**. Modeling of diastole. *Cardiol Clin* 18: 459-487, 2000.

11.   **Kovács SJ, Rosado J, Manson McGuire AL, and Hall AF**. Can trasmitral Doppler E-waves differentiate hypertensive hearts from normal? *Hypertension* 30: 788-795, 1997.

12.   **Kovács SJ, Setser R, and Hall AF**. Left ventricular chamber stiffness from model-based image processing of transmitral Doppler E-waves. *Coron Artery Dis* 8: 179-187, 1997.

13.   **Lipton P**. Testing hypotheses: prediction and prejudice. *Science* 307: 219-221, 2005.

14.   **Lisauskas J, Singh J, Courtois M, and Kovács SJ**. The relation of the peak Doppler E-wave to peak mitral annulus velocity ratio to diastolic function. *Ultrasound Med Biol* 27: 499-507, 2001.

15.   **Lisauskas JB, Singh J, Bowman AW, and Kovács SJ**. Chamber properties from transmitral flow: prediction of average and passive left ventricular diastolic stiffness. *J Appl Physiol (1985)* 91: 154-162, 2001.

16.   **Manson AL, Nudelman SP, Hagley MT, Hall AF, and Kovács SJ**. Relationship of the third heart sound to transmitral flow velocity deceleration. *Circulation* 92: 388-394, 1995.

17.   **Matsubara H, Takaki M, Yasuhara S, Araki J, and Suga H**. Logistic time constant of isovolumic relaxation pressure-time curve in the canine left ventricle. Better alternative to exponential time constant. *Circulation* 92: 2318-2326, 1995.

18.   **McGuire AM, Hagley MT, Hall AF, and Kovács SJ**. Relationship of the fourth heart sound to atrial systolic transmitral flow deceleration. *Am J Physiol* 272: H1527-1536, 1997.

19.   **Mossahebi S, Shmuylovich L, and Kovács SJ**. The thermodynamics of diastole: kinematic modeling-based derivation of the P-V loop to transmitral flow energy relation with in vivo validation. *Am J Physiol Heart Circ Physiol* 300: H514-521, 2011.

20.   **Mossahebi S, Zhu S, Chen H, Shmuylovich L, Ghosh E, and Kovács SJ**. Quantification of global diastolic function by kinematic modeling-based analysis of transmitral flow via the Parametrized Diastolic Filling formalism. *J Vis Exp (In Press)* 2014.

21.   **Nagueh SF, Appleton CP, Gillebert TC, Marino PN, Oh JK, Smiseth OA, Waggoner AD, Flachskampf FA, Pellikka PA, and Evangelista A**. Recommendations for the evaluation of left ventricular diastolic function by echocardiography. *J Am Soc Echocardiogr* 22: 107-133, 2009.

22.   **Riordan MM, and Kovács SJ**. Absence of diastolic mitral annular oscillations is a marker for relaxation-related diastolic dysfunction. *Am J Physiol Heart Circ Physiol* 292: H2952-2958, 2007.

23.   **Riordan MM, and Kovács SJ**. Stiffness- and relaxation-based quantitation of radial left ventricular oscillations: elucidation of regional diastolic function mechanisms. *J Appl Physiol (1985)* 102: 1862-1870, 2007.

24.   **Shmuylovich L, and Kovács SJ**. Load-independent index of diastolic filling: model-based derivation with in vivo validation in control and diastolic dysfunction subjects. *J Appl Physiol (1985)* 101: 92-101, 2006.

25.   **Shmuylovich L, and Kovács SJ**. Stiffness and relaxation components of the exponential and logistic time constants may be used to derive a load-independent index of isovolumic pressure decay. *Am J Physiol Heart Circ Physiol* 295: H2551-2559, 2008.

26.   **Weiss JL, Frederiksen JW, and Weisfeldt ML**. Hemodynamic determinants of the time-course of fall in canine left ventricular pressure. *J Clin Invest* 58: 751-760, 1976.

27.   **Yang SS, Bentivoglio L, Maranhao V, and Goldberg H**. *From Cardiac Catheterization Data to Hemodynamic Parameter* Philadelphia: F. A. Davis Company, 1988.

Chapter 3: Thermodynamics of Diastole

3.1   Abstract

Pressure-volume (P-V) loop based analysis facilitates thermodynamic assessment of LV function in terms of work and energy. Typically these quantities are calculated for a cardiac cycle using the entire P-V loop, though thermodynamic analysis may be applied to a selected phase of the cardiac cycle, specifically, diastole. Diastolic function (DF) is routinely quantified by analysis of transmitral Doppler E-wave contours. The first law of thermodynamics requires that energy $\mathcal{E}$ computed from the Doppler E-wave ($\mathcal{E}_{\text{E-wave}}$) and the same portion of the P-V loop ($\mathcal{E}_{\text{PV-E-wave}}$) be equivalent. These energies have not been previously derived nor has their predicted equivalence been experimentally validated. To test the hypothesis that $\mathcal{E}_{\text{PV-E-wave}}$ and $\mathcal{E}_{\text{E-wave}}$ are equivalent we employed a validated kinematic model of filling to derive $\mathcal{E}_{\text{E-wave}}$ in terms of chamber stiffness (k), relaxation/viscoelasticity (c) and load (x_o). For validation, simultaneous (conductance catheter) P-V and echocadiographic data from 12 subjects (205 total cardiac cycles) having a range of DF were analyzed. For each E-wave, $\mathcal{E}_{\text{E-wave}}$ was compared to $\mathcal{E}_{\text{PV-E-wave}}$ calculated from simultaneous P-V data. Linear regression yielded:

$\mathcal{E}_{\text{PV-E-wave}} = \alpha \mathcal{E}_{\text{E-wave}} + b$ (R^2=0.67), where $\alpha = 0.95$, and $b = 6E\text{ -}05$.

We conclude that E-wave derived energy for suction initiated, early rapid filling $\mathcal{E}_{\text{E-wave}}$, quantitated via kinematic modeling is equivalent to invasive, P-V defined filling energy. Hence, the thermodynamics of diastole via $\mathcal{E}_{\text{E-wave}}$ generates a novel, mechanism-based index of DF suitable for in-vivo phenotypic characterization.

3.2   Introduction

Diastolic dysfunction (DD) is predictor of, and a precursor to, diastolic heart failure (DHF), or heart failure with normal ejection fraction (HFNEF), a growing clinical syndrome that has reached epidemic proportions (17, 24, 41). Critical to diagnosis and management of DHF is quantitative diastolic function (DF) assessment. Although left ventricular (LV) hemodynamics constitutes the gold standard for characterizing DF, echocardiography remains the preferred method clinically. Acknowledged limitations of current echo-derived clinical DF indexes justify the continued quest for novel, physiologic, mechanism-based rather than merely echocardiographic waveform phenomenology-based, DF indexes that correlate with dysfunction.

In previous work we have developed and validated novel, mechanism-based indexes of DF, via a kinematic modeling approach, called the parameterized diastolic filling (PDF) formalism (13, 19, 20). The PDF formalism models the kinematics of suction initiated filling as the recoil, from rest, of an equivalent damped oscillator. Model predicted velocity and clinical E-wave contours have shown superb agreement. Using any clinically recorded E-wave as input and suitable mathematical methods, unique chamber stiffness, viscoelasticity/relaxation and load parameters are generated as output, thereby solving the 'inverse problem of diastole'(13). The three PDF parameters (k, c, x_o) can be used to generate indexes with rigorous physiologic analogues such as peak instantaneous pressure gradient (kx_o) among others (1).

Although previous work has shown that subjects with DD may have stiffer chambers (29) or altered values for chamber viscoelasticity/relaxation (29) relative to controls, the physiology of diastole, and early rapid filling in particular, has not been fully elucidated in thermodynamic terms. Indeed, while both systolic and diastolic energies may be calculated from P-V loops, it is

not known whether P-V loop derived measures of energy have a direct non-invasive E-wave derived analogue. Thus in this work we derive an E-wave based expression for the energy associated with early, rapid filling, and hypothesize that in accordance with the first law of thermodynamics, the energy of filling computed from Doppler echocardiography (a relative measure) should be linearly related to energy calculated from simultaneously acquired pressure-volume data (an absolute measure).

3.3   Methods

3.3.1 <u>Subject Selection</u>

Datasets from twelve patients (mean age 64, 8 men) were selected from our existing cardiovascular laboratory database of simultaneous echocardiography-high fidelity hemodynamic (Millar conductance catheter) recordings (6, 22). Subjects underwent elective cardiac catheterization to determine presence of coronary artery disease at the request of their referring physicians. The data selection criteria for the study included a broad range of LVEDP representative of a patient population encountered clinically, normal left ventricular ejection fraction (LVEF > 50%), normal sinus rhythm, clearly discernible E-waves followed by a diastatic interval, and normal valvular function. Prior to data acquisition, subjects provided signed, IRB approved informed consent for participation in accordance with Washington University Human Research Protection Office (HRPO) approved criteria. The method of simultaneous echocardiographic transmitral flow and pressure-volume data recording is well established and has been previously detailed (3, 21, 23). Among the 12 datasets, 5 had end-diastolic pressure (LVEDP) less than 15 mm Hg, 4 had 15 mm Hg < LVEDP < 20 mm Hg and 3 had LVEDP >20 mm Hg. A total of 205 cardiac cycles of simultaneous echocardiographic-high fidelity hemodynamic (conductance catheter) data was analyzed. The clinical descriptors of the 12 subjects and their hemodynamic and echocardiographic indexes are shown in Table 3.1.

Table 3.1 Clinical descriptors, hemodynamic and echocardiographic indexes of subjects.

Clinical descriptors of 12 subjects including hemodynamic and echocardiographic indexes.

N	12
Age (y)	64 ± 13
Gender (male/female)	8 / 4
Heart Rate (bpm)	62 ± 8
Ejection Fraction (LVEF) (%) [*]	75 ± 12
LVEDP (mmHg)	18 ± 6
LVEDV (ml)	145 ± 35
$P_{Diastasis}$ (mmHg)	15 ± 5
E/A	2.2 ± 0.7
PDF parameter x_o (cm)	9.3 ± 4.6
PDF parameter k ($1/s^2$)	211 ± 84
PDF parameter c (1/s)	17.3 ± 12

LVEF=left ventricular ejection fraction; LVEDP=left ventricular end-diastolic pressure; LVEDV=left ventricular end-diastolic volume; E/A, ratio of E_{peak} and A_{peak}.

* LVEF determined by ventriculography

Data are presented as mean ± standard deviation.

3.3.2   <u>Data Acquisition</u>

The simultaneous high-fidelity, P-V and echocardiographic transmitral flow data recording method has been previously detailed (3, 21, 23). Briefly, LV pressure and volume were acquired using micromanometric conductance catheter (SPC-560, SPC-562, or SSD-1043, Millar Instruments, Houston, TX) at the commencement of elective cardiac catheterization, prior to the administration of iodinated contrast agents. Pressure signals from the transducers were fed into a clinical amplifier system (Quinton Diagnostics, Bothell, WA, and General Electric). Conductance catheterization signals were fed into a custom personal computer via a standard interface (Sigma-5, CD Leycom). Conductance volume data were recorded in five channels. Data from low-noise channels providing physiological readings were selected, suitably averaged and calibrated using absolute volumes obtained by calibrated ventriculography during the same procedure.

Prior to arterial access, in the catheterization laboratory, a full 2-D echo-Doppler study is performed by an ASE certified sonographer in accordance with ASE criteria (27). After appropriate sterile skin prep and drape, local anesthesia (1% xylocaine) is given and percutaneous right or left femoral arterial access is obtained in preparation for catheterization and angiography, using a valved sheath (6-F, Arrow Inc, Reading, PA). After arterial access and placement of a 64 cm sheath (Arrow Inc, Reading, PA), a 6F micromanometer-tipped pigtail (triple pressure transducer) pressure-volume, conductance catheter (Model 560-1, 560-5, Millar Instruments, Houston, TX) is directed into the mid-LV in a retrograde fashion across the aortic valve under fluoroscopic control. Prior to insertion, the manometer-tipped catheter is calibrated against "zero" by submersion just below the surface of NS bath at 37° C, an again after insertion relative to hydrostatic "zero" using the lumen with respect to the mid-thoracic fluid filled

transducer (HP). It is balanced using a transducer control unit (Model TC-510, Millar Instruments, Houston, TX) and pressure are fed to the catheterization laboratory amplifier (Quinton Diagnostics, Bothell, WA or GE Healthcare, Milwaukee, WI) and simultaneously into the input ports of the physiological amplifier of the Doppler imaging system for synchronization (Philips iE33). With the patient supine, apical four-camber views using a 2.5 MHz transducer are obtained by the sonographer, with the sample volume gated at 1.5 to 5 mm directed between the tips of the mitral valve leaflets and orthogonal to the MV plane. Continuous wave Doppler is used to record aortic outflow and mitral inflow from the apical view for determination of the lateral IVRT using a sweep speed of 10cm/s. Doppler tissue imaging (DTI) of the medial and the lateral mitral annulus and M-mode images are also recorded. To synchronize the hemodynamic data with the Doppler data a fiducial marker in the form of a square wave is fed from the catheter-transducer control unit. The LV and AO pressure, LV volume from the conductance catheter and one ECG channel are also simultaneously recorded on disk. Simultaneous Doppler data, LVP and conductance volume are obtained for a minimum of 30 consecutive beats during quiet respiration. After data acquisition, the diagnostic catheterization procedure is performed in the usual manner.

3.3.3   Doppler E-wave Analysis

For each subject, approximately 1-2 minutes of continuous transmitral flow data were recorded in the pulsed-wave Doppler mode. Echocardiographic data acquisition is performed in accordance with published American Society of Echocardiography (27) criteria. Briefly, immediately before catheterization, patients are imaged in a supine position using a Philips

(Andover, MA.) iE33 system. Two dimensional images in apical 2- and 4-chamber views were obtained. In accordance with convention, the apical 4-chamber view was used for Doppler E-wave recording with the sample volume located at the leaflet tips. An average of 17 beats per subject were analyzed (205 cardiac cycles total for the 12 subjects). All E-waves were analyzed via the Parameterized Diastolic Filling (PDF) formalism via model-based image processing to yield E-wave specific kinematic parameters (chamber viscoelasticity/relaxation parameter (c), stiffness parameter (k), load parameter (x_o)) (19, 21).

The PDF Formalism

The PDF formalism models the kinematics of early rapid LV filling in analogy to the motion of a damped simple harmonic oscillator (19, 41). The governing equation of motion is:

$$m\frac{d^2x}{dt^2} + c\frac{dx}{dt} + kx = 0 \qquad [3.1]$$

The formalism solves the 'inverse problem' by providing (mathematically) unique parameters c, k, and x_o that determine each Doppler E-wave contour (19, 20, 41). The initial displacement of the oscillator x_o (cm) is linearly related to the E-wave VTI (i.e. a measure of volumetric preload), chamber stiffness ($\Delta P/\Delta V$) is linearly related to the model's spring constant k (g/s^2) while the oscillator's damping constant or chamber viscoelasticity/relaxation index c (g/s) characterizes the resistance (relaxation/viscosity) and energy loss associated with filling (20, 40). E-waves with long concave up deceleration portions ('delayed relaxation pattern') have high c values, while E-waves that approximate symmetric sine waves have low c values. The contour of the clinical E-wave is predicted by the (underdamped) solution for the velocity of a damped oscillator, given by:

$$v(t) = -\frac{x_o k}{\omega} \exp(-ct/2)\sin(\omega t)$$ [3.2]

where $\omega = \sqrt{4mk - c^2}/2m$.

PDF parameter values for c, k, and x_o and are determined using the Levenberg-Marquardt algorithm to fit to the E-wave maximum velocity envelope via a custom Lab VIEW (National Instruments, Austin, TX) interface (3, 7, 20, 29, 40). By setting $m = 1$, we can calculate the parameters per unit mass.

3.3.4 Hemodynamic Analysis

Hemodynamics were determined from the high-fidelity Millar LV pressure and volume data from each beat. A custom MATLAB program was used to find the end-systolic and diastatic P-V data points. Diastatic points were defined by ECG P-wave onset, and according to convention, mitral valve opening pressure on the continuous LVP tracing was estimated to be equal to LVEDP (4, 15, 25, 26).

3.3.5 Definition of P-V area During the E-wave

The diastolic pressure-volume (P-V) area, as defined in Figure 3.1, represents the work done by recoiling chamber during early rapid filling (E-wave). This area was computed numerically from P-V data directly, and is defined in the P-V plane as the area under the P-V curve from mitral valve opening (MVO) to diastasis.
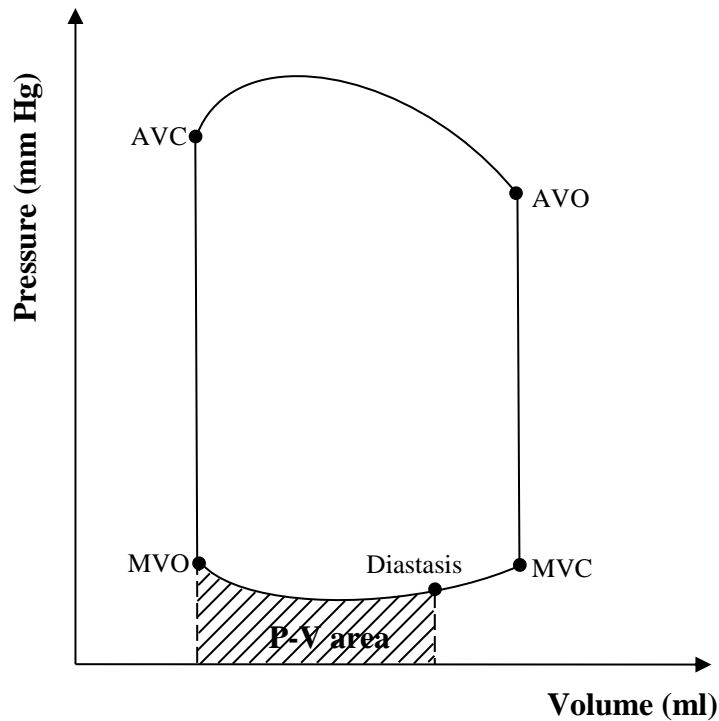
Figure 3.1 Schematic P-V loop defining P-V area.

Schematic P-V loop defining P-V area as a measure of energy, from mitral valve opening to diastasis, encompassing the suction initiated, early rapid filling (Doppler E-wave) interval. AVC, aortic valve closure; AVO, aortic valve opening; MVO, mitral valve opening; MVC, mitral valve closure. See text for details.

3.3.6 **Derivation and Calculation of the Kinematic Energy**

For a damped simple harmonic oscillator, with spring constant k and initial displacement x_o recoiling from rest, the potential energy prior to recoil is $1/2kx_o^2$. Because the oscillator is damped, only a fraction of the total potential energy is available as external work during the E-wave. Because work is defined as $\int Fdx$, where F is force and dx is displacement. Expressing the result in terms of PDF parameters we obtain

$$\int F dx = \left(\frac{1}{2} k x_o^{\,2} \right) KFEI \qquad\qquad [3.3]$$

where *KFEI*, the kinematic filling efficiency index (always<1) is the proportionality constant that determines what fraction of the total potentially energy $1/2 k x_o^{\,2}$ is delivered as external [*Fdx*] work (38).

To gain more insights into the physiologic determinants of E-wave energy and since the PDF formalism provides closed form algebraic expression for transmitral flow velocity *v(t)* as a function of time we expressed LV pressure *P* in terms of *v(t)* and acceleration *dv(t)/dt* using Bernoulli's equation for non-steady flow (35, 37).

To incorporate the near perfect constant-volume attribute of the 4-chambered and 2-chambered heart, left heart atrioventricular external geometry was modeled as a right circular cylinder having a fixed height (L) and fixed cross sectional area A. It is subdivided into upper and lower chambers representing the left atrium (LA) and left ventricle (LV), respectively.

v_E and $v_{E'}$ are the Doppler derived mitral inflow velocity and DTI recorded mitral annulus velocity. With the constraint that LV mass is conserved between systole and diastole and noting that the combined atrial and ventricular blood volume remains essentially constant between systole and diastole, we can write (10):

$$MVA \cdot v_E = A \cdot v_{E'} \qquad\qquad [3.4]$$

The volume of heart and volume of LV can be written as A·L and L·x, respectively. By taking derivative of the LV volume and using [3.4]

$$dV_{LV} = A \cdot dx = A \cdot v_{E'} dt = MVA \cdot v_E dt \qquad\qquad [3.5]$$

The relation between kinematic energy $\mathcal{E}_{\text{E-wave}}$ and PDF parameters can be derived from

Bernoulli's equation for non-steady flow:

$$\Delta P = LAP - LVP = \frac{1}{2}\rho v_E{}^2 + \rho \int_{LA}^{LV} \frac{\partial v(s,t)}{\partial t}\, ds \qquad [3.6]$$

where LAP and LVP are left atrial and left ventricular pressure, and ρ is the density of blood.

The integral can be rewritten as $M(dv_E/dt)$, where M (constant) is the mitral inertiance (35, 37, 40). Equation [3.6] becomes:

$$LVP = -\frac{1}{2}\rho v_E{}^2 - M\frac{dv_E}{dt} + LAP \qquad [3.7]$$

where M can be obtained by noting that at $t=DT$ the time of pressure crossover, LAP=LVP (40).

$$\Delta P = 0 = \frac{1}{2}\rho v_E{}^2 \bigg|_{t=DT} + M\frac{dv_E}{dt}\bigg|_{t=Dt} \qquad [3.8]$$

$$M = -\frac{\dfrac{1}{2}\rho v_E^2 \bigg|_{t=DT}}{\dfrac{dv_E}{dt}\bigg|_{t=Dt}} = \frac{1}{2}\rho x_o\left(\frac{\sqrt{k}}{c}\right)\exp\left(-\frac{cDT}{2}\right) \qquad [3.9]$$

where $DT = \dfrac{\pi}{\omega} - \dfrac{1}{\omega}\operatorname{Arc\,tan}\left(\dfrac{2\omega}{c}\right)$.

Substituting $y \equiv \dfrac{c}{2\sqrt{k}}$, the LV pressure at any time t (Equation [3.7]) is:

$$LVP = -\frac{1}{2}\rho\left[v_E(t)^2 + x_o\left(\frac{1}{2y}\right)\exp\left(-\frac{y\left(\pi - \cos^{-1}(y)\right)}{\sqrt{1-y^2}}\right)\dot{v}_E(t)\right] + LAP \qquad [3.10]$$

We obtain the area under the E-wave portion of the P-V loop by integrating the Bernoulli equation derived expression for P in $\int PdV$, as a function of volume, from MVO to diastasis. By

integrating [3.10] over the volume of LV we can derive P-V area (kinematic energy $\mathcal{E}_{\text{E-wave}}$) in term of PDF parameters. The result is:

$$\mathcal{E}_{\text{E-wave}} = \int_{V(0)}^{V(\frac{\pi}{\omega})} LVP \cdot dV_{LV}$$

$$= -\frac{1}{2}\rho \int_{V(0)}^{V(\frac{\pi}{\omega})} \left[v_E(t)^2 + x_o \left(\frac{1}{2y}\right) \exp\left(-\frac{y\left(\pi - \cos^{-1}(y)\right)}{\sqrt{1-y^2}}\right) \dot{v}_E(t) \right] \cdot dV_{LV} + \underbrace{\int_{V(0)}^{V(\frac{\pi}{\omega})} LAP \cdot dV_{LV}}_{C'}$$

$$[3.11]$$

Since dV_{LV} is originally equal to $A \cdot v_{E'} dt$, limits are determined by the duration of E'-wave $(0 - \dfrac{\pi}{\omega'})$ and LAP is treated as a constant of integration

$$\mathcal{E}_{\text{E-wave}} = -\frac{1}{2}\rho \int_{0}^{\frac{\pi}{\omega'}} \left[v_E(t)^2 + x_o \left(\frac{1}{2y}\right) \exp\left(-\frac{y\left(\pi - \cos^{-1}(y)\right)}{\sqrt{1-y^2}}\right) \dot{v}_E(t) \right] \cdot MVA \cdot v_E(t) dt + C' \qquad [3.12]$$

$$\mathcal{E}_{\text{E-wave}} = -\frac{1}{2}\rho \cdot MVA \left[\int_{0}^{\frac{\pi}{\omega'}} v_E(t)^3 dt + x_o \left(\frac{1}{2y}\right) \exp\left(-\frac{y\left(\pi - \cos^{-1}(y)\right)}{\sqrt{1-y^2}}\right) \int_{v_E(0)}^{v_E(\frac{\pi}{\omega'})} v_E(t) dv_E \right] + C' \quad [3.13]$$

where v_E the E-wave velocity from PDF model is given by $v(t) = -\dfrac{x_o k}{\omega} \exp(-ct/2)\sin(\omega t)$.

Since the specific relation between E-wave and E'-wave PDF parameters depends on chamber geometry, the useful approximation for the upper limit of both integrals is $t=DT$, the time of the peak of E-wave inflection. After taking the integrals, we get:

$$\mathcal{E}_{\text{E-wave}} = \rho \cdot MVA \left(\frac{1}{2} k x_o^{\,3} \right) \left[\frac{4}{3(1+8y^2)} \left(1 - y(5+8y^2)\right) \exp\left(-\frac{3y\,\text{Arctan}\left(\frac{\sqrt{1-y^2}}{y} \right)}{\sqrt{1-y^2}} \right) + \left(\frac{1}{4y} \exp\left(-\frac{3y\left(\pi - \cos^{-1}(y)\right)}{\sqrt{1-y^2}} \right) \right) \right] + C' \quad [3.14]$$

For E-waves whose contours are well fit by the underdamped oscillation regime (

$\sqrt{4k - c^2} > 0$) or $y < 1$, the equation becomes

$$\mathcal{E}_{\text{E-wave}} \approx \rho \cdot MVA \left(\frac{1}{2} k x_o^{\,3} \right) \left(\frac{4}{3} + \frac{1}{4y} \exp\left(-\frac{3y\left(\pi - \cos^{-1}(y)\right)}{\sqrt{1-y^2}} \right) \right) + C' \qquad [3.15]$$

This yields the expression for diastolic kinematic energy $\mathcal{E}_{\text{E-wave}}$ in terms of PDF

parameters (c, k and x_o) and deceleration time of E-wave:

$$\mathcal{E}_{\text{E-wave}} \approx \rho \cdot MVA \left(\frac{1}{2} k x_o^{\,3} \right) \left(\frac{4}{3} + \left(\frac{\sqrt{k}}{2c} \right) \exp\left(-\frac{3cDT}{2} \right) \right) + C' \qquad [3.16]$$

where MVA is the effective (constant) mitral valve area, ρ is the density of blood, and DT is the

deceleration time of the E-wave. For simplicity, MVA was constant (4 cm^2) and the density of

blood was 1.060 g/ml.

3.4   Results

3.4.1 <u>Pressure-Volume Area vs. Energy as $\left(\frac{1}{2}kx_o^2\right) \cdot KFEI$</u>

Pressure-Volume (P-V) area and the potential energy of the damped simple harmonic oscillator were highly correlated ($R^2 = 0.62$) for all analyzed beats (Figure 3.2).

Number of beats = 205

$$y = 0.13x + 0.04$$
$$R^2 = 0.62$$

P-V Area (J)
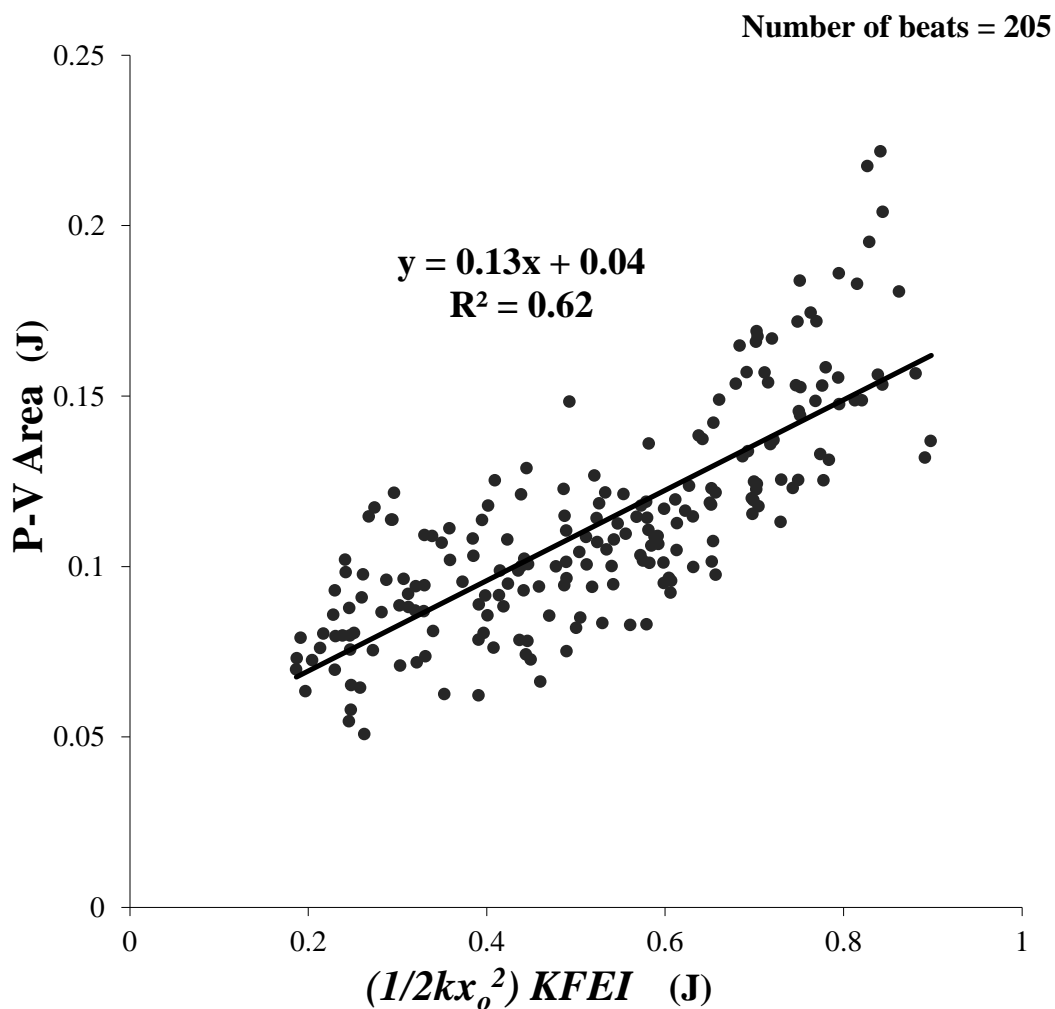
$(1/2kx_o^2)$ $KFEI$ (J)

Figure 3.2 Correlation between P-V area and potential energy.

Correlation between experimentally measured pressure-volume area (P-V Area) as the ordinate and E-wave determined potential energy ($(\frac{1}{2}kx_o^2) \cdot KFEI$) as the abscissa. See text for details.

When analyzed on an individual basis the high correlation between P-V area and potential energy ($R^2 > 0.69$) was maintained. Individual linear regression for each dataset is shown in Table 3.2. We compared potential energy vs. P-V area (as the reference). ANOVA derived p-values < 0.05 were considered statistically significant.

Table 3.2 Individual slopes and intercepts for P-V area vs. potential energy.

Individual least mean square linear regression slopes and intercepts for Pressure-Volume area vs. kinematic model derived potential energy expressed as $(\frac{1}{2}kx_o{}^2) \cdot KFEI$ for 12 subjects.

Subject	Linear fit slope	Linear fit intercept	R^2
1	0.03	2E-03	0.79
2	0.05	1E-04	0.75
3	0.09	1E-01	0.83
4	0.12	2E-02	0.80
5	0.02	6E-02	0.77
6	0.05	2E-02	0.75
7	0.06	3E-02	0.81
8	0.04	4E-02	0.83
9	0.03	5E-02	0.76
10	0.06	2E-02	0.69
11	0.07	3E-02	0.87
12	0.03	4E-02	0.77

3.4.2 <u>Pressure-Volume Area vs. Kinematic Energy $\mathcal{E}_{\text{E-wave}}$</u>

As we expected Pressure-Volume (P-V) area and kinematic energy $\mathcal{E}_{\text{E-wave}}$ derived from

E-wave analysis were highly correlated ($R^2 = 0.67$) for all analyzed beats (Figure 3.3).
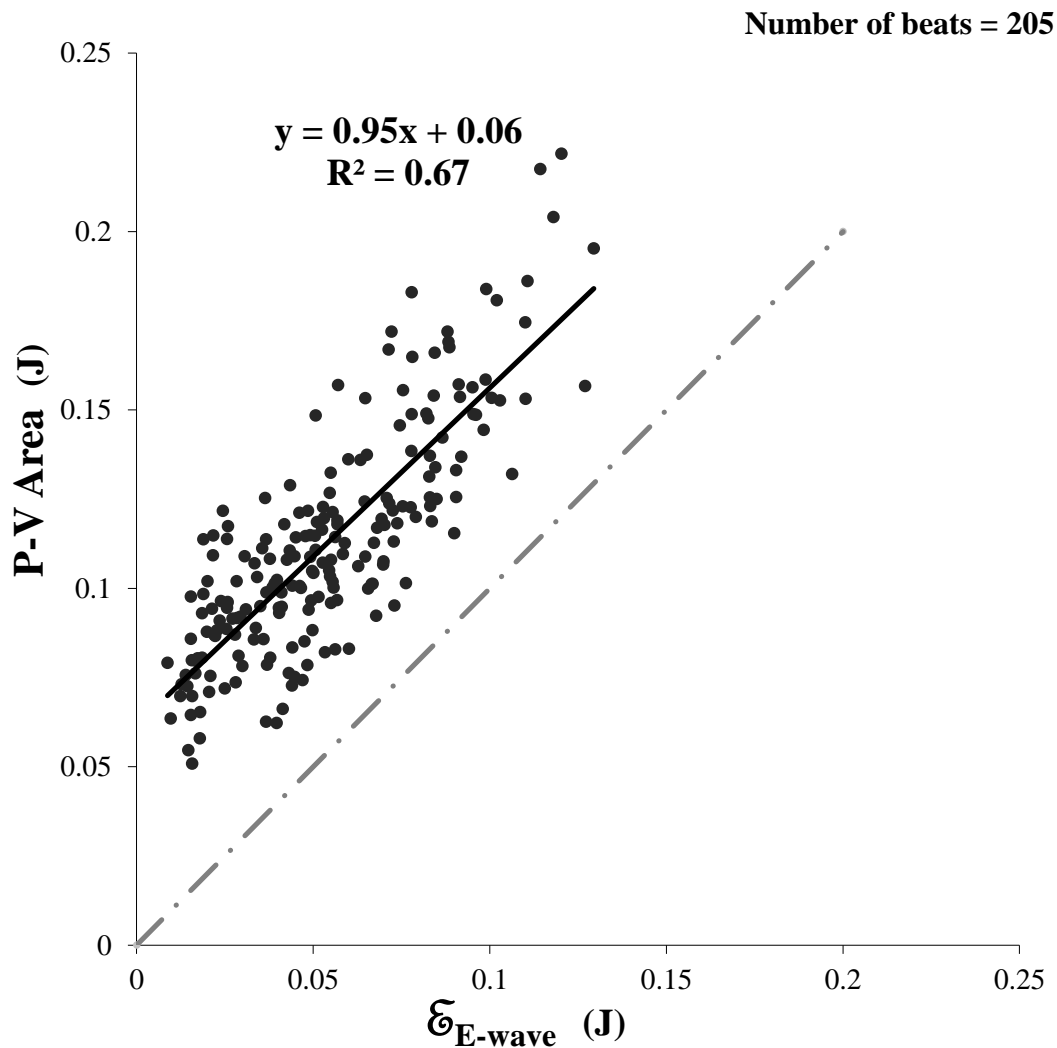
Figure 3.3 Correlation between P-V Area and kinematic energy.

Correlation between experimentally measured pressure-volume area (P-V Area) as the ordinate and model-predicted kinematic energy ($\mathcal{E}_{\text{E-wave}}$) as the abscissa. See text for details.

When analyzed individually, data for all 12 subjects showed that P-V area strongly

correlated with kinematic energy ($R^2 > 0.60$). Individual linear regressions for the subjects are

shown in Table 3.3. For all subjects kinematic energy vs. P-V area, analyzed using ANOVA yielded p-values < 0.05, and were statistically significant.

Table 3.3 Individual slopes and intercepts for P-V area vs. kinematic energy.

Individual least mean square linear regression slopes and intercepts for Pressure-Volume area vs. kinematic energy $\mathcal{E}_{\text{E-wave}}$ (Equation [3.16]) incorporating Bernoulli equation and near constant volume physiology, for 12 subjects.

Subject	Linear fit slope	Linear fit intercept	R^2
1	0.92	5E-02	0.69
2	1.19	5E-02	0.67
3	1.69	9E-05	0.85
4	3.58	2E-02	0.78
5	0.62	7E-02	0.80
6	1.41	4E-02	0.77
7	1.46	4E-02	0.60
8	1.20	6E-02	0.88
9	0.57	8E-02	0.69
10	1.76	5E-02	0.69
11	1.50	4E-02	0.87
12	0.74	6E-02	0.79

3.5   Discussion

3.5.1 <u>Pressure-Volume Area vs. Kinematic</u>

Echocardiography is the preferred method of diastolic function assessment. To provide a more complete set of causality based DF indexes we utilized thermodynamic principles. We determined the E-wave derived analogue of invasively measured (P-V loop derived) diastolic energy. While stroke work is a familiar energy-based index, the energy associated with diastolic recoil, a necessary component for total energy balance, has not been fully appreciated. Elastic strain energy, stored during the prior systole is unmasked during relaxation and drives diastolic recoil. It results in mechanical suction of atrial blood by generating an atrioventricular pressure gradient resulting in the E-wave (12, 14, 16, 30). Using complementary methods and mathematical modeling, we derived two expressions for diastolic energy in terms of parameters obtained from the E-wave alone. We tested the validity of our derived energy expressions for the same physiologic event by determining the correlation between values obtained using simultaneous invasive (P-V loop) vs. noninvasive (echo) data in 12 subjects. In accordance with thermodynamic requirements, we found a strong correlation. This represents the first study where expressions for diastolic energy have been derived from first principles and validated employing simultaneous invasive and noninvasive data acquisition methods.

3.5.2 __Thermodynamics and the Heart__

The total LV generated external work (stoke work) per cardiac cycle (joules) is given by ∫PdV around the pressure-volume loop. Systolic pressure-volume area, a measure of total mechanical energy generated by ventricular contraction, closely correlates with cardiac oxygen consumption under a variety of loading conditions for a given contractile (inotropic) state (32-34). Similarly, the tension-time integral or force-time integral (11) can convey work done by the chamber. Efficiency of the chamber has been computed as the ratio of output or external work (joules) divided by input (myocardial oxygen consumption) (18). These measurements typically yield an efficiency of about 25%. Instead of the entire cycle, we consider the external work during diastole, since diastolic energy, a component of ∫PdV has not, to our knowledge, ever been specifically calculated or analyzed.

By considering the early, rapid filling phase of diastole we define the diastolic pressure-volume area as the measure of external work done by the chamber during the E-wave. We obtain this experimentally from the area of the P-V loop [∫PdV] from MVO to diastasis (See Figure 3.1). This area represents the absolute (invasive) measure of external PdV work of the chamber during the E-wave ($\mathcal{E}_{PV\text{-}E\text{-}wave}$).

An independent, transmitral flow based relative measure of E-wave energy can be obtained via kinematic modeling of suction initiated filling ($\mathcal{E}_{E\text{-}wave}$). Thermodynamic laws require that relative and absolute measurements of the same event be linearly related, and differ by a constant of integration.

3.5.3 <u>Kinematic Filling Efficiency Index (KFEI)</u>

Systole stores elastic strain energy (potential energy) which is unmasked by relaxation and powers the mechanical recoil/ventricular suction process. The PDF formalism provides a simple expression, $1/2kx_o^2$, for energy available to power an idealized, lossless and symmetric (about its peak) E-wave. But actual E-waves must be asymmetric, and the extent of asymmetry reflects filling related energy losses. We have previously computed a kinematic filling efficiency index (KFEI) as actual E-wave volume (parameterized by x_o, c and k) divided by the maximum possible (idealized) E-wave volume, parameterized by identical x_o and k, but generated in the absence of viscous losses ($c = 0$ kinematics) (38). KFEI therefore incorporates viscous losses/relaxation effects associated with the balance between chamber damping (c) and chamber stiffness (k).

The KFEI index differentiated E-waves of normal LVEF diabetic hearts from E-waves of normal LVEF non-diabetic controls more robustly than traditional clinical parameters such as deceleration time (38). KFEI's connection to E-wave energy provides valuable insight into the current work. In analogy to KFEI, the potential energy of the oscillator ($1/2kx_o^2$) can also be considered in the ideal lossless ($c = 0$) setting and the actual, in- vivo ($c \neq 0$) setting. In the lossless setting KFEI=1, all of the oscillator's potential energy is converted to kinetic energy (velocity) and no energy is lost as viscous dissipation. In the actual, in-vivo setting some energy is always lost to dissipation, and only a fraction of the initial $1/2kx_o^2$ energy is delivered as kinetic energy of filling. Because KFEI is a dimensionless index of kinematic filling efficiency, it is appropriate to estimate the actual delivered energy powering filling as the product of KFEI and ideal energy powering filling ($1/2kx_o^2$).

As we expected from the correlations between P-V area and the potential energy of the

damped simple harmonic oscillator, $1/2kx_o^2$.KFEI, (as shown in Figure 3.2) and P-V area vs. kinematic energy $\mathcal{E}_{E\text{-wave}}$ (as shown in Figure 3.3), there is a good correlation (R^2=0.88) between potential energy $1/2kx_o^2$.KFEI and kinematic energy $\mathcal{E}_{E\text{-wave}}$ (Figure 3.4).
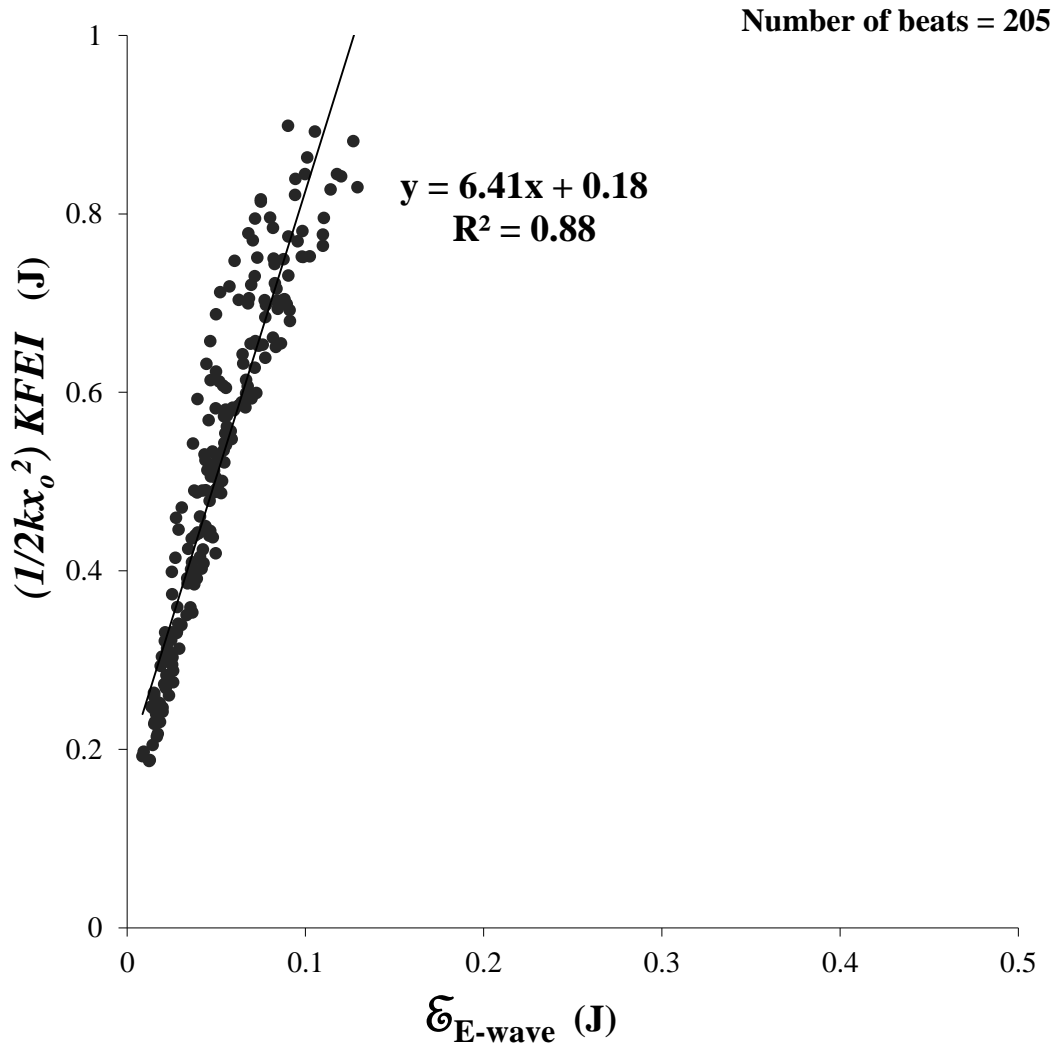
Figure 3.4 Correlation between potential energy and kinematic energy.

Correlation between potential energy $(\frac{1}{2}kx_o^2) \cdot KFEI$ and kinematic energy $\mathcal{E}_{E\text{-wave}}$ (theoretical P-V area). See text for details.

3.5.4 <u>Theoretical P-V Loop</u>

Using the non-steady Bernoulli equation and PDF formalism derived expressions for flow (E-wave) velocity *v(t)* and acceleration *dv(t)/dt*, expressions for LV pressure and volume as a function of time can be derived. Eliminating time provides pressure as a function of volume. This yields kinematic and fluid mechanics-based modeling derived algebraic expressions for the early filling portion of the P-V loop, in terms of PDF parameters k, c and x_o. To find the area under the pressure-volume loop during early filling, the derived P(V) expression is integrated from MVO to diastasis, coinciding with E-wave duration.

In previous work we have modeled the pressure-volume loop kinematically, and demonstrated that the model-derived analog of maximum elastance was a function only of intrinsic model parameters rather than initial conditions and therefore the analogous E_{max} relationship was load independent (28). However that approach relied on modeling the entire cardiac cycle. In this work we instead focus on the early rapid filling related portion of the P-V loop, and we do this by applying the non-steady Bernoulli equation.

3.5.5 <u>Application of Non-Steady Bernoulli Equation</u>

Previous work has demonstrated the importance of including both convective and inertial terms in the Bernoulli equation when modeling transmitral flow (9). By approximating the inertial term as the product of mitral inertiance and acceleration, and applying the proper limit, we are able to derive an expression for the atrioventricular pressure gradient in terms of PDF parameters (Equation [3.10]). In constructing a pressure volume loop from this expression, we treat the atrial pressure term as an unknown constant in order to extract ventricular pressure

alone. This introduces a systematic offset in our final expression, and in the area under the theoretically constructed pressure volume loop. Thus the non-zero asymptote present in Figure 3.3 is primarily the result of treating the atrial pressure term as an unknown constant. This linear offset is the expected consequence of comparing an absolute catheterization based measure (P-V area) to a relative measure (theoretical PV loop area derived from E-wave alone), and the correlation seen in Figure 3.3 is expected to be stronger and have an intercept closer to zero if atrial pressure recording was available and contributed to ΔP in the construction of the final expression. The value of the intercept in Figure 3.3 was consistent across subjects (see Table 3.3).

3.5.6 <u>Determining Diastolic Recoil Energy in the Context of ‘Absolute’ vs. ‘Relative’ Measurement</u>

Diastolic recoil energy from the P-V loop shown graphically in Figure 3.1 can be computed in alternate ways. For the P-V loop in Figure 3.1, atmospheric zero is, by convention, the fiducial reference. However, for the E-wave derived expression for energy (Equation [3.16]), the offset relative to atmospheric zero or any fiducial value cannot be specified (it is the constant of integration, C’ in Equation [3.16]).

Indeed, when we compare diastolic recoil energies determined from the invasive (an ‘absolute’ measure) and non-invasive (a ‘relative’ measure) approaches (Figure 3.3), we observe a non-zero intercept. The non-zero intercept is the experimental equivalent of C’ in Equation [3.16]. It is the result of the alternate choice of atmospheric zero vs. mean atrial pressure or diastatic pressure as the reference fiducial pressure relative to which energy variation is

computed. Using the diastatic P-V curve as a reference constitutes another option (39). We tested the extent to which choice of fiducial pressure (atmospheric vs. zero reference) affects the regression between E-wave derived and P-V derived energies. The correlations between kinematic energy using 0 as the constant of integration vs. actual PV area were unaltered. Therefore, the observed offset introduced by the choice of reference pressure has no effect on the expected linear correlation between invasive ('absolute') vs. noninvasive ('relative') measures of recoil energies.

3.5.7   **Future Studies**

This initial work is focused on deriving and validating the predicted relationship between invasive and noninvasive measures of diastolic energy. Broader clinical application should include a spectrum of suitably selected pathophysiologic states such as heart failure with normal ejection fraction (HFNEF), hypertension, diabetes, infiltrative disease, etc. Furthermore, energy based indexes are suitable for studies where each subject serves as their own control, and response to selected therapies for diastolic dysfunction are assessed using conventional methods and in terms of repeated measures of recoil energy. Although expected to be load-dependent, diastolic recoil energy indexes can be trended in concert with a previously derived and validated load independent index of diastolic function obtained by suitable analysis of the E-wave (31).

3.6   Limitations

3.6.1 <u>Conductance Volume</u>

The conductance catheter method of volume determination has known limitations related to noise, saturation and calibration that we have previously acknowledged (1, 3, 22). In this study, the channels which provided physiologically consistent P-V loops were selected and averaged. However, since there was no significant drift of volume signal during recording, any systematic offset related to calibration of the volume channels did not affect the result when the limits of conductance volume was calibrated via quantitative ventriculography.

3.6.2 <u>P-V Measurements</u>

Our assumption that MVO pressure approximates LVEDP has limitations. It has been shown (36) that this assumption is valid in the setting of normal physiology. In an abnormal case (abnormal valve function and LVEF) where MVO pressure and EDP are significantly different, the use of EDP in the P-V area will introduce a systematic error, but will still represent a reasonable estimate of energy during early filling, and it will affect the offset of the correlation of P-V area and $\mathcal{E}_{E\text{-wave}}$. To minimize any systematic difference between MVO pressure and LVEDP in our analysis of 205 heart beats in 12 subjects, we selected datasets only for subjects with normal valve function, and normal LVEF (4, 15, 26, 40).

3.6.3   E-wave Selection

Although the PDF formalism is applicable to all E-waves, the most robust analysis is achieved for E-waves that have a clear termination and are followed by diastasis. E-wave analysis becomes less reliable when the A-wave merges with the E-wave and covers more than two-thirds of the E-wave deceleration portion. This typically occurs at HR > 90 beats/min (2). In the present study we used datasets with clearly discernible E-waves followed by a diastatic interval (average heart rate= 62 bpm).

3.6.4   Choosing the Limits of Integral in Bernoulli's Equation

We assumed simultaneous E- and E'-wave onset in deriving kinematic energy. It is possible that some E'-waves are slightly delayed (by a few ms) beyond E-wave onset (5). For simplicity and consistency and for ease of the integration we assumed that E'-wave duration and DT are comparable as shown in Figure 3.5. This assumption only effects magnitude of $\mathcal{E}_{\text{E-wave}}$ for every single beat, and has no significant effect on the slope and the correlation between $\mathcal{E}_{\text{PV-E-wave}}$ and $\mathcal{E}_{\text{E-wave}}$.
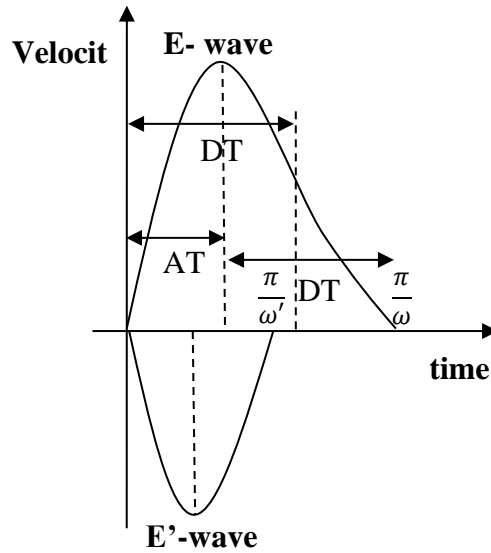
Figure 3.5 Schematic diagrams showing E-wave and E'-wave.

AT, acceleration time; DT, deceleration time. See text for details.

3.6.5 <u>Application of Bernoulli's Equation</u>

In deriving the expression for the kinematic energy ($\mathscr{E}_{\text{E-wave}}$), we apply a form of the Bernoulli equation for an ideal fluid, where fluid viscosity is ignored. This approach has been applied by previous investigators (35, 37) and studies have demonstrated its validity (8, 9). Recall that the PDF model (damped oscillation) accounts for energy loss in kinematic terms via the parameter c, hence by using the PDF derived expression for velocity in the Bernoulli equation, we automatically include the effects of losses in the system (damping) as part of the kinetic energy term in the Bernoulli equation. In effect the expression for fluid velocity and acceleration includes the parameter c, and therefore already includes energy losses as part of the resulting expression for pressure. This insures that energy conservation is maintained in accordance with Bernoulli's law, and includes the dominant form of energy loss due to kinematic

105

modeling derived viscoelastic losses rather than (negligible) fluid viscosity losses.

3.6.6   Sample Size

The number of datasets (n=12) is a minor limitation to the study, since the total number of cardiac cycles analyzed (n=205) mitigates it to an acceptable degree.

3.7   Conclusions

By deriving thermodynamics-based and kinematic modeling-based expressions for the work of suction initiated filling (E-wave) and utilizing in-vivo, human, simultaneous P-V and transmitral echocardiographic data for validation, we showed (to within an additive constant of integration) the predicted equivalence between echo-derived (relative) and P-V loop derived (absolute) measures of diastolic energy. These results establish energy ($1/2kx_o^2$) as a legitimate, mechanism-based, echo-derived diastolic function index obtainable via kinematic modeling based analysis of clinically recorded E-waves.

3.8   References

1.   **Bauman L, Chung CS, Karamanoglu M, and Kovács SJ**. The peak atrioventricular pressure gradient to transmitral flow relation: kinematic model prediction with in vivo validation. *J Am Soc Echocardiogr* 17: 839-844, 2004.

2.   **Cheng CP, Igarashi Y, and Little WC**. Mechanism of augmented rate of left ventricular filling during exercise. *Circ Res* 70: 9-19, 1992.

3.   **Chung CS, Ajo DM, and Kovács SJ**. Isovolumic pressure-to-early rapid filling decay rate relation: model-based derivation and validation via simultaneous catheterization echocardiography. *J Appl Physiol (1985)* 100: 528-534, 2006.

4.   **Chung CS, Karamanoglu M, and Kovács SJ**. Duration of diastole and its phases as a function of heart rate during supine bicycle exercise. *Am J Physiol Heart Circ Physiol* 287: H2003-2008, 2004.

5.   **Chung CS, and Kovács SJ**. Consequences of increasing heart rate on deceleration time, the velocity-time integral, and E/A. *Am J Cardiol* 97: 130-136, 2006.

6.   **Chung CS, and Kovács SJ**. Physical determinants of left ventricular isovolumic pressure decline: model prediction with in vivo validation. *Am J Physiol Heart Circ Physiol* 294: H1589-1596, 2008.

7.   **Dent CL, Bowman AW, Scott MJ, Allen JS, Lisauskas JB, Janif M, Wickline SA, and Kovács SJ**. Echocardiographic characterization of fundamental mechanisms of abnormal diastolic filling in diabetic rats with a parameterized diastolic filling formalism. *J Am Soc Echocardiogr* 14: 1166-1172, 2001.

8.   **Falsetti HL, Verani MS, Chen CJ, and Cramer JA**. Regional pressure differences in the left ventricle. *Cathet Cardiovasc Diagn* 6: 123-134, 1980.

9.   **Firstenberg MS, Vandervoort PM, Greenberg NL, Smedira NG, McCarthy PM, Garcia MJ, and Thomas JD**. Noninvasive estimation of transmitral pressure drop across the normal mitral valve in humans: importance of convective and inertial forces during left ventricular filling. *J Am Coll Cardiol* 36: 1942-1949, 2000.

10.   **Ghosh E, Shmuylovich L, and Kovacs SJ**. Determination of early diastolic LV vortex

formation time (T*) via the PDF formalism: a kinematic model of filling. *Conf Proc IEEE Eng Med Biol Soc* 2009: 2883-2886, 2009.

11.   **Goto Y, Slinker BK, and LeWinter MM**. Decreased contractile efficiency and increased nonmechanical energy cost in hyperthyroid rabbit heart. Relation between O2 consumption and systolic pressure-volume area or force-time integral. *Circ Res* 66: 999-1011, 1990.

12.   **Granzier H, and Labeit S**. Cardiac titin: an adjustable multi-functional spring. *J Physiol* 541: 335-342, 2002.

13.   **Hall AF, and Kovács SJ**. Automated method for characterization of diastolic transmitral Doppler velocity contours: early rapid filling. *Ultrasound Med Biol* 20: 107-116, 1994.

14.   **Helmes M, Trombitás K, and Granzier H**. Titin develops restoring force in rat cardiac myocytes. *Circ Res* 79: 619-626, 1996.

15.   **Ishida Y, Meisner JS, Tsujioka K, Gallo JI, Yoran C, Frater RW, and Yellin EL**. Left ventricular filling dynamics: influence of left ventricular relaxation and left atrial pressure. *Circulation* 74: 187-196, 1986.

16.   **Jöbsis PD, Ashikaga H, Wen H, Rothstein EC, Horvath KA, McVeigh ER, and Balaban RS**. The visceral pericardium: macromolecular structure and contribution to passive mechanical properties of the left ventricle. *Am J Physiol Heart Circ Physiol* 293: H3379-3387, 2007.

17.   **Kass DA, Bronzwaer JG, and Paulus WJ**. What mechanisms underlie diastolic dysfunction in heart failure? *Circ Res* 94: 1533-1542, 2004.

18.   **Knaapen P, Germans T, Knuuti J, Paulus WJ, Dijkmans PA, Allaart CP, Lammertsma AA, and Visser FC**. Myocardial energetics and efficiency: current status of the noninvasive approach. *Circulation* 115: 918-927, 2007.

19.   **Kovács SJ, Barzilai B, and Pérez JE**. Evaluation of diastolic function with Doppler echocardiography: the PDF formalism. *Am J Physiol* 252: H178-187, 1987.

20.   **Kovács SJ, Meisner JS, and Yellin EL**. Modeling of diastole. *Cardiol Clin* 18: 459-487, 2000.

21.   **Kovács SJ, Setser R, and Hall AF**. Left ventricular chamber stiffness from model-based image processing of transmitral Doppler E-waves. *Coron Artery Dis* 8: 179-187, 1997.

22.   **Lisauskas J, Singh J, Courtois M, and Kovács SJ**. The relation of the peak Doppler E-wave to peak mitral annulus velocity ratio to diastolic function. *Ultrasound Med Biol* 27: 499-507, 2001.

23.   **Lisauskas JB, Singh J, Bowman AW, and Kovács SJ**. Chamber properties from transmitral flow: prediction of average and passive left ventricular diastolic stiffness. *J Appl Physiol (1985)* 91: 154-162, 2001.

24.   **Maeder MT, and Kaye DM**. Heart failure with normal left ventricular ejection fraction. *J Am Coll Cardiol* 53: 905-918, 2009.

25.   **Miki S, Murakami T, Iwase T, Tomita T, Nakamura Y, and Kawai C**. Doppler echocardiographic transmitral peak early velocity does not directly reflect hemodynamic changes in humans: importance of normalization to mitral stroke volume. *J Am Coll Cardiol* 17: 1507-1516, 1991.

26.   **Murakami T, Hess OM, Gage JE, Grimm J, and Krayenbuehl HP**. Diastolic filling dynamics in patients with aortic stenosis. *Circulation* 73: 1162-1174, 1986.

27.   **Nagueh SF, Appleton CP, Gillebert TC, Marino PN, Oh JK, Smiseth OA, Waggoner AD, Flachskampf FA, Pellikka PA, and Evangelista A**. Recommendations for the evaluation of left ventricular diastolic function by echocardiography. *J Am Soc Echocardiogr* 22: 107-133, 2009.

28.   **Oommen B, Karamanoglu M, and Kovács S**. Modeling Time Varying Elastance: The Meaning of "Load-Independence". *Cardiovascular Engineering* 3: 123-130, 2003.

29.   **Riordan MM, Chung CS, and Kovács SJ**. Diabetes and diastolic function: stiffness and relaxation from transmitral flow. *Ultrasound Med Biol* 31: 1589-1596, 2005.

30.   **Robinson TF, Factor SM, and Sonnenblick EH**. The heart as a suction pump. *Sci Am* 254: 84-91, 1986.

31.   **Shmuylovich L, and Kovács SJ**. Load-independent index of diastolic filling: model-based derivation with in vivo validation in control and diastolic dysfunction subjects. *J Appl Physiol (1985)* 101: 92-101, 2006.

32.   **Suga H**. Cardiac energetics: from E(max) to pressure-volume area. *Clin Exp Pharmacol Physiol* 30: 580-585, 2003.

33.   **Suga H**. Theoretical Analysis of a Left-Ventricular Pumping Model Based on the Systolic Time-Varying Pressure/Volume Ratio. *IEEE Trans Biomed Eng* 24: 29-38, 1977.

34.   **Suga H, Goto Y, Futaki S, Kawaguchi O, Yaku H, Hata K, and Takasago T**. Systolic pressure-volume area (PVA) as the energy of contraction in Starling's law of the heart. *Heart Vessels* 6: 65-70, 1991.

35.   **Thomas JD, Newell JB, Choong CY, and Weyman AE**. Physical and physiological determinants of transmitral velocity: numerical analysis. *Am J Physiol* 260: H1718-1731, 1991.

36.   **Wu Y, and Kovács SJ**. Frequency-based analysis of the early rapid filling pressure-flow relation elucidates diastolic efficiency mechanisms. *Am J Physiol Heart Circ Physiol* 291: H2942-2949, 2006.

37.   **Yellin E**. *Mitral Valve Motion, Intracardiac Dynamics and Flow Pattern Modelling: Physiology and Pathophysiology. In: Advances in Cardiovascular Physics*. Basel, Switzerland: 1983, p. 137-161.

38.   **Zhang W, Chung CS, Riordan MM, Wu Y, Shmuylovich L, and Kovács SJ**. The kinematic filling efficiency index of the left ventricle: contrasting normal vs. diabetic physiology. *Ultrasound Med Biol* 33: 842-850, 2007.

39.   **Zhang W, and Kovács SJ**. The diastatic pressure-volume relationship is not the same as the end-diastolic pressure-volume relationship. *Am J Physiol Heart Circ Physiol* 294: H2750-2760, 2008.

40.   **Zhang W, Shmuylovich L, and Kovacs SJ**. The pressure recovery ratio: The invasive index of LV relaxation during filling. Model-based prediction with in-vivo validation. *Conf Proc IEEE Eng Med Biol Soc* 2009: 3940-3943, 2009.

41.   **Zile MR, and Brutsaert DL**. New concepts in diastolic dysfunction and diastolic heart failure: Part I: diagnosis, prognosis, and measurements of diastolic function. *Circulation* 105: 1387-1393, 2002.

Chapter 4: Diastatic Chamber Stiffness

4.1   Abstract

The slope of the diastatic pressure-volume relationship (D-PVR) defines passive left ventricular (LV) stiffness K. Although K is a relative measure, cardiac catheterization, which is an absolute measurement method is used to obtain it. Echocardiography, including transmitral flow velocity (Doppler E-wave) analysis, is the preferred quantitative diastolic function (DF) assessment method. However, E-wave analysis can provide only relative, rather than absolute pressure information. We hypothesized that physiologic mechanism based modeling of E-waves allows derivation of the D-PVR$_{E-wave}$ whose slope, K_{E-wave}, provides E-wave derived diastatic, passive chamber stiffness. Our kinematic model of filling and Bernoulli's equation were used to derive expressions for diastatic pressure and volume on a beat-by-beat basis, thereby generating D-PVR$_{E-wave}$, and K_{E-wave}. For validation, simultaneous (conductance catheter) P-V and echocadiographic E-wave data from 30 subjects (444 total cardiac cycles) having normal LV ejection fraction (LVEF) were analyzed. For each subject (15 beats average) model predicted K_{E-wave} was compared to experimentally measured K_{CATH} via linear regression yielding: $K_{E-wave} = \alpha K_{CATH} + b$ (R^2=0.92), where, α=0.995 and $b = 0.02$.

We conclude that echocardiographically determined diastatic passive chamber stiffness K_{E-wave}, provides an excellent estimate of simultaneous, gold standard (P-V) defined diastatic stiffness, K_{CATH}.   Hence, in chambers at diastasis, passive LV stiffness can be accurately determined by suitable analysis of Doppler E-waves (transmitral flow).

4.2   Introduction

Heart failure with normal ejection fraction (HFNEF), considered to be a consequence of diastolic dysfunction (DD), is a clinical syndrome that has reached epidemic proportions (17, 26, 42). Accordingly, the ability to quantitate DF and the presence and severity of DD is important. Among the invasive DF indexes, chamber stiffness remains an area of active investigation (6, 36). Classically, chamber stiffness determination has required catheterization-based measurement of the simultaneous change in LV pressure and volume ($\Delta P/\Delta V$). Conventionally LV chamber stiffness is measured as the slope of the LV end-diastolic pressure-volume relation (EDPVR) (16). However, end-diastole, defined by termination of atrial systole and the Doppler A-wave generates P-V data that is confounded by the properties of the contracted atrium (40). Passive chamber stiffness is achieved at diastasis. During diastasis, LV and LA pressures are equal, therefore the pressure gradient across the mitral valve is zero (7), and the resultant forces generated by and acting on the ventricle are balanced (but not zero) (32). No atrioventricular blood flow (4, 7, 23) or tissue motion is present (31, 35), the atrium and ventricle are both relaxed and pressure remains constant ($dP/dt \cong 0$). Accordingly, diastasis comprises the static equilibrium state of the passive LV (24, 39). Since LV volume, (i.e. load) changes physiologically on a beat-by-beat basis, diastasis is achieved at slightly different ventricular volumes and pressures generating a series of slightly different equilibrium states. The locus of these load-varying diastasis P-V points define the diastatic P-V relationship (D-PVR), whose slope (K_{CATH}) provides the passive stiffness of the LV (Figure 4.1). The P-V range, i.e. load-range, due to normal beat-to-beat physiologic variation during cardiac catheterization is somewhat narrower than can be possibly achieved under more aggressive load changing

115

maneuvers (pharmacologic agents, rapid volume infusion, etc.). However physiologic variation

has the advantage of being easily reproduced by other investigators and avoids the activation of

reflex mechanisms in response to aggressive methods.
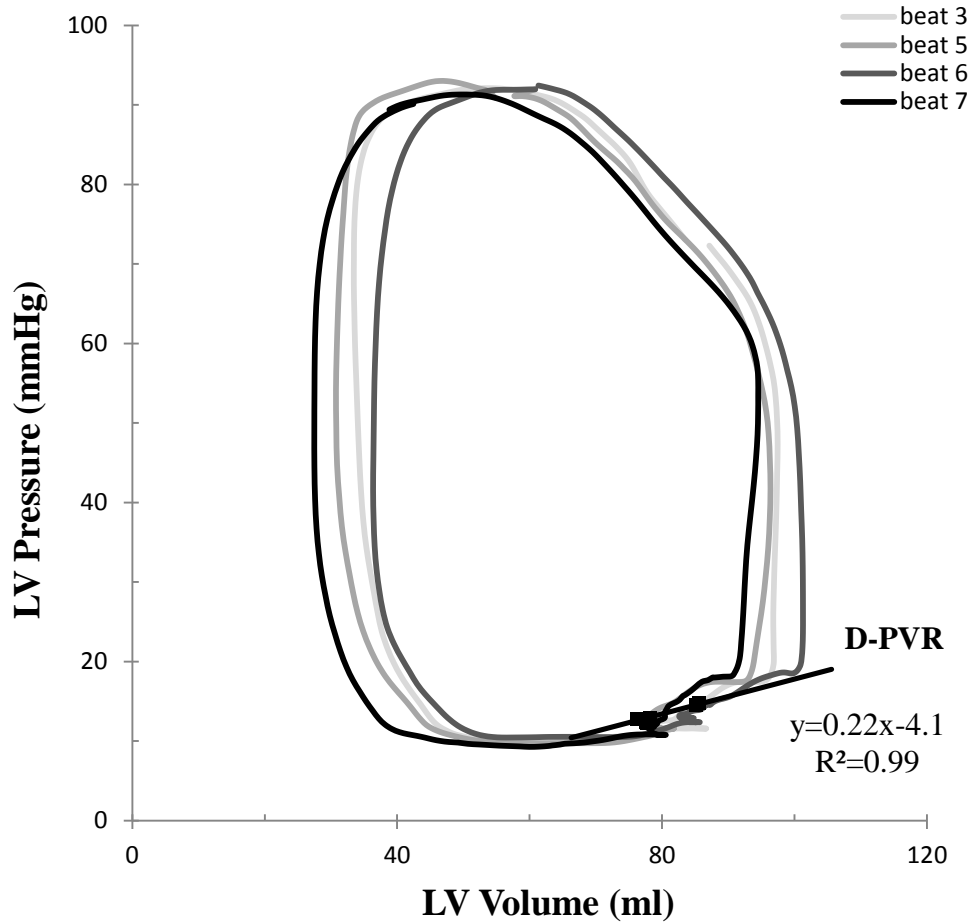
Figure 4.1 Typical P-V loops illustrating beat-by-beat response to physiologic load alteration.
For clarity beat #3, #5, #6 and #7, i.e. 4 of 15 analyzed beats are shown. Linear fit to diastatic locus of
points yields the diastatic pressure-volume relation (D-PVR), whose slope K_{CATH} defines diastatic
stiffness. See text for details.

In order to obtain the D-PVR we fit the P-V data using a linear, rather than exponential

fit, since previous work (40) shows that a linear or exponential fit to the same data yields a

similar measure of goodness of fit. Importantly, for a given chamber, the in-vivo equilibrium

volume of the LV is diastasis (24, 39) and chamber stiffness of the diastatic P-V relation has been shown to be distinct from, and to be always lower than, chamber stiffness in the same chamber measured at end-diastole (40).

Quantification of DD has remained a challenge without direct, invasive measurement. Doppler echocardiography has become the standard, and preferred method for quantitative DF assessment (12, 15, 18, 30). In previous work we have developed and validated novel, mechanism-based DF indexes via a kinematic modeling approach, called the parametrized diastolic filling (PDF) formalism (14, 20, 21). The PDF formalism models the kinematics of suction-initiated filling in analogy to the recoil from rest, of an equivalent damped oscillator. Model predicted velocity and clinical E-wave contours have shown superb agreement (21). Using a clinically recorded E-wave as input and suitable mathematical methods, unique chamber stiffness (k), viscoelasticity/relaxation (c) and load (x_o) parameters are generated as output, thereby solving the 'inverse problem of diastole' (17). The three PDF parameters (k, c, x_o) can be used to generate indexes with rigorous physiologic analogues including the peak instantaneous pressure gradient (kx_o) driving filling, and the potential energy driving the recoil/suction process ($1/2kx_o^2$) (2, 28).

Although obtaining the D-PVR itself involves an absolute measurement (LVP), the slope of the D-PVR is a relative index. The chamber's diastatic (passive) stiffness (K_{CATH}) is achieved at the end of each E-wave. Because Doppler E-waves are generated by the atrioventricular pressure gradient (a relative measure) rather than the individual values of either atrial or ventricular pressure (absolute measures individually) E-wave analysis should provide LV diastatic stiffness.

Thus in this work we derive an expression for diastatic stiffness from the E-wave

($K_{\text{E-wave}}$), and test the hypothesis, that $K_{\text{E-wave}}$ provides an excellent estimate of diastatic stiffness, K_{CATH}, determined using simultaneous invasive, catheterization-based P-V (gold-standard) methods. This is the first work to use Doppler data to measure the diastatic pressure-volume relationship in the heart.

4.3   Methods

4.3.1 <u>Subject Selection</u>

Datasets from 30 patients (mean age 57 years, 18 men) were selected from our cardiovascular biophysics laboratory database of simultaneous echocardiography-high fidelity hemodynamic (Millar conductance catheter) recordings (5, 24). Subjects underwent elective cardiac catheterization to determine presence of coronary artery disease at the request of their referring physicians. The data selection criteria included a broad range of LV end-diastolic pressure (LVEDP) representative of a patient population encountered clinically, normal LVEF ($> 50\%$), normal sinus rhythm, clearly discernible E-waves followed by a diastatic interval, and normal valvular function. Prior to data acquisition, subjects provided signed, IRB approved informed consent for participation in accordance with Washington University Human Research Protection Office (HRPO) criteria.

Among the 30 datasets, 13 had end-diastolic pressure (LVEDP) < 15 mm Hg, 9 had 15 mm Hg < LVEDP < 20 mm Hg and 8 had LVEDP >20 mm Hg. A total of 444 cardiac cycles of simultaneous echocardiographic-high fidelity hemodynamic (conductance catheter) data was analyzed.

The clinical descriptors of the 30 subjects and their hemodynamic and echocardiographic indexes are shown in Table 4.1.

Table 4.1 Clinical descriptors including hemodynamic and echocardiographic indexes.

N	30
Age (y)	57 ± 12
Gender (male/female)	18 / 12
Heart Rate (bpm)	62 ± 7
Ejection Fraction (LVEF) (%) [*]	69 ± 6
LVEDP (mmHg)	16 ± 4
LVEDV (ml)	133 ± 26
$P_{Diastasis}$ (mmHg)	13 ± 3
E/A	1.4 ± 0.2
PDF parameter x_o (cm)	9.4 ± 1.4
PDF parameter k ($1/s^2$)	205 ± 24
PDF parameterc c (1/s)	16.5 ± 3.1

LVEF, left ventricular ejection fraction; LVEDP, left ventricular end-diastolic pressure; LVEDV, left ventricular end-diastolic volume; PDF parameter x_o, c, and k precision is shown by the level of significant figures.

E/A, ratio of E_{peak} and A_{peak}.

* LVEF determined by ventriculography

Data are presented as mean $\pm$ standard deviation.

4.3.2 <u>Data Acquisition</u>

Our simultaneous high-fidelity, P-V and echocardiographic transmitral flow data recording method has been previously detailed (2, 3, 21, 22, 24, 28). Briefly, LV pressure and

volume were acquired using a micromanometric conductance catheter (SPC-560, SPC-562, or SSD-1043, Millar Instruments, Houston, TX) at the commencement of elective cardiac catheterization, prior to the administration of iodinated contrast agents. Pressure signals from the transducers were fed into a clinical amplifier system (Quinton Diagnostics, Bothell, WA, and General Electric). Conductance catheterization signals were fed into a custom personal computer via a standard interface (Sigma-5, CD Leycom). Conductance volume data were recorded in five channels. Data from low-noise channels providing physiological readings were selected, suitably averaged and calibrated using absolute volumes obtained by calibrated ventriculography during the same procedure.

Prior to arterial access, in the catheterization laboratory, a full 2-D echo-Doppler study is performed by an ASE certified sonographer in accordance with ASE criteria (29). After appropriate sterile skin prep and drape, local anesthesia (1% xylocaine) is given and percutaneous right or left femoral arterial access is obtained in preparation for catheterization and angiography, using a valved sheath (6-F, Arrow Inc, Reading, PA). After arterial access and placement of a 64 cm sheath (Arrow Inc, Reading, PA), a 6F micromanometer-tipped pigtail (triple pressure transducer) pressure-volume, conductance catheter (Model 560-1, 560-5, Millar Instruments, Houston, TX) is directed into the mid-LV in a retrograde fashion across the aortic valve under fluoroscopic control. Prior to insertion, the manometer-tipped catheter is calibrated against "zero" by submersion just below the surface of NS bath at 37° C, and again after insertion relative to hydrostatic "zero" using the lumen with respect to the mid-thoracic fluid filled transducer (HP). It is balanced using a transducer control unit (Model TC-510, Millar Instruments, Houston, TX) and pressure are fed to the catheterization laboratory amplifier (Quinton Diagnostics, Bothell, WA or GE Healthcare, Milwaukee, WI) and simultaneously into

the input ports of the physiological amplifier of the Doppler imaging system for synchronization (Philips iE33). With the patient supine, apical four-camber views using a 2.5 MHz transducer are obtained by the sonographer, with the sample volume gated at 1.5 to 5 mm directed between the tips of the mitral valve leaflets and orthogonal to the MV plane. Continuous wave Doppler is used to record aortic outflow and mitral inflow from the apical view for determination of the lateral IVRT using a sweep speed of 10cm/s. Doppler tissue imaging (DTI) of the medial and the lateral mitral annulus and M-mode images are also recorded. To synchronize the hemodynamic data with the Doppler data a fiducial marker in the form of a square wave is fed from the catheter-transducer control unit. The LV and AO pressure, LV volume from the conductance catheter and one ECG channel are also simultaneously recorded on disk. Simultaneous Doppler data, LVP and conductance volume are obtained for a minimum of 30 consecutive beats during quiet respiration. After data acquisition, the diagnostic catheterization procedure is performed in the usual manner.

4.3.3   <u>Doppler E-wave Analysis</u>

For each subject, approximately 1-2 minutes of continuous transmitral flow data were recorded in the pulsed-wave Doppler mode (Appendix 1). Echocardiographic data acquisition is performed in accordance with American Society of Echocardiography (29) criteria. Briefly, immediately before catheterization, patients were imaged in a supine position using a Philips (Andover, MA.) iE33 system. Two dimensional images in apical 2- and 4-chamber views were obtained. In accordance with convention, the apical 4-chamber view was used for Doppler E-wave recording with the sample volume located at the leaflet tips. An average of 15 beats per

subject were analyzed (444 cardiac cycles total for the 30 subjects). All E-waves were analyzed using the Parametrized Diastolic Filling (PDF) formalism via model-based image processing to yield E-wave specific kinematic parameters (chamber viscoelasticity/relaxation parameter (c), stiffness parameter (k), load parameter (x_o)) for each cardiac cycle (19, 20, 23).

The PDF Formalism

The PDF formalism models the kinematics of early rapid LV filling in analogy to the motion of a damped simple harmonic oscillator (20, 21). The governing equation of motion is:

$$m\frac{d^2 x}{dt^2} + c\frac{dx}{dt} + kx = 0 \qquad [4.1]$$

The displacement of the PDF model's analog oscillator is x (cm), and its physiologic equivalent is the velocity-time integral of the E-wave (cm). The inertial term for the oscillator is m, and without loss of generality Equation [4.1] can be divided by m, providing the parameters k and c on a per unit mass basis (20, 21). The formalism solves the 'inverse problem' by using the Doppler E-wave contour as input and providing (mathematically) unique parameters c, k, and x_o that determine each wave, as output (13, 19-21).

The initial displacement of the equivalent oscillator x_o (cm) is linearly related to the E-wave velocity–time integral (i.e. a measure of volumetric preload), kinematic chamber stiffness ($\Delta P/\Delta V$) is linearly related to the model's spring constant k (g/s^2) while the oscillator's damping constant c (g/s) characterizes the resistance (relaxation/viscosity) and energy loss associated with recoil initiated filling (21). E-waves with long concave up deceleration portions ('delayed relaxation pattern') have high c values, while E-waves that approximate nearly symmetric sine

123

waves have low c values (34). The contour of the clinical E-wave is predicted by the (underdamped) solution of Equation [4.1] for the velocity of a damped oscillator, as:

$$v_E(t) = -\frac{x_o k}{\omega} \exp(-ct/2)\sin(\omega t)$$ [4.2]

where $\omega = \sqrt{4mk - c^2}/2m$.

PDF parameter values for c, k, and x_o are determined as output using the Levenberg-Marquardt algorithm using the E-wave maximum velocity envelope as input via a custom Lab VIEW (National Instruments, Austin, TX) interface (4, 8, 21, 33).

4.3.4 <u>Determination of Diastatic Stiffness Using P-V Data</u>

Hemodynamics were determined from the high-fidelity Millar LV pressure and volume data from each beat. After ventriculography-based calibration of conductance volume, LV pressure and volume at diastasis were measured beat-by-beat using a custom MATLAB program. Although relaxation is often fully complete at the end of the E-wave, when diastasis begins, to assure full relaxation and the passive state of the LV we analyzed data at the end of diastasis. We selected cardiac cycles having diastatic intervals during which pressure as a function of time was essentially constant or varied by < 2mmHg during all of diastasis. The end-diastasis points were defined by ECG P wave onset (28, 41). For each subject diastatic P-V data points were fit by linear regression, from which K_{CATH} was computed in the usual manner.

4.3.5 <u>Derivation of Pressure, Volume and Diastatic Stiffness from E-wave Analysis</u>

The change in volume of the left ventricle due to the E-wave is (28)

$$dV_{LV} = MVA \cdot v_E dt \qquad [4.3]$$

where *MVA* is the effective mitral valve area and v_E is E-wave velocity.

Therefore, the diastatic volume which is attained at the end of E-wave is:

$$V_{dias} = MVA \cdot \int_0^{\frac{\pi}{\omega}} v_E(t)dt + ESV \qquad [4.4]$$

where *MVA* is the effective (constant) mitral valve area and *ESV* is the constant of integration which is the end systolic volume or equivalently LV volume at mitral valve opening. The PDF formalism provides closed form algebraic expression for transmitral flow velocity *v(t)* as a function of time. Physiologically diastatic pressure (P_{dias}) and volume (V_{dias}) are achieved when the E-wave velocity becomes zero. The analog in the PDF model Equation [4.2] is when the damped sinusoid has its first zero crossing at $\omega t = \pi$, at time $t = \dfrac{\pi}{\omega}$. Using Equation [4.2] for *v(t)* and integrating yields the desired expression incorporating the PDF parameters given by:

$$V_{dias} = MVA \cdot |x_o| \cdot \left(\exp(\frac{-c\pi}{2\omega}) + 1 \right) + ESV \qquad [4.5]$$

For simplicity, *MVA* was approximated as constant (5 cm^2).

We can express LV pressure P in terms of *v(t)* and acceleration *dv(t)/dt* using Bernoulli's equation for non-steady flow (37, 38)

$$\Delta P = LAP - LVP = \frac{1}{2}\rho v_E^2 + \rho \int_{LA}^{LV} \frac{\partial v(s,t)}{\partial t} ds \qquad [4.6]$$

where LAP and LVP are left atrial (LA) and LV pressure, and ρ is the density of blood (1.06 g/ml). The integral can be rewritten as $M(dv_E/dt)$, where M (constant) is the mitral inertiance (28, 37, 38, 41).

Equation [4.6] becomes:

$$LVP = -\frac{1}{2}\rho v_E^2 - M\frac{dv_E}{dt} + LAP \qquad [4.7]$$

where M can be obtained at $t{=}DT,$ the time of pressure crossover, LAP=LVP (28, 41) yielding:

$$\Delta P = 0 = \frac{1}{2}\rho v_E^2\bigg|_{t=DT} + M\frac{dv_E}{dt}\bigg|_{t=Dt}$$

$$M = -\frac{\frac{1}{2}\rho v_E^2\big|_{t=DT}}{\frac{dv_E}{dt}\big|_{t=DT}} = \frac{1}{2}\rho x_o\left(\frac{\sqrt{k}}{c}\right)\exp\left(-\frac{c\cdot DT}{2}\right) \qquad [4.8]$$

where $DT = \frac{\pi}{\omega} - \frac{1}{\omega}\text{Arctan}\left(\frac{2\omega}{c}\right)$, denotes E-wave deceleration time, defined by the time from E-wave peak to E-wave termination. The sum of E-wave acceleration time (AT) and DT is equal to duration of E-wave (π/ω in PDF formalism) (34).

By setting time in Equation [4.7] equal to E-wave duration ($t = \frac{\pi}{\omega}$) and using Equation [4.8], the relation between the diastatic pressure involving PDF parameters can be derived:

126

$$P_{dias} = -\frac{1}{2}\rho\frac{x_o^2 k^{\frac{3}{2}}}{c}\exp\left(\frac{-c}{2}(\frac{\pi}{\omega} + DT)\right) + LAP \qquad\qquad [4.9]$$

where DT is the deceleration time of the E-wave, and LAP is t LA pressure approximated by its

mean, constant, but unknown value. Recall that in computing stiffness dP/dV =[dP/dt]/[dV/dt],

the derivatives of constants vanish. The P, V points so derived were fit via linear regression to

generate the D-PVR$_{\text{E-wave}}$ from whose slope, diastatic stiffness $K_{\text{E-wave}}$ was computed.

4.4 Results

4.4.1 Invasive and Non-invasive Diastatic Stiffness

We analyzed 444 beats from the datasets of 30 patients (~15 beats per person, 18 men). In accordance with the derivation, E-wave derived diastatic stiffness ($K_{E\text{-wave}}$) and diastatic stiffness derived from P-V data (K_{CATH}) were highly correlated ($R^2=0.92$) for all analyzed subjects (Figure 4.2).

Number of data sets =30 (444 cardiac cycles)
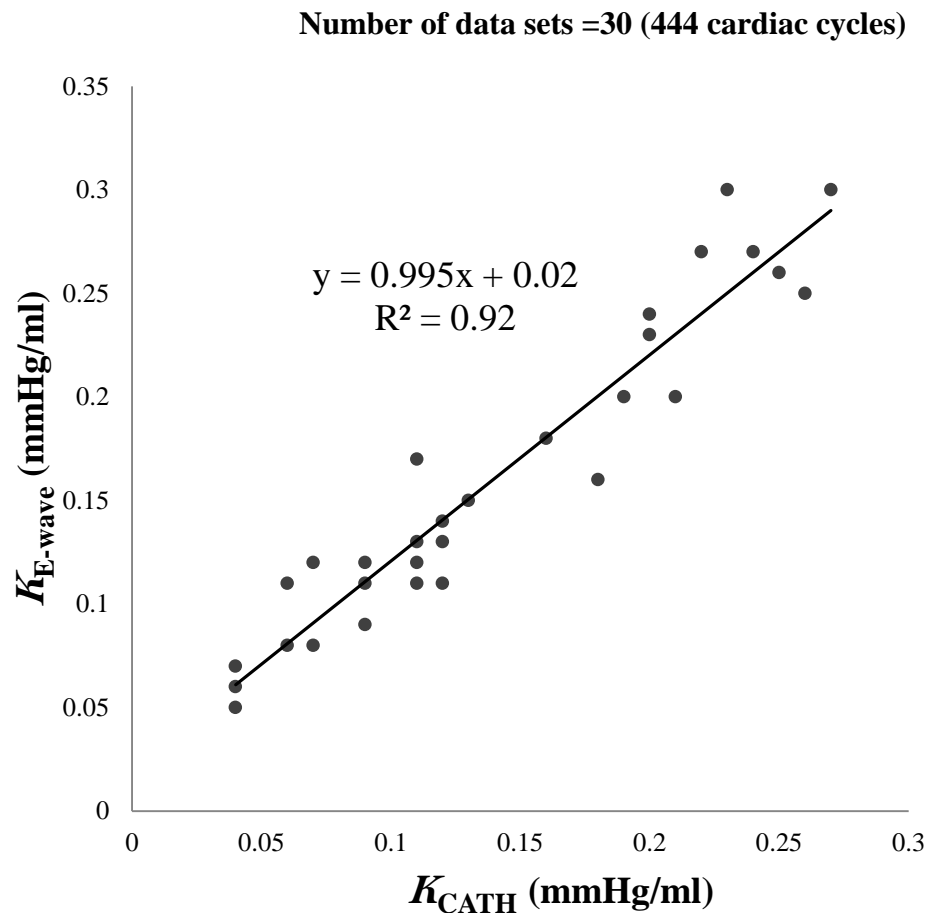
Figure 4.2 Correlation between P-V and E-wave derived diastatic stiffness.

Correlation between experimentally measured pressure-volume derived diastatic stiffness (K_{CATH}) as the ordinate and E-wave derived diastatic stiffness ($K_{E\text{-wave}}$) as the abscissa. The mean and standard deviation for both methods yields $K_{E\text{-wave (average)}} = 0.16 \pm 0.07$, $K_{CATH \text{ (average)}} = 0.14 + 0.07$. Alternatively the calculated confidence interval, with a level of significance of 0.05 (i.e. meaning a confidence level of 95%), for the mean stiffness of all 30 subjects for both methods, written as $K=K_{average} \pm \%95CI$ is: $K_{E\text{-wave}} = 0.16 \pm 0.03$, and $K_{CATH} = 0.14 + 0.03$. See Figure 4.4 and text for details.

For each subject D-PVR slope was computed using multiple beats using both E-wave and simultaneous beat-by-beat P-V data (Figure 4.3).

Number of beats = 15

$$y = 0.20\ x + 1.53$$
$$R^2 = 0.51$$

$$y = 0.21\ x - 3.56$$
$$R^2 = 0.50$$

- E-wave
- CATH
- —— D-PVR (E-wave)
- —— D-PVR (CATH)

Pressure-Diastasis (mmHg)

Volume-Diastasis (ml)
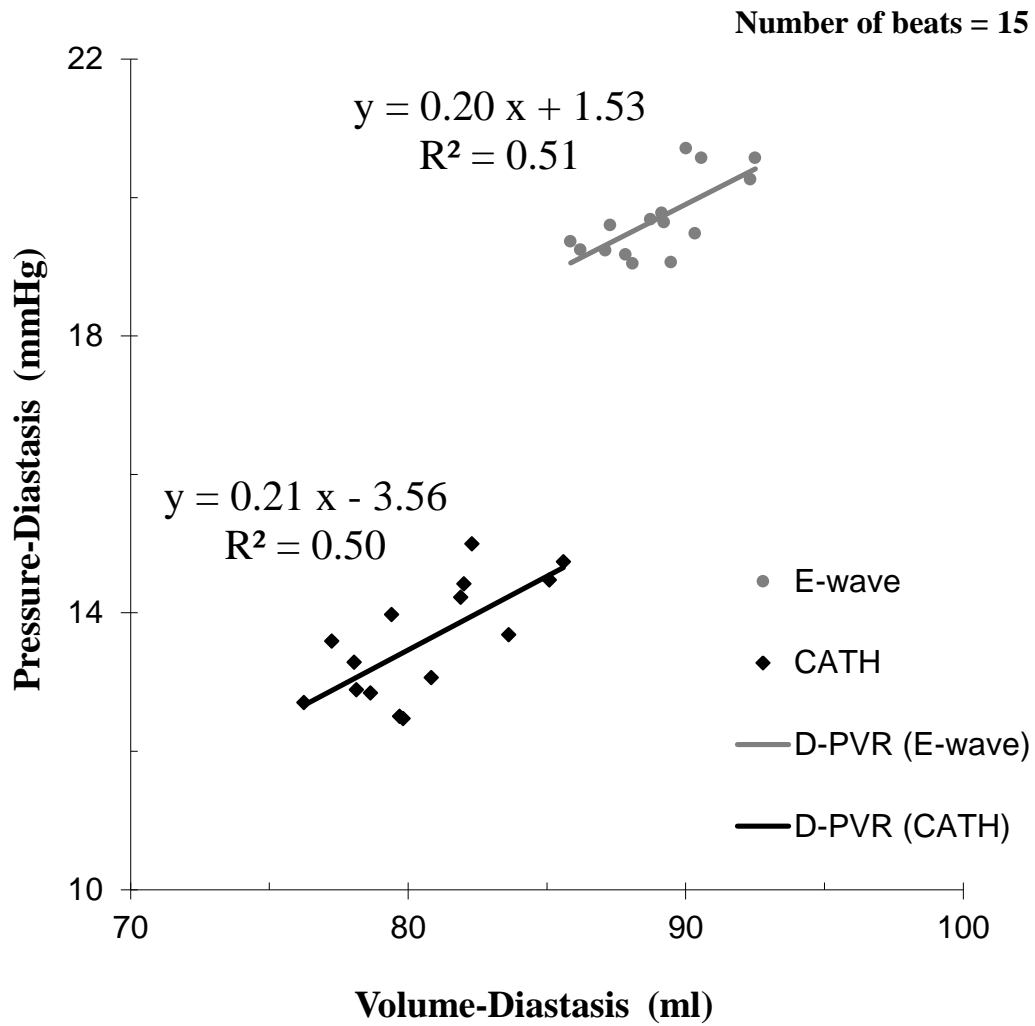
Figure 4.3 Diastatic stiffness from P-V data and E-wave analysis.

Diastatic stiffness is the slope (K_{CATH} = 0.21 mmHg/ml) of the (black) linear regression line for cath-based P-V data. Simultaneous E-wave derived P-V data provides the slope of the (gray) linear regression line ($K_{E\text{-}wave}$ = 0.20 mmHg/ml). Data for one typical subject is shown. Note expected offset between cath (absolute measurement method) vs. echo (relative measurement method) data but close similarity of regression slopes. Micromanometric conductance catheter P-V measurement precision is < 0.1 (mmHg), and 2 (ml). See text for details.

Analysis yielded a range of high correlation ($0.50 < R^2 < 0.84$) for the entire dataset. Individual linear regression values for each dataset are shown in Table 4.2.

Table 4.2 Individual diastatic stiffness (K_{CATH} and $K_{E\text{-wave}}$).

Individual least mean square linear regression slopes for diastatic pressure-volume relationship (K_{CATH} and $K_{E\text{-wave}}$) for 30 subjects.

Subject	$K_{E\text{-wave}}$		K_{CATH}	
	Linear fit slope	R^2	Linear fit slope	R^2
1	0.05	0.50	0.04	0.57
2	0.11	0.62	0.06	0.68
3	0.07	0.60	0.04	0.55
4	0.23	0.72	0.20	0.63
5	0.17	0.50	0.11	0.54
6	0.26	0.62	0.25	0.57
7	0.12	0.58	0.09	0.55
8	0.24	0.52	0.20	0.59
9	0.12	0.61	0.07	0.56
10	0.06	0.51	0.04	0.59
11	0.08	0.55	0.06	0.50
12	0.15	0.50	0.13	0.60
13	0.09	0.51	0.09	0.63
14	0.16	0.52	0.18	0.51
15	0.20	0.51	0.21	0.50

16	0.30	0.54	0.23	0.60
17	0.12	0.63	0.11	0.54
18	0.27	0.60	0.24	0.67
19	0.27	0.54	0.22	0.67
20	0.30	0.60	0.27	0.72
21	0.25	0.70	0.26	0.60
22	0.11	0.51	0.12	0.50
23	0.13	0.53	0.11	0.70
24	0.11	0.56	0.11	0.65
25	0.20	0.51	0.19	0.60
26	0.11	0.57	0.09	0.53
27	0.14	0.61	0.12	0.79
28	0.18	0.70	0.1	0.55
29	0.13	0.56	0.12	0.50
30	0.08	0.70	0.07	0.84

4.4.2 <u>Bland-Altman Analysis</u>

Bland-Altman analysis (Figure 4.4) shows that diastatic stiffness has very good agreement between the two (experimental vs. model-predicted) methods. Less than 5% of all measurements reside outside 1.96 SD of the percentage difference, in keeping with the criteria of Bland and Altman (3), representing a 95% confidence interval in the result. The solid line

represents the mean difference or the estimated bias. As expected, when comparing an absolute measurement method (cath) vs. a relative measurement method (echo) the bias is not exactly zero, indicating the expected systematic difference between the two methods.
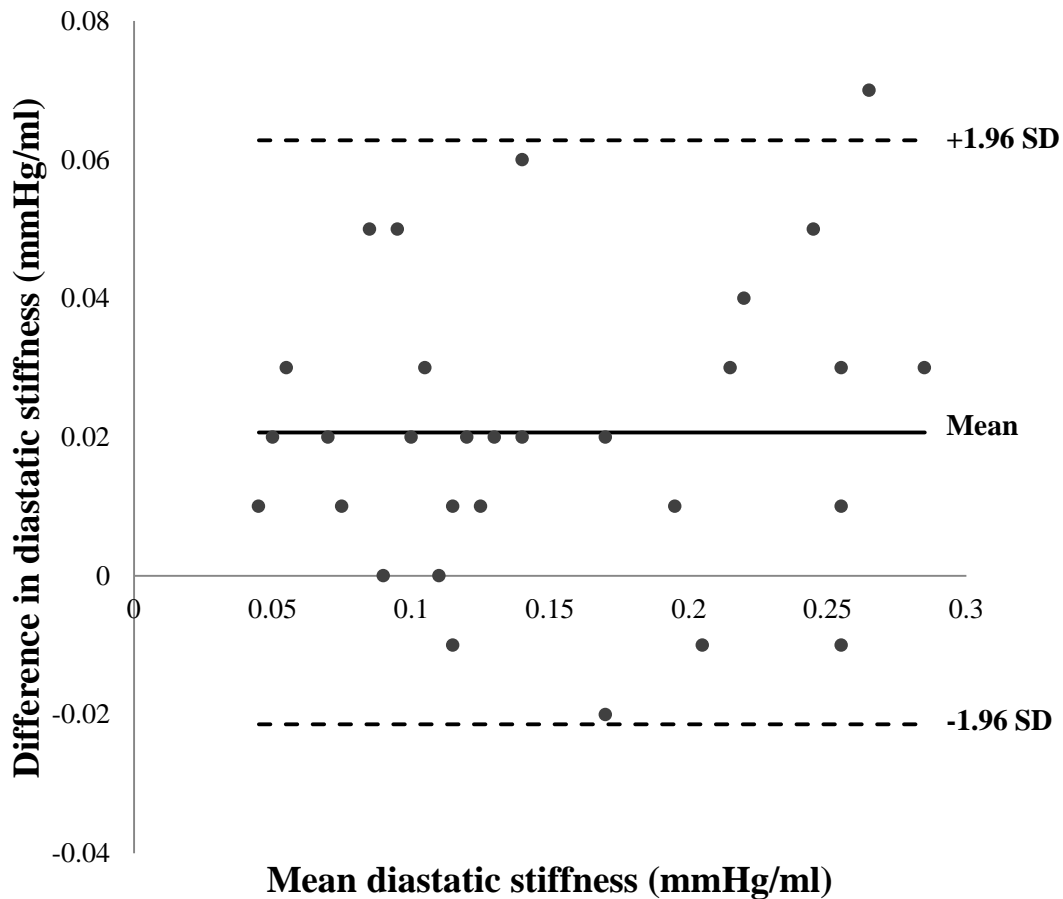
Figure 4.4 Bland-Altman plot of the diastatic stiffness measurement.
Less than 5% of all of the measurements lie outside 1.96 SD of the percent difference, assuring a 95% confidence in the measurement showing the equivalence of the two methods. The solid line represents the mean difference or the estimated bias. The dashed lines show the limits of agreement between two methods. The plots indicate very good agreement between both methods. See text for details.

4.5 Discussion

4.5.1 <u>Invasive Chamber Stiffness</u>

Chamber stiffness is an established determinant of DF (6, 36). Chamber stiffness – defined by the slope $\Delta P/\Delta V$ of the P-V relation has remained a key feature of cardiovascular physiology. A physiologically and thermodynamically more clearly defined state is achieved by the LV during diastasis – when wall motion and transmitral flow cease – and the chamber is in transient static equilibrium. Accordingly a method to determine passive diastatic chamber stiffness noninvasively constitutes an important advance.

4.5.2 <u>Non-invasive Chamber Stiffness</u>

E-waves are generated by the atrioventricular pressure gradient, not by the absolute values of either atrial or ventricular pressures by themselves, as such. Hence, E-wave information can only provide a relative measure concerning pressures. Similarly, chamber stiffness is defined by the slope (a relative measure) of the applicable P-V relationship, rather than where in the P-V plane, i.e. how far above the $P = 0$ axis, (an absolute measure) the P-V relationship resides. Therefore, it is legitimate to expect that suitable kinematic modeling and mathematical reasoning based analysis of a relative measure (Doppler E-wave) can provide diastatic (passive) chamber stiffness – another relative measure.

Doppler E-wave derived indexes of chamber stiffness such as K_{LV} have been proposed (25) but have important limitations, particularly when encountering the 'delayed relaxation' pattern, when the deceleration portion of the E-wave contour has an inflection point (1, 34).

133

Furthermore, K_{LV} determined from the DT of the E-wave was correlated with stiffness determined from the LV EDPVR (25), which is inscribed after atrial systole.

In previous work relating chamber stiffness to transmitral flow (24) for each subject one beat was used to determine the instantaneous stiffness during the E-wave, k_E and the corresponding $(\Delta P/ \Delta V)_E$ due to the E-wave itself. As in previous work (24) ΔP_E was defined as a difference between minimum LV pressure P_{min} and diastatic LV pressure P_{dias} and ΔV_E was the volume change due to the deceleration portion of the E-wave (after P_{min} up to P_{dias}). In contrast, in the present work we use the average value of k computed from 15 beats per subject using the duration of the entire E-wave while we determine the incremental change in volume ΔV during the entire E-wave from the volume channel of the conductance catheter. The beat-to-beat variation and range of values of P_{dias} and V_{dias} provides the P-V data points whose slope via linear regression yields the diastatic P-V relationship. To clarify further, in previous work $(\Delta P/\Delta V)_E$ relied on a combination of invasive (P) and non-invasive (ΔV_E) methods whereas in the present work, we used invasively (conductance catheter) recorded P-V data to compute diastatic stiffness and compare it to diastatic stiffness computed entirely non-invasively from E-wave analysis.

The present work seeks to establish a firmer causal line of reasoning by relating chamber stiffness at diastasis with stiffness derived from simultaneous E-waves ($K_{E\text{-wave}}$) via the Bernoulli equation. As the results indicate $K_{E\text{-wave}}$ and K_{CATH} are not only very tightly correlated with $K_{E\text{-wave}} = \alpha K_{CATH} + b$ (R^2=0.92), where $\alpha = 0.995$, and $b = 0.02$ as predicted but Bland-Altman analysis underscores the legitimacy of the causal relationship.

The value of diastatic stiffness (K_{CATH}) in the 30 subjects (Table 4.2) ranged from 0.04 mmHg/ml to 0.27 mmHg/ml. Interestingly, others have encountered the same range in humans

when making measurements of chamber stiffness (9).

Although encouraging, these methodologic results need to be viewed as preliminary while application in selected pathophysiologic groups is undertaken. However, the overall results reinforce the power of kinematic modeling and associated mathematical reasoning through which the full range of DF determinants can be characterized and elucidated.

4.6 Limitations

4.6.1 Conductance Volume

The conductance catheter method of volume determination has known limitations related to noise, saturation and calibration that we have previously acknowledged (2, 4, 21, 22, 24, 27, 28, 40). In this study, the channels which provided physiologically consistent P-V loops were selected. However, since there was no significant volume signal drift during recording, any systematic offset related to calibration of the volume channels did not affect the result when the limits of conductance volume was calibrated via quantitative ventriculography.

4.6.2 E-wave Selection

Although the PDF formalism is applicable to all E-waves, the most robust analysis is achieved for E-waves that have a clear termination and are followed by diastasis. E-wave analysis becomes less reliable when the A-wave merges with the E-wave and covers more than two-thirds of the E-wave deceleration portion. This typically occurs at HR > 90 beats/min (13). In the present study our inclusion criteria required use of datasets with clearly discernible E-waves followed by a diastatic interval (average heart rate= 62 bpm).

4.6.3 Application of Bernoulli's Equation

In deriving the expression for diastatic pressure (P_{dias}), we apply a form of the Bernoulli equation for an ideal fluid, where fluid viscosity is ignored. This approach has been applied by

previous investigators (37, 38) and studies have demonstrated its validity (10, 11).

4.6.4 <u>Assumption of Some Variables as Constants</u>

Although MVA, LAP and ESV may or may not be the same from subject to subject the key justification for not explicitly measuring them and including them is because they are 'absolute' metrics of the physiology. Our goal is to show that two independent measures of stiffness (a relative measure) are equivalent. In other words we are measuring the slope (derivative) of a straight line, rather than the absolute location (y-intercept) of the line. This is explicitly shown in Figure 4.3, where the offset of the two sets of data points is explained by treating some absolute variables as constants.

4.6.5 <u>Sample Size</u>

The number of datasets (n=30) is a minor limitation to the study, since the total number of cardiac cycles analyzed (n=444) mitigates it to an acceptable degree.

4.7   Conclusions

We derived diastatic stiffness $K_{\text{E-wave}}$ from E-wave based kinematic modeling and Bernoulli's equation. We utilized in-vivo, human, simultaneous P-V and transmitral echocardiographic E-wave data for validation. Our results show that kinematic modeling predicted diastatic chamber stiffness $K_{\text{E-wave}}$ using echo data is experimentally validated using P-V loop derived diastatic chamber stiffness K_{CATH}. This novel method of echocardiographic, quantitative DF assessment facilitates accurate *in-vivo* determination of passive (diastatic) chamber stiffness.

4.8   References

1.   **Appleton CP, Hatle LK, and Popp RL**. Relation of transmitral flow velocity patterns to left ventricular diastolic function: new insights from a combined hemodynamic and Doppler echocardiographic study. *J Am Coll Cardiol* 12: 426-440, 1988.

2.   **Bauman L, Chung CS, Karamanoglu M, and Kovács SJ**. The peak atrioventricular pressure gradient to transmitral flow relation: kinematic model prediction with in vivo validation. *J Am Soc Echocardiogr* 17: 839-844, 2004.

3.   **Bland JM, and Altman DG**. Statistical methods for assessing agreement between two methods of clinical measurement. *Lancet* 1: 307-310, 1986.

4.   **Chung CS, Ajo DM, and Kovács SJ**. Isovolumic pressure-to-early rapid filling decay rate relation: model-based derivation and validation via simultaneous catheterization echocardiography. *J Appl Physiol (1985)* 100: 528-534, 2006.

5.   **Chung CS, and Kovács SJ**. Physical determinants of left ventricular isovolumic pressure decline: model prediction with in vivo validation. *Am J Physiol Heart Circ Physiol* 294: H1589-1596, 2008.

6.   **Chung CS, Strunc A, Oliver R, and Kovács SJ**. Diastolic ventricular-vascular stiffness and relaxation relation: elucidation of coupling via pressure phase plane-derived indexes. *Am J Physiol Heart Circ Physiol* 291: H2415-2423, 2006.

7.   **Courtois M, Kovács SJ, and Ludbrook PA**. Transmitral pressure-flow velocity relation. Importance of regional pressure gradients in the left ventricle during diastole. *Circulation* 78: 661-671, 1988.

8.   **Dent CL, Bowman AW, Scott MJ, Allen JS, Lisauskas JB, Janif M, Wickline SA, and Kovács SJ**. Echocardiographic characterization of fundamental mechanisms of abnormal diastolic filling in diabetic rats with a parameterized diastolic filling formalism. *J Am Soc Echocardiogr* 14: 1166-1172, 2001.

9.   **Dumont CA, Monserrat L, Peteiro J, Soler R, Rodriguez E, Bouzas A, Fernández X, Pérez R, Bouzas B, and Castro-Beiras A**. Relation of left ventricular chamber stiffness at rest to exercise capacity in hypertrophic cardiomyopathy. *Am J Cardiol* 99: 1454-1457, 2007.

10.	**Falsetti HL, Verani MS, Chen CJ, and Cramer JA**. Regional pressure differences in the left ventricle. *Cathet Cardiovasc Diagn* 6: 123-134, 1980.

11.	**Firstenberg MS, Vandervoort PM, Greenberg NL, Smedira NG, McCarthy PM, Garcia MJ, and Thomas JD**. Noninvasive estimation of transmitral pressure drop across the normal mitral valve in humans: importance of convective and inertial forces during left ventricular filling. *J Am Coll Cardiol* 36: 1942-1949, 2000.

12.	**Garcia MJ, Thomas JD, and Klein AL**. New Doppler echocardiographic applications for the study of diastolic function. *J Am Coll Cardiol* 32: 865-875, 1998.

13.	**Hall A, and Kovács S**. Processing parameter effects on the robustness of the solution to the "Inverse Problem" of diastole from Doppler echocardiographic data. *15th Annual International Conference, IEEE Engineering in Medicine & Biology Society* I385-387, 1993.

14.	**Hall AF, and Kovács SJ**. Automated method for characterization of diastolic transmitral Doppler velocity contours: early rapid filling. *Ultrasound Med Biol* 20: 107-116, 1994.

15.	**Haney S, Sur D, and Xu Z**. Diastolic heart failure: a review and primary care perspective. *J Am Board Fam Pract* 18: 189-198, 2005.

16.	**Kass DA**. Assessment of diastolic dysfunction. Invasive modalities. *Cardiol Clin* 18: 571-586, 2000.

17.	**Kass DA, Bronzwaer JG, and Paulus WJ**. What mechanisms underlie diastolic dysfunction in heart failure? *Circ Res* 94: 1533-1542, 2004.

18.	**Khouri SJ, Maly GT, Suh DD, and Walsh TE**. A practical approach to the echocardiographic evaluation of diastolic function. *J Am Soc Echocardiogr* 17: 290-297, 2004.

19.	**Kovács S, MD M, and CS P**. Modelling cardiac fluid dynamics and diastolic function. *Philosophical Transactions of the Royal Society (A)* 359: 1299-1314, 2001.

20.	**Kovács SJ, Barzilai B, and Pérez JE**. Evaluation of diastolic function with Doppler echocardiography: the PDF formalism. *Am J Physiol* 252: H178-187, 1987.

21.	**Kovács SJ, Meisner JS, and Yellin EL**. Modeling of diastole. *Cardiol Clin* 18: 459-487, 2000.

22.	**Kovács SJ, Setser R, and Hall AF**. Left ventricular chamber stiffness from model-based

image processing of transmitral Doppler E-waves. *Coron Artery Dis* 8: 179-187, 1997.

23.   **Lisauskas J, Singh J, Courtois M, and Kovács SJ**. The relation of the peak Doppler E-wave to peak mitral annulus velocity ratio to diastolic function. *Ultrasound Med Biol* 27: 499-507, 2001.

24.   **Lisauskas JB, Singh J, Bowman AW, and Kovács SJ**. Chamber properties from transmitral flow: prediction of average and passive left ventricular diastolic stiffness. *J Appl Physiol (1985)* 91: 154-162, 2001.

25.   **Little WC, Ohno M, Kitzman DW, Thomas JD, and Cheng CP**. Determination of left ventricular chamber stiffness from the time for deceleration of early left ventricular filling. *Circulation* 92: 1933-1939, 1995.

26.   **Maeder MT, and Kaye DM**. Heart failure with normal left ventricular ejection fraction. *J Am Coll Cardiol* 53: 905-918, 2009.

27.   **Mossahebi S, and Kovács SJ**. The isovolumic relaxation to early rapid filling relation: kinematic model based prediction with in vivo validation. *Physiol Rep* 2: e00258, 2014.

28.   **Mossahebi S, Shmuylovich L, and Kovács SJ**. The thermodynamics of diastole: kinematic modeling-based derivation of the P-V loop to transmitral flow energy relation with in vivo validation. *Am J Physiol Heart Circ Physiol* 300: H514-521, 2011.

29.   **Nagueh SF, Appleton CP, Gillebert TC, Marino PN, Oh JK, Smiseth OA, Waggoner AD, Flachskampf FA, Pellikka PA, and Evangelista A**. Recommendations for the evaluation of left ventricular diastolic function by echocardiography. *J Am Soc Echocardiogr* 22: 107-133, 2009.

30.   **Nishimura RA, and Tajik AJ**. Evaluation of diastolic filling of left ventricle in health and disease: Doppler echocardiography is the clinician's Rosetta Stone. *J Am Coll Cardiol* 30: 8-18, 1997.

31.   **Oki T, Tabata T, Mishiro Y, Yamada H, Abe M, Onose Y, Wakatsuki T, Iuchi A, and Ito S**. Pulsed tissue Doppler imaging of left ventricular systolic and diastolic wall motion velocities to evaluate differences between long and short axes in healthy subjects. *J Am Soc Echocardiogr* 12: 308-313, 1999.

32.   **Omens JH, and Fung YC**. Residual strain in rat left ventricle. *Circ Res* 66: 37-45, 1990.

33.   **Riordan MM, Chung CS, and Kovács SJ**. Diabetes and diastolic function: stiffness and relaxation from transmitral flow. *Ultrasound Med Biol* 31: 1589-1596, 2005.

34.   **Shmuylovich L, and Kovács SJ**. E-wave deceleration time may not provide an accurate determination of LV chamber stiffness if LV relaxation/viscoelasticity is unknown. *Am J Physiol Heart Circ Physiol* 292: H2712-2720, 2007.

35.   **Støylen A, Slørdahl S, Skjelvan GK, Heimdal A, and Skjaerpe T**. Strain rate imaging in normal and reduced diastolic function: comparison with pulsed Doppler tissue imaging of the mitral annulus. *J Am Soc Echocardiogr* 14: 264-274, 2001.

36.   **Suga H, Sagawa K, and Shoukas AA**. Load independence of the instantaneous pressure-volume ratio of the canine left ventricle and effects of epinephrine and heart rate on the ratio. *Circ Res* 32: 314-322, 1973.

37.   **Thomas JD, Newell JB, Choong CY, and Weyman AE**. Physical and physiological determinants of transmitral velocity: numerical analysis. *Am J Physiol* 260: H1718-1731, 1991.

38.   **Yellin E**. *Mitral Valve Motion, Intracardiac Dynamics and Flow Pattern Modelling: Physiology and Pathophysiology. In: Advances in Cardiovascular Physics*. Basel, Switzerland: 1983, p. 137-161.

39.   **Zhang W, Chung CS, Shmuylovich L, and Kovács SJ**. Is left ventricular volume during diastasis the real equilibrium volume, and what is its relationship to diastolic suction? *J Appl Physiol (1985)* 105: 1012-1014, 2008.

40.   **Zhang W, and Kovács SJ**. The diastatic pressure-volume relationship is not the same as the end-diastolic pressure-volume relationship. *Am J Physiol Heart Circ Physiol* 294: H2750-2760, 2008.

41.   **Zhang W, Shmuylovich L, and Kovács SJ**. The E-wave delayed relaxation pattern to LV pressure contour relation: model-based prediction with in vivo validation. *Ultrasound Med Biol* 36: 497-511, 2010.

42.   **Zile MR, and Brutsaert DL**. New concepts in diastolic dysfunction and diastolic heart failure: Part I: diagnosis, prognosis, and measurements of diastolic function. *Circulation* 105: 1387-1393, 2002.

Chapter 5: Chamber Stiffness Determination in Atrial Fibrillation vs. Normal Sinus Rhythm

5.1 Abstract

Echocardiographic diastolic function (DF) assessment remains a challenge in atrial fibrillation (AF), because indexes such as E/A cannot be used and because chronic, rate controlled AF causes chamber remodeling. To determine if echocardiography can accurately characterize diastolic chamber properties we compared 15 chronic AF subjects to 15, age matched normal sinus rhythm (NSR) subjects using simultaneous echocardiography-cardiac catheterization (391 beats analyzed). Conventional DF parameters (DT, E_{peak}, AT, E_{dur}, E-VTI, E/E') and validated, E-wave derived, kinematic modeling based chamber stiffness parameter (k), were compared. For validation, chamber stiffness (*dP/dV*) was independently determined from simultaneous, multi-beat P-V loop data. Results show that neither AT, E_{peak} nor E-VTI differentiated between groups. Although DT, E_{dur} and E/E' did differentiate between groups (DT_{NSR} vs. DT_{AF} $p < 0.001$, E_{durNSR} vs. E_{durAF} $p < 0.001$, E/E'$_{NSR}$ vs. E/E'$_{AF}$ $p < 0.05$), the model derived chamber stiffness parameter k was the only parameter specific for chamber stiffness, (k_{NSR} vs. k_{AF} $p < 0.005$). The invasive gold standard determined end-diastolic stiffness in NSR was indistinguishable from end-diastolic (i.e. diastatic) stiffness in AF ($p = 0.84$). Importantly, the analysis provided mechanistic insight by showing that diastatic stiffness in AF was significantly greater than diastatic stiffness in NSR ($p < 0.05$).

We conclude that passive (diastatic) chamber stiffness is increased in normal LVEF chronic, rate controlled AF hearts relative to normal LVEF NSR controls and that in addition to DT, the E-wave derived, chamber stiffness specific index k, differentiates between AF vs. NSR groups, even when invasively determined end-diastolic chamber stiffness fails to do so.

145

5.2 Introduction

Atrial fibrillation (AF) is strongly associated with heart failure, coronary artery disease (CAD), valvular heart disease, diabetes mellitus, and hypertension (11, 16). If present when AF manifests they are viewed as risk factors. However, the actual causal relationship between these comorbidities and AF is incompletely understood. The ultimate relationship is certainly more complex than the term 'risk factor' implies. The mechanisms by which risk factors cause AF and the long-term consequences of AF on diastolic chamber properties remain topics of investigation (10, 27). The 'epidemic' of heart failure with normal ejection fraction (3, 25, 33) has cast a spotlight on diastolic function (DF) and its determinants such as chamber stiffness, whose gold-standard method of measurement requires invasive, simultaneous, LV pressure and volume change ($\Delta P/\Delta V$) data. Doppler echocardiography is the standard method for DF assessment; with E-wave deceleration time (DT) being the most common chamber stiffness correlate (18). DF can also be analyzed via the Parametrized Diastolic Filling (PDF) formalism (Appendix 1) which provides unique E-wave derived chamber stiffness (k), chamber relaxation/viscoelasticity (c) and load (x_o) parameters (14). Importantly, k is specific for chamber stiffness whereas E-wave DT is jointly determined by LV chamber stiffness (k) and LV relaxation/viscoelasticity (c) (29).

The chamber stiffness gold standard is the end-diastolic pressure-volume relation (ED-PVR). Load-varying ED-PV data can be fit using exponential, power law, or linear functions (12). The slope, dP/dV of the ED-PVR is a relative index that defines chamber stiffness, whereas LVEDP itself is an absolute index (19).

We hypothesized that because echocardiography can compute only relative rather than absolute pressure related indexes, it should be able to determine whether chamber stiffness is

altered in AF compared to NSR. To test this hypothesis we compared conventional and PDF model-derived E-wave based chamber stiffness metrics between groups. For independent validation we analyzed simultaneous micromanometric pressure-volume data.

Considering the ED-PVR in the setting of chronic atrial fibrillation (AF) raises a concern. In normal sinus rhythm (NSR), the ED-PVR includes the effect of both (atrial and ventricular) chambers and therefore includes atrial contractile properties. In rate controlled AF, the ED-PVR lacks atrial contractile effects and relies only on diastatic chamber effects. Thus, comparison of NSR vs. AF stiffness that relies on end-diastole incorporates chamber properties confounded by atrial contraction, thereby masking potential differences in passive ventricular diastatic chamber stiffness (see Figure 5.1). Indeed, in NSR, stiffness measured at end-diastole is always greater than stiffness at diastasis (31, 35). Importantly, the D-PVR and the ED-PVR are distinguishable and distinct relations (35). Accordingly, chamber stiffness was computed at two distinct physiologic portions of (NSR) P-V loops, as the slope of the ED-PVR and the slope of the diastatic pressure-volume relation (D-PVR) (35).
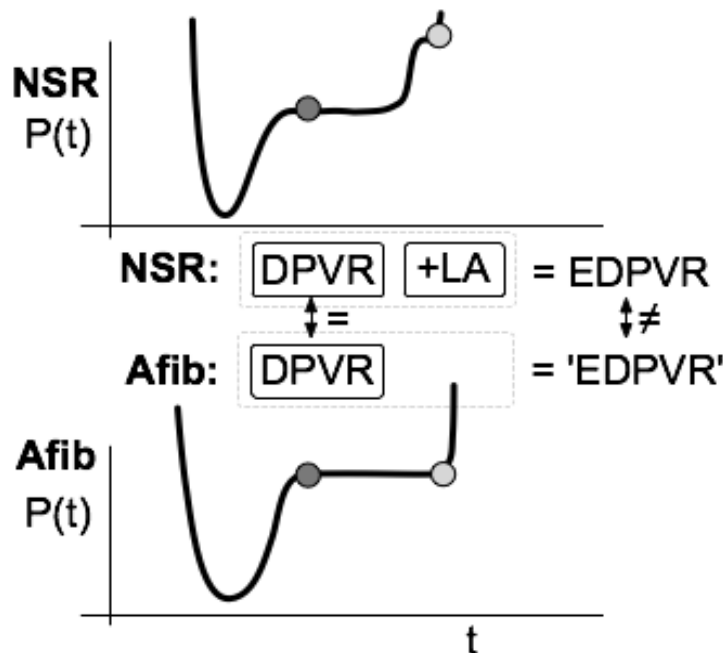
Figure 5.1 Schematic of LV pressure in NSR and AF.

In NSR, end-diastolic pressure and volume are jointly determined by diastolic LV chamber and systolic LA properties. In AF, diastasis and end-diastole inscribe the same pressure and volume values. Thus comparison of NSR vs. AF chamber stiffness requires comparison of diastatic rather than end-diastolic hemodynamics. NSR, normal sinus rhythm; Afib, atrial fibrillation; DPVR, diastatic pressure-volume relation; EDPVR, end-diastolic pressure-volume relation. See text for details.

5.3   Methods

5.3.1 Subject Selection

Thirty datasets were selected from the Cardiovascular Biophysics Laboratory database. All subjects were referred for elective cardiac catheterization and coronary angiography to rule out suspected coronary artery disease. All participants provided informed consent prior to the procedure using a protocol approved by the Washington University Human Research Protection Office (HRPO).

Fifteen subjects were in NSR, 15 subjects had chronic AF (average duration 7.2 ± 4.2 years) and were in AF during data acquisition. Selection criteria for the NSR group were: no active ischemia, normal valvular function, normal LV ejection fraction (LVEF$\geq$50%), no history of myocardial infarction, peripheral vascular disease, or bundle branch block, and clear diastatic intervals following E-waves. Selection criteria for the AF group were similar, with the exception that four of the 15 AF subjects had LVEF somewhat $< 50\%$. No subjects were in heart failure, and all subjects were normotensive at the time of data acquisition. Because our intent is to compare grouped averages primarily differentiated by AF vs. NSR physiology, we specifically included a range of LV end-diastolic pressures (LVEDP) encountered in practice, including elevated LVEDP. See Table 5.1.

Table 5.1 The clinical descriptors of NSR and AF groups.

Clinical Descriptors	NSR	AF Group	Significance
N	15	15	N.A.
Age (y)	62±9	61±9	0.65
Gender (M/F)	7/8	12/3	N.A.
Heart Rate (bpm)	66±7	76±9	<0.005
Ejection Fraction	76±12	55±17	<0.0005
Height (cm)	170±9	178±11	N.S.
Weight (kg)	88±12	99±19	N.S.

LVEF, left ventricular ejection fraction (via calibrated ventriculography); NSR, normal sinus rhythm; AF, atrial fibrillation; N.S., not significant; N.A., not applicable

Data are presented as mean ± standard deviation.

5.3.2   <u>Data Acquisition</u>

The high fidelity, simultaneous echocardiographic transmitral flow and pressure-volume data recording method has been previously described (5). Briefly, immediately prior to arterial access a complete 2-D echo-Doppler study is performed according to ASE criteria (8). After arterial access and placement of a 64-cm, 6-Fr sheath (Arrow, Reading, PA), a 6-Fr micromanometer conductance catheter (SPC-560, SPC-562, or SSD-1034, Millar Instruments, Houston, TX) was directed across the aortic valve under fluoroscopic control. Pressure and volume signals were processed through clinical amplifier systems (Quinton Diagnostics, General Electric, CD Leycom) and recorded by a custom PC via a standard interface (Sigma-5).

Simultaneous transmitral Doppler images were obtained (8). Using a clinical imaging system (Acuson, Sequoia C256, Mountain View, CA or Philips, Model iE33, Eindhoven, the Netherlands). Following data acquisition, end-systolic and end-diastolic volumes (ESV, EDV) were determined by calibrated quantitative ventriculography.

5.3.3   Load Variation

As previously described (35), respiratory physiologic load variation was present in all 30 datasets. In 10 out of 15 NSR subjects, additional physiologic load variation derived data included the recovery phase of the Valsalva maneuver. In the remaining 5 NSR subjects, additional load variation data included cardiac cycles following either catheter generated or isolated spontaneous premature ventricular contractions (PVC).

5.3.4   Data Analysis

After ventriculography-based calibration of volume, LV pressures and volumes at both diastasis (P_D, V_D) and end diastole (P_{ED}, V_{ED}) were determined for 8-12 cardiac cycles with a custom LabView interface (National Instruments, Austin, TX). For AF subjects, only cardiac cycles with R-R intervals generating essentially constant diastatic pressures and volumes following E-waves were included. Because of the time delay inherent in electro-mechanical coupling, end-diastole was identified by ECG R-wave peaks. ECG P-wave peaks identified end-diastasis for NSR, and by ECG R-wave peaks in AF subjects.

5.3.5 <u>Doppler E-wave Analysis</u>

Approximately 5 (continuous) Doppler transmitral E-wave contours per subject were selected and analyzed using the triangle shape approximations (1), yielding peak E-wave velocity (E_{peak}), deceleration time (DT), velocity-time integral (E-VTI), E/E', and peak A-wave velocity (A_{peak}).

The parameterized diastolic filling (PDF) formalism was also used to analyze E-waves (9, 14) to yield k_{AF}, k_{NSR} respectively. Specifically, k is the analog of invasively determined chamber stiffness (17).

The PDF Formalism

The kinematics of filling can be modeled using the Parametrized Diastolic Filling (PDF) formalism, which uses a linear, bi-directional spring to approximate early filling according to the motion of a damped, simple harmonic oscillator (SHO) (14). Newton's second law is the equation of motion:

$$\frac{d^2 x}{dt^2} + c_{PDF}\frac{dx}{dt} + k_{PDF}x = 0 \qquad\qquad [5.1]$$

where x (cm) is oscillator displacement, c_{PDF} is a damping (relaxation), and k_{PDF} is stiffness. Because the E-wave has zero initial velocity, the model's initial velocity is zero ($v(0)=0$). However, the SHO has a non-zero initial spring displacement, x_o. Systole stores elastic strain in tissue, which, at mitral valve opening, is available to power mechanical recoil and the ventricular suction process. The parameters c_{PDF} and k_{PDF} are computed per unit mass. The contour of the

clinical E-wave is predicted by the solution for the SHO velocity (Equation [5.1]), which for 'underdamped' motion is:

$$v(t) = -\frac{x_o k_{PDF}}{\omega} e^{-\alpha t} \sin(\omega t)$$ [5.2]

where $\alpha = c_{PDF}/2$, $\omega = \sqrt{4k_{PDF} - c_{PDF}^2}/2$. The determination of PDF parameters from each E-wave by solving the 'inverse problem' results in a unique set of x_o, c_{PDF}, and k_{PDF} (9) values for each E-wave. PDF stiffness parameter k_{PDF} is the analog of invasively measured chamber stiffness (15, 17). PDF relaxation/viscoelasticity parameter c_{PDF} is one of the two determinants of E- wave deceleration time (29) and it differentiates diabetic hearts from non-diabetic controls (7, 26).

To obtain x_o, c, and k, ultrasonic images are cropped, the mitral E-wave maximum velocity envelope is identified and fit by the PDF solution to the E-wave using the Levenberg-Marquardt algorithm (23) to yield the best-fit x_o, c, and k parameters as well as a measure of goodness of fit. The fitting process is achieved using a custom LABVIEW (National Instruments, Austin, TX) interface (9). Additional PDF-derived DF indexes include: 1) stored elastic strain energy available for ventricular suction ($1/2kx_o^2$) (20), 2) the volume equivalent delivered by a unit amount of potential energy ($VTI_E/(1/2kx_o^2)$), 3) the peak atrio-ventricular pressure gradient (kx_o) (2) and 4) the load independent index of diastolic function M obtained as the slope of the kx_o vs. cE_{peak} regression relation obtained from load-varying E-waves (30).

5.3.6 <u>Multiple Beat Estimates of Stiffness</u>

To construct the ED-PVR, and D-PVR V_{ED}, P_{ED} and V_D, P_D were measured at physiologically varying load states as previously described (35). Thus for each subject the ED-PVR was generated by the best-fit linear regression to the 8-12 measured (V_{ED}, P_{ED}) locus of points (see Figure 5.2). Previous work (35) showed that linear or exponential fits yielded similar goodness of fit (by mean square error), and therefore linear regression was used. The D-PVR was generated similarly using (V_D, P_D) data. For the AF group, end-diastatic and end-diastolic data was identical, hence only a D-PVR was generated.

For NSR subjects chamber stiffness was determined from both ED-PVR and D-PVR slopes (dP/dV_{NSR-ED}, dP/dV_{NSR-D} respectively) whereas, for AF subjects chamber stiffness was computed from the D-PVR slope (dP/dV_{AF}). It is generally accepted that LV relaxation is complete after an elapsed time of 3.5 tau after peak –dP/dt. To minimize the possible effect of insufficient time to achieve relaxation in generating the D-PVR we took care to use P, V data recorded at the END of diastasis, both in NSR (ECG P-wave) and in AF (ECG R-wave). Tau values for all subjects indicate that on average in NSR 6 tau intervals elapsed between peak -dP/dt and end-diastasis, while at least 4 tau intervals elapsed between peak -dP/dt and end-diastasis in AF.
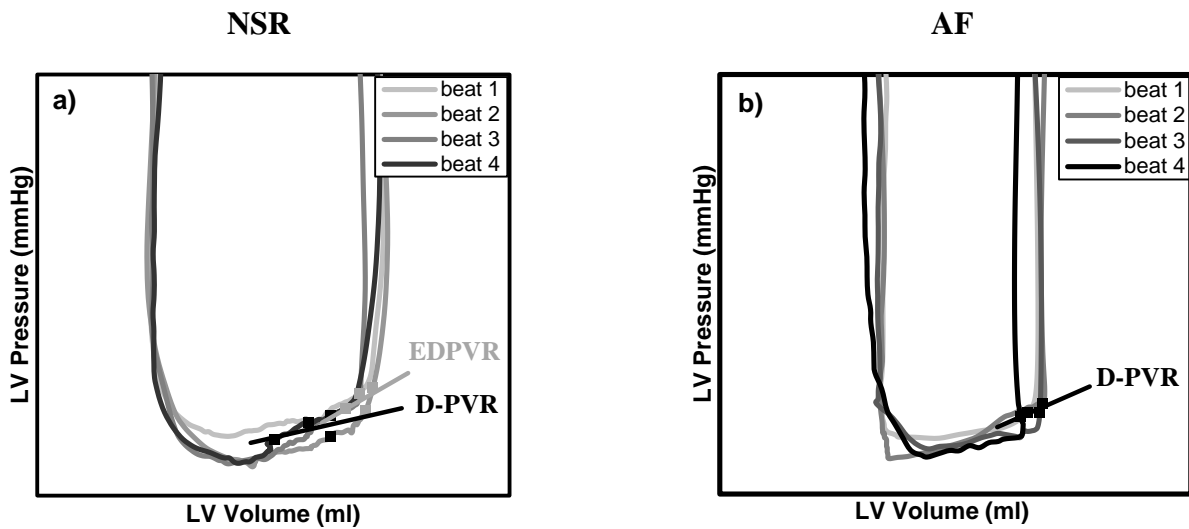
Figure 5.2 P-V loops, D-PVR and ED-PVR of NSR subject and D-PVR of AF subject.

In-vivo pressure-volume loops showing diastatic pressure-volume relation (D-PVR) and end-diastolic pressure-volume relation (ED-PVR) from selected NSR subject (panel a) and D-PVR for selected AF subject (panel b). For clarity only 4 of 10 analyzed beats are shown. Black line, D-PVR via linear regression for all 10 beats. Gray line, ED-PVR in NSR subject via linear regression for all 10 beats. See text for details.

5.3.7 <u>Statistical Analysis</u>

For each subject, parameters were averaged for the beats selected. Within the NSR group P_D, V_D and dP/dV_{NSR-D} were compared to P_{ED}, V_{ED} and dP/dV_{NSR-ED} by paired t-test. Comparisons of dP/dV, DT, k, and other parameters between NSR and AF groups were carried out by Student's t-test using MS-Excel (Microsoft, Redmond, WA).

5.4   Results

5.4.1 Absolute Index (Volume and Pressure) Comparison

NSR diastatic volumes and pressures were significantly smaller than corresponding NSR end-diastolic pressures and volumes (V_D vs. V_{ED}:   118±31ml vs. 153±26ml $p<0.001$; P_D: 13±3mmHg vs. 19±5mmHg $p<0.001$). Diastatic (same as end-diastolic) pressures and volumes in the AF group were indistinguishable from end-diastolic pressures and volumes in the NSR group (AF V_D vs. NSR V_{ED}: 169±56ml vs. 153±26ml, $p=0.96$; AF P_D vs. NSR P_{ED}: 18±4 mmHg vs. 19±5 mmHg, $p=0.51$). See Table 5.2 for additional hemodynamic details.

5.4.2 Conventional Index Comparison

The groups were age matched with AF (62±9 yrs) vs. NSR (61±9 yrs) yielding $p=0.65$. Heart rate in AF was higher than in NSR (76±9 bpm vs. 66±7, $p<0.005$). E-wave peak (E_{peak}) in AF and NSR were similar (0.90±0.28 m/s vs. 0.76±0.17 m/s, respectively, $p=0.12$). E-wave velocity-time integral (E-VTI) in AF and NSR were indistinguishable (11.4±0.04 cm vs. 11.2±0.03 cm, respectively, $p=0.93$). Peak E-wave to peak E'-wave ratio (E/E') in AF was higher than in NSR (6.0±1.9 vs. 4.7±1.8, respectively, $p<0.05$). Both groups had normal mean LVEF>50%, although LVEF in the NSR group tended to be higher 76±12% vs. 55±17% in the AF group. If the four AF subjects with LVEF <50% are removed from the intergroup comparison, the p value becomes 0.2 and all of the conclusions remain unchanged.

5.4.3 <u>Relative Index (Chamber Stiffness) Comparison</u>

Invasive Measures of Chamber Stiffness

Concordant with previous findings (35), chamber stiffness in the NSR group at end-diastole, from the ED-PVR ($dP/dV_{\text{NSR-ED}}$) was significantly greater than stiffness measured at diastasis, from the D-PVR ($dP/dV_{\text{NSR-D}}$) (0.16±0.10 mmHg/ml vs. 0.10±0.07 mmHg/ml $p<0.001$). Between AF and NSR groups, comparing the hemodynamics at the same phase of diastole, revealed that diastatic chamber stiffness, $dP/dV_{\text{AF-D}}$ was significantly higher than diastatic chamber stiffness $dP/dV_{\text{NSR-D}}$ (0.16±0.08 mmHg/ml vs. 0.10±0.07 mmHg/ml, $p<0.05$) in NSR.

Noninvasive Measures of Chamber Stiffness

E-wave deceleration time (DT) was significantly shorter in AF than in NSR (170±21 msec vs. 210±26msec, $p<0.001$). The PDF stiffness parameter in AF was significantly higher than in NSR (k_{AF} vs. k_{NSR}: 249±75/s^2 vs. 183±35/s^2, $p<0.005$). Higher k means increased stiffness.

Table 5.2 Hemodynamic and echocardiographic data in NSR and AF groups.

	NSR	AF (n=15)	p	p NSR_{ED} vs. NSR_D
Hemodynamic Parameters:				
P_{ED} (mmHg)	19±5	18±4	0.51	<0.001
V_{ED} (ml)	153±26	169±56	0.96	<0.001
P_D (mmHg)	13±3	18±4	<0.005	
V_D (ml)	118±31	169±56	<0.005	
dP/dV_{ED} (mmHg/ml)	0.16±0.10	0.16±0.08	0.84	<0.001
dP/dV_D (mmHg/ml)	0.10±0.07	0.16±0.08	<0.05	
Echocardiographic Parameters				
Peak E-wave velocity (E_{peak})	76±17	90±28	0.12	
E-wave acceleration time (AT)	92±9	87±17	0.32	
E-wave deceleration time (DT)	210±26	170±21	<0.001	
E-wave duration time (E_{dur}) (ms)	302±30	257±34	<0.001	
k_{PDF} ($1/s^2$)	183±35	249±75	<0.005	
E-VTI (cm)	11.2±0.03	11.4±0.04	0.93	
E/E'	4.7±1.8	6.0±1.9	<0.05	

AF, atrial fibrillation; NSR, normal sinus rhythm; NSR_{ED} , end-diastolic values for NSR group; NSR_D , diastatic values for NSR group; P_{ED}, left ventricular end-diastolic pressure; V_{ED}, left ventricular end-diastolic volume; P_D, left ventricular diastatic pressure. V_D, left ventricular diastatic volume; E_{peak}, peak E-wave velocity; AT, E-wave acceleration time; DT, E-wave deceleration time; E_{dur}, E-wave duration; k_{PDF}, Kinematic model-based, E-wave derived chamber stiffness; E-VTI, E-wave velocity-time integral; E/E', ratio of E_{peak} and Peak E'-wave velocity N.A., not applicable.

Data are presented as mean ± standard deviation.

5.5   Discussion

5.5.1 <u>Noninvasive Indexes</u>

We assessed E-wave derived chamber stiffness (DT, k) (15, 17, 18) in NSR and AF groups. To validate E-wave predicted stiffness we used chamber stiffness from simultaneous catheterization-derived multiple beat P-V data.

The PDF derived chamber stiffness k and DT both showed significant difference between the AF and NSR groups, with the AF group having increased stiffness. The shorter DT in the AF group is <u>not</u> due to the higher average heart rate (HR) of the AF group because all AF E-waves were followed by a diastatic interval. As long as diastasis is present, E-wave DT remains essentially unchanged as HR increases (6) while diastasis shortens. In addition, it is relevant that E-wave DT is determined <u>jointly</u> by stiffness and relaxation (k_{PDF} and c_{PDF} in PDF formalism terminology) rather than stiffness alone (29), and therefore k_{PDF} is the physiologically more specific index of stiffness than DT.

5.5.2 <u>Invasive Indexes</u>

Stiffness measures use end-diastolic P-V data. In chambers with chronic AF, however, end-diastole and diastasis (when R-R intervals are sufficiently long) are physiologically and hemodynamically the same (same point on the P-V plane). This is not the case in NSR. This and previous work (35) show that in NSR, the diastatic and end-diastolic PVR are physiologically distinct and distinguishable. The feature responsible for this distinction is atrial systole, which

expands the ventricle beyond its diastatic, equilibrium volume. This stiffens the chamber at end-diastole with the concomitant confounding of the ED-PVR by atrial systolic properties.

In NSR diastatic stiffness, is consistently lower than at end-diastole, after atrial systole. As a result, end-diastolic stiffness between AF and NSR groups would systematically overestimate NSR stiffness relative to AF stiffness. Indeed in the current work, AF chamber stiffness (0.16±0.08 mmHg/ml) is indistinguishable from NSR chamber stiffness (0.16±0.10 mmHg/ml) measured at <u>end-diastole</u> (p=0.84). The AF chamber stiffness (0.16±0.08 mmHg/ml) measured at <u>diastasis</u> is significantly (p<0.05) higher than diastatic NSR chamber stiffness (0.10±0.07 mmHg/ml). These are concordant with the simultaneous, and independent chamber stiffness findings from E-wave DT and the PDF formalism parameter k. Hence, when diastatic phases are not matched, and are merely referred to as 'diastolic chamber stiffness' the significant differences between AF and NSR stiffness is lost (dP/dV_{AF-D} vs. dP/dV_{NSR-ED}: 0.16±0.08 mmHg/ml vs. 0.16±0.10 mmHg/ml, p=0.84).

Although elucidation of mechanisms is beyond the scope of the current work, the likeliest explanation for the increased diastatic stiffness observed in chronic AF vs. NSR is chamber remodeling (4, 13, 21, 24).

5.5.3 <u>Equilibrium Volume</u>

Diastasis defines the hemodynamic/physiologic P-V point for passive chamber stiffness measurement. Elastic elements, displaced from equilibrium by systole, recoil toward their equilibrium diastatic position and power suction-initiated early rapid filling. At diastasis there is no bulk tissue or fluid movement and the chamber is momentarily static; there is no

atrioventricular pressure gradient, no net force, and no net flow. As previously detailed (28, 34), diastasis defines the in-vivo equilibrium chamber volume, and represents the most relaxed and passive in-vivo state. Displacement above equilibrium volume by atrial systole loads elastic elements and couples the contracted atrium itself in series with a now, passively stretched ventricle, generating a state stiffer than the relaxed diastatic state (35). Thus while conventionally one uses end-diastole for chamber stiffness, measuring stiffness at the equilibrium (diastatic) volume provides a physiologically more accurate measure of actual passive stiffness.

5.5.4   Chamber Stiffness in Sinus Rhythm and Atrial Fibrillation

There are few studies that compare DF between AF and NSR groups. Pozzoli et al followed heart failure subjects over 2 years and compared DF parameters between 18 subjects that developed chronic AF, and 34 control subjects in NSR (22). While they found values of DT consistent with the current study, and a decrease in DT between AF and NSR subjects, the difference was not significant. However all of their subjects had systolic heart failure (average EF=25%). In contrast, all NSR subjects in the current study had normal EF, and this may help explain the more significant DT difference between groups observed in the current study. Furthermore, Pozzoli et al did not include simultaneous, invasive measures of chamber stiffness to support their echocardiographic DT based findings.

Takagaki et al, compared myocardial compliance in sheep before and after induction of atrial fibrillation (32). This is the only other AF vs. NSR invasive study where chamber stiffness was compared. Interestingly, they found no difference in invasive ED-PVR results between AF

and NSR. However, they compared 'end-diastole' in AF with 'end-diastole' in NSR. End-diastole in (rate controlled) AF allows achievement of diastasis, and therefore a comparison of the D-PVR between AF and NSR sheep in the Takagaki et al study would have been more appropriate. Indeed, we found that chamber stiffness between AF and NSR groups showed no significant difference when end-diastole was used, but showed significant difference when diastasis was employed. By using end-diastole, Takagaki et al likely over-estimated the NSR chamber stiffness relative to AF Another important difference between the Takagaki study and the present work is that our subjects had chronic AF of several years duration – and therefore sufficient time for chamber remodeling - whereas the Takagaki study measured compliance before and after induction of AF.

5.6   Limitations

5.6.1 <u>Conductance Volume</u>

The conductance catheter method of volume determination has known limitations related

to noise, saturation and calibration that we have previously acknowledged (1, 5, 17, 35). Only

physiologically consistent P-V loops were selected and averaged. If the two absolute measures

(ESV, EDV) have slight systematic differences, resulting in a systematic volume calibration

offset, the absolute values of the slopes could be innacurate. However, comparison of slopes

between groups remain valid, because a systematic offset would affect all measurements equally.

Indeed the absolute location of the D-PVR or ED-PVR in the pressure-volume axes should not

affect the slope of the pressure-volume relation.

As previously (35), the P-V measurements in NSR subjects utilized ECG R- and P-

waves having an interobserver dependence of <5%.

5.6.2 <u>Load Variation Approach</u>

An average of 7 beats per subject in NSR and 19 beats per subject in AF were used to

construct respective D-PVR because in NSR, the observed physiologic load variation was

primarily the result of respiration, with PVC or Valsalva also utilized. For PVC and Valsalva the

D-PVR was measured during the compensatory period. Although the amount of load variation

after these maneuvers is modest, the P-V relationship constructed from an average of 7 beats in

NSR is sufficient (35). In contrast we used only respiratory variation in AF patients to determine

D-PVR, so a greater number of cardiac cycles per subject was included in the analysis. Previous

D-PVR work (35), demonstrated that even though the heart may respond differently to Valsalva maneuver and PVC, the D-PVR and ED-PVR measurements using the two load-varying methods do not differ significantly.

In P-V relationship determining physiology experiments, inotropic state may be varied by pharmacologic means. Data obtained during the course of cardiac catheterization and the associated informed consent procedure did not allow for interventions involving external (non-physiologic) inotropic agents. This limitation is obviated by the fact that load variation was entirely physiologic and did not activate reflex mechanisms associated with pharmacologic interventions.

5.6.3   Heart Rate Limitation

The D-PVR requires the presence of diastasis and therefore a suitable HR. In the current study HR was such that every analyzed cardiac cycle in AF or NSR had a clear, diastatic pressure interval and an E-wave followed by diastasis.

5.7   Conclusions

We determined if echocardiography is able to reliably characterize chamber properties in AF vs. NSR. Conventional DF parameters (DT, E_{peak}, AT, E_{dur}, E-VTI, E/E',) and E-wave derived, stiffness specific PDF parameter (k), were computed. Although AT, E_{peak} and E-VTI failed to differentiate between groups, DT, E_{dur} and E/E' and stiffness parameter k showed that AF hearts are stiffer than NSR hearts. In contrast, chamber stiffness from simultaneous ED-PVR data showed no difference between groups! We resolved the discordance and gained mechanistic insight when we found that diastatic stiffness in the AF group is significantly greater than diastatic stiffness in NSR group. We conclude that passive (diastatic) chamber stiffness is increased in normal LVEF chronic, rate controlled AF hearts relative to normal LVEF, NSR hearts and that in addition to DT, the E-wave derived, chamber stiffness specific index k, differentiates between AF vs. NSR groups, even when invasive hemodynamic P-V loop derived end-diastolic chamber stiffness fails to do so.

5.8   References

1.   **Appleton CP, Firstenberg MS, Garcia MJ, and Thomas JD**. The echo-Doppler evaluation of left ventricular diastolic function. A current perspective. *Cardiol Clin* 18: 513-546, ix, 2000.

2.   **Bauman L, Chung CS, Karamanoglu M, and Kovács SJ**. The peak atrioventricular pressure gradient to transmitral flow relation: kinematic model prediction with in vivo validation. *J Am Soc Echocardiogr* 17: 839-844, 2004.

3.   **Bhatia RS, Tu JV, Lee DS, Austin PC, Fang J, Haouzi A, Gong Y, and Liu PP**. Outcome of heart failure with preserved ejection fraction in a population-based study. *N Engl J Med* 355: 260-269, 2006.

4.   **Chen YH, Xu SJ, Bendahhou S, Wang XL, Wang Y, Xu WY, Jin HW, Sun H, Su XY, Zhuang QN, Yang YQ, Li YB, Liu Y, Xu HJ, Li XF, Ma N, Mou CP, Chen Z, Barhanin J, and Huang W**. KCNQ1 gain-of-function mutation in familial atrial fibrillation. *Science* 299: 251-254, 2003.

5.   **Chung CS, Ajo DM, and Kovács SJ**. Isovolumic pressure-to-early rapid filling decay rate relation: model-based derivation and validation via simultaneous catheterization echocardiography. *J Appl Physiol (1985)* 100: 528-534, 2006.

6.   **Chung CS, and Kovács SJ**. Consequences of increasing heart rate on deceleration time, the velocity-time integral, and E/A. *Am J Cardiol* 97: 130-136, 2006.

7.   **Dent CL, Bowman AW, Scott MJ, Allen JS, Lisauskas JB, Janif M, Wickline SA, and Kovács SJ**. Echocardiographic characterization of fundamental mechanisms of abnormal diastolic filling in diabetic rats with a parameterized diastolic filling formalism. *J Am Soc Echocardiogr* 14: 1166-1172, 2001.

8.   **Gottdiener JS, Bednarz J, Devereux R, Gardin J, Klein A, Manning WJ, Morehead A, Kitzman D, Oh J, Quinones M, Schiller NB, Stein JH, Weissman NJ, and**

Echocardiography ASo. American Society of Echocardiography recommendations for use of echocardiography in clinical trials. *J Am Soc Echocardiogr* 17: 1086-1119, 2004.

9.   **Hall AF, and Kovács SJ**. Automated method for characterization of diastolic transmitral Doppler velocity contours: early rapid filling. *Ultrasound Med Biol* 20: 107-116, 1994.

10.   **Kannel WB, Abbott RD, Savage DD, and McNamara PM**. Coronary heart disease and atrial fibrillation: the Framingham Study. *Am Heart J* 106: 389-396, 1983.

11.   **Kannel WB, Wolf PA, Benjamin EJ, and Levy D**. Prevalence, incidence, prognosis, and predisposing conditions for atrial fibrillation: population-based estimates. *Am J Cardiol* 82: 2N-9N, 1998.

12.   **Kass DA**. Assessment of diastolic dysfunction. Invasive modalities. *Cardiol Clin* 18: 571-586, 2000.

13.   **Khan A, Moe GW, Nili N, Rezaei E, Eskandarian M, Butany J, and Strauss BH**. The cardiac atria are chambers of active remodeling and dynamic collagen turnover during evolving heart failure. *J Am Coll Cardiol* 43: 68-76, 2004.

14.   **Kovács SJ, Barzilai B, and Pérez JE**. Evaluation of diastolic function with Doppler echocardiography: the PDF formalism. *Am J Physiol* 252: H178-187, 1987.

15.   **Kovács SJ, Setser R, and Hall AF**. Left ventricular chamber stiffness from model-based image processing of transmitral Doppler E-waves. *Coron Artery Dis* 8: 179-187, 1997.

16.   **Ling LH, Khammy O, Byrne M, Amirahmadi F, Foster A, Li G, Zhang L, dos Remedios C, Chen C, and Kaye DM**. Irregular rhythm adversely influences calcium handling in ventricular myocardium: implications for the interaction between heart failure and atrial fibrillation. *Circ Heart Fail* 5: 786-793, 2012.

17.   **Lisauskas JB, Singh J, Bowman AW, and Kovács SJ**. Chamber properties from transmitral flow: prediction of average and passive left ventricular diastolic stiffness. *J Appl Physiol (1985)* 91: 154-162, 2001.

18. **Little WC, Ohno M, Kitzman DW, Thomas JD, and Cheng CP**. Determination of left ventricular chamber stiffness from the time for deceleration of early left ventricular filling. *Circulation* 92: 1933-1939, 1995.

19. **Mossahebi S, and Kovács SJ**. Kinematic modeling-based left ventricular diastatic (passive) chamber stiffness determination with in-vivo validation. *Ann Biomed Eng* 40: 987-995, 2012.

20. **Mossahebi S, Shmuylovich L, and Kovács SJ**. The thermodynamics of diastole: kinematic modeling-based derivation of the P-V loop to transmitral flow energy relation with in vivo validation. *Am J Physiol Heart Circ Physiol* 300: H514-521, 2011.

21. **Neilan TG, Shah RV, Abbasi SA, Farhad H, Groarke JD, Dodson JA, Coelho-Filho O, McMullan CJ, Heydari B, Michaud GF, John RM, van der Geest R, Steigner ML, Blankstein R, Jerosch-Herold M, and Kwong RY**. The incidence, pattern, and prognostic value of left ventricular myocardial scar by late gadolinium enhancement in patients with atrial fibrillation. *J Am Coll Cardiol* 62: 2205-2214, 2013.

22. **Pozzoli M, Cioffi G, Traversi E, Pinna GD, Cobelli F, and Tavazzi L**. Predictors of primary atrial fibrillation and concomitant clinical and hemodynamic changes in patients with chronic heart failure: a prospective study in 344 patients with baseline sinus rhythm. *J Am Coll Cardiol* 32: 197-204, 1998.

23. **Press W, Teukolsky S, Vetterling W, and Flannery B**. *Numerical Recipes in C: The Art of Scientific Computing.* Cambridge, MA: Cambridge University Press, 1992.

24. **Reant P, Lafitte S, Jaïs P, Serri K, Weerasooriya R, Hocini M, Pillois X, Clementy J, Haïssaguerre M, and Roudaut R**. Reverse remodeling of the left cardiac chambers after catheter ablation after 1 year in a series of patients with isolated atrial fibrillation. *Circulation* 112: 2896-2903, 2005.

25. **Redfield MM**. Understanding "diastolic" heart failure. *N Engl J Med* 350: 1930-1931, 2004.

26.   **Riordan MM, Chung CS, and Kovács SJ**. Diabetes and diastolic function: stiffness and relaxation from transmitral flow. *Ultrasound Med Biol* 31: 1589-1596, 2005.

27.   **Saba S, and Adelstein E**. The atria are fibrillating: does it matter to the resynchronized ventricles? *Circ Heart Fail* 5: 547-549, 2012.

28.   **Shmuylovich L, Chung CS, and Kovács SJ**. Point: Left ventricular volume during diastasis is the physiological in vivo equilibrium volume and is related to diastolic suction. *J Appl Physiol (1985)* 109: 606-608, 2010.

29.   **Shmuylovich L, and Kovács SJ**. E-wave deceleration time may not provide an accurate determination of LV chamber stiffness if LV relaxation/viscoelasticity is unknown. *Am J Physiol Heart Circ Physiol* 292: H2712-2720, 2007.

30.   **Shmuylovich L, and Kovács SJ**. Load-independent index of diastolic filling: model-based derivation with in vivo validation in control and diastolic dysfunction subjects. *J Appl Physiol (1985)* 101: 92-101, 2006.

31.   **Swanson JC, Krishnamurthy G, Kvitting JP, Miller DC, and Ingels NB**. Electromechanical coupling between the atria and mitral valve. *Am J Physiol Heart Circ Physiol* 300: H1267-1273, 2011.

32.   **Takagaki M, McCarthy PM, Inoue M, Chung M, Connor JT, Dessoffy R, Ochiai Y, Howard M, Doi K, Kopcak M, Mazgalev TN, and Fukamachi K**. Myocardial compliance was not altered after acute induction of atrial fibrillation in sheep. *Med Sci Monit* 11: BR147-153, 2005.

33.   **Zakeri R, Borlaug BA, McNulty SE, Mohammed SF, Lewis GD, Semigran MJ, Deswal A, LeWinter M, Hernandez AF, Braunwald E, and Redfield MM**. Impact of atrial fibrillation on exercise capacity in heart failure with preserved ejection fraction: a RELAX trial ancillary study. *Circ Heart Fail* 7: 123-130, 2014.

34.   **Zhang W, Chung CS, Shmuylovich L, and Kovács SJ**. Is left ventricular volume during diastasis the real equilibrium volume, and what is its relationship to diastolic suction? *J Appl Physiol (1985)* 105: 1012-1014, 2008.

35.   **Zhang W, and Kovács SJ**. The diastatic pressure-volume relationship is not the same as the end-diastolic pressure-volume relationship. *Am J Physiol Heart Circ Physiol* 294: H2750-2760, 2008.

Chapter 6: The Isovolumic Relaxation to Early Rapid Filling Relation

6.1 Abstract

Although catheterization is the gold standard, Doppler echocardiography is the preferred diastolic function (DF) characterization method. The physiology of diastole requires continuity of left ventricular pressure (LVP) generating forces before and after mitral valve opening (MVO). Correlations between isovolumic relaxation (IVR) indexes such as tau (time-constant of IVR) and non-invasive, Doppler E-wave derived metrics, such as peak A-V gradient or deceleration time (DT), have been established. However, what has been missing is the model predicted causal link that connects isovolumic relaxation (IVR) to suction initiated filling (E-wave). The physiology requires that model-predicted terminal force of IVR ($F_{t\ IVR}$) and model-predicted initial force of early rapid filling ($F_{i\ E\text{-}wave}$) after MVO be correlated. For validation, simultaneous (conductance catheter) P-V and E-wave data from 20 subjects (mean age 57 years, 13 men) having normal LV ejection fraction (LVEF>50%) and a physiologic range of LV end-diastolic pressure (LVEDP) were analyzed. For each cardiac cycle the previously validated kinematic (Chung) model for isovolumic pressure decay and the Parametrized Diastolic Filling (PDF) kinematic model for the subsequent E-wave provided $F_{t\ IVR}$ and $F_{i\ E\text{-}wave}$ respectively. For all 20 subjects (15 beats/subject, 308 beats) linear regression yielded $F_{t\ IVR} = \alpha\ F_{i\ E\text{-}wave} + b$ (R=0.80) where α=1.62 and b=1.32.

We conclude that model-based analysis of IVR and of the E-wave elucidates DF mechanisms common to both. The observed in-vivo relationship provides novel insight into diastole itself and the model-based causal mechanistic relationship that couples IVR to early rapid filling.

6.2   Introduction

Diastolic dysfunction (DD) is predictor of and a precursor to diastolic heart failure (DHF), a clinical syndrome that has reached epidemic proportions (2, 14, 24, 25, 28, 37, 40). Critical to the management of this epidemic is the quantitative assessment of diastolic function (DF). DF determinants such as stiffness and relaxation, measured clinically, reflecting global chamber function have causal components at the cellular level. Physiologists and clinicians know that the LVP contour is smooth and continuous during the 'isovolumic relaxation - mitral valve opening - early rapid filling' interval. The physiology of relaxation and filling requires continuity of left ventricular (LV) pressure generating forces before and after mitral valve opening (MVO). Correlations between invasive measures of isovolumic relaxation (IVR) such as tau (time-constant of IVR) and E-wave derived parameters, such as peak atrioventricular gradient or deceleration time (DT), have been established (3). However the known physiologic continuity that links these two phases has not been assessed in terms of the applicable kinematic models that individually allow computation of the model-predicted force at the end of IVR and its relationship to the model-predicted force at the beginning of suction initiated filling (E-wave).

Quantification of diastolic dysfunction (DD) has remained a challenge without direct, invasive measurement. Doppler echocardiography has become the standard, and preferred method for quantitative DF assessment (7, 10, 16, 34). In previous work we have developed and validated novel, mechanism-based DF indexes using a kinematic modeling approach, called the parametrized diastolic filling (PDF) formalism (9, 17, 18). The PDF formalism models the kinematics of suction-initiated filling in analogy to the recoil from rest, of an equivalent damped oscillator. Model predicted velocity and clinical E-wave contour velocity have shown superb

173

agreement (19). Using a clinically recorded E-wave as input and suitable mathematical methods, unique chamber stiffness (k), viscoelasticity/relaxation (c) and load (x_o) parameters are generated as output, thereby solving the 'inverse problem of diastole' (19). The three PDF parameters (k, c, x_o) can be used to generate indexes with rigorous physiological analogues including the peak instantaneous pressure gradient (kx_o), and the potential energy driving the recoil/suction process ($1/2kx_o^2$) (1, 31). We have also previously derived and validated the 'Chung model', a kinematic model of isovolumic pressure decay (IVPD) applicable during IVR (5). The model accurately characterizes the wide range of physiologically observed IVPD contours when viewed as pressure phase plane (PPP) trajectories. It was shown that IVPD is governed by the interplay of inertial, stiffness and relaxation forces (5). Importantly, the Chung model is linear, it uses invasive high fidelity pressure contour as input and generates unique model parameters as output for each cardiac cycle. Furthermore, for the first time, the model unified the previous disparate characterizations of IVR in terms of τ or the logistic time constant τ_L by modeling the forces responsible and showing that linear (τ) and curved (τ_L) fits to IVPD phases in the PPP are in fact parametric limits of a single unifying (Chung) model of IVR (5).

Thus in this work we employ the Chung model for IVPD and the PDF model for transmitral flow and compute the Chung model-predicted expression for terminal force during IVR and PDF model-predicted initial force initiating early rapid filling. Because the physiology is continuous, we hypothesize that the Chung model predicted terminal force of IVR ($F_{t\ IVR}$) and the PDF model predicted initial force of early rapid filling ($F_{i\ E\text{-}wave}$) after MVO should be correlated.

174

6.3   Methods

6.3.1 Subject Selection

Datasets from 20 patients (mean age 57 years, 13 men) were selected from our cardiovascular biophysics laboratory database of simultaneous echocardiography-high fidelity hemodynamic (Millar conductance catheter) recordings (5, 23). Subjects were referred by their personal physician for elective diagnostic cardiac catheterization to determine the possibility of coronary artery disease. Prior to data acquisition, subjects provided signed, IRB approved informed consent for participation in accordance with Washington University Human Research Protection Office (HRPO) criteria. The criteria for data selection from the database included: a range of LV end-diastolic pressure (LVEDP) representative of a patient population encountered clinically, normal LVEF (> 50%), normal sinus rhythm, clearly discernible E-waves followed by a diastatic interval, and normal valvular function. Subject's inclusion in the study required the subject to have no pacemaker, be in normal sinus rhythm, have no evidence of valvular disease, and have no active ischemia. Among the 20 datasets, 8 had end-diastolic pressure (LVEDP) < 15 mm Hg, 8 had 15 mm Hg < LVEDP < 20 mm Hg and 4 had LVEDP >20 mm Hg. A total of 308 cardiac cycles of simultaneous echocardiographic-high fidelity hemodynamic (conductance catheter) data was analyzed. The clinical descriptors of the 20 subjects and their hemodynamic and echocardiographic indexes are shown in Table 6.1.

Table 6.1 Clinical descriptors including hemodynamic and echocardiographic indexes.

N	20
Age (y)	57 ± 11
Gender (male/female)	13 / 7
Heart Rate (bpm)	63 ± 6
Ejection Fraction (LVEF) (%) [*]	70 ± 7
LVEDP = MVOP (mmHg)	16 ± 4
LVEDV (ml)	127 ± 29
E/A	1.3 ± 0.2
PDF parameter x_o (cm)	9.6 ± 1.6
PDF parameter k ($1/s^2$)	211 ± 44
PDF parameterc c (1/s)	16.6 ± 4.1
Chung parameter E_k ($1/s^2$)	1552 ± 763
Chung parameter μ (s)	0.013 ± 0.009

LVEF, left ventricular ejection fraction (via calibrated ventriculography); LVEDP, left ventricular end-diastolic pressure; LVEDV, left ventricular end-diastolic volume; MVOP, mitral valve opening pressure; E/A, ratio of E_{peak} and A_{peak}.

Data are presented as mean ± standard deviation.

6.3.2 <u>Data Acquisition</u>

Our simultaneous high-fidelity, P-V and echocardiographic transmitral flow data recording method has been previously detailed (3, 19, 20, 23, 31). Briefly, LV pressure was acquired using a micromanometric conductance catheter (SPC-560, SPC-562, or SSD-1043,

Millar Instruments, Houston, TX) at the commencement of elective cardiac catheterization, prior to the administration of iodinated contrast agents. Pressures signals were fed into the catheterization laboratory amplifier (Quinton Diagnostics, Bothell, WA, and General Electric) and simultaneously into the input ports of the physiological amplifier of the Doppler imaging system for synchronization (Philips iE33). Conductance catheterization signals were fed into a custom personal computer via a standard interface (Sigma-5, CD Leycom). Although conductance volume data were recorded, analysis of the data was not necessary in this study.

6.3.3 Doppler E-wave Analysis

For each subject, approximately 1-2 minutes of continuous transmitral flow data were recorded in the pulsed-wave Doppler mode. Echocardiographic data acquisition is performed in accordance with American Society of Echocardiography (33) criteria. Briefly, immediately before catheterization, patients were imaged in a supine position using a Philips (Eindhoven, the Netherlands) iE33 system. Two dimensional images in apical 2- and 4-chamber views were obtained. In accordance with convention, the apical 4-chamber view was used for Doppler E-wave recording with the sample volume located at the leaflet tips. An average of 15 beats per subject were analyzed (308 cardiac cycles total for the 20 subjects). All E-waves were analyzed using the Parametrized Diastolic Filling (PDF) formalism to yield E-wave specific kinematic parameters (chamber viscoelasticity/relaxation parameter (c), stiffness parameter (k), load parameter (x_o)) for each cardiac cycle (17, 18, 22, 23).

The PDF Formalism

The PDF formalism characterizes Doppler transmitral velocity profiles (E- and A-waves) kinematically in analogy to the motion of a damped simple harmonic oscillator (SHO) (18). Thus transmitral blood flow velocity is the result of a balance between elastic, inertial, and damping forces. During early rapid filling, the elastic driving force, due to the previous systolic loading of elastic elements in the ventricle (titin, elastin, the visceral pericardium, and collagen (11, 13, 15, 29, 35) etc.), generates both acceleration-generating forces that encounter acceleration-opposing inertial and resistive (damping) forces. The relative balance of these three forces is reflected in the values of the three mathematically independent model-derived parameters: k, c, and x_o. The SHO equation of motion for the E-wave is given by:

$$\frac{d^2x}{dt^2} + c\frac{dx}{dt} + kx = 0 \qquad [6.1]$$

where the terms from left to right represent the inertial, resistive, and elastic forces, per unit mass respectively. In Equation [6.1] x is the initial displacement of oscillator spring, dx/dt is the velocity of oscillator, and d^2x/dt^2 is the acceleration of oscillator. Without loss of generality Equation [6.1] allows computation of the parameters per unit mass by dividing through by m.

This is Newton's second law and solves the 'inverse problem' of diastole by providing three unique parameters, k, c, and x_o, which specify each E-wave contour (20). The closed form solution of Equation [6.1] yields E-wave velocity, given by:

$$v(t) = \frac{-x_0 \cdot k}{\omega} e^{-\alpha t} \sin(\omega \cdot t) \qquad [6.2a]$$

where $\omega = \frac{\sqrt{4k - c^2}}{2}$ and $\alpha = \frac{c}{2}$, when $4k > c^2$ (underdamped kinematic regime), ω is the

178

angular frequency of SHO. The phase shift in sinusoidal function is zero because at the initial condition (at t=0) the E-wave starts from zero velocity, and

$$v(t) = \frac{-x_0 \cdot k}{\beta} e^{-\alpha t} \sinh(\beta \cdot t)$$ [6.2b]

where $\beta = \frac{\sqrt{c^2 - 4k}}{2}$, when $4k < c^2$ (overdamped kinematic regime)

Using the digitized E-wave contour as input, best-fit, mathematically unique (x_o, c, k) parameters are obtained for each E-wave. The three lumped parameters c, k and x_o account for all the global physiologic determinants of the contour. The initial displacement of the oscillator x_o (cm) is the model's analogue to the velocity-time integral (VTI) of the E-wave (i.e. related to volumetric preload) (20). Chamber stiffness (dP/dV) is linearly related to the spring constant k (g/s^2) (20, 23), while the chamber viscoelasticity/relaxation index c (g/s) characterizes the resistance of the filling process (9, 21). It has been shown that PDF analysis of the Doppler E-wave can accurately determine LV diastatic (passive) stiffness (30).

6.3.4 Pressure Analysis

Hemodynamics were recorded using high-fidelity Millar LV pressure catheter for each beat. Kinematic model parameters of Chung model (μ, E_k, and P_∞), are extracted as previously described (5) for each individual beat by applying the Levenberg-Marquardt (LM) algorithm to the P(t) and dP(t)/dt data for isovolumic pressure decay.

Kinematic Model of Isovolumic Relaxation (Chung Model)

In an effort to completely characterize the wide range of physiologically observed IVPD PPP trajectories Chung et. al. proposed a general model of IVPD governed by the physically intuitive interplay of inertial, stiffness and relaxation forces. These forces determine, via Newton's law, motion of the chamber manifesting as (small) displacements (isovolumic torsion, chamber shape change) (5). Utilizing Laplace's law to transform displacements to pressures, Chung et al used Newton's Law (per unit mass) to account for IVPD:

$$\frac{d^2P}{dt^2} + \frac{1}{\mu}\frac{dP}{dt} + E_k(P - P_\infty) = 0 \qquad [6.3]$$

where μ is a relaxation parameter, E_k is a stiffness parameter, and P_∞ is the pressure asymptote.

When the recoil (E_kP) and relaxation $[(1/\mu)dP/dt]$ terms numerically dominate the inertial term ($d^2P/dt^2 \approx 0$) (36), the solution to Equation [6.3] reduces to the familiar monoexponential solution for IVPD with $\tau = 1/\mu E_k$. As a further benefit of the approach, note that neither the monoexponential (38) nor the logistic parameter-predicted pressure decay (26) can characterize the range of physiologically encountered IVPD (as it appears in the PPP in Figure 6.1) and the data before dP/dt_{min} (5).
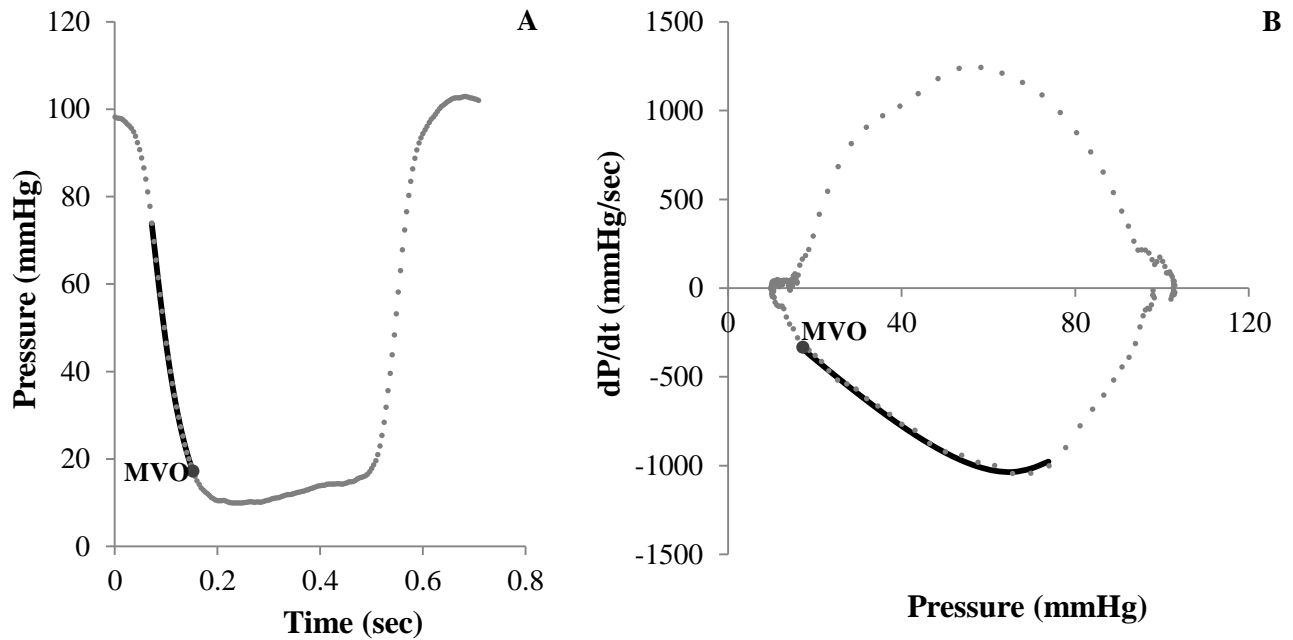
Figure 6.1 Chung model predicted isovolumic pressure decay.

Chung model predicted isovolumic pressure decay up to mitral valve opening (MVO) employing elastic (E_k) and relaxation (μ) parameters. A) Raw data (grey dots) showing pressure vs. time with model fit (solid black line) superimposed. B) Chung model fit to same data in the pressure phase plane (dP/dt vs. P). Note ability of Chung model to fit curvilinear feature of IVR phase plane segment commencing at pressures greater than that at which negative dP/dt was greatest. See text for details.

6.3.5 <u>Determination of Terminal Force of IVR Using Catheterization-derived Pressure Data</u>

Pressure is defined as force per unit area. When the Chung model (Figure 6.1) predicted value of the pressure at MVO (P_{MVO}) is multiplied by the effective (constant) mitral valve area (MVA) it provides the model predicted terminal force of IVR. For simplicity, effective MVA was considered as a constant (4 cm^2). Therefore, the terminal force of IVR ($F_{t\,IVR}$) is given by:

$$F_{t\,IVR} = P_{MVO} \cdot MVA \qquad\qquad [6.4]$$

181

Because left atrial pressure is not routinely recorded during cardiac catheterization P_{MVO} very well approximated by LVEDP (4, 12, 27, 32), and was the value used for terminating the Chung model predicted pressure in this study. Chung parameters which are computed per unit mass gives the force per unit mass (by setting m=1), therefore, the unit of force becomes m/sec^2.

6.3.6 <u>Determination of Initial Force of Early Rapid Filling Using Echocardiographic Data</u>

PDF formalism solves the 'inverse problem' of diastole by providing three unique parameters, k, c, and x_o, which specify each E-wave contour. According to the PDF formalism k is the stiffness parameter for early rapid filling. The initial displacement at MVO is given by x_o (cm). The force generated by a recoiling spring is the product of its stiffness and displacement. Therefore, the initial model-predicted force of early rapid filling ($F_{i\ E\text{-}wave}$) applicable to E-wave analysis is:

$$F_{i\ E-wave} = kx_o \qquad [6.5]$$

As in previous work, PDF parameter values for c, k, and x_o are determined as output using the Levenberg-Marquardt algorithm using the E-wave maximum velocity envelope as input via a custom Lab VIEW (National Instruments, Austin, TX) interface (3, 6, 19, 39). As the PDF parameters (c and k) are computed per unit mass, the force computed from those parameters are computed per unit mass (by setting m=1), therefore, the unit of force becomes m/sec^2.

6.4   Results

We analyzed 308 beats from 20 patients' datasets (~15 beats per person, 13 men). Table 6.1 also lists mean heart rate, LVEF, LVEDV and LVEDP (=MVOP).

When analyzed individually, a close linear relationship was found for the terminal force of IVR ($F_{t\ IVR}$) and the initial force of early rapid filling ($F_{i\ E-wave}$) in accordance with the derivation (R > 0.71). Data from one subject is shown in Figure 6.2. Individual linear regression for each data set is shown in Table 6.2.
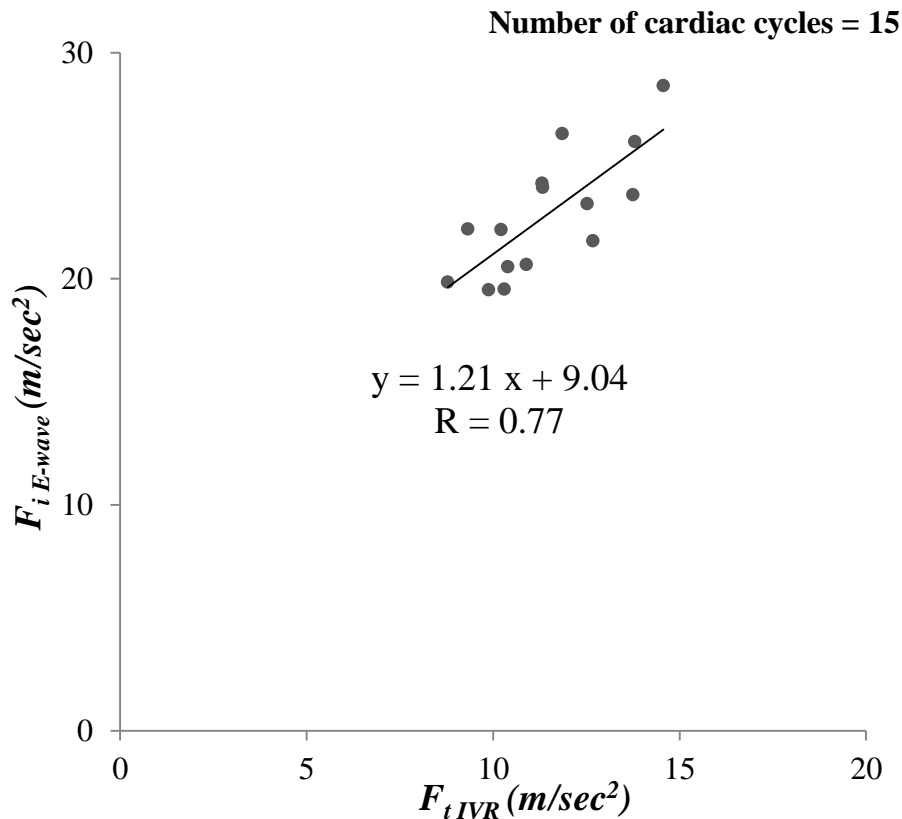
Figure 6.2 Initial force of early rapid filling vs. terminal force of IVR in one subject.
Initial force of early rapid filling ($F_{i\ E-wave}$) vs. terminal force of isovolumic relaxation ($F_{t\ IVR}$) in one selected subject. 15 cardiac cycles were analyzed. Very good linear correlation was observed. See text for details.

Table 6.2 Individual slopes for force relationship.

Individual least mean square linear regression slopes for force relationship ($F_{t\,IVR}$ and $F_{i\,E\text{-}wave}$) for 20 subjects.

Subject	$F_{i\,E\text{-}wave}$ vs. $F_{t\,IVR}$	
	Linear fit slope	R
1	1.42	0.77
2	1.21	0.77
3	1.88	0.79
4	1.69	0.88
5	1.28	0.72
6	0.86	0.71
7	1.44	0.72
8	1.72	0.82
9	1.16	0.71
10	0.94	0.79
11	0.95	0.74
12	1.46	0.84
13	1.67	0.80
14	0.54	0.72
15	1.86	0.77
16	1.36	0.71
17	1.63	0.76
18	3.10	0.81
19	1.06	0.78
20	2.28	0.81

The relationship between $F_{i\ E\text{-}wave}$ and $F_{t\ IVR}$ for the 20 datasets (308 beats) is shown in Figure 6.3. It yielded a very good linear relationship R=0.80.

20 Subjects (308 cardiac cycles)

$$y = 1.62\ x + 1.32$$
$$R = 0.80$$

y-axis: $F_{i\ E\text{-}wave}\ (m/sec^2)$

x-axis: $F_{t\ IVR}\ (m/sec^2)$
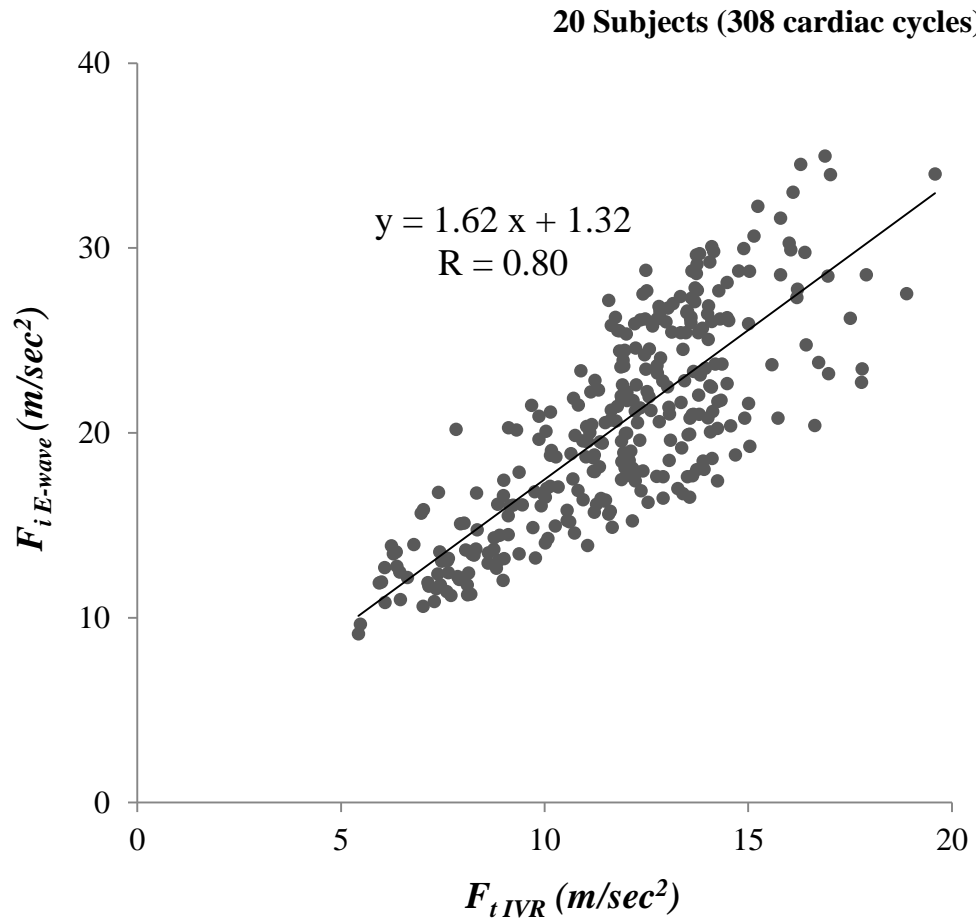
Figure 6.3 Initial force of early rapid filling vs. terminal force of IVR of the entire dataset.

Initial force of early rapid filling ($F_{i\ E\text{-}wave}$) vs. terminal force of isovolumic relaxation ($F_{t\ IVR}$) for the entire (20 normal) dataset consisting of 308 cardiac cycles. Very good linear correlation was observed. See text for details.

6.5   Discussion

Echocardiography is the preferred method of DF assessment. To provide a more complete set of causality- and mechanism-based DF indexes, we used separate, independent kinematic models for IVR and early rapid filling phases of diastole. The advantage of these models is that they are linear, and therefore are 'invertible' generating numerically unique model parameters for each recorded IVR and subsequent E-wave. In addition, both models use (Newton's) equations of motion (Equation [6.1], Equation [6.3]) and quantify the roles that inertial, resistive and restoring forces play in IVR and early rapid filling.

6.5.1   Isovolumic Relaxation Models

Left ventricular isovolumic pressure decline is commonly characterized by the traditional relaxation indexes τ (the time-constant of IVR) and τ_L (the logistic time-constant). A more visually revealing and convenient way to characterize the IVR portion, and to assess model predicted fit to the data, is to plot it in the PPP i.e. a plot of the time derivative of pressure [dP/dt] vs. time-varying pressure [P(t)] (Figure 6.1-B). In the Weiss model, the rate of pressure decline as a function of time is assumed to be proportional to pressure itself, and the Weiss model generates $-1/\tau$ as the slope of the linear fit to the IVR segment, commencing below peak $-$dP/dt and terminating just above LVEDP in the PPP (38). In the logistic model, the pressure decay during IVR is proportional to the square of the pressure, and it fits PPP trajectories having curvilinear, rather than linear IVR segments of (26). In other words, the Weiss model can only generate a straight line (linear) fit to the IVR portion of the PPP, whereas the logistic model can only generate a curvilinear fit to IVR contours in the PPP and no physiologic connection

between τ and τ_L has been established and neither can be used to fit the PPP data before dP/dt$_{min}$ (5).

In contrast, the Chung model provides excellent fits to the full range (linear or curved) IVR pressure decay contours encountered in the PPP and also fits PPP data before dP/dt$_{min}$ (5). Importantly, the Chung model reveals that linear or curved IVR portions encountered in the PPP are mechanistically identical and correspond to parametric limits of a mechanistically single (Chung) model.

6.5.2   Early Rapid Filling Model

The PDF formalism models suction initiated early rapid filling (E-wave). The relation between catheterization-determined chamber stiffness (dP/dV) and k, and the viscoelasticity/ relaxation parameter c and the time-constant of IVR τ have been previously established (9, 20, 21, 23, 31).

6.5.3   Expected Correlation of Isovolumic Relaxation and Early Rapid Filling Measures

Correlations between invasive isovolumic relaxation (IVR) measures, such as tau (time-constant of IVR) and E-wave derived parameters, such as peak A-V gradient, have also been established (3). Continuity of LVP contours during the 'isovolumic relaxation - mitral valve opening - early rapid filling' interval and the physiology of relaxation and filling requires that the forces before and after mitral valve opening (MVO) should be continuous and therefore its

model predicted analogues should be correlated. Because LVP measurement (Chung model parameters) is an 'absolute' pressure measurement method, whereas echocardiography (PDF parameters) can only provide 'relative' rather than 'absolute' pressure information, we expect the model predicted forces to correlate, rather than be numerically identical.

Chung et al (5) have characterized the relationship between IVR and early rapid filling. They showed that the rate of pressure decay during IVR, $1/\tau$, is related to the chamber's viscous damping/relaxation (PDF) index c, and also the peak atrioventricular pressure gradient kx_o which is also equal to the initial force of early rapid filling ($F_{i\ E\text{-}wave}$). It was also shown that there is correlation between traditional IVR (IVRT, τ) and early filling (DT) measures.

6.5.4 Low Ejection Fraction, High Heart Rate and Elevated LVEDP

All ventricles at mitral valve opening must initiate filling by being mechanical suction pumps (dP/dV<0). Therefore, the kinematics that connects IVR to suction initiated early rapid filling remain unaltered, i.e. the same equations of motion for IVR (Chung model) and the E-wave (PDF formalism) apply for low EF, high HR and elevated LVEDP. Thus, the Chung parameters and the PDF parameters will change accordingly but the correlations between terminal force of IVR and initial rapid filling force are expected to remain essentially the same, although the magnitudes of the forces are expected to be different than the forces in the "normal" cases.

6.5.5 Clinical Importance and Implications

The physiologic and clinical importance of this method is that it can approximate complex physiology of IVR and suction initiated early rapid filling using Newton's Law – provides for a linear model of events. Furthermore, linearity assures unique parameter values in solving the 'inverse problem' and thereby allows (clinicians and physiologists) direct determination of lumped parameters that govern the system from direct in-vivo data obtainable during routine studies.

We conclude that kinematic model-based analysis of IVR and of the E-wave elucidates DF mechanisms common to both. The observed in-vivo relationship provides novel insight into diastole itself and the causal, mechanistic, model-based relationship that couples IVR to early rapid filling.

6.6   Limitations

6.6.1   E-wave Selection

Although the PDF formalism is applicable to all E-waves, the most robust analysis is achieved for E-waves that have a clear termination and are followed by diastasis. E-wave analysis becomes less reliable when the A-wave merges with the E-wave and covers more than two-thirds of the E-wave deceleration portion. This typically occurs at HR > 90 beats/min (8). In the present study our inclusion criteria required use of datasets with clearly discernible E-waves followed by a diastatic interval (average heart rate= 62 bpm).

6.6.2   Sample Size

The number of datasets (n=20) may be viewed as a minor limitation but the total number of cardiac cycles analyzed (n=308) mitigates it to an acceptable degree.

6.7   Conclusions

We derived terminal force of IVR ($F_{t\ IVR}$) from kinematic modeling of IVR (Chung model) and the initial force of early rapid filling ($F_{i\ E\text{-}wave}$) from E-wave based kinematic modeling (PDF formalism). We utilized in-vivo, human, simultaneous P and transmitral echocardiographic E-wave data for validation. Our results show that terminal force of IVR and initial force of early rapid filling are closely correlated. These observed in-vivo relationships provide novel, model-based insight into physiological isovolumic relaxation mechanisms and the mechanism of early rapid filling via a link of model predicted force generating chamber properties.

6.8   References

1.   **Bauman L, Chung CS, Karamanoglu M, and Kovács SJ**. The peak atrioventricular pressure gradient to transmitral flow relation: kinematic model prediction with in vivo validation. *J Am Soc Echocardiogr* 17: 839-844, 2004.

2.   **Benjamin EJ, Levy D, Anderson KM, Wolf PA, Plehn JF, Evans JC, Comai K, Fuller DL, and Sutton MS**. Determinants of Doppler indexes of left ventricular diastolic function in normal subjects (the Framingham Heart Study). *Am J Cardiol* 70: 508-515, 1992.

3.   **Chung CS, Ajo DM, and Kovács SJ**. Isovolumic pressure-to-early rapid filling decay rate relation: model-based derivation and validation via simultaneous catheterization echocardiography. *J Appl Physiol (1985)* 100: 528-534, 2006.

4.   **Chung CS, Karamanoglu M, and Kovács SJ**. Duration of diastole and its phases as a function of heart rate during supine bicycle exercise. *Am J Physiol Heart Circ Physiol* 287: H2003-2008, 2004.

5.   **Chung CS, and Kovács SJ**. Physical determinants of left ventricular isovolumic pressure decline: model prediction with in vivo validation. *Am J Physiol Heart Circ Physiol* 294: H1589-1596, 2008.

6.   **Dent CL, Bowman AW, Scott MJ, Allen JS, Lisauskas JB, Janif M, Wickline SA, and Kovács SJ**. Echocardiographic characterization of fundamental mechanisms of abnormal diastolic filling in diabetic rats with a parameterized diastolic filling formalism. *J Am Soc Echocardiogr* 14: 1166-1172, 2001.

7.   **Garcia MJ, Thomas JD, and Klein AL**. New Doppler echocardiographic applications for the study of diastolic function. *J Am Coll Cardiol* 32: 865-875, 1998.

8.   **Hall A, and Kovács S**. Processing parameter effects on the robustness of the solution to the "Inverse Problem" of diastole from Doppler echocardiographic data. *15th Annual International Conference, IEEE Engineering in Medicine & Biology Society* I385-387, 1993.

9.   **Hall AF, and Kovács SJ**. Automated method for characterization of diastolic transmitral Doppler velocity contours: early rapid filling. *Ultrasound Med Biol* 20: 107-116, 1994.

10.   **Haney S, Sur D, and Xu Z**. Diastolic heart failure: a review and primary care

perspective. *J Am Board Fam Pract* 18: 189-198, 2005.

11.   **Helmes M, Trombitás K, and Granzier H**. Titin develops restoring force in rat cardiac myocytes. *Circ Res* 79: 619-626, 1996.

12.   **Ishida Y, Meisner JS, Tsujioka K, Gallo JI, Yoran C, Frater RW, and Yellin EL**. Left ventricular filling dynamics: influence of left ventricular relaxation and left atrial pressure. *Circulation* 74: 187-196, 1986.

13.   **Jöbsis PD, Ashikaga H, Wen H, Rothstein EC, Horvath KA, McVeigh ER, and Balaban RS**. The visceral pericardium: macromolecular structure and contribution to passive mechanical properties of the left ventricle. *Am J Physiol Heart Circ Physiol* 293: H3379-3387, 2007.

14.   **Kass DA, Bronzwaer JG, and Paulus WJ**. What mechanisms underlie diastolic dysfunction in heart failure? *Circ Res* 94: 1533-1542, 2004.

15.   **Katz L**. The role played by the ventricular relaxation process in filling the ventricle. *Am J Physiol* 95: 542-553, 1930.

16.   **Khouri SJ, Maly GT, Suh DD, and Walsh TE**. A practical approach to the echocardiographic evaluation of diastolic function. *J Am Soc Echocardiogr* 17: 290-297, 2004.

17.   **Kovács S, MD M, and CS P**. Modelling cardiac fluid dynamics and diastolic function. *Philosophical Transactions of the Royal Society (A)* 359: 1299-1314, 2001.

18.   **Kovács SJ, Barzilai B, and Pérez JE**. Evaluation of diastolic function with Doppler echocardiography: the PDF formalism. *Am J Physiol* 252: H178-187, 1987.

19.   **Kovács SJ, Meisner JS, and Yellin EL**. Modeling of diastole. *Cardiol Clin* 18: 459-487, 2000.

20.   **Kovács SJ, Setser R, and Hall AF**. Left ventricular chamber stiffness from model-based image processing of transmitral Doppler E-waves. *Coron Artery Dis* 8: 179-187, 1997.

21.   **Lakshminarayan K, Hall A, and Kovács S**. Doppler echocardiographic determination of mitral valvular resistance to inertiance ratio. *IEEE Engineering in Medicine & Biology Society* I551-553, 1993.

22.   **Lisauskas J, Singh J, Courtois M, and Kovács SJ**. The relation of the peak Doppler E-

wave to peak mitral annulus velocity ratio to diastolic function. *Ultrasound Med Biol* 27: 499-507, 2001.

23. **Lisauskas JB, Singh J, Bowman AW, and Kovács SJ**. Chamber properties from transmitral flow: prediction of average and passive left ventricular diastolic stiffness. *J Appl Physiol (1985)* 91: 154-162, 2001.

24. **Maceira AM, Prasad SK, Khan M, and Pennell DJ**. Normalized left ventricular systolic and diastolic function by steady state free precession cardiovascular magnetic resonance. *J Cardiovasc Magn Reson* 8: 417-426, 2006.

25. **Maeder MT, and Kaye DM**. Heart failure with normal left ventricular ejection fraction. *J Am Coll Cardiol* 53: 905-918, 2009.

26. **Matsubara H, Takaki M, Yasuhara S, Araki J, and Suga H**. Logistic time constant of isovolumic relaxation pressure-time curve in the canine left ventricle. Better alternative to exponential time constant. *Circulation* 92: 2318-2326, 1995.

27. **Miki S, Murakami T, Iwase T, Tomita T, Nakamura Y, and Kawai C**. Doppler echocardiographic transmitral peak early velocity does not directly reflect hemodynamic changes in humans: importance of normalization to mitral stroke volume. *J Am Coll Cardiol* 17: 1507-1516, 1991.

28. **Miller TR, Grossman SJ, Schectman KB, Biello DR, Ludbrook PA, and Ehsani AA**. Left ventricular diastolic filling and its association with age. *Am J Cardiol* 58: 531-535, 1986.

29. **Mizuno J, Araki J, Mikane T, Mohri S, Imaoka T, Matsubara H, Okuyama H, Kurihara S, Ohe T, Hirakawa M, and Suga H**. Logistic time constant of isometric relaxation force curve of ferret ventricular papillary muscle: reliable index of lusitropism. *Jpn J Physiol* 50: 479-487, 2000.

30. **Mossahebi S, and Kovács SJ**. Kinematic modeling-based left ventricular diastatic (passive) chamber stiffness determination with in-vivo validation. *Ann Biomed Eng* 40: 987-995, 2012.

31. **Mossahebi S, Shmuylovich L, and Kovács SJ**. The thermodynamics of diastole: kinematic modeling-based derivation of the P-V loop to transmitral flow energy relation with in vivo validation. *Am J Physiol Heart Circ Physiol* 300: H514-521, 2011.

32.   **Murakami T, Hess OM, Gage JE, Grimm J, and Krayenbuehl HP**. Diastolic filling dynamics in patients with aortic stenosis. *Circulation* 73: 1162-1174, 1986.

33.   **Nagueh SF, Appleton CP, Gillebert TC, Marino PN, Oh JK, Smiseth OA, Waggoner AD, Flachskampf FA, Pellikka PA, and Evangelista A**. Recommendations for the evaluation of left ventricular diastolic function by echocardiography. *J Am Soc Echocardiogr* 22: 107-133, 2009.

34.   **Nishimura RA, and Tajik AJ**. Evaluation of diastolic filling of left ventricle in health and disease: Doppler echocardiography is the clinician's Rosetta Stone. *J Am Coll Cardiol* 30: 8-18, 1997.

35.   **Robinson TF, Factor SM, and Sonnenblick EH**. The heart as a suction pump. *Sci Am* 254: 84-91, 1986.

36.   **Shmuylovich L, and Kovács SJ**. Load-independent index of diastolic filling: model-based derivation with in vivo validation in control and diastolic dysfunction subjects. *J Appl Physiol (1985)* 101: 92-101, 2006.

37.   **Slotwiner DJ, Devereux RB, Schwartz JE, Pickering TG, de Simone G, Ganau A, Saba PS, and Roman MJ**. Relation of age to left ventricular function in clinically normal adults. *Am J Cardiol* 82: 621-626, 1998.

38.   **Weiss JL, Frederiksen JW, and Weisfeldt ML**. Hemodynamic determinants of the time-course of fall in canine left ventricular pressure. *J Clin Invest* 58: 751-760, 1976.

39.   **Zhang W, Shmuylovich L, and Kovács SJ**. The E-wave delayed relaxation pattern to LV pressure contour relation: model-based prediction with in vivo validation. *Ultrasound Med Biol* 36: 497-511, 2010.

40.   **Zile MR, and Brutsaert DL**. New concepts in diastolic dysfunction and diastolic heart failure: Part I: diagnosis, prognosis, and measurements of diastolic function. *Circulation* 105: 1387-1393, 2002.

Chapter 7: Fractionation Method

7.1   Abstract

The mechanical suction-pump feature of the left ventricle aspirates atrial blood and generates a rapid rise and fall in transmitral flow (Doppler E-wave). Initially, E-wave deceleration time (DT), a routine index of clinical diastolic function, was thought to be determined only by chamber stiffness. Kinematic modeling of filling, in analogy to damped oscillatory motion (Parametrized Diastolic Filling (PDF) formalism), has been extensively validated and accurately predicts clinically observed E-wave contours while, revealing that DT is actually an algebraic function of both stiffness (PDF parameter k) and relaxation (PDF parameter c). We hypothesize that kinematic modeling based E-wave analysis accurately predicts the stiffness (DT_s) and relaxation (DT_r) components of DT such that $DT = DT_s + DT_r$.

For validation, pressure-volume (P-V) and E-wave data from 12 control (DT<220msec) and 12 delayed-relaxation (DT>220msec) subjects, 738 beats total, were analyzed. For each E-wave, DT_s and DT_r was compared to simultaneous, gold-standard, high fidelity (Millar catheter) determined, chamber stiffness ($K=\Delta P/\Delta V$) and chamber relaxation (time-constant of isovolumic relaxation - τ), respectively. For the group linear regression yielded $DT_s = \alpha K + \beta$ (R=0.82) with $\alpha = -0.38$ and $\beta = 0.20$, and $DT_r = m \tau + b$ (R=0.94) with m=2.88 and b=-0.12.

We conclude that PDF-based E-wave analysis provides the DT_s and DT_r components of DT with simultaneous chamber stiffness (K) and relaxation (τ) respectively, as primary determinants. This kinematic modeling based method of E-wave analysis is immediately translatable clinically and can assess the effects of pathology and pharmacotherapy as causal determinants of DT.

7.2   Introduction

The clinical syndrome formerly referred to as 'diastolic heart failure' is now called 'heart failure with normal' or 'heart failure with preserved ejection fraction'. It has been recognized as a major cause of cardiovascular morbidity and mortality and has reached epidemic proportions (15, 20, 24, 36, 48). Hence, the ability to quantitate diastolic function (DF) and the presence and severity of diastolic dysfunction is important. Among invasive DF indices, left ventricular (LV) chamber stiffness ($\Delta P/\Delta V$) and relaxation (τ) comprise the gold-standard (15, 32, 47, 48). Conventionally, chamber stiffness has been computed from $\Delta P_{avg}/\Delta V_{avg}$ using invasive methods (11, 21, 22, 31, 39). Although obtaining chamber stiffness, $\Delta P_{avg}/\Delta V_{avg}$ itself usually involves an 'absolute' measurement of LV pressure requiring catheterization, chamber stiffness, being the ratio of two derivatives, is a 'relative' index and can be determined using 'relative measurement' methodology, such as echocardiography, which is the preferred method of quantitative DF characterization. Hence, Doppler E-wave contours can only provide relative, rather than absolute, pressure information. It is known that model-based analysis of the inflow pattern, i.e. Doppler E-waves, generated by the atrioventricular pressure gradient (a relative measure), can accurately determine LV diastatic (passive) stiffness (also a relative measure) (27).

Based on the work of Thomas (40, 42) and Flachskampf (10), Little et al (23) used physiologic modeling to predict that E-wave DT is determined by stiffness alone. Their equation relating stiffness K_{LV} to DT was:

$$K_{LV} = \frac{\rho L}{A} \left(\frac{\pi}{2} \frac{1}{DT} \right)^2 \qquad [7.1]$$

where ρ=density of blood, L=effective mitral plug-flow length, and A=mitral area.

The prediction was experimentally validated (r^2=0.88) in conscious dogs by invasively determining LV stiffness ($\Delta P_{avg}/\Delta V_{avg}$) (23). An alternative kinematic modeling based analysis that incorporates the mechanical suction-pump feature of the physiology (the Parametrized Diastolic Filling (PDF) formalism) showed (19) that the PDF parameter k (the analog of stiffness) is the algebraic equivalent of K_{LV}. For E-wave contours well fit by the 'underdamped' oscillatory regime of motion, the relationship between the PDF stiffness parameter k and Little's expression for stiffness K_{LV} is given by $k = 1.16[A/(\rho L)]\, K_{LV}+41$, r^2=0.92.

Although Little et al (23) proposed that DT is determined by chamber stiffness (K_{LV}) alone, Shmuylovich et al (38) showed that two subjects can have indistinguishable E-wave DTs, but can have significantly different catheterization determined (gold standard) chamber stiffness (dP/dV). They showed that DT is actually jointly determined by both stiffness (PDF stiffness parameter k) and relaxation (PDF relaxation parameter c) (38).

LV relaxation is conventionally characterized by the time constant (τ) of isovolumic relaxation (IVR) (43), where τ is the e-folding time (the time interval during which the pressure falls by a factor of 1/e) assuming pressure, after peak $-dP/dt$ to mitral valve opening, declines exponentially. The interval from aortic valve closure to mitral valve opening, the isovolumic relaxation time (IVRT), non-invasive echocardiographic measurement, is another commonly used, but less, specific surrogate (41). Chamber stiffness, the slope ($\Delta P/\Delta V$) of the end-diastolic pressure-volume relationship, is usually determined from multiple beats. Diastatic (passive) stiffness is the slope of the diastatic pressure-volume relationship, inscribed by the locus of load varying P-V points achieved at the end of each diastatic interval after E-wave termination, after the chamber has fully relaxed (6, 21, 22, 34, 44). During diastasis, LV and left atrial pressures are equal, the pressure gradient across the mitral valve is zero (6), there is no transmitral flow, hence

the resultant forces generated by and acting on the ventricle are balanced (but not zero) (35). Accordingly, diastasis comprises the static equilibrium state of the passive LV. In engineering terms, the volume at diastasis is the resting (equilibrium) volume relative to which the chamber oscillates.

7.3   Methods

7.3.1 Subject Selection

Datasets from 24 patients (mean age 61, 16 men) were selected from our cardiovascular biophysics laboratory database of simultaneous echocardiography-high fidelity hemodynamic (Millar conductance catheter) recordings (5, 22). Subjects underwent elective cardiac catheterization to determine presence of suspected coronary artery disease at the request of their referring physicians. Prior to data acquisition, subjects provided signed, IRB approved informed consent for participation in accordance with Washington University Human Research Protection Office (HRPO) criteria. In addition to normal LV ejection fraction (LVEF) (> 50%), normal sinus rhythm, normal valvular function, datasets were also selected based on the presence of an echocardiographic normal or a delayed relaxation (DR) pattern. DR was defined as previously (12, 42) as E/A (ratio of E_{peak} and A_{peak} (peak of late filling)) < 1 and a DT > 220 ms (12 subjects), normal relaxation pattern was defined as E/A > 1, DT < 220ms and normal Doppler tissue velocity (E' > 8 cm/s) (12 subjects). Both groups included the range of LV end diastolic pressure (LVEDP) representative of a patient population encountered clinically. Among the 12 normal deceleration time datasets, 8 had normal end-diastolic pressure (LVEDP<14 mmHg), 2 had 15 mmHg < LVEDP < 20 mmHg and 2 had elevated LVEDP (>21 mmHg). The distribution of LVEDPs in the 12 DR group datasets were: 4 with LVEDP<14, 4 with 15<LVEDP<20 mmHg and 4 with LVEDP>21. A total of 738 cardiac cycles (31 beats/subject) of simultaneous echocardiographic-high fidelity hemodynamic (conductance catheter) data were analyzed. The clinical descriptors of the 24 subjects and their hemodynamic and echocardiographic indices are shown in Table 7.1.

Table 7.1 Clinical descriptors including hemodynamic and echocardiographic indexes.

Clinical Descriptors	Normal Relaxation Group	Delayed Relaxation Group	Significance
N	12	12	N.A.
Age (y)	56±11	67±11	0.02
Gender (male/female)	7/5	9/3	N.A.
Heart Rate (bpm)	62±10	58±4	0.20
LVEF (%) [*]	71±7	72±1	0.89
LVEDP (mmHg)	16±5	18±3	0.37
LVEDV (ml)	129±25	149±43	0.17
DT (msec)	185±21	252±24	<0.0001
DT_r (msec)	45±13	98±13	<0.0001
DT_s (msec)	140±11	154±16	<0.03
$R = DT_r / DT$ (%)	24±6	39±3	<0.0001
$S = DT_s / DT$ (%)	76±6	61±3	<0.0001
E/A (dimensionless)	1.16±0.19	0.84±0.13	<0.0005
IVRT (msec)	75±6	95±9	<0.0001
τ (msec)	58±6	75±5	<0.0001

LVEF, left ventricular ejection fraction (via calibrated ventriculography); LVEDP, left ventricular end-diastolic pressure; LVEDV, left ventricular end-diastolic volume; DT, deceleration time of E-wave; DT_r, relaxation component of DT; DT_s, stiffness component of DT; E/A, ratio of Epeak and Apeak; IVRT, isovolumic relaxation time; τ, time-constant of isovolumic relaxation; N.A., not applicable. DT, DT_r, DT_s precision is shown by the level of significant figures.

Data are presented as mean ± standard deviation.

7.3.2 <u>Data Acquisition</u>

Our simultaneous high-fidelity, P-V and echocardiographic transmitral flow data recording method has been previously detailed (1, 3, 18, 19, 22, 28). Briefly, LV pressure and volume were acquired using a micromanometric conductance catheter (SPC-560, SPC-562, or SSD-1043, Millar Instruments, Houston, TX) at the commencement of elective cardiac catheterization, prior to the administration of iodinated contrast agents. Pressure signals from the transducers were fed into a clinical amplifier system (Quinton Diagnostics, Bothell, WA, and General Electric). Conductance catheterization signals were fed into a custom personal computer via a standard interface (Sigma-5, CD Leycom). Conductance volume data were recorded in five channels. Data from low-noise channels providing physiological readings were selected, suitably averaged and calibrated using absolute volumes obtained by calibrated ventriculography during the same procedure.

7.3.3 <u>Doppler E-wave Analysis</u>

For each subject, approximately 1-2 minutes of continuous transmitral flow data were recorded in the pulsed-wave Doppler mode. Echocardiographic data acquisition is performed in accordance with published American Society of Echocardiography (30) criteria. Briefly, immediately before catheterization, patients are imaged in a supine position using a Philips (Andover, MA.) iE33 system. In accordance with convention, the apical 4-chamber view was used for Doppler E-wave recording with the sample volume located at the leaflet tips. An average of 31 beats per subject of simultaneous echocardiographic-hemodynamic data were analyzed (738 cardiac cycles total for the 24 subjects). DT was measured manually using

standard criteria (9) as the base of the triangle approximating the deceleration portion of the E wave. Each E-wave was also analyzed via PDF formalism to yield mathematically unique PDF parameters for each E-wave (stiffness parameter (k), chamber viscoelasticity/relaxation parameter (c), load parameter (x_o)) (16, 17, 22).

The PDF Formalism

The parametrized diastolic filling (PDF) formalism characterizes Doppler transmitral velocity profiles kinematically according to damped simple harmonic oscillatory (SHO) motion (17). Thus transmitral blood flow velocity is the result of simultaneous elastic, inertial, and damping forces. The relative roles of these forces are reflected in the values of the three mathematically independent model-derived parameters: k, c, and x_o. The SHO equation of motion for the E-wave is given by:

$$\frac{d^2x}{dt^2} + c\frac{dx}{dt} + kx = 0 \qquad [7.2]$$

where the terms, from left to right, represent the inertial, resistive, and elastic forces, respectively and we calculate the parameters per unit mass. Without loss of generality the parameters k and c are computed on a per unit mass basis (17, 18).

Newton's second law governs the process and solves the 'inverse problem' of diastole by providing three unique parameters of k, c, and x_o, for each E-wave contour (13). The solution of Equation [7.2] yields E-wave velocity, given by:

$$v(t) = -\frac{x_o k}{\omega}\exp(-ct/2)\sin(\omega t) \qquad [7.3a]$$

where $\omega = \sqrt{4k - c^2}/2$, when $4k>c^2$ underdamped kinematic regime characteristic of NR, and

$$v(t) = -\frac{x_o k}{\beta}\exp(-ct/2)\sinh(\beta t) \qquad [7.3b]$$

where $\beta = \sqrt{c^2 - 4k}/2$, when $4k<c^2$ overdamped kinematic regime, characteristic of DR.

The three parameters c, k and x_o encompass the (lumped) physiologic determinants of all E-wave contours. The initial oscillator displacement x_o (cm) is linearly related to the velocity-time integral (VTI) of the E-wave (19). Chamber stiffness (dP/dV) is linearly related to the spring constant k (g/s^2) (18, 21), while the chamber viscoelasticity/relaxation index c (g/s) characterizes the resistance of the process (18, 19). E-waves with long concave up deceleration portions are fit by the overdamped solution and have higher c values, while E-waves that approximate nearly symmetric sine waves are fit by the underdamped solution and have lower c values (38).

PDF parameter c, k, and x_o values are determined via the Levenberg-Marquardt algorithm as a part of generating the fit to the E-wave maximum velocity envelope via a custom Lab VIEW (National Instruments, Austin, TX) interface (13). The algorithm provides parameter values and a simultaneous measure of goodness of fit.

Because DT has been shown to explicitly depend on both stiffness and relaxation (38), in this work we provide the method that decomposes E-wave DT into its stiffness (DT$_s$) and relaxation (DT$_r$) components. Accordingly DT = DT$_s$ + DT$_r$. The decomposition utilizes (PDF) analysis of Doppler E-waves. For validation, we determine the relationship between DT$_s$ and DT$_r$ and conventional and gold-standard (simultaneous) invasive DF parameters of stiffness (slope of diastatic pressure-volume relationship) and relaxation (τ, IVRT). The diastatic pressure-volume

relationship is obtained by a linear (or exponential) fit to diastatic load-varying P-V data. Since previous work (45) has shown that a linear or exponential fit to the same diastatic P-V data yields a similar measure of goodness of fit, a linear fit was used.

7.3.4   <u>Determination of Diastatic Stiffness from P-V Data</u>

Hemodynamics were determined from the high-fidelity Millar LV P-V data from each beat. The method used to compute volumes has been previously detailed (22, 27, 28, 45). Quantitative ventriculography was used to determine end-systolic and end-diastolic volumes which defined (calibrated) the systolic and diastolic volume limits of conductance catheter recorded continuous volume signal. After calibration of conductance volume, LV pressure and volume at diastasis were measured beat-by-beat using a custom MATLAB program. Although relaxation is often fully complete at the end of the E-wave, when diastasis begins, to assure full relaxation and achievement of the passive state of the LV we analyzed data at the end of diastasis, i.e. at ECG P-wave onset. We selected cardiac cycles having diastatic intervals during which pressure as a function of time was essentially constant or varied by $< 2\text{mmHg}$ during all of diastasis. At sufficiently low heart rates, end-diastasis points were defined by ECG P-wave onset (28, 45, 46). In our analyzed subjects the average heart rate was 62 ± 10 bpm for the normal relaxation (NR) group and 58 ± 4 bpm for the DR group. As previously (28, 45, 46), for each subject diastatic P-V data points were fit by linear regression, from which diastatic chamber stiffness was determined as the slope (K) of diastatic pressure-volume relationship. Micromanometric conductance catheter P measurement precision is < 0.1 (mmHg).

7.3.5 Determination of Time-constant of Isovolumic Relaxation from Pressure Data

The monoexponential model of isovolumic pressure decay assumes that the time derivative of pressure decay is proportional to pressure (43). The governing differential equation for pressure decay is:

$$\tau \frac{dP}{dt} + (P - P_\infty) = 0 \qquad [7.4]$$

where τ is the time-constant of IVR, and P_∞ is the pressure asymptote.

As previously described (8) the pressure phase plane (dP/dt vs. P) was used to determine τ (conventional invasive relaxation index) for each beat in each subject.

7.3.6 Graphical Determination of Stiffness and Relaxation Components of E-wave Deceleration Time

The duration of the E-wave (E_{dur}), acceleration time (AT), and DT are measured as usual from Doppler echo data, by approximating E-wave shape as a triangle (Figure 7.1). PDF parameters (k, c, and x_o) can be obtained for each E-wave (defined as the original E-wave) via PDF analysis. The effect of delayed relaxation on an ideal (generated by recoil only) E-wave is to decrease its peak amplitude and lengthen its DT.

Accordingly, DT_r is determined by setting PDF relaxation parameter zero ($c=0$) and generating an ideal contour via the PDF formalism, using the same x_o and k as the original E-wave. Therefore, the model predicted ideal E-wave has the same stiffness and initial load (displacement from the equilibrium) as the actual E-wave being analyzed, but recoils (oscillates)

without resistance. Subtracting the ideal E-wave duration from actual PDF fit total DT yields

DT_r (as shown in Figure 7.1). Therefore, E-wave DT becomes $DT = DT_s + DT_r$.
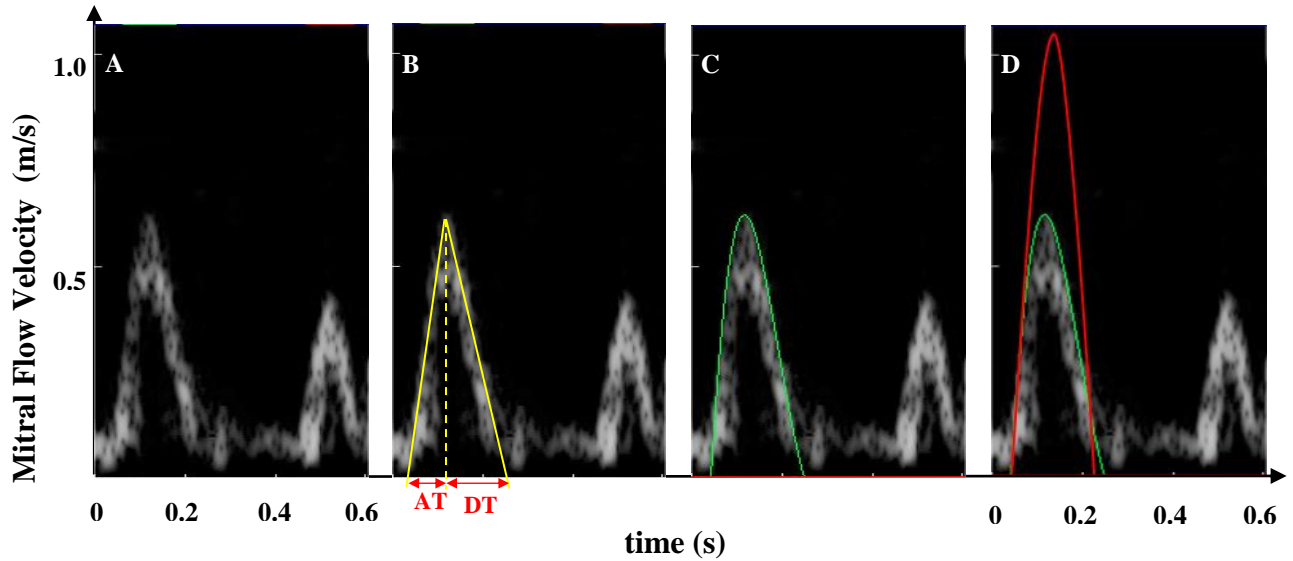
Figure 7.1 Overview of DT_s and DT_r computation.

A) A typical Doppler velocity profile. B) AT and DT determination using triangle method. C) PDF model fit to E-wave (green) provides PDF parameters c=14.6/s, k=287/s^2, x_o= 6 cm. D) Model predicted E-wave with c=0 (red), with same xo, k as original (green) E-wave. DT_r lengthens DT, hence green DT (where $c\neq0$) is longer than red DT (where c=0). Nonzero c decreases peak amplitude and increases DT. $DT_s = DT - DT_r$. DT=0.132 s, DT_r=0.022 s and DT_s=0.110 s. See text for details.

By determining DT_s and DT_r of each E-wave, the total DT can be normalized and fractionated as the fraction due to stiffness (S=DT_s/DT) and the fraction of DT due to relaxation (R=DT_r/DT) for each cardiac cycle such that S+R=1.

209

7.3.7 <u>Algebraic Determination of Stiffness and Relaxation Components of E-wave Deceleration Time</u>

The velocity of damped simple oscillator for underdamped regime can be expressed as:

$$v(t) = -\frac{x_o k}{\omega} \exp(-ct/2) \sin(\omega t) \qquad [7.5]$$

where $\omega = \sqrt{4k - c^2}/2$.

Using above equation E-wave acceleration time (AT), deceleration time (DT) and duration of actual E-wave (sum of AT and DT) for underdamped regime can be written as (38):

$$AT = (1/\omega)\arctan(2\omega/c) \qquad [7.6]$$

$$DT = \pi/\omega - (1/\omega)\arctan(2\omega/c) \qquad [7.7]$$

$$E_{dur}(c \neq 0) = \pi/\omega \qquad [7.8]$$

where $\omega = \sqrt{4k - c^2}/2$.

In an ideal E-wave (where $c=0$), $\omega = \sqrt{k}$ and the duration of the ideal E-wave using the PDF model is:

$$E_{dur}(c = 0) = \pi/\sqrt{k} \qquad [7.9]$$

The duration of the actual ($c \neq 0$) and ideal E-wave ($c=0$) for the 'underdamped' ($c^2 < 4k$) regime of oscillation from the PDF model are π/ω and $\pi/\sqrt{k}$. Therefore, the relaxation component of DT (DT$_r$) defined by the difference between actual and ideal E-wave durations is:

$$DT_r = E_{dur}(c \neq 0) - E_{dur}(c = 0) = \pi\left[1/\omega - 1/\sqrt{k}\right] \qquad [7.10]$$

210

And the stiffness component of DT (DT_s) defined by the difference between DT (Equation [7.7]) and DT_r (Equation [7.10]) can be written as:

$$DT_s = DT - DT_r = \pi / \sqrt{k} - (1/\omega)\arctan(2\omega/c) \qquad [7.11]$$

7.4 Results

7.4.1 <u>Stiffness and Relaxation Components of Deceleration Time</u>

We analyzed 738 beats from 24 datasets (12 normal relaxation, 12 delayed relaxation). Figure 7.2 shows strong correlation between DT measured by triangle method vs. DT_s ($R^2=0.63$) and DT_r ($R^2=0.89$) in 738 analyzed cardiac cycles from 24 subjects. DT_s did not significantly correlate with DT_r ($R^2=0.30$) across all subjects.
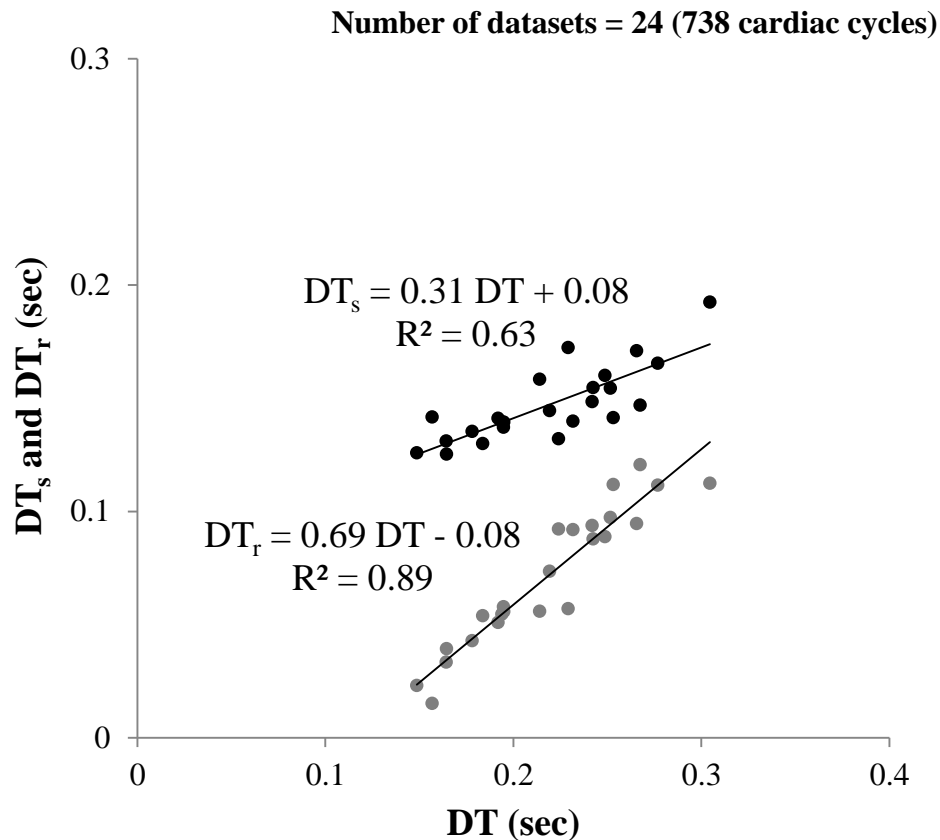
Figure 7.2 Relaxation and stiffness components of DT vs DT.

Least mean square determined linear fit between DT_r vs. DT (grey) and DT_s vs. DT (black) in 24 subjects (738 beats analyzed). DT measured by triangle method. See text for details.

Table 7.2 shows the average deceleration time components in all subjects (12 normal relaxation and 12 delayed relaxation datasets).

Table 7.2 Deceleration time components in all 24 subjects.

	Normal Relaxation		Delayed Relaxation	
	DT_r (msec)	DT_s (msec)	DT_r (msec)	DT_s (msec)
Subject 1	53±4	139±6	88±12	155±17
Subject 2	54±7	130±9	94±11	148±10
Subject 3	24±3	127±10	112±19	192±18
Subject 4	53±8	141±12	92±12	140±17
Subject 5	56±5	158±13	111±18	165±13
Subject 6	22±2	142±7	77±11	144±14
Subject 7	51±10	137±12	95±13	171±15
Subject 8	39±6	125±5	89±11	160±15
Subject 9	44±6	139±9	121±13	147±15
Subject 10	33±5	131±5	92±12	132±13
Subject 11	56±7	153±5	112±14	141±14
Subject 12	57±7	152±11	97±12	154±12

DT_r, relaxation component of DT; DT_s, stiffness component of DT.

7.4.2 <u>Stiffness Component of Deceleration Time and Diastatic Stiffness</u>

As hypothesized DT_s and diastatic stiffness derived from P-V data (K) were correlated ($DT_s = -0.38\ K + 0.20$, $R^2 = 0.67$) (Figure 7.3).

The negative slope in DT_s vs. K correlation was expected from the inverse relation between DT (and stiffness component of DT) and chamber stiffness.

Number of datasets = 24 (738 cardiac cycles)

$$DT_s = -0.38\ K + 0.20$$
$$R^2 = 0.67$$
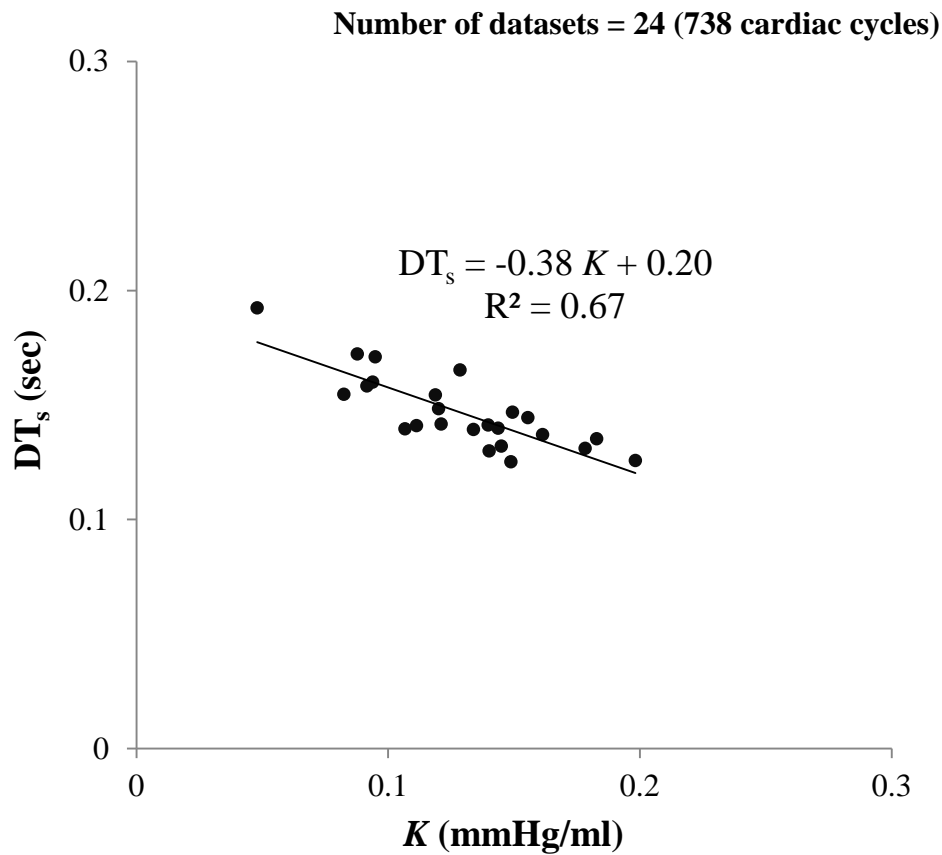
Figure 7.3 Stiffness component of DT (DT_s) vs diastatic stiffness (K).

Least mean square determined linear fit of stiffness component of DT (DT_s) and diastatic stiffness (K) in 24 subjects (738 beats analyzed). See text for details.

7.4.3 Relaxation Component of Deceleration Time and Relaxation Indexes

DT$_r$, the relaxation component of DT, was highly correlated with the time constant (τ) of IVR (DT$_r$ = 2.88 τ – 0.12, R^2=0.89) (Figure 7.4). Similarly, DT$_r$ was highly correlated with IVRT (DT$_r$ = 2.13 IVRT – 0.11, R^2=0.80) (Figure 7.5).

Number of datasets = 24 (738 cardiac cycles)

$$DT_r = 2.88\ \tau - 0.12$$
$$R^2 = 0.89$$
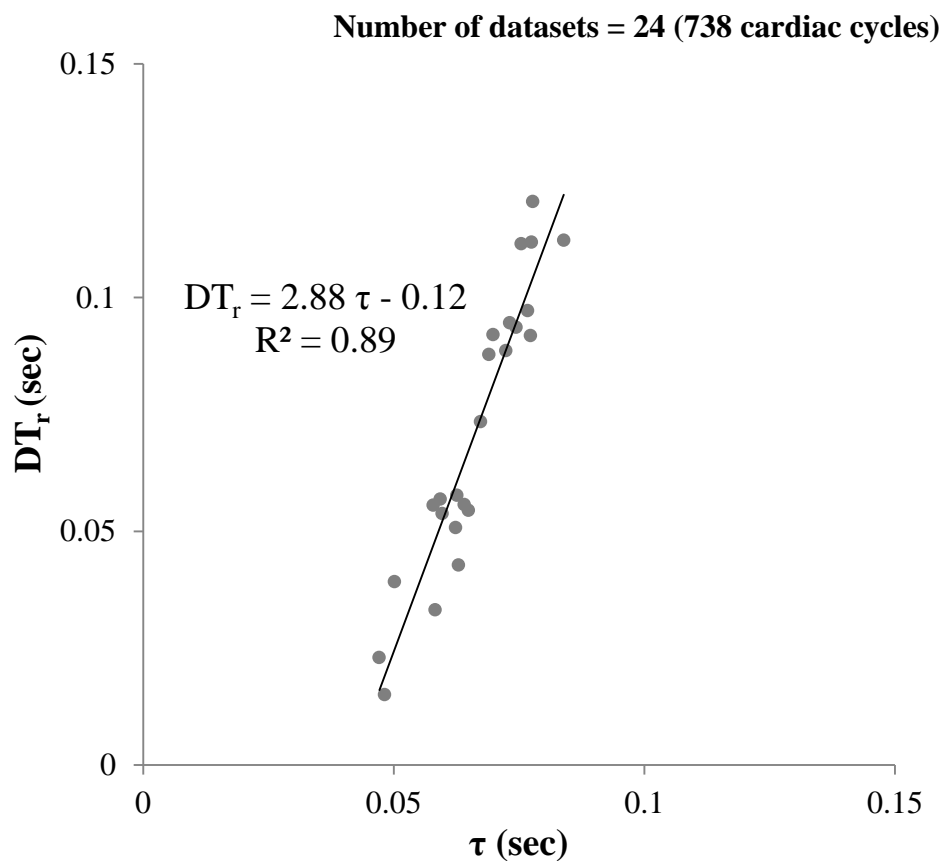
Figure 7.4 Relaxation component of DT vs the time constant of IVR.

Least mean square determined linear fit of relaxation component of DT (DT$_r$) and the time constant of IVR (τ) in 24 subjects (738 beats analyzed). See text for details.
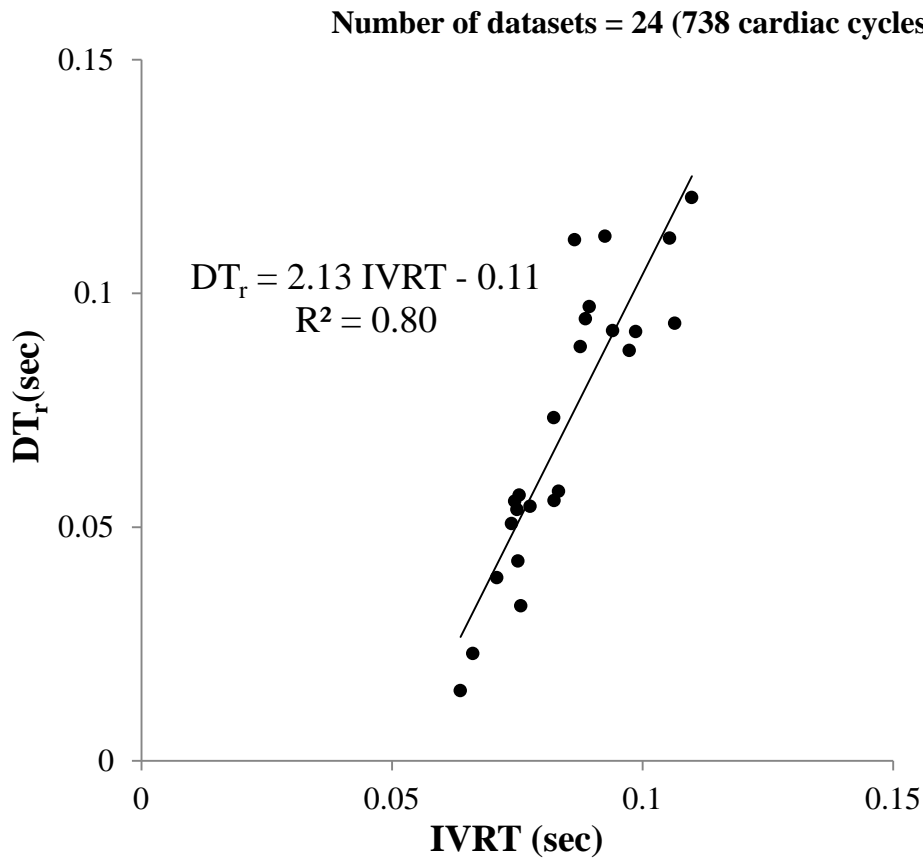
Figure 7.5 Relaxation component of DT vs isovolumic relaxation time.

Least mean square determined linear fit of relaxation component of DT (DT_r) and isovolumic relaxation time (IVRT) in 24 subjects (738 beats analyzed). See text for details.

7.4.4 <u>Fractionation of Deceleration Time in terms of Stiffness and Relaxation Components in Normal and Delayed Relaxation</u>

For the 12 NR datasets 76% of total DT is due to stiffness and 24% is due to relaxation. For the 12 DR datasets 61% of DT is due to stiffness and 39% is due to relaxation (Figure 7.6).

These differences are significant ($p < 0.0001$). Figure 7.6 shows the fraction of DT accounted for by stiffness (S) in the DR group is significantly less than in the NR group

(P<0.0001), and the fraction of DT due to the relaxation (R) in the DR group is significantly

higher than in the NR group (P<0.0001).

Normalized DT Comparison Between Groups
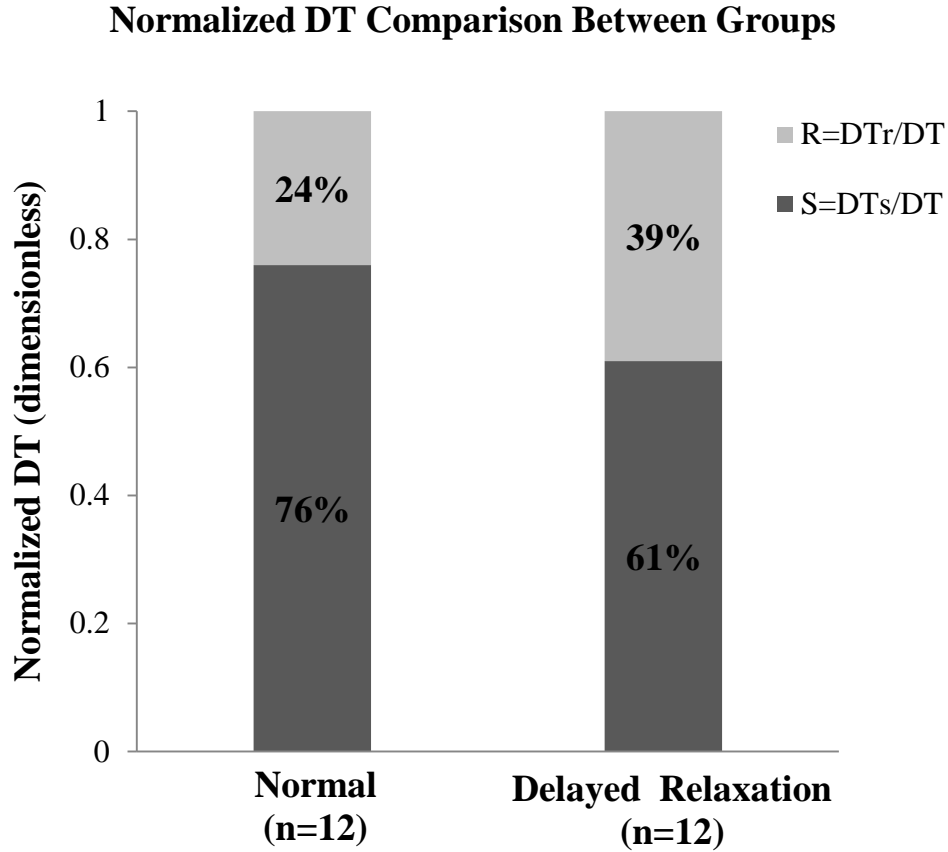
Figure 7.6 Normalized DT in NL and DR groups.

Intergroup comparison of the percentage of normalized DT due to stiffness (S) and relaxation (R).

A significantly larger percentage of total DT is due relaxation in the DR group. See text for details.

7.4.5 <u>Interobserver Variability and Bland-Altman Analysis</u>

As in previous work (2), interobserver variability in applying the PDF formalism for E-wave analysis of the current data was $\leq 8\%$. Two months after the initial analysis, we carried out an inter-observer variability study where datasets were reanalyzed in random order. Bland-Altman analysis shows that PDF parameters, AT, and DT have very good agreement between

observers (Figure 7.7 and 7.8). Less than 5% of all measurements reside outside 1.96 SD of the percentage difference, in keeping with the criteria of Bland and Altman, representing 95% confidence intervals in the results.
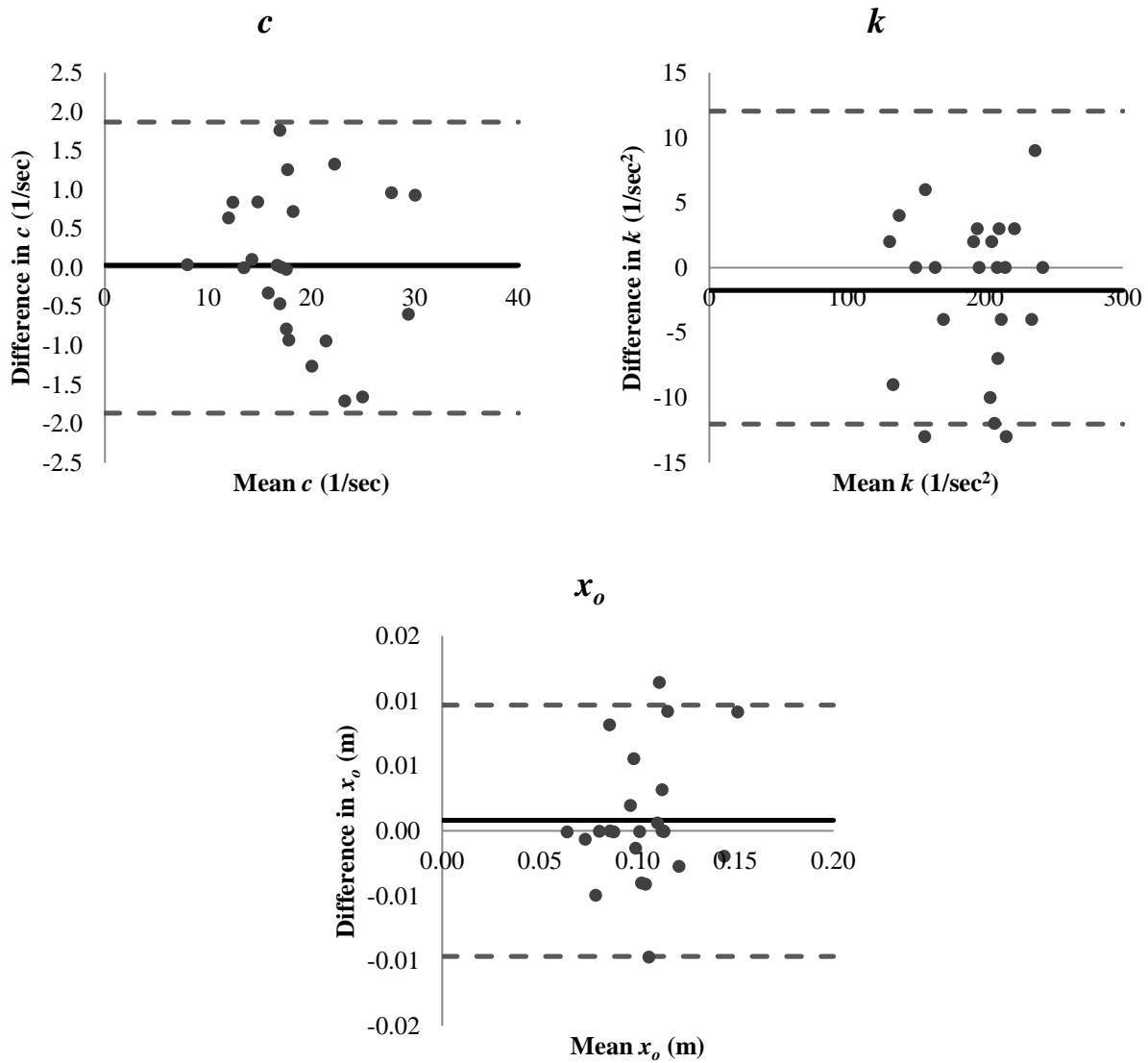
Figure 7.7 Bland-Altman plots of PDF parameters.

Bland-Altman analysis shows that PDF parameters have very good agreement between observers. Less than 5% of all measurements reside outside 1.96 SD of the percentage difference, in keeping with the criteria of Bland and Altman, representing 95% confidence intervals in the results. In each plot the solid line represents the mean difference or the estimated bias and the dashed lines are ±1.96 SD of the percentage difference.
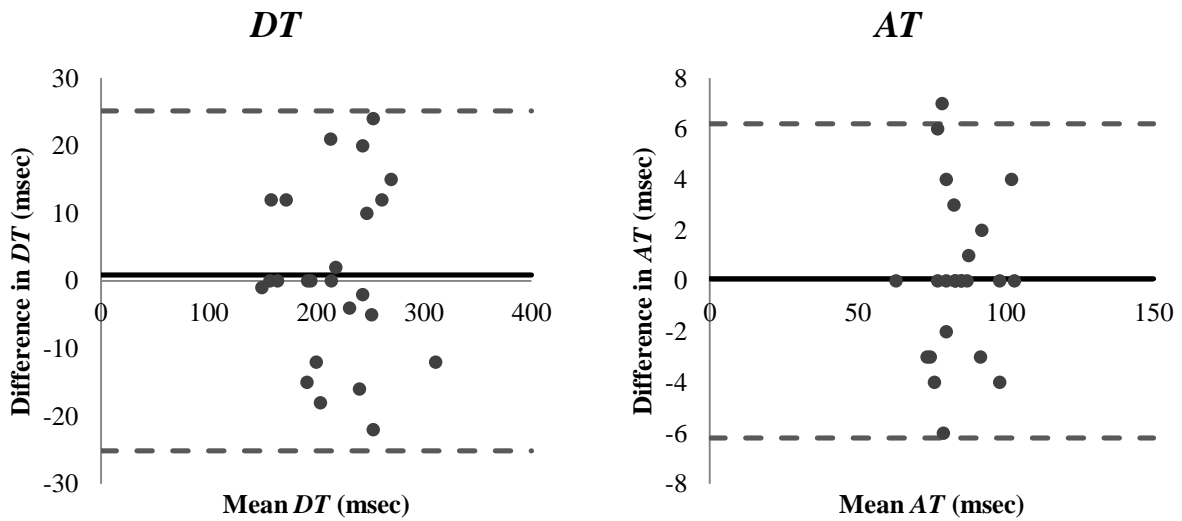
Figure 7.8 Bland-Altman plots of acceleration and deceleration times.

Bland-Altman analysis shows that acceleration time (AT) and deceleration time (DT) of E-wave have very good agreement between observers. Less than 5% of all measurements reside outside 1.96 SD of the percentage difference, in keeping with the criteria of Bland and Altman, representing 95% confidence intervals in the results. In each plot the solid line represents the mean difference or the estimated bias and the dashed lines are ±1.96 SD of the percentage difference.

7.5   Discussion

7.5.1   Stiffness and Relaxation Indexes

Doppler transmitral velocity contours can be accurately approximated by the prediction of a kinematic model (PDF formalism) that incorporates the mechanical suction-pump attribute of all LV chambers (18, 19). The model is linear, it is invertible (provides unique model parameters for each E-wave) and approximates the kinematics of chamber recoil in analogy to damped simple harmonic oscillatory motion (13, 17, 18). Transmitral blood flow is modeled as the result of the interaction of simultaneous elastic, inertial, and damping forces. Linearity assures invertability and mathematically unique values for chamber stiffness (k), viscoelasticity/relaxation (c) and load parameters (x_o) for each E-wave. Chamber stiffness (11, 21, 22, 25, 31, 39) is defined by the slope $\Delta P/\Delta V$ of the P-V relation. Lisauskas et al. has demonstrated the expected high correlation between PDF parameter k and $\Delta P_{avg}/\Delta V_{avg}$ in a large dataset. Little et al (23) have proposed that chamber stiffness (K_{LV}) is related to E-wave DT as:

$$
K_{LV} = \frac{\rho L}{A}\left(\frac{\pi}{2}\frac{1}{DT}\right)^2
$$

indicating an inverse square relationship between stiffness and DT. K_{LV} was shown to correlate with stiffness determined from the LV end-diastolic pressure-volume relationship.

Considering the physiology in kinematic modeling terms that incorporates the suction-pump attribute of the LV, Shmuylovich et al. (38) have shown that DT is jointly (algebraically) determined by stiffness (PDF parameter k) and relaxation (PDF parameter c). Importantly, Shmuylovich et al. have also shown that two subjects with *indistinguishable* E-wave determined DTs, mitral valve areas, and chamber volumes (LVEDV) can have *distinguishable*

catheterization-determined values of chamber stiffness, because of differences in the viscoelastic/relaxation parameter (PDF parameter c) in the two subjects.

Relaxation can be characterized by the time constant (τ) or the logistic time constant (τ_L), from cardiac catheterization data, or by IVRT and DT from echocardiography. The concordance of delayed-relaxation (DT>220ms) and associated prolonged τ indicates that impaired relaxation is a feature of diastolic dysfunction (15, 32, 47, 48). The PDF chamber relaxation/viscosity parameter c has been shown: 1) to have a significant linear correlation with $1/\tau$ (3) and with the 'pressure recovery ratio,' directly determined from the LV waveform after mitral valve opening (46), and 2) differentiate diabetic from non-diabetic hearts in animals (7) and in humans (37).

Because constrictive-restrictive E-wave patterns inscribe tall and narrow E-waves with short DT, the E-wave fits generate higher (compared to normal) PDF parameter k values, indicating increased stiffness, relative to normal DT patterns. In contrast, PDF fits to delayed relaxation patterns (long DT) generate higher c values, indicating delayed relaxation.

In the current study we analyzed simultaneous LV P-V and transmitral flow (echo) data and decomposed E-wave DT is to stiffness (DT_s) and relaxation (DT_r) components. As expected DT_s was highly correlated with (simultaneous) invasively determined (passive) diastatic chamber stiffness (45). Similarly, very strong correlation was observed between DT_r and the time-constant of IVR (τ) from simultaneous high fidelity pressure data and between IVRT determined by echocardiography.

Our study provides a novel methodologic approach employing rigorous causal analytical and modeling methods, that, for the first time, fractionates total DT into its stiffness and relaxation components.

7.5.2   The Load Dependence of DT_s and DT_r

Because all conventional indexes of diastolic function are load-dependent we assessed the correlation between total DT, DT_s, DT_r and load. Although mitral valve opening pressure is the ideal index of load, it was not available, hence we employed LVEDP as the load surrogate, since LVEDP and mitral valve opening pressure are known to be closely correlated (14, 26, 29, 33). The results, for the group as a whole are that DT vs. LVEDP (R^2<0.17), DT_s vs. LVEDP (R^2<0.13), and DT_r vs. LVEDP (R^2<0.20)] indicating that DT, DT_s, DT_r are very weakly load-dependent as expected.

7.5.3   The Heart Rate Dependence of DT_s and DT_r

The heart rate (HR) dependence of the duration of diastole and its phases (E-wave, diastasis and A-wave) have been previously detailed (4). Importantly, for a 100% increase in HR, E-wave duration diminishes by 15%; hence we expect that DT, DT_s, DT_r would only be weakly heart rate dependent. Our results, for the group as a whole, indicate that DT vs. HR (R^2<0.21), DT_s vs. HR (R^2<0.16), and DT_r vs. HR (R^2<0.20) justify this conclusion.

7.6 Limitations

7.6.1 <u>Conductance Volume</u>

The conductance catheter method of volume determination has known limitations related to noise, saturation and calibration that we have previously acknowledged (22, 27, 28, 45). In this study, the channels which provided physiologically consistent P-V loops were selected and averaged. However, since there was no significant volume signal drift during recording, any systematic offset related to calibration of the volume channels did not affect the result when the limits of conductance volume were calibrated via quantitative ventriculography.

7.6.2 <u>Sample Size</u>

Although the number of subjects (n=24) is modest, and may be viewed as a minor limitation, the total number of cardiac cycles analyzed (n=738) and the very high R^2 values observed, mitigates the sample size limitation to an acceptable degree.

7.7   Conclusions

We used the PDF formalism to decompose E-wave deceleration time into its stiffness and relaxation components and utilized in-vivo, human, simultaneous P-V and transmitral echocardiographic data to validate model prediction. We showed that DT_s is primarily determined by the diastatic (passive) chamber stiffness (K), and DT_r is determined by relaxation (τ). This method is general and can be used to decompose any E-wave into its stiffness and relaxation components. It therefore facilitates rigorous noninvasive assessment of the differential effects of pathophysiology and of alternative therapies as determinants of DT and its components.

7.8 References

1.   **Bauman L, Chung CS, Karamanoglu M, and Kovács SJ**. The peak atrioventricular pressure gradient to transmitral flow relation: kinematic model prediction with in vivo validation. *J Am Soc Echocardiogr* 17: 839-844, 2004.

2.   **Boskovski MT, Shmuylovich L, and Kovács SJ**. Transmitral flow velocity-contour variation after premature ventricular contractions: a novel test of the load-independent index of diastolic filling. *Ultrasound Med Biol* 34: 1901-1908, 2008.

3.   **Chung CS, Ajo DM, and Kovács SJ**. Isovolumic pressure-to-early rapid filling decay rate relation: model-based derivation and validation via simultaneous catheterization echocardiography. *J Appl Physiol (1985)* 100: 528-534, 2006.

4.   **Chung CS, Karamanoglu M, and Kovács SJ**. Duration of diastole and its phases as a function of heart rate during supine bicycle exercise. *Am J Physiol Heart Circ Physiol* 287: H2003-2008, 2004.

5.   **Chung CS, and Kovács SJ**. Physical determinants of left ventricular isovolumic pressure decline: model prediction with in vivo validation. *Am J Physiol Heart Circ Physiol* 294: H1589-1596, 2008.

6.   **Courtois M, Kovács SJ, and Ludbrook PA**. Transmitral pressure-flow velocity relation. Importance of regional pressure gradients in the left ventricle during diastole. *Circulation* 78: 661-671, 1988.

7.   **Dent CL, Bowman AW, Scott MJ, Allen JS, Lisauskas JB, Janif M, Wickline SA, and Kovács SJ**. Echocardiographic characterization of fundamental mechanisms of abnormal diastolic filling in diabetic rats with a parameterized diastolic filling formalism. *J Am Soc Echocardiogr* 14: 1166-1172, 2001.

8.   **Eucker SA, Lisauskas JB, Singh J, and Kovács SJ**. Phase plane analysis of left ventricular hemodynamics. *J Appl Physiol (1985)* 90: 2238-2244, 2001.

9.   **Feigenbaum H**. *Echocardiography*. Baltimore, MD: Williams & Wilkins, 1993.

10.   **Flachskampf FA, Weyman AE, Guerrero JL, and Thomas JD**. Calculation of atrioventricular compliance from the mitral flow profile: analytic and in vitro study. *J Am Coll*

Cardiol 19: 998-1004, 1992.

11.   **Garcia MJ, Firstenberg MS, Greenberg NL, Smedira N, Rodriguez L, Prior D, and Thomas JD**. Estimation of left ventricular operating stiffness from Doppler early filling deceleration time in humans. *Am J Physiol Heart Circ Physiol* 280: H554-561, 2001.

12.   **Hall AF, Aronovitz JA, Nudelman SP, and Kovács SJ**. Automated method for characterization of diastolic transmitral Doppler velocity contours: late atrial filling. *Ultrasound Med Biol* 20: 859-869, 1994.

13.   **Hall AF, and Kovács SJ**. Automated method for characterization of diastolic transmitral Doppler velocity contours: early rapid filling. *Ultrasound Med Biol* 20: 107-116, 1994.

14.   **Ishida Y, Meisner JS, Tsujioka K, Gallo JI, Yoran C, Frater RW, and Yellin EL**. Left ventricular filling dynamics: influence of left ventricular relaxation and left atrial pressure. *Circulation* 74: 187-196, 1986.

15.   **Kass DA, Bronzwaer JG, and Paulus WJ**. What mechanisms underlie diastolic dysfunction in heart failure? *Circ Res* 94: 1533-1542, 2004.

16.   **Kovács S, MD M, and CS P**. Modelling cardiac fluid dynamics and diastolic function. *Philosophical Transactions of the Royal Society (A)* 359: 1299-1314, 2001.

17.   **Kovács SJ, Barzilai B, and Pérez JE**. Evaluation of diastolic function with Doppler echocardiography: the PDF formalism. *Am J Physiol* 252: H178-187, 1987.

18.   **Kovács SJ, Meisner JS, and Yellin EL**. Modeling of diastole. *Cardiol Clin* 18: 459-487, 2000.

19.   **Kovács SJ, Setser R, and Hall AF**. Left ventricular chamber stiffness from model-based image processing of transmitral Doppler E-waves. *Coron Artery Dis* 8: 179-187, 1997.

20.   **Lee DS, Gona P, Vasan RS, Larson MG, Benjamin EJ, Wang TJ, Tu JV, and Levy D**. Relation of disease pathogenesis and risk factors to heart failure with preserved or reduced ejection fraction: insights from the framingham heart study of the national heart, lung, and blood institute. *Circulation* 119: 3070-3077, 2009.

21.   **Lisauskas J, Singh J, Courtois M, and Kovács SJ**. The relation of the peak Doppler E-wave to peak mitral annulus velocity ratio to diastolic function. *Ultrasound Med Biol* 27: 499-

507, 2001.

22.   **Lisauskas JB, Singh J, Bowman AW, and Kovács SJ**. Chamber properties from transmitral flow: prediction of average and passive left ventricular diastolic stiffness. *J Appl Physiol (1985)* 91: 154-162, 2001.

23.   **Little WC, Ohno M, Kitzman DW, Thomas JD, and Cheng CP**. Determination of left ventricular chamber stiffness from the time for deceleration of early left ventricular filling. *Circulation* 92: 1933-1939, 1995.

24.   **Maeder MT, and Kaye DM**. Heart failure with normal left ventricular ejection fraction. *J Am Coll Cardiol* 53: 905-918, 2009.

25.   **Marino P, Little WC, Rossi A, Barbieri E, Anselmi M, Destro G, Prioli A, Lanzoni L, and Zardini P**. Can left ventricular diastolic stiffness be measured noninvasively? *J Am Soc Echocardiogr* 15: 935-943, 2002.

26.   **Miki S, Murakami T, Iwase T, Tomita T, Nakamura Y, and Kawai C**. Doppler echocardiographic transmitral peak early velocity does not directly reflect hemodynamic changes in humans: importance of normalization to mitral stroke volume. *J Am Coll Cardiol* 17: 1507-1516, 1991.

27.   **Mossahebi S, and Kovács SJ**. Kinematic modeling-based left ventricular diastatic (passive) chamber stiffness determination with in-vivo validation. *Ann Biomed Eng* 40: 987-995, 2012.

28.   **Mossahebi S, Shmuylovich L, and Kovács SJ**. The thermodynamics of diastole: kinematic modeling-based derivation of the P-V loop to transmitral flow energy relation with in vivo validation. *Am J Physiol Heart Circ Physiol* 300: H514-521, 2011.

29.   **Murakami T, Hess OM, Gage JE, Grimm J, and Krayenbuehl HP**. Diastolic filling dynamics in patients with aortic stenosis. *Circulation* 73: 1162-1174, 1986.

30.   **Nagueh SF, Appleton CP, Gillebert TC, Marino PN, Oh JK, Smiseth OA, Waggoner AD, Flachskampf FA, Pellikka PA, and Evangelista A**. Recommendations for the evaluation of left ventricular diastolic function by echocardiography. *J Am Soc Echocardiogr* 22: 107-133, 2009.

31.   **Nikolić S, Yellin EL, Tamura K, Vetter H, Tamura T, Meisner JS, and Frater RW**.

Passive properties of canine left ventricle: diastolic stiffness and restoring forces. *Circ Res* 62: 1210-1222, 1988.

32.   **Oh JK, Appleton CP, Hatle LK, Nishimura RA, Seward JB, and Tajik AJ**. The noninvasive assessment of left ventricular diastolic function with two-dimensional and Doppler echocardiography. *J Am Soc Echocardiogr* 10: 246-270, 1997.

33.   **Ohte N, Nakano S, Mizutani Y, Samoto T, and Fujinami T**. [Relation of mitral valve motion to left ventricular end-diastolic pressure assessed by M-mode echocardiography]. *J Cardiogr* 16: 115-120, 1986.

34.   **Oki T, Tabata T, Mishiro Y, Yamada H, Abe M, Onose Y, Wakatsuki T, Iuchi A, and Ito S**. Pulsed tissue Doppler imaging of left ventricular systolic and diastolic wall motion velocities to evaluate differences between long and short axes in healthy subjects. *J Am Soc Echocardiogr* 12: 308-313, 1999.

35.   **Omens JH, and Fung YC**. Residual strain in rat left ventricle. *Circ Res* 66: 37-45, 1990.

36.   **Owan TE, Hodge DO, Herges RM, Jacobsen SJ, Roger VL, and Redfield MM**. Trends in prevalence and outcome of heart failure with preserved ejection fraction. *N Engl J Med* 355: 251-259, 2006.

37.   **Riordan MM, Chung CS, and Kovács SJ**. Diabetes and diastolic function: stiffness and relaxation from transmitral flow. *Ultrasound Med Biol* 31: 1589-1596, 2005.

38.   **Shmuylovich L, and Kovács SJ**. E-wave deceleration time may not provide an accurate determination of LV chamber stiffness if LV relaxation/viscoelasticity is unknown. *Am J Physiol Heart Circ Physiol* 292: H2712-2720, 2007.

39.   **Templeton GH, and Nardizzi LR**. Elastic and viscous stiffness of the canine left ventricle. *J Appl Physiol* 36: 123-127, 1974.

40.   **Thomas JD, Choong CY, Flachskampf FA, and Weyman AE**. Analysis of the early transmitral Doppler velocity curve: effect of primary physiologic changes and compensatory preload adjustment. *J Am Coll Cardiol* 16: 644-655, 1990.

41.   **Thomas JD, Flachskampf FA, Chen C, Guererro JL, Picard MH, Levine RA, and Weyman AE**. Isovolumic relaxation time varies predictably with its time constant and aortic and left atrial pressures: implications for the noninvasive evaluation of ventricular relaxation. *Am*

Heart J 124: 1305-1313, 1992.

42. **Thomas JD, Newell JB, Choong CY, and Weyman AE**. Physical and physiological determinants of transmitral velocity: numerical analysis. *Am J Physiol* 260: H1718-1731, 1991.

43. **Weiss JL, Frederiksen JW, and Weisfeldt ML**. Hemodynamic determinants of the time-course of fall in canine left ventricular pressure. *J Clin Invest* 58: 751-760, 1976.

44. **Zhang W, Chung CS, Shmuylovich L, and Kovács SJ**. Is left ventricular volume during diastasis the real equilibrium volume, and what is its relationship to diastolic suction? *J Appl Physiol (1985)* 105: 1012-1014, 2008.

45. **Zhang W, and Kovács SJ**. The diastatic pressure-volume relationship is not the same as the end-diastolic pressure-volume relationship. *Am J Physiol Heart Circ Physiol* 294: H2750-2760, 2008.

46. **Zhang W, Shmuylovich L, and Kovács SJ**. The E-wave delayed relaxation pattern to LV pressure contour relation: model-based prediction with in vivo validation. *Ultrasound Med Biol* 36: 497-511, 2010.

47. **Zile MR, Baicu CF, and Gaasch WH**. Diastolic heart failure--abnormalities in active relaxation and passive stiffness of the left ventricle. *N Engl J Med* 350: 1953-1959, 2004.

48. **Zile MR, and Brutsaert DL**. New concepts in diastolic dysfunction and diastolic heart failure: Part I: diagnosis, prognosis, and measurements of diastolic function. *Circulation* 105: 1387-1393, 2002.

Chapter 8: Fractionation Method Application in Normal Sinus Rhythm vs. Atrial Fibrillation

8.1 Abstract

Although the electrophysiologic derangement responsible for atrial fibrillation (AF) has been elucidated, how AF remodels the ventricular chamber and affects diastolic function (DF) has not been fully characterized. The previously validated Parametrized Diastolic Filling (PDF) formalism models suction-initiated filling kinematically and generates error-minimized fits to E-wave contours using unique load (x_o), relaxation (c), and stiffness (k) parameters. It predicts that E-wave deceleration time (DT) is a function of both stiffness and relaxation. Ascribing DT_s to stiffness and DT_r to relaxation such that $DT = DT_s + DT_r$ is legitimate because of causality and their predicted and observed high correlation (r=0.82 and r=0.94) with simultaneous (diastatic) chamber stiffness (dP/dV) and isovolumic relaxation (tau), respectively.

We analyzed simultaneous echocardiography-cardiac catheterization data and compared 16 age matched, chronic AF subjects to 16, normal sinus rhythm (NSR) subjects (650 beats). All subjects had diastatic intervals. Conventional DF parameters (DT, AT, E_{peak}, E_{dur}, E-VTI, E/E') and E-wave derived PDF parameters (c, k, DT_s, DT_r) were compared. Total DT and DT_s, DT_r in AF were shorter than in NSR (p<0.005), chamber stiffness, (k) in AF was higher than in NSR (p<0.001). For NSR, 75% of DT was due to stiffness and 25% was due to relaxation whereas for AF 81% of DT was due to stiffness and 19% was due to relaxation (p<0.005).

We conclude that compared to NSR, increased chamber stiffness is one measurable consequence of chamber remodeling in chronic, rate controlled AF. A larger fraction of E-wave DT in AF is due to stiffness compared to NSR. By trending individual subjects, this method can elucidate and characterize the beneficial or adverse long-term effects on chamber remodeling due to alternative therapies in terms of chamber stiffness and relaxation.

8.2   Introduction

Atrial fibrillation (AF) is a known correlate of heart failure (HF) and affects millions of patients worldwide. Investigators have demonstrated that AF and HF are concordant and increase overall mortality rate (7, 10, 22, 34). Significant progress has been made in the diagnosis, electrophysiologic mechanism, and treatment of AF (1, 4, 6, 7, 10-12, 22, 30, 34). However, the mechanistic consequences of AF on left ventricular (LV) function, chamber stiffness and relaxation, and global LV diastolic function (DF) in particular, remain incompletely characterized.

The instantaneous slope of the left ventricular (LV) pressure-volume relation, dP/dV, defines chamber stiffness and serves as one of the two main parameters (the other is relaxation) by which global diastolic function (DF) is quantitated (17, 31, 38, 39). Traditionally, LV chamber stiffness is determined invasively from the slope (ΔP/ΔV) of the end-diastolic pressure volume relationship (EDPVR). However, due to the lack of atrial contraction, end-diastole in AF and NSR are different physiologic states. Hence the EDPVR cannot be used to compare the chamber stiffness in AF with that in NSR. Therefore, the diastatic pressure volume relationship (D-PVR) provides the appropriate physiologic metric for AF vs. NSR chamber stiffness comparison. It has been established that (passive) diastatic chamber stiffness, i.e. the slope of D-PVR, is significantly elevated in AF compared to NSR (27).

Chamber stiffness (ΔP/ΔV) is a 'relative' index and can be determined using 'relative' (echo), rather than 'absolute' (cath) measurement methods. Little et al (24) used physiologic modeling to predict that E-wave DT is determined by stiffness (K_{LV}) alone. However, for E-wave contours well fit by underdamped oscillatory kinematics, the PDF formalism (21) parameter k is

233

the algebraic equivalent of K_{LV}.

Clinicians know that tall, narrow E-waves having a short DT, referred to as the 'constrictive-restrictive' pattern, are associated with stiff chambers. Similarly, long DT is referred to as a manifestation of the 'delayed relaxation' pattern. Therefore, from an intuitive clinical perspective it is self-evident that both stiffness and relaxation must be DT determinants. This intuitive role of stiffness and relaxation as DT determinants has been made physiologically precise by Shmuylovich et al who have shown that two subjects having echocardiographically indistinguishable DT can have significantly distinguishable values of chamber stiffness and relaxation (tau) on simultaneous hemodynamic analysis. Using PDF-based analysis, the derived algebraic expression for DT was shown to be a function of both stiffness (PDF parameter k) and relaxation (PDF parameter c) (33). The aforementioned naturally justifies decomposition of E-wave DT into its stiffness (DT_s) and relaxation (DT_r) components such that $DT = DT_s + DT_r$ (25). The expected causal relationship between DT_s and DT_r and simultaneous stiffness ($\Delta P/\Delta V$) and relaxation (tau) has been firmly established by the high observed correlation (r=0.82 and r=0.94 respectively) (25).

We hypothesized that AF LVs are stiffer than NSR LVs. Consequently, decomposition of E-wave DT into stiffness (DT_s) and relaxation (DT_r) components will show that, compared to NSR, DT_s is shorter in AF and a larger percentage of E-wave DT in AF is due to stiffness than to relaxation.

8.3 Methods

8.3.1 <u>Subject Selection</u>

Thirty two datasets (mean age 61, 22 men) were selected from the Cardiovascular Biophysics Laboratory database (8). Subjects underwent elective cardiac catheterization to determine presence of suspected coronary artery disease at the request of their referring physicians. All participants provided informed consent prior to the procedure using a protocol approved by the Washington University Human Research Protection Office (HRPO). The clinical descriptors of the 32 subjects are shown in Table 8.1.

Table 8.1 The clinical descriptors of NSR and AF groups.

Clinical Descriptors	NSR Group	AF Group	Significance
N	16	16	N.A.
Age (y)	61±8	61±9	0.92
Gender (M/F)	10/6	12/4	N.A.
Heart Rate (bpm)	62±9	76±9	<0.001
Ejection Fraction (LVEF) (%)	73±8	55±17	<0.01
Height (cm)	172±10	178±10	N.S.
Weight (kg)	89±14	99±18	N.S.

LVEF, left ventricular ejection fraction (via calibrated ventriculography); NSR, normal sinus rhythm; AF, atrial fibrillation; N.S., not significant; N.A., not applicable.

Data are presented as mean ± standard deviation.

Sixteen datasets of subjects in NSR, were selected so they were aged matched with the 16 subjects of the chronic AF group (average duration 7.3±4.1 years). All were in AF during data acquisition. Selection criteria for the NSR group were: no active ischemia, normal valvular function, normal LV ejection fraction (LVEF≥50%), no history of myocardial infarction, peripheral vascular disease, or bundle branch block, and clear diastatic intervals following E-waves. Selection criteria for the AF group were similar, with the exception that four of the 16 AF subjects had LVEF somewhat < 50%.

Among the 16 NSR datasets, 9 had normal LV end-diastolic pressure (LVEDP<14 mmHg), 3 had 15 mmHg < LVEDP < 20 mmHg and 4 had elevated LVEDP (>21 mmHg). The distribution of LVEDPs in the 15 AF group datasets were: 3 with LVEDP<14, 9 with 15<LVEDP<20 mmHg and 4 with LVEDP>21. A total of 650 cardiac cycles (20 beats/subject) of simultaneous echocardiographic-high fidelity hemodynamic (conductance catheter) data were analyzed. The hemodynamic and echocardiographic indices of 32 subjects are shown in Table 8.2.

Table 8.2 Hemodynamic and echocardiographic data in NSR and AF groups.

	NSR	AF	Significance
Hemodynamic Parameters:			
LVEDP (mmHg)	17±5	18±4	0.48
LVEDV (ml)	159±12	167±55	0.59
Diastatic stiffness (mmHg/ml)	0.11±0.05	0.18±0.08	<0.01
τ (msec)	59±7	50±10	<0.01
Echocardiographic Parameters			
Peak E-wave velocity (E_{peak}) (cm/s)	71±15	89±26	<0.05
E-wave acceleration time (AT) (ms)	89±11	84±8	0.13
E-wave deceleration time (DT) (ms)	192±19	153±22	<0.001
E-wave duration time (E_{dur}) (ms)	281±27	236±26	<0.001
E/E'(dimensionless)	4.7±1.8	6.0±1.9	<0.05
x_o (cm)	10.2±2.5	10.1±2.9	0.93
k (1/sec^2)	191±41	274±70	<0.001
c (1/sec)	15.7±3.0	16.3±3.5	0.65
DT_r (msec)	50±10	30±12	<0.001
DT_s (msec)	142±14	123±20	<0.005
R = DT_r/ DT (%)	25±3	19±7	<0.005
S = DT_s/ DT (%)	75±3	81±7	<0.005

LVEDP, left ventricular end-diastolic pressure; LVEDV, left ventricular end-diastolic volume; τ, time constant of isovolumic relaxation; E/E', ratio of Epeak and E'peak; E-VTI, E-wave velocity-time integral; k, PDF stiffness parameter; c, PDF relaxation parameter; DT_r, relaxation component of DT; DT_s, stiffness component of DT. Data are presented as mean ± standard deviation.

8.3.2   <u>Data Acquisition</u>

The high fidelity, simultaneous echocardiographic transmitral flow and pressure-volume (P-V) data recording method has been previously described (3, 8, 20, 21, 23, 28). Briefly, immediately prior to arterial access a complete 2-D echo-Doppler study in a supine position using a Philips (Andover, MA.) iE33 system is performed according to American Society of Echocardiography (ASE) criteria (15). After arterial access and placement of a 64-cm, 6-Fr sheath (Arrow, Reading, PA), a 6-Fr micromanometer conductance catheter (SPC-560, SPC-562, or SSD-1034, Millar Instruments, Houston, TX) was directed across the aortic valve under fluoroscopic control. Pressure and volume signals were processed through clinical amplifier systems (Quinton Diagnostics, General Electric, CD Leycom) and recorded by a custom personal computer via a standard interface (Sigma-5). Simultaneous transmitral Doppler images were obtained (15) using a clinical imaging system (Philips iE33, Andover, MA). Following data acquisition, end-systolic and end-diastolic volumes (ESV, EDV) were determined by calibrated quantitative ventriculography.

8.3.3   <u>Doppler E-wave Analysis</u>

For each subject, approximately 1-2 minutes of continuous transmitral flow data were recorded in the pulsed-wave Doppler mode. Echocardiographic data acquisition is performed in accordance with published ASE (29) guidelines. In accordance with convention, the apical 4-chamber view was used for Doppler E-wave recording with the sample volume located at the leaflet tips. An average of 20 beats per subject were analyzed (650 cardiac cycles total for the 32 subjects).

Doppler transmitral E-wave contours were analyzed using the conventional triangle shape approximation (2, 13), yielding peak E-wave velocity (E_peak), acceleration time (AT), deceleration time (DT), velocity-time integral (E-VTI), E/E'.

Each E-wave was also analyzed via the Parametrized Diastolic Filling (PDF) formalism to yield, mathematically unique PDF parameters for each E-wave (stiffness parameter (k), chamber viscoelasticity/relaxation parameter (c), load parameter (x_o)) (18, 19, 23).

The PDF Formalism

The kinematics of filling is modeled using the Parameterized Diastolic Filling (PDF) formalism which uses a linear, bi-directional spring to approximate early filling in accordance with the velocity of a damped SHO (19). In accordance with Newton's second law, the equation of motion is:

$$\frac{d^2x}{dt^2} + c\frac{dx}{dt} + kx = 0 \qquad [8.1]$$

Because the E-wave has zero initial velocity, the model's initial velocity is zero ($v(0)=0$). However, the SHO has a non-zero initial spring displacement, x_o. Systole stores elastic strain in tissue, which at mitral valve opening, is available to power mechanical recoil and the ventricular suction process. Equation [8.1] allows calculation of parameters c and k per unit mass. The predicted contour of the clinical E-wave is obtained from the solution for the SHO velocity. The underdamped solution is:

$$v(t) = -\frac{x_o k}{\omega}\exp(-ct/2)\sin(\omega t) \qquad [8.2]$$

where $\omega = \sqrt{4k - c^2}/2$. The determination of PDF parameters from each E-wave solves the

239

'inverse problem' of diastole and generates a unique set of x_o, c, and k (16) values for each contour. The three parameters x_o, c, and k encompass the (lumped) physiologic determinants of all E-wave contours. The initial oscillator displacement x_o (cm) is linearly related to the velocity-time integral (VTI) of the E-wave (21). Chamber stiffness (dP/dV) is linearly related to the spring constant k (g/s^2) (20, 21, 23), while the chamber viscoelasticity/relaxation index c (g/s) characterizes the resistance of the process (20, 21). E-waves with long concave up deceleration portions ('delayed relaxation pattern') are fit by the overdamped solution and have higher c values, while E-waves that approximate nearly symmetric sine waves are fit by the underdamped solution and have lower c values (33).

Briefly, echocardiographic images are cropped, the mitral E-wave maximum velocity envelopes are identified and fit by the PDF generated solution using the Levenberg-Marquardt algorithm to yield the best-fit PDF parameter x_o, c, and k, values. The process is achieved using a custom LabVIEW (National Instruments, Austin, TX) interface (16). In addition to providing parameter values the algorithm also provides a simultaneous measure of goodness of fit. Additional PDF-derived indexes include the stored elastic strain energy available for ventricular suction ($1/2kx_o^2$) at the onset of filling, and the peak atrio-ventricular pressure gradient (kx_o) (3, 28).

As in previous work (5, 8), interobserver variability in applying the PDF formalism for E-wave analysis was $\leq 8\%$.

Determination of Stiffness and Relaxation Components of E-wave Deceleration Time

PDF model predicts that E-wave deceleration time (DT) is a function of both stiffness and relaxation (33). PDF-based E-wave analysis provides a method for fractionating total DT

into its stiffness (DT_s) and relaxation (DT_r) components such that $DT=DT_s+DT_r$. The fractionation method has been previously validated with DT_s and DT_r correlating with simultaneous stiffness (dP/dV) and relaxation (tau) with r=0.82 and r=0.94 respectively (25).

The duration of the E-wave, AT, and DT are measured as usual from Doppler echo images using a triangle to approximate E-wave shape (Figure 8.1). The effect of delayed relaxation on an ideal (generated by recoil only) E-wave is to decrease its peak amplitude and lengthen its DT. Accordingly, DT_r is determined by using the same x_o and k as the original E-wave but setting $c=0$ and thereby providing the PDF generated ideal contour. Subtracting the ideal E-wave duration from actual total duration yields DT_r (Figure 8.1). Therefore, E-wave DT is decomposed into its determinants as $DT = DT_s + DT_r$. It is known that DT_s, DT_r are only weakly load and heart rate dependent (25).

Stiffness (DT_s) and relaxation (DT_r) components of DT were computed via the fractionation method employed previously (25) such that $DT=DT_s+DT_r$. By determining DT_s and DT_r of each E-wave, the total DT can be expressed as the fraction due to stiffness ($S=DT_s/DT$) and the fraction of DT due to relaxation ($R=DT_r/DT$) for each E-wave analyzed.

241
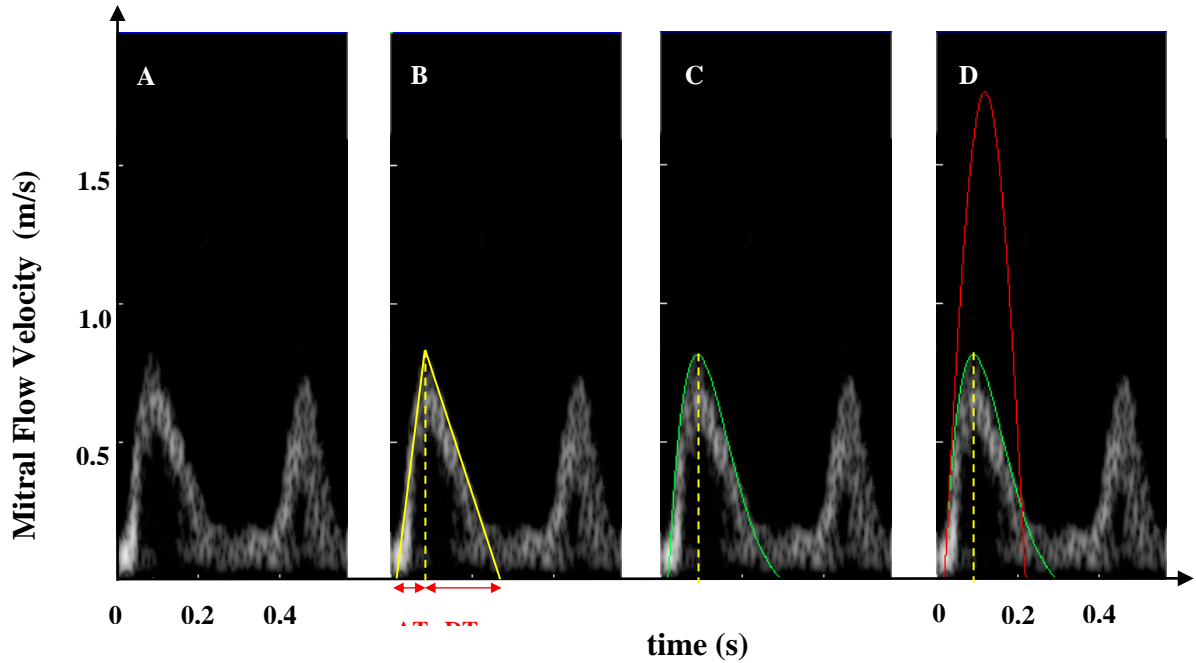
Figure 8.1 Overview of DT_s and DT_r computation.

A) A typical Doppler velocity profile. Note diastatic interval between E- and A-waves. B) AT and DT determination using triangle method. C) PDF model-predicted fit to E-wave (green) provides numerically unique PDF parameters $c=21.8$/s, $k=248$/s2, $x_o=11.2$cm for each analyzed E-wave. D) Model predicted E-wave (red) having same x_o, k values as original (green) E-wave but with PDF parameter $c=0$, assumes relaxation plays no role in determining waveform. The effect of relaxation (where $c\neq0$) is to lengthen DT and decrease E-wave amplitude. Hence, green DT is longer and its amplitude is less than red waveform. The numerical difference between actual green ($c\neq0$) DT minus red DT ($c=0$) equals DT_r. $DT_s = DT - DT_r$. DT=0.206 s, DT_r=0.077 s and DT_s=0.129 s. See text for details.

8.3.4 <u>Determination of Diastatic Stiffness from P-V Data</u>

Hemodynamics were determined from the high-fidelity Millar LV P-V data from each beat. The quantitative ventriculography was used to determine end-systolic and end-diastolic volumes which defined the limits of volume tracing of conductance catheter has been previously detailed (23, 26, 28, 36). After calibration of conductance volume, LV pressure and

volume at diastasis were measured beat-by-beat using a custom MATLAB program. End-diastasis points were defined by ECG P wave onset (26, 28, 36, 37). As previously (28, 36) for each subject, diastatic P-V data points generated by load varying cardiac cycles were fit via linear regression, to provide diastatic chamber stiffness as the slope (K) of D-PVR.

8.3.5   Statistical Analysis

For each subject, parameters were averaged for the beats selected. Comparisons of diastatic stiffness, AT, DT, E_{dur}, PDF parameters, and other parameters between NSR and AF groups were carried out by Student's t-test using MS-Excel (Microsoft, Redmond, WA).

8.4   Results

8.4.1 <u>Diastatic Stiffness and other Invasive Measurements in NSR and AF</u>

LV (passive) chamber stiffness measured as the slope of the D-PVR is significantly higher in the AF group than that in the NSR group (0.18 ± 0.08 mmHg/ml vs. 0.11 ± 0.05 mmHg/ml, $p<0.01$). In contrast to NSR, (where diastatic pressure and volume is different than end-diastolic pressure and volume at end atrial systole), in AF, diastatic pressure and volume is the <u>same</u> as end-diastolic pressure and volume since there is no atrial contraction in AF. In AF diastatic pressure and volume are similar to the diastatic pressure and volume in NSR (18 ± 4 mmHg for AF vs. 17 ± 5 mmHg for NSR, $p=0.48$ and 167 ± 55 ml for AF vs. 159 ± 12 ml for NSR, $p=0.59$).

8.4.2 <u>Triangle Method Measurements of E-waves in NSR and AF</u>

Figure 8.2 shows that E-wave DT and E-wave duration (E_{dur}) are significantly shorter in the AF group than NSR group (DT: 153 ± 22 msec vs. 192 ± 19 msec, $p<0.001$, E_{dur}: 236 ± 26 msec vs. 281 ± 27 msec, $p<0.001$). E-wave acceleration time (AT) is not significantly different between the two groups (84 ± 8 msec vs. 89 ± 11 msec, $p=0.13$).
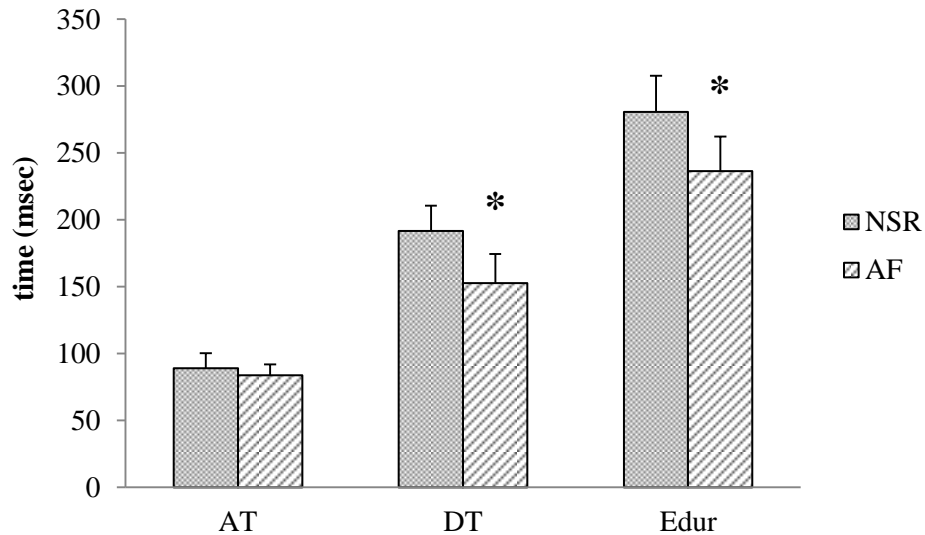
Figure 8.2 AT, DT, and E_{dur} in NSR and AF groups.

AT, DT, and E_{dur} determined by approximating E-wave shape as a triangle in NSR group (16 subjects) and AF group (16 subjects). Significant differences between DT and E_{dur} are denoted by asterisk (*). (DT: p<0.001, Edur: p<0.001) between groups. See Table 2 and text for details.

8.4.3   PDF Measurements in NSR and AF

Results from PDF analysis show (Figure 8.3) that PDF stiffness parameter (k) in AF group is higher (stiffer) than NSR group (274 ± 70 $1/\sec^2$ vs. 191 ± 41 $1/\sec^2$, p<0.001). PDF parameters c, x_o are not significantly different between AF and NSR groups (c: 15.7 ± 3.0 $1/\sec$ vs. 16.3 ± 3.5 $1/\sec$, p=0.65 and x_o: 10.2 ± 2.5 cm vs. 10.1 ± 2.9 cm, p=0.93).
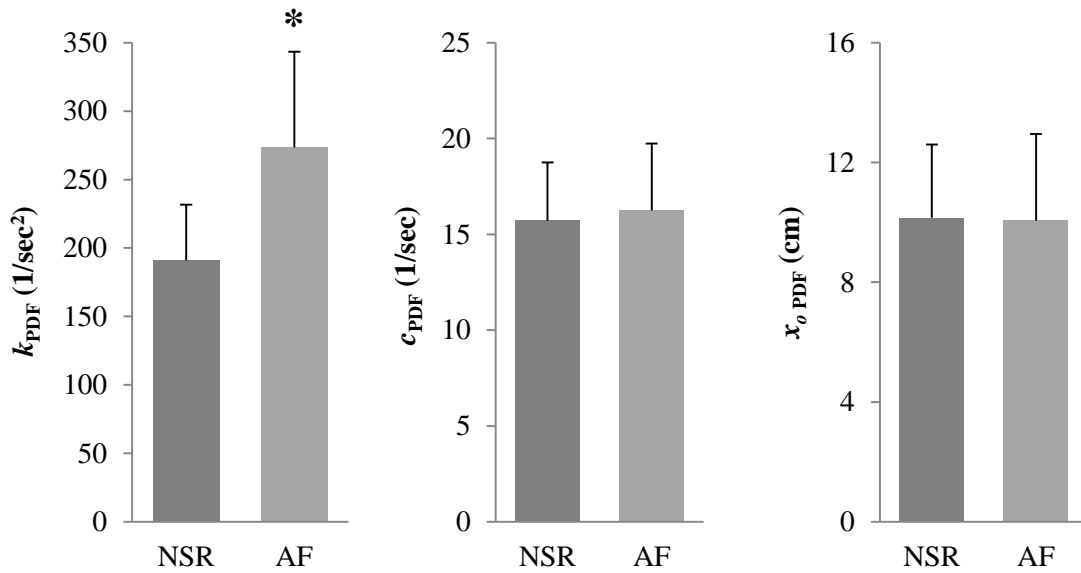
Figure 8.3 PDF parameters in NSR and AF groups.

PDF parameters (k, c, and x_o) in NSR group (16 subjects) and AF group (16 subjects). Significant ($p<0.001$) differences between groups for k are denoted by asterisk (*) indicating that AF chambers at diastasis are stiffer than NSR chambers at diastasis. See text for details.

8.4.4 Fractionation of Deceleration Time into Stiffness and Relaxation Components in NSR and AF

Figure 8.4 shows the stiffness and relaxation components in both groups and their contribution to DT. The relaxation (DT_r) component of DT in AF is shorter than in NSR ($DT_{r\ AF}=30\pm12$ vs. $DT_{r\ NSR}=50\pm10$, $p<0.001$). The stiffness (DT_s) component of DT in AF, which is inversely related to chamber stiffness, is shorter than in NSR ($DT_{s\ AF}=123\pm20$ vs. $DT_{s\ NSR}=142\pm14$, $p<0.005$). The shorter DT_s in AF and the known inverse relation between DT_s and (diastatic) stiffness indicates that AF chambers are stiffer than NSR chambers.
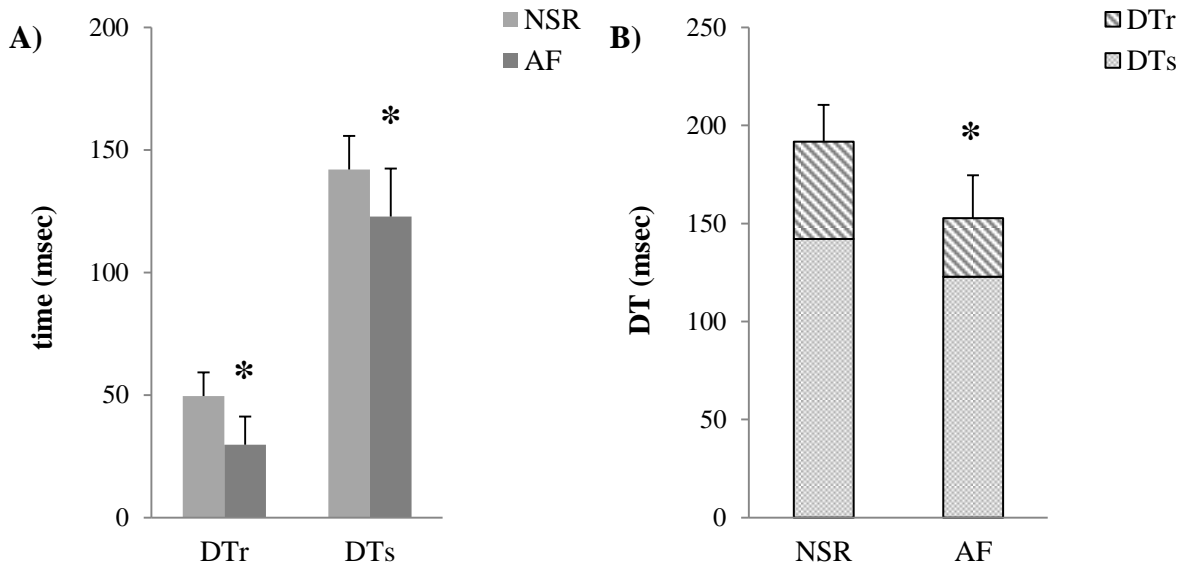
Figure 8.4 DT, stiffness and relaxation components of DT in NSR and AF groups.

A) Comparison of stiffness (DT_s), relaxation (DT_r) components of total DT according to group. Asterisk (*) indicates DTs and DTr are both significantly shorter in AF than in NSR.

B) Comparison of total DT between groups indicates significant difference (*). When DT is decomposed into its DT_s, DT_r components in NSR and AF groups, significant intergroup differences in components persist as shown in Panel A. See text for details.

DT_r and time constant of isovolumic relaxation (τ) were highly correlated in both NSR and AF groups (NSR: $DT_r = 1.30 \tau - 0.03$, $R^2=0.84$, AF: $DT_r = 1.11 \tau - 0.03$, $R^2=0.77$) (Figure 8.5). DT_s and diastatic stiffness derived from P-V data (K) were highly correlated in both NSR and AF groups (NSR: $DT_s = -0.21 K + 0.16$, $R^2=0.57$, AF: $DT_s = -0.19 K + 0.16$, $R^2=0.56$) (Figure 8.6).
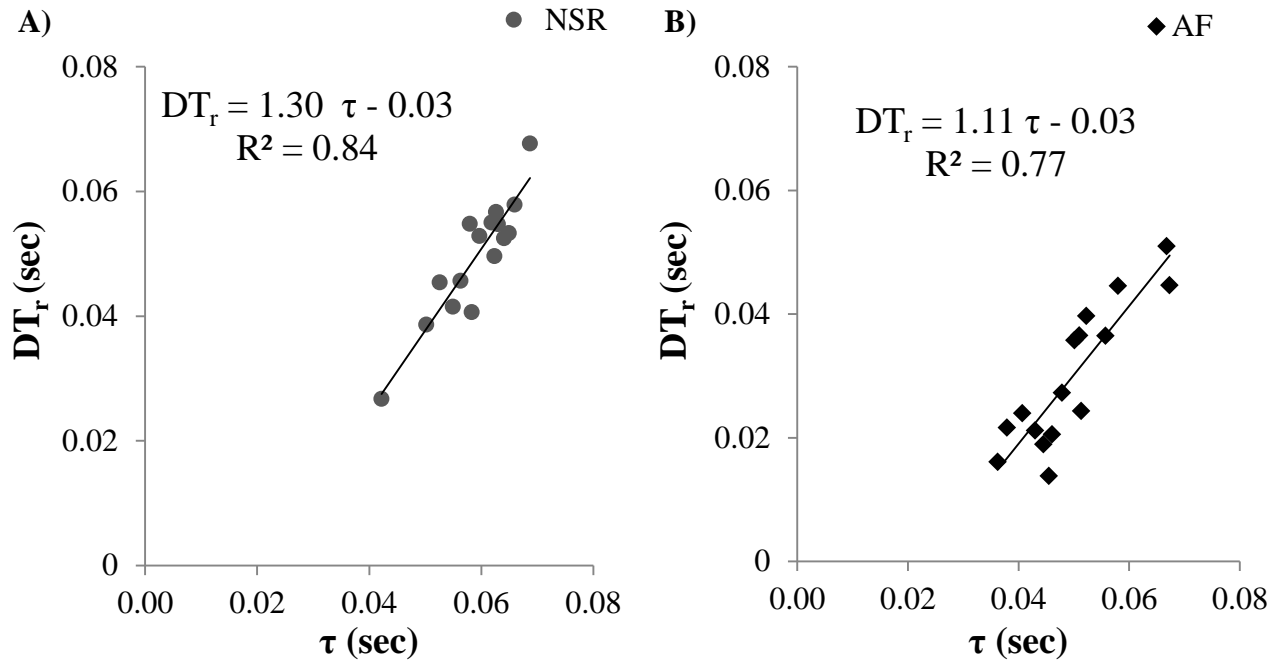
Figure 8.6 Relaxation component of DT vs time constant of IVR in NSR and AF groups.

A) Least mean square determined linear fit of relaxation component of DT (DT_r) vs. time constant of isovolumic relaxation (τ) in A) 16 NSR subjects, B) 16 AF subjects. See text for details.
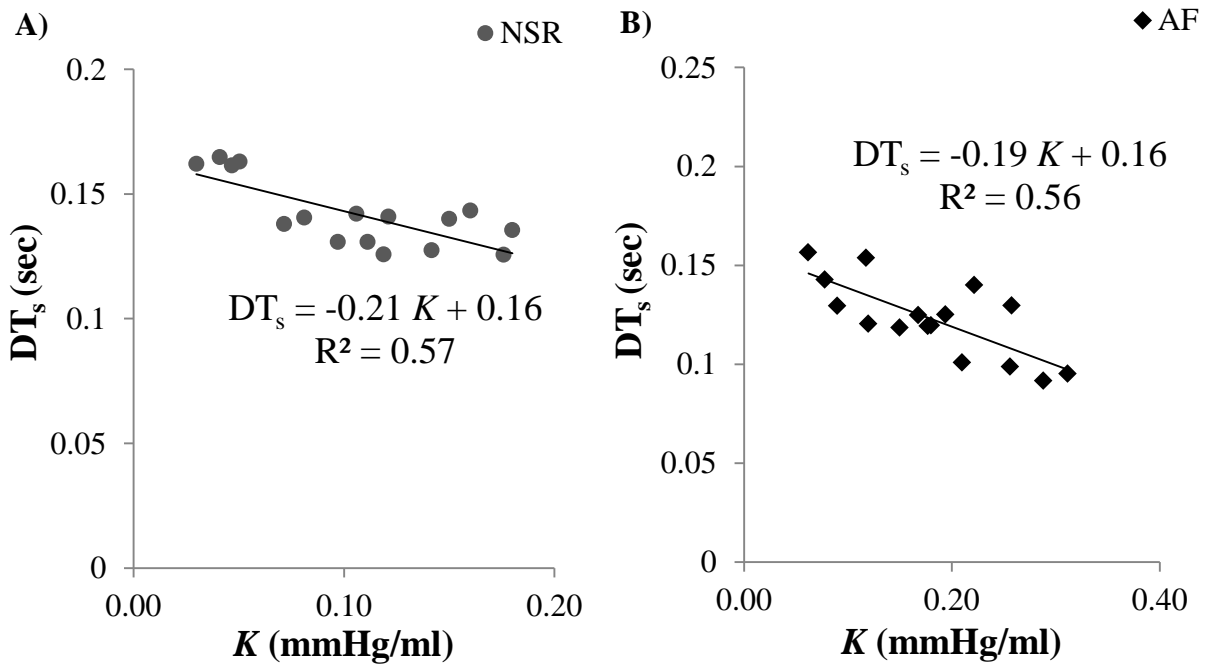
Figure 8.5 Stiffness component of DT vs diastatic stiffness in NSR and AF groups.

A) Least mean square determined linear fit of stiffness component of DT (DT_s) vs. diastatic stiffness (K) in A) 16 NSR subjects, B) 16 AF subjects. See text for details.

248

For the 16 NSR datasets 75% of total DT is due to stiffness and 25% is due to relaxation. For the 16 AF datasets 81% of DT is due to stiffness and 19% is due to relaxation (Figure 8.7). These differences are significant (p<0.005). If the four AF subjects with LVEF <50% are removed from the intergroup comparison, all of the conclusions remain unaltered.
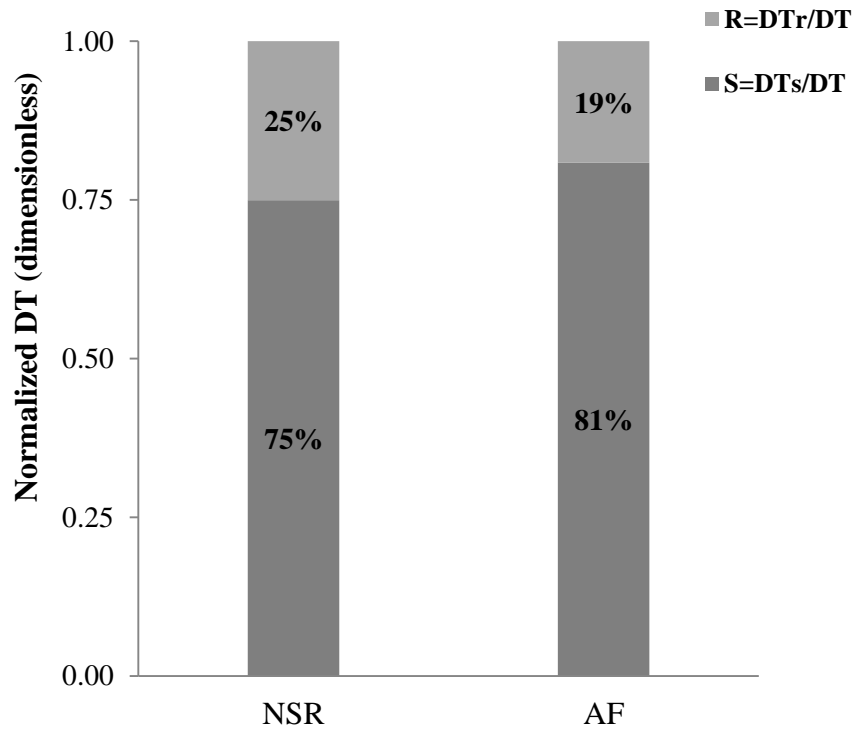
Figure 8.7 Normalized DT in NSR and AF groups.

Intergroup comparison of normalized DT showing percentage due to stiffness (S) and relaxation (R). A significantly larger percentage of total DT is due stiffness in the AF group. See text for details.

8.5   Discussion

8.5.1 Invasive and Non-invasive Measurements of AF Chamber Stiffness

Although multiple methods for LV chamber stiffness determination using echocardiography have been proposed (14, 23, 24, 32), one of the most important methods for characterizing passive chamber stiffness has been the end-diastolic pressure volume relation (EDPVR), defined by the locus of points inscribed by end-diastolic pressures and volumes at varying loads (17). Considering the EDPVR in the setting of chronic AF raises a concern, however. Because there is no atrial contraction, end-diastole in (rate controlled) AF is the hemodynamic equivalent of diastasis. During diastasis the ventricle is in static equilibrium (for a brief period), atrial and ventricular pressures are equal and net transmitral flow is absent (35). This equivalence between end-diastole and diastasis does not exist in NSR, and previous work (36) has shown that in the same NSR heart, the D-PVR and EDPVR are physiologically distinct relations, with significantly different slopes and therefore different values for chamber stiffness. Hence, the D-PVR is the only physiologically justified invasive method available for chamber stiffness determination in AF. The use of D-PVR requires the determination of load-varying diastatic pressure and volume points.

In addition to invasive approaches, the stiffness of the LV chamber can also be estimated noninvasively. The PDF parameter k obtained from echocardiographic E-wave analysis is mathematically (21) and experimentally related to the invasively measured chamber stiffness ($\Delta P/\Delta V$) during early rapid filling (23). E-wave deceleration time (DT) has also been correlated with stiffness as proposed by Little et al. (24). It was shown that an inverse square relationship

250

exists between stiffness and E-wave DT.

Both the triangle based (DT) and PDF model based (k) non-invasive estimates of chamber stiffness showed significant difference between the AF and NSR groups, consistent with the invasive chamber stiffness findings between groups at diastasis (27). The significantly shorter DT in the AF group is not likely to be explained by the higher average HR of the AF group since it is known that in the presence of a diastatic interval, E-wave DT remains essentially unchanged when HR increases (9).

8.5.2 <u>Deceleration Time of E-wave Correlation with Chamber Stiffness and Relaxation</u>

Average left ventricular (LV) chamber stiffness, $\Delta P/\Delta V$, is an important diastolic function (DF) metric. An E-wave based determination of $\Delta P/\Delta V$ by Little et al predicted that deceleration time (DT) is related to stiffness according to $\Delta P/\Delta V = A/(DT)^2$ (24). This implies that if the DTs of two LVs are indistinguishable, their stiffness should be similarly indistinguishable. Shmuylovich et al. (33) have shown that two subjects with indistinguishable E-wave determined DTs can have distinguishable catheterization-determined values of chamber stiffness, because of differences in relaxation, i.e. the viscoelastic parameter (PDF parameter c) in the two subjects. We found E-wave DT and its stiffness component are significantly (DT: p<0.001, DT_s: 0.005) shorter in the AF group (DT=153±22 msec, DT_s=123±20) than NSR group (DT=192±19 msec, DT_s=142±14). The shorter DT in AF group is primarily an effect of stiffness because the relaxation parameter c is similar in the two groups (p=0.65).

8.5.3 Decomposition of E-wave Deceleration Time to Stiffness and Relaxation Components

Because E-wave DT depends on both stiffness (k) and relaxation (c) we have previously proposed (25) a method by which E-wave DT can be decomposed to stiffness (DT_s) and relaxation (DT_r) components. We have shown (25) that DT_s was highly correlated (r=0.82) with (simultaneous) invasively determined (passive) diastatic chamber stiffness, and DT_r and the time-constant of IVR (τ) from simultaneous high fidelity pressure data and IVRT determined by echocardiography were highly correlated (r=0.94, r=0.89).

In the current study we analyzed simultaneous LV P-V and transmitral flow (echo) data and decomposed E-wave DT in to stiffness (DT_s) and relaxation (DT_r) components in NSR and AF groups. As expected diastatic stiffness and PDF stiffness parameter k were higher in AF group compared to NSR group and AF E-wave DT was shorter than in NSR. Figure 8.7 shows the fraction of DT accounted for by stiffness (S) in the AF group is significantly higher than in the NSR group (p<0.005), and the fraction of DT due to the relaxation (R) in the AF group is significantly lower than in the NSR group (p<0.005). Although the numerical value of the PDF relaxation parameter c is similar in NSR and AF, the fraction of the total DT due to relaxation (R = DT_r / DT (%)) is less in AF than in NSR because DT and DT_r in AF group is shorter (See Figure 8.7) than in NSR. This is underscored by the difference in stiffness parameter k, being higher (stiffer) in AF vs NSR. This method is totally general. It fractionates total DT into its stiffness and relaxation components and thereby reflects actual chamber properties. As such, the method allows for longitudinal assessment and trending of beneficial vs. adverse effects of alternative treatment strategies on chamber properties of stiffness and relaxation in clinical settings where echocardiography is utilized.

8.6 Limitations

8.6.1 <u>Conductance Volume</u>

The conductance catheter method of volume determination has known limitations related to noise, saturation and calibration that we have previously acknowledged (3, 8, 20, 21, 23, 36). In this study, the channels which provided physiologically consistent P-V loops were selected and averaged. However, since there was no significant volume signal drift during recording, any systematic offset related to calibration of the volume channels did not affect the result when the limits of conductance volume were calibrated via quantitative ventriculography.

8.6.2 <u>HR Limitation</u>

The D-PVR is defined by a linear, least mean-squared error fit to the load varying locus of points at which diastasis is achieved. At elevated heart rates diastasis is usually eliminated. In this study datasets were selected such that for every analyzed cardiac cycle in AF or NSR a clear, diastatic interval was present after E-wave termination, prior to the onset of the next systole in AF, or prior to the onset of the Doppler A-wave in NSR.

8.6.3 <u>Sample Size</u>

Although the number of subjects (n=32) is modest, and may be viewed as a minor limitation regarding statistics, the total number of cardiac cycles analyzed (n=650) mitigates the sample size limitation to an acceptable degree.

8.7   Conclusions

We used the PDF formalism to decompose E-wave deceleration time into its stiffness and relaxation components in NSR and AF groups where E-waves were always followed by a diastatic interval. We found that AF chambers have increased (diastatic) stiffness compared to NSR chambers at diastasis. In addition, a larger percentage of E-wave DT in AF is due to stiffness than to relaxation compared to NSR. This novel method allows clinicians to track and trend the effect of alternative pharmacologic therapies in terms of DT_s and DT_r not only as DF determinants, but as metrics of beneficial vs. adverse remodeling and as determinants of prognosis and rehospitalization in clinical settings where echocardiography is employed.

8.8 References

1.   **Allessie M, Ausma J, and Schotten U**. Electrical, contractile and structural remodeling during atrial fibrillation. *Cardiovasc Res* 54: 230-246, 2002.

2.   **Appleton CP, Firstenberg MS, Garcia MJ, and Thomas JD**. The echo-Doppler evaluation of left ventricular diastolic function. A current perspective. *Cardiol Clin* 18: 513-546, ix, 2000.

3.   **Bauman L, Chung CS, Karamanoglu M, and Kovács SJ**. The peak atrioventricular pressure gradient to transmitral flow relation: kinematic model prediction with in vivo validation. *J Am Soc Echocardiogr* 17: 839-844, 2004.

4.   **Bosch RF, Zeng X, Grammer JB, Popovic K, Mewis C, and Kühlkamp V**. Ionic mechanisms of electrical remodeling in human atrial fibrillation. *Cardiovasc Res* 44: 121-131, 1999.

5.   **Boskovski MT, Shmuylovich L, and Kovács SJ**. Transmitral flow velocity-contour variation after premature ventricular contractions: a novel test of the load-independent index of diastolic filling. *Ultrasound Med Biol* 34: 1901-1908, 2008.

6.   **Casaclang-Verzosa G, Gersh BJ, and Tsang TS**. Structural and functional remodeling of the left atrium: clinical and therapeutic implications for atrial fibrillation. *J Am Coll Cardiol* 51: 1-11, 2008.

7.   **Cha YM, Redfield MM, Shen WK, and Gersh BJ**. Atrial fibrillation and ventricular dysfunction: a vicious electromechanical cycle. *Circulation* 109: 2839-2843, 2004.

8.   **Chung CS, Ajo DM, and Kovács SJ**. Isovolumic pressure-to-early rapid filling decay rate relation: model-based derivation and validation via simultaneous catheterization echocardiography. *J Appl Physiol (1985)* 100: 528-534, 2006.

9.   **Chung CS, and Kovács SJ**. Consequences of increasing heart rate on deceleration time, the velocity-time integral, and E/A. *Am J Cardiol* 97: 130-136, 2006.

10.   **Dries DL, Exner DV, Gersh BJ, Domanski MJ, Waclawiw MA, and Stevenson LW**. Atrial fibrillation is associated with an increased risk for mortality and heart failure progression in patients with asymptomatic and symptomatic left ventricular systolic dysfunction: a

retrospective analysis of the SOLVD trials. Studies of Left Ventricular Dysfunction. *J Am Coll Cardiol* 32: 695-703, 1998.

11.   **Everett TH, Li H, Mangrum JM, McRury ID, Mitchell MA, Redick JA, and Haines DE**. Electrical, morphological, and ultrastructural remodeling and reverse remodeling in a canine model of chronic atrial fibrillation. *Circulation* 102: 1454-1460, 2000.

12.   **Falk RH**. Atrial fibrillation. *N Engl J Med* 344: 1067-1078, 2001.

13.   **Feigenbaum H**. *Echocardiography*. Baltimore, MD: Williams & Wilkins, 1993.

14.   **Garcia MJ, Firstenberg MS, Greenberg NL, Smedira N, Rodriguez L, Prior D, and Thomas JD**. Estimation of left ventricular operating stiffness from Doppler early filling deceleration time in humans. *Am J Physiol Heart Circ Physiol* 280: H554-561, 2001.

15.   **Gottdiener JS, Bednarz J, Devereux R, Gardin J, Klein A, Manning WJ, Morehead A, Kitzman D, Oh J, Quinones M, Schiller NB, Stein JH, Weissman NJ, and Echocardiography ASo**. American Society of Echocardiography recommendations for use of echocardiography in clinical trials. *J Am Soc Echocardiogr* 17: 1086-1119, 2004.

16.   **Hall AF, and Kovács SJ**. Automated method for characterization of diastolic transmitral Doppler velocity contours: early rapid filling. *Ultrasound Med Biol* 20: 107-116, 1994.

17.   **Kass DA**. Assessment of diastolic dysfunction. Invasive modalities. *Cardiol Clin* 18: 571-586, 2000.

18.   **Kovács S, MD M, and CS P**. Modelling cardiac fluid dynamics and diastolic function. *Philosophical Transactions of the Royal Society (A)* 359: 1299-1314, 2001.

19.   **Kovács SJ, Barzilai B, and Pérez JE**. Evaluation of diastolic function with Doppler echocardiography: the PDF formalism. *Am J Physiol* 252: H178-187, 1987.

20.   **Kovács SJ, Meisner JS, and Yellin EL**. Modeling of diastole. *Cardiol Clin* 18: 459-487, 2000.

21.   **Kovács SJ, Setser R, and Hall AF**. Left ventricular chamber stiffness from model-based image processing of transmitral Doppler E-waves. *Coron Artery Dis* 8: 179-187, 1997.

22.   **Li D, Fareh S, Leung TK, and Nattel S**. Promotion of atrial fibrillation by heart failure in dogs: atrial remodeling of a different sort. *Circulation* 100: 87-95, 1999.

23.   **Lisauskas JB, Singh J, Bowman AW, and Kovács SJ**. Chamber properties from transmitral flow: prediction of average and passive left ventricular diastolic stiffness. *J Appl Physiol (1985)* 91: 154-162, 2001.

24.   **Little WC, Ohno M, Kitzman DW, Thomas JD, and Cheng CP**. Determination of left ventricular chamber stiffness from the time for deceleration of early left ventricular filling. *Circulation* 92: 1933-1939, 1995.

25.   **Mossahebi S, and Kovács SJ**. Kinematic Modeling Based Decomposition of Transmitral Flow (Doppler E-wave) Deceleration Time into Stiffness and Relaxation Components. *Cardiovascular Engineering & Technology* 5: 25-34, 2014.

26.   **Mossahebi S, and Kovács SJ**. Kinematic modeling-based left ventricular diastatic (passive) chamber stiffness determination with in-vivo validation. *Ann Biomed Eng* 40: 987-995, 2012.

27.   **Mossahebi S, Shmuylovich L, and Kovács SJ**. The Challenge of Chamber Stiffness Determination in Chronic Atrial Fibrillation vs. Normal Sinus Rhythm: Echocardiographic Prediction with Simultaneous Hemodynamic Validation. *Journal of Atrial Fibrillation* 6: 46-51, 2013.

28.   **Mossahebi S, Shmuylovich L, and Kovács SJ**. The thermodynamics of diastole: kinematic modeling-based derivation of the P-V loop to transmitral flow energy relation with in vivo validation. *Am J Physiol Heart Circ Physiol* 300: H514-521, 2011.

29.   **Nagueh SF, Appleton CP, Gillebert TC, Marino PN, Oh JK, Smiseth OA, Waggoner AD, Flachskampf FA, Pellikka PA, and Evangelista A**. Recommendations for the evaluation of left ventricular diastolic function by echocardiography. *J Am Soc Echocardiogr* 22: 107-133, 2009.

30.   **Nattel S**. New ideas about atrial fibrillation 50 years on. *Nature* 415: 219-226, 2002.

31.   **Oh JK, Appleton CP, Hatle LK, Nishimura RA, Seward JB, and Tajik AJ**. The noninvasive assessment of left ventricular diastolic function with two-dimensional and Doppler echocardiography. *J Am Soc Echocardiogr* 10: 246-270, 1997.

32.   **Ohno M, Cheng CP, and Little WC**. Mechanism of altered patterns of left ventricular filling during the development of congestive heart failure. *Circulation* 89: 2241-2250, 1994.

33.	**Shmuylovich L, and Kovács SJ**. E-wave deceleration time may not provide an accurate determination of LV chamber stiffness if LV relaxation/viscoelasticity is unknown. *Am J Physiol Heart Circ Physiol* 292: H2712-2720, 2007.

34.	**Wang TJ, Larson MG, Levy D, Vasan RS, Leip EP, Wolf PA, D'Agostino RB, Murabito JM, Kannel WB, and Benjamin EJ**. Temporal relations of atrial fibrillation and congestive heart failure and their joint influence on mortality: the Framingham Heart Study. *Circulation* 107: 2920-2925, 2003.

35.	**Zhang W, Chung CS, Shmuylovich L, and Kovács SJ**. Is left ventricular volume during diastasis the real equilibrium volume, and what is its relationship to diastolic suction? *J Appl Physiol (1985)* 105: 1012-1014, 2008.

36.	**Zhang W, and Kovács SJ**. The diastatic pressure-volume relationship is not the same as the end-diastolic pressure-volume relationship. *Am J Physiol Heart Circ Physiol* 294: H2750-2760, 2008.

37.	**Zhang W, Shmuylovich L, and Kovács SJ**. The E-wave delayed relaxation pattern to LV pressure contour relation: model-based prediction with in vivo validation. *Ultrasound Med Biol* 36: 497-511, 2010.

38.	**Zile MR, Baicu CF, and Gaasch WH**. Diastolic heart failure--abnormalities in active relaxation and passive stiffness of the left ventricle. *N Engl J Med* 350: 1953-1959, 2004.

39.	**Zile MR, and Brutsaert DL**. New concepts in diastolic dysfunction and diastolic heart failure: Part I: diagnosis, prognosis, and measurements of diastolic function. *Circulation* 105: 1387-1393, 2002.

Chapter 9: Fractionation Method Application in Pseudonormal vs Normal Filling

In Review as: Mossahebi S, Kovács SJ. Fractionating E-wave Deceleration Time into its Stiffness and Relaxation Components Distinguishes Pseudonormal from Normal Filling

9.1   Abstract

Pseudonormal (PN) Doppler E-wave filling patterns indicate diastolic dysfunction but are indistinguishable from the normal filling (NL) pattern. For accurate classification, maneuvers to alter load or to additionally measure peak E' are required. E-wave deceleration time (DT) has been fractionated into stiffness (DT_s) and relaxation (DT_r) components ($DT = DT_s + DT_r$) by analyzing E-waves via the Parametrized Diastolic Filling (PDF) formalism. The method has been previously validated with DT_s and DT_r correlating with simultaneous catheterization (MILLAR) derived stiffness (dP/dV) and relaxation (tau) with r=0.82 and r=0.94, respectively. We hypothesize that DT fractionation can: 1) distinguish between unblinded (E' known) NL vs. PN age-matched groups with normal LVEF, and 2) distinguish between blinded (E' unknown) NL vs. PN groups, based solely on E-wave analysis.

Data (763 E-waves) from 15 age matched, PN (elevated E/E') and 15 NL subjects was analyzed. Conventional echocardiographic and PDF stiffness (*k*) and relaxation (*c*) parameters, and DT_s, DT_r were compared. Conventional diastolic function (DF) parameters did not differentiate between unblinded groups, whereas *k*, *c* (p<0.001), and DT_s, DT_r (p<0.001) did. Blinded (E' not provided) analysis of 42 subjects (581 E-waves) showed that R (=DT_r/DT) had high sensitivity (0.90) and specificity (0.86) in predicting PN from NL once E' revealed actual classification.

We conclude that PDF based E-wave analysis (*k*, *c* or DT_s and DT_r) can differentiate NL vs. PN filling patterns without requiring knowledge of E'.

9.2   Introduction

Diastolic dysfunction (DD) plays a role in heart failure with preserved ejection fraction (HFpEF) (19, 37, 41). Traditionally, diastolic function (DF) has been evaluated invasively by measuring left ventricular (LV) diastolic pressure-volume relations and/or tau, the time-constant of isovolumic relaxation (IVR). During early rapid filling, determinants of LV pressure include relaxation and passive chamber properties (30-32). In early diastole, relaxation usually dominates (passive) stiffness effects and their modification strongly influences diastolic function (31, 32).

However, invasive methods can be complimented by echocardiography to characterize additional aspects of filling (17). Doppler echocardiography has become the standard, and preferred noninvasive clinical quantitative DF assessment method. Selected aspects of LV filling dynamics can be assessed from features of the Doppler transmitral (E- and A-wave) and mitral annular (E'-wave) velocity waveforms approximated as triangles. The three major abnormal transmitral flow patterns, associated with dysfunction are 'impaired relaxation', 'pseudonormal' and 'restrictive' (34). The inflow patterns and related cardiac fluid dynamic mechanisms including the dynamics of atrioventricular (AV) valve plane motion, diastolic function alterations accompanying chamber enlargement and failure have been previously investigated (30).

The pressure gradient between left atrium (LA) and LV determines E-waves directly while E' reflects longitudinal chamber volume accommodation. The peak early rapid filling to peak late filling (E/A) and peak E to peak mitral annulus velocity (E/E') ratios are common DF correlates. In normal filling patterns (NL), E/A>1 and peak E' velocity is greater than 10 cm/sec (or E/E'<8) (27).

Mathematical models have been effective in promoting an understanding of diastolic function as well as alteration of chamber properties in selected cardiovascular diseases (20, 30, 32). One such model is the Parametrized Diastolic Filling (PDF) formalism which can assess DF quantitatively by subjecting E-waves to model-based analysis (14). The PDF formalism models the kinematics of suction-initiated filling in analogy to the recoil from rest, of an equivalent damped oscillator. Model predicted fit to the clinical E-wave is excellent and the fitting process yields three unique parameters for each analyzed E-wave: k, the stiffness constant; c, the viscoelasticity/relaxation constant; and x_o, the load. Using a clinical E-wave contour as input and suitable mathematical methods, unique k, c and x_o parameters are generated as output for each E-wave (7). The PDF parameters also generate indexes with rigorous physiologic analogues such as the peak instantaneous pressure gradient (kx_o), and the potential energy driving the recoil/suction process ($1/2kx_o^2$) (2, 24). The details and the required tools so anyone can perform PDF based analysis of E-waves for diastolic function quantitation are available at Journal of Visualized Experiments (25).

Prior work by Little et al (18) predicted that Doppler E-wave deceleration time (DT) is determined by stiffness alone. E-wave analysis via PDF revealed that DT is actually jointly determined by stiffness (PDF parameter k) and relaxation (PDF parameter c) (38). Using PDF-based analysis, we have predicted and validated that E-wave DT can be decomposed into its stiffness (DT_s) and relaxation (DT_r) components such that $DT=DT_s+DT_r$ (21, 22). The predicted causal relationship between DT_s and DT_r and stiffness ($\Delta P/\Delta V$) and relaxation (tau) was validated using simultaneous, high fidelity hemodynamic and echocardiographic data, by the high, observed correlation (r=0.82 and r=0.94 respectively) (21, 22).

The effect of delayed relaxation (which lengthens the E-wave) can be masked by

263

increased stiffness (which shortens the E-wave) by generating increased atrial pressure and thereby increasing E-wave amplitude (31, 32). Pseudonormalized (PN) filling patterns indicate diastolic dysfunction (grade 2 diastolic dysfunction). In PN filling LV and LA pressures are increased, and relaxation is slower (17). Although inscribed at a higher absolute pressure, the early diastolic pressure **gradient** is similar to NL filling, resulting indistinguishable E-wave shapes and E/A ratios. With progressive impairment of relaxation, the E′ peak is reduced and delayed (16). Thus, PN can be distinguished from NL by a reduced and delayed E′ and increase in the E/E′ ratio or by respiratory maneuvers (straining) that transiently alter load (17, 27).

In this work, we test two hypotheses: 1) that PDF based analysis of E-waves suffices to differentiate PN from NL in unblinded groups, i.e. where E' is known in advance, and 2) that PDF analysis can differentiate PN from NL in blinded groups, when E' is not known in advance. We fractionate DT into its stiffness and relaxation components and determine if they can distinguish between NL and PN filling in unblinded and blinded age matched groups having normal E-wave patterns and indistinguishable E_{peak}, DT, and E_{dur}.

9.3   Methods

9.3.1 Subject Selection

Unblinded Analysis Group:

Thirty datasets (mean age 59, 16 men) were selected from the Cardiovascular Biophysics Laboratory database (3). All participants provided informed consent prior to the procedure using a protocol approved by the Washington University Human Research Protection Office (HRPO).

Fifteen NL filling pattern datasets were selected so they were age matched with the 15 PN filling datasets according to American Society of Echocardiography (ASE) (27) criteria. In both groups $0.8 < E/A < 1.5$ and 160 msec $<$ DT $<$ 200 msec. Selection criteria for the NL group were: no active ischemia, normal valvular function, normal LV ejection fraction (LVEF$\geq$50%), no history of myocardial infarction or peripheral vascular disease or bundle branch block, and clear diastatic intervals following E-waves.

Among the 15 NL filling datasets, 12 had normal end-diastolic pressure (LVEDP<14 mmHg), 3 had 14 mmHg < LVEDP < 16 mmHg. The distributions of LVEDPs in the 15 PN filling datasets were: 6 with 15<LVEDP<20 mmHg and 9 with LVEDP>21. Selection criteria for the PN group (27, 28, 39) were: indistinguishable E-wave peak, DT, and E-wave duration compared to the NL group, normal LV function (EF > 50%) with impaired annular peak velocity (lateral E'<10) and prolonged tau (τ>50 msec). The PN datasets were age matched with the NL group since DF depends on age (9). A total of 763 cardiac cycles (25 beats/subject) were analyzed. The clinical descriptors of the 30 subjects are shown in Table 9.1.

Table 9.1 The clinical descriptors of NL and PN groups in single-blind analysis.

Clinical Descriptors	NL Group	PN Group	Significance
N	15	15	N.A.
Age (y)	59±8	59±9	0.87
Gender (M/F)	8/7	8/7	N.A.
Heart Rate (bpm)	68±7	66±7	0.47
Ejection Fraction (LVEF) (%)	71±8	71±8	0.81
Height (cm)	170±11	165±8	0.16
Weight (kg)	88±16	86±15	0.78

LVEF, left ventricular ejection fraction (via calibrated ventriculography); NL, normal filling; PN, pseudonormalized filling; N.A., not applicable.

Data are presented as mean ± standard deviation.

The hemodynamic and echocardiographic indices of 30 subjects are shown in Table 9.2.

Table 9.2 Hemodynamic and echocardiographic data in NL and PN groups.

	NL	PN	Significance
Hemodynamic Parameters:			
LVEDP (mmHg)	13±2	20±3	<0.001
LVESV (ml)	39±17	36±12	0.63
LVEDV (ml)	134±43	128±38	0.66
τ (msec)	46±2	65±5	<0.001
Echocardiographic Parameters			
Peak E-wave velocity (E) (cm/sec)	82±6	83±13	0.62
E-wave deceleration time (DT) (msec)	180±16	185±13	0.31
E-wave duration time (E_{dur}) (msec)	262±17	258±23	0.60
E-VTI (cm)	10.5±1.9	11.1±1.9	0.35
Peak A-wave velocity (A) (cm/sec)	72±9	73±15	0.82
E/A(dimensionless)	1.2±0.1	1.2±0.4	0.49
Peak E'-wave velocity (E') (cm/sec)	15±3	8±1	<0.001
E/E'(dimensionless)	5.1±0.9	10.9±1.4	<0.001
k (1/sec^2)	212±17	263±28	<0.001
c (1/sec)	15.7±1.6	23.9±6.0	<0.001
DT_r (msec)	44±12	64±14	<0.001
DT_s (msec)	136±8	121±11	<0.001
R = DTr / DT (%)	24±5	34±6	<0.001
S = DTs / DT (%)	76±5	66±6	<0.001

NL, normal filling; PN, pseudonormalized filling; LVEDP, left ventricular end-diastolic pressure; LVESV, left ventricular end-systolic volume; LVEDV, left ventricular end-diastolic volume; τ, time constant of isovolumic relaxation; E-VTI, E-wave velocity-time integral; E/A, ratio of peak E-wave and peak A-wave; E/E', ratio of peak E-wave and peak E'-wave; k, PDF stiffness parameter; c, PDF relaxation parameter; DT_r, relaxation component of DT; DT_s, stiffness component of DT.

Data are presented as mean + standard deviation.

Blinded Analysis Group:

The 30 datasets from the unblinded study were combined with twelve additional datasets (42 total) meeting inclusionary criteria from the Cardiovascular Biophysics Laboratory database (3) and subjected to a blinded analysis by a member (SZ) of our research group. In the blinded study 42 datasets consisting only of E-waves were provided for analysis to the independent collaborator (SZ). The clinical descriptors of the blinded group are shown in Table 9.3.

Table 9.3 The clinical descriptors of NL and PN groups in double-blind analysis.

Clinical Descriptors	NL Group	PN Group	Significance
N	21	21	N.A.
Age (y)	59±8	59±10	0.84
Gender (M/F)	11/10	13/8	N.A.
Heart Rate (bpm)	67±7	66±7	0.77
Ejection Fraction (LVEF) (%)	73±8	71±8	0.52
Height (cm)	171±10	165±9	0.10
Weight (kg)	85±18	87±15	0.67

LVEF, left ventricular ejection fraction (via calibrated ventriculography); NL, normal filling; PN, pseudonormalized filling; N.A., not applicable.

Data are presented as mean ± standard deviation.

9.3.2 <u>Data Acquisition</u>

The database is a repository of high fidelity, simultaneous echocardiographic transmitral flow and pressure-volume data employing standard recording methods that have been previously detailed (2, 3, 12, 14, 16, 24). Briefly, immediately prior to arterial access a complete 2-D echo-Doppler study is performed with subjects in supine position using a Philips (Andover, MA) iE33 system according to ASE criteria (6, 27). Only the echocardiographic portion of the dataset was utilized in this study.

9.3.3 <u>Doppler E-wave Analysis</u>

For each subject, approximately 1-2 minutes of simultaneous hemodynamic and continuous transmitral flow data were recorded in the pulsed-wave Doppler mode. In accordance with convention, the apical 4-chamber view was used for Doppler E-wave recording with the sample volume located at the leaflet tips. For the 30 subject unblinded analysis an average of 25 beats per subject were analyzed (763 E-waves).

Doppler transmitral E- and A-wave contours and mitral annulus velocity (E'-wave) were analyzed using the conventional triangle shape approximation (1, 4), yielding peak E-wave velocity (E), acceleration time (AT), deceleration time (DT), velocity-time integral (E-VTI), peak A-wave velocity (A), E/A ratio, peak E'-wave velocity (E'), and E/E' ratio.

Each E-wave was also analyzed via the Parametrized Diastolic Filling (PDF) formalism to yield, mathematically unique PDF parameters for each E-wave (stiffness parameter (k), chamber viscoelasticity/relaxation parameter (c), load parameter (x_o)) (10, 11, 16).

The PDF Formalism

Suction initiated filling is modeled via the Parameterized Diastolic Filling (PDF) formalism. The model uses a linear, bi-directional spring to approximate the kinematics of early filling in analogy to the recoil from rest of a damped, simple harmonic oscillator (SHO) (11). In accordance with Newton's second law, the equation of motion is:

$$\frac{d^2x}{dt^2} + c\frac{dx}{dt} + kx = 0 \qquad [9.1]$$

Because the E-wave has zero initial velocity, the model's initial velocity is zero ($v(0)=0$). However, the simple harmonic oscillator (SHO) has a non-zero initial spring displacement, x_o. Systole stores elastic strain in tissue, which at mitral valve opening, is available to power mechanical recoil and the ventricular suction process. Equation [9.1] allows calculation of parameters c and k per unit mass. The predicted contour of the clinical E-wave is obtained from the solution for the SHO velocity, which for underdamped ($c^2<4k$) kinematics is:

$$v(t) = -\frac{x_o k}{\omega}\exp(-ct/2)\sin(\omega t) \qquad [9.2]$$

where $\omega = \sqrt{4k-c^2}/2$. The determination of PDF parameters from each E-wave generates a unique set of x_o, c, and k (7) values for each contour. The three parameters x_o, c, and k encompass the (lumped) physiologic determinants of all E-wave contours. The initial oscillator displacement x_o (cm) is linearly related to the velocity-time integral (VTI) of the E-wave (14). Chamber stiffness (dP/dV) is linearly related to the spring constant k (g/s^2) (14, 16), while the chamber viscoelasticity/relaxation index c (g/s) characterizes the resistance of the process (12, 14). PDF analysis of Doppler E-waves can accurately determine diastatic (passive) LV chamber stiffness (23). E-waves with long concave up deceleration portions ('delayed relaxation pattern') are fit by the 'overdamped' solution ($c^2>4k$) and have higher c values, while E-waves that resemble the

first half of a sine wave are fit by the underdamped solution and have lower c values (38).

Briefly, echocardiographic images are cropped, the mitral E-wave maximum velocity envelopes are identified and fit by the PDF generated solution using the Levenberg-Marquardt algorithm to yield the best-fit PDF parameter x_o, c, and k, values. The process is achieved using a custom Lab VIEW (National Instruments, Austin, TX) interface (7). In addition to providing parameter values the algorithm also provides a simultaneous measure of goodness of fit. The details of methods are available at Journal of Visualized Experiments (26). These algorithms are available for download for any user on our website: http://CBL1.wustl.edu

Determination of Stiffness and Relaxation Components of E-wave Deceleration Time

PDF model predicts that E-wave deceleration time (DT) is a function of both stiffness and relaxation (22, 38). PDF-based E-wave analysis provides a method for fractionating total DT into its stiffness (DT_s) and relaxation (DT_r) components such that $DT=DT_s+DT_r$. The fractionation method has been validated with DT_s and DT_r correlating with simultaneous stiffness (dP/dV) and relaxation (tau) with r=0.82 and r=0.94 respectively (22).
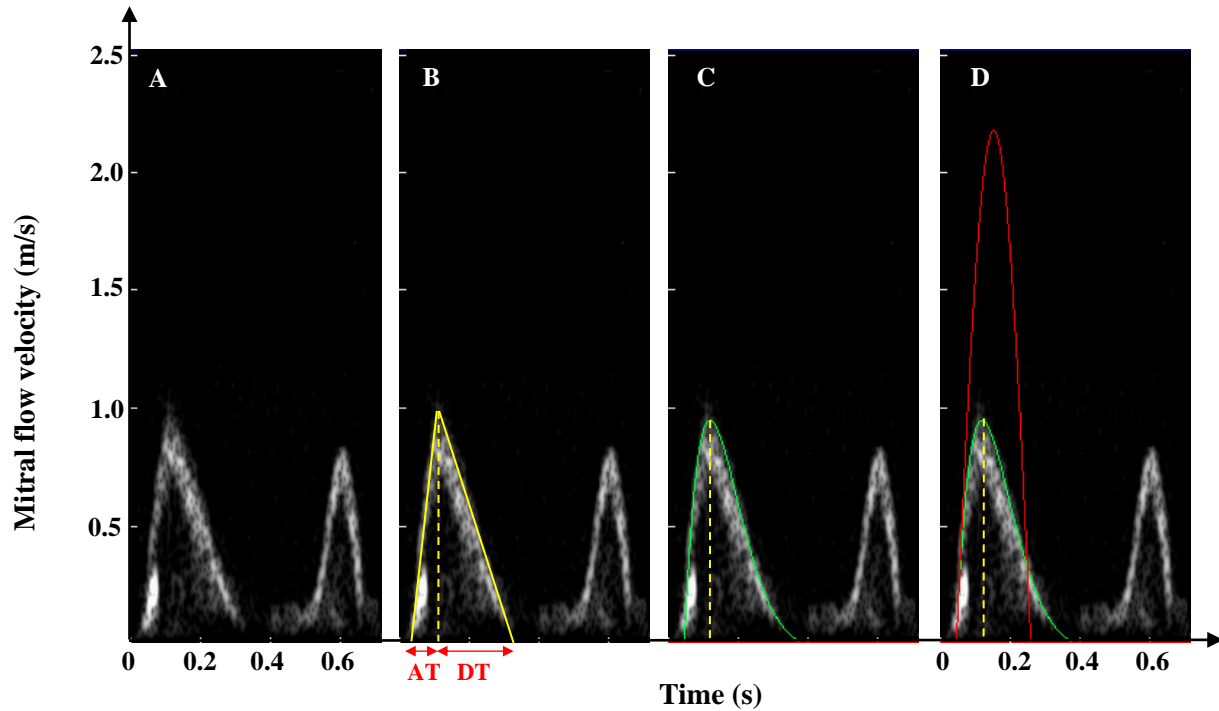
Figure 9.1 Overview of DT_s and DT_r computation.

A) Typical Doppler velocity profile. B) AT, DT, Edur determination using triangle approximation to E-wave contour. C) PDF model fit to E-wave (green) determined via model-based image processing provides PDF parameters c=22.7/s, k=217/s2, x_o=14.8 cm. D) DT_r is determined by setting c=0 thereby generating an ideal, model predicted E-wave (red curve), with same x_o, k as original E-wave (green curve). DT_r is defined as the time difference between duration of the actual E-wave (green curve) using triangle method and the ideal (c=0) E-wave (red curve). DTs is then determined by subtracting DT_r from total DT ($DT_s = DT - DT_r$). DT=202 msec, DT_r=77 msec and DT_s=125 msec. DT, E-wave deceleration time; Edur, E-wave duration; DT_s, stiffness component of E-wave deceleration time; DT_r, relaxation component of E-wave deceleration time; c, PDF chamber relaxation parameter; k, PDF chamber stiffness parameter; x_o, PDF load parameter. See text for details.

The duration of the E-wave, AT, and DT are measured as usual from Doppler echo images using the conventional triangle approximation to E-wave shapes (Figure 9.1). The effect of delayed relaxation on an ideal (generated by recoil only) E-wave is to decrease its peak amplitude and lengthen its DT. Accordingly, DT_r is determined by using the same x_o and k as the original E-wave but setting c=0 and thereby providing the PDF generated ideal contour.

Subtracting the ideal E-wave's shorter duration from actual total duration yields DT_r (See Figure 9.1). Therefore, E-wave DT is decomposed into its components as $DT = DT_s + DT_r$. Alternatively, DT can be determined via use of the PDF method solely –as detailed in (22). It is known that DT_s, DT_r are only weakly load and heart rate dependent (22). Fractionation is achieved by dividing by DT yielding $1 = S + R$, where S is the fraction of total DT due to stiffness and R is the fraction of total DT due to relaxation. Hence, $S = DT_s/DT$, and $R = DT_r/DT$.

Sensitivity and specificity were determined using the logistic regression model (ROC analysis) to compare the diagnostic performance of parameter R (or S) over the full range of thresholds by classifying groups in accordance with E/E' and tau. Using the logistic regression model the cutpoint was selected as that value of R that maximized both sensitivity and specificity (where the sensitivity and specificity curves vs. all possible cutpoints cross) with the highest likelihood ratio (8).

9.3.4 <u>Blinded Analysis</u>

An average of 14 beats per subject (581 cardiac cycles total for the 42 subjects) were analyzed by one author (SZ) blinded to E'-wave and LVEDP data. PDF parameters, stiffness and relaxation components of DT (DT_s and DT_r), and the fraction of DT due to stiffness and relaxation (S and R) were computed for each E-wave. Based on the selected cutpoint for R (or S) from the unblinded study, sensitivity and specificity of blinded study was determined relative to NL and PN classification based on E' values and tau.

9.4　Results

9.4.1　<u>Hemodynamics in NL and PN</u>

As expected LVEDP and tau are significantly higher in PN than that in NL filling group (LVEDP: 20 ± 4 mmHg vs. 13 ± 2 mmHg, $p<0.001$, τ: 65 ± 5 msec vs. 46 ± 2 mmHg, $p<0.001$). The ESV and EDV are similar in both groups (ESV: 36 ± 12 ml for PN vs. 39 ± 17 ml for NL, $p=0.63$ and EDV: 128 ± 38 ml for PN vs. 134 ± 43 ml for NL, $p=0.66$).

9.4.2　<u>Conventional E-wave, A-wave and E'-wave Features in NL and PN</u>

Figure 9.2 shows that the peak E-wave velocity (E), peak A-wave velocity (A) and E/A ratio do not significantly differ between groups (E: 82 ± 6 cm/sec vs. 83 ± 13 cm/sec, $p=.62$, A: 72 ± 9 cm/sec vs. 73 ± 15 cm/sec, $p=0.82$, E/A: 1.2 ± 0.1 vs. 1.2 ± 0.4, $p=0.49$). As expected peak E'-wave velocity (E') is significantly lower in PN than NL (E': 8 ± 1 cm/sec vs. 15 ± 3, $p<0.001$). E/E' is higher in PN than in NL (E/E': 10.9 ± 1.4 vs. 5.1 ± 0.9, $p<0.001$).

E-wave DT, E-wave duration (E_{dur}) and E-VTI do not significantly differ between NL and PN filling groups as shown in Figure 9.3 (DT: 180 ± 16 msec vs. 185 ± 13 msec, $p=0.31$, E_{dur}: 262 ± 17 msec vs. 258 ± 23 msec, $p=0.60$, E-VTI: 10.5 ± 1.9 cm vs. 11.1 ± 1.9 cm, $p=0.35$).
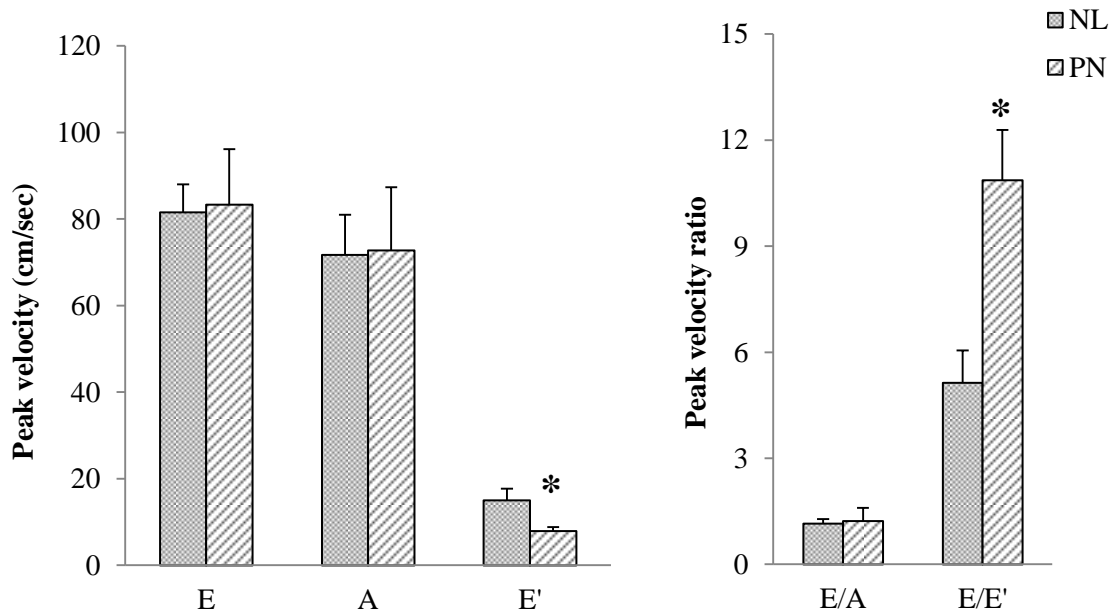
Figure 9.3 Conventional echo parameters in NL and PN groups.

A) Peak E-wave, A-wave, and E'-wave velocities, B) E/A and E/E' ratios in NL group (15 subjects) and PN group (15 subjects). E' and E/E' ratio were significantly different (E': p<0.001, E/E': p<0.001) between two groups. NL, normal filling; PN, pseudonormalized filling. See text for details.

Figure 9.2 DT, E_{dur}, and E-VTI in NL and PN groups.

DT, E_{dur}, and E-VTI from triangle method in normal (NL) filling group (15 subjects) and pseudonormal (PN) filling group (15 subjects). DT, E_{dur}, and E-VTI were not significantly different (DT: p=0.31, Edur: p=0.60, E-VTI: p=0.35) between two groups. DT, E-wave deceleration time; E_{dur}, E-wave duration; E-VTI, E-wave velocity-time integral. See text for details.

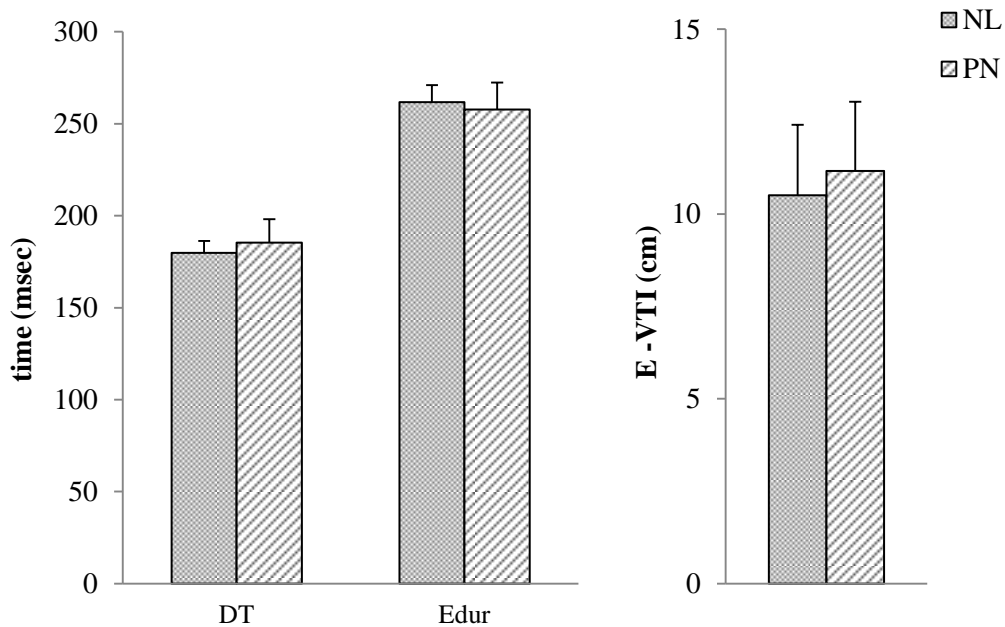## 9.4.3 PDF Parameters in NL and PN

PDF analysis reveals that PDF stiffness parameter (k) and PDF relaxation parameter in PN group are higher (worse) than NL group as shown in Figure 9.4 (k: 263 ± 28 1/sec^2 vs. 212 ± 17 1/sec^2, p<0.001, c: 23.9 ± 6.0 1/sec vs. 15.7 ± 1.6 1/sec, p<0.001).
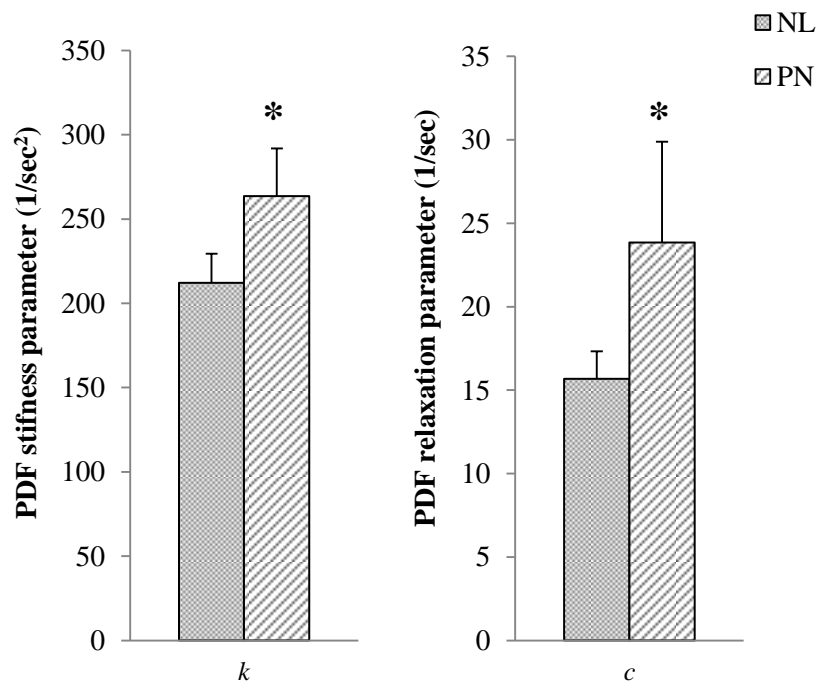
Figure 9.4 PDF stiffness and relaxation parameters in NL and PN groups.

PDF stiffness and relaxation parameters (k and c) in NL group (15 subjects) and PN group (15 subjects). Higher k in PN group than NL group (p<0.001) showed that PN hearts were stiffer than NL hearts. Higher c in PN group than NL group (p<0.001) showed that relaxation is slower in PN group than NL group. NL, normal filling; PN, pseudonormalized filling. See text for details.

9.4.4 <u>Fractionation of Deceleration Time into Stiffness and Relaxation Components in NL and PN</u>

Figure 9.5 illustrates Relaxation component of DT (DT$_r$) in PN group is longer than NL group (DT$_{r\,PN}$=64±14 msec vs. DT$_{r\,NL}$=44±12 msec, p<0.001). The longer DT$_r$ in PN and the direct correlation between DT$_r$ and the time constant of IVR (τ) and IVR time (IVRT) show that the relaxation is impaired in PN compared to NL. Stiffness component of DT (DT$_s$) in PN group (inversely related to chamber stiffness) is shorter (stiffer) than NL group as shown in Figure 9.5 (DT$_{s\,PN}$=121±11 msec vs. DT$_{s\,NL}$=136±8 msec, p<0.001). The shorter DT$_s$ in PN quantifies the extent to which PN chambers are stiffer than NL.
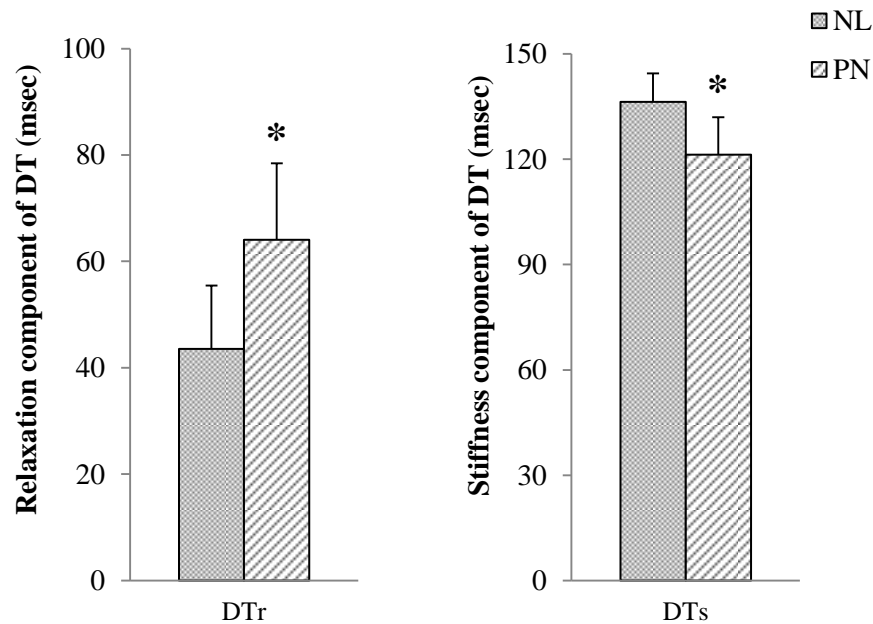

Figure 9.5 Stiffness and relaxation components of DT in NL and PN groups.
Stiffness (DT$_s$) and relaxation (DT$_r$) components of DT in NL group (15 subjects) and PN group (15 subjects). DT$_s$ is shorter in PN group than NL group (p<0.001). DTr is longer in PN group than NL group (p<0.001). NL, normal filling; PN, pseudonormalized filling. See text for details.

For the 15 NL datasets S=0.76 and R=0.24 hence, 76% of total DT is due to stiffness and 24% is due to relaxation. For the 15 PN datasets S=0.66 and R=0.34, hence 66% of DT is due to stiffness and 34% is due to relaxation (Figure 9.6). These differences are significant ($p<0.001$).
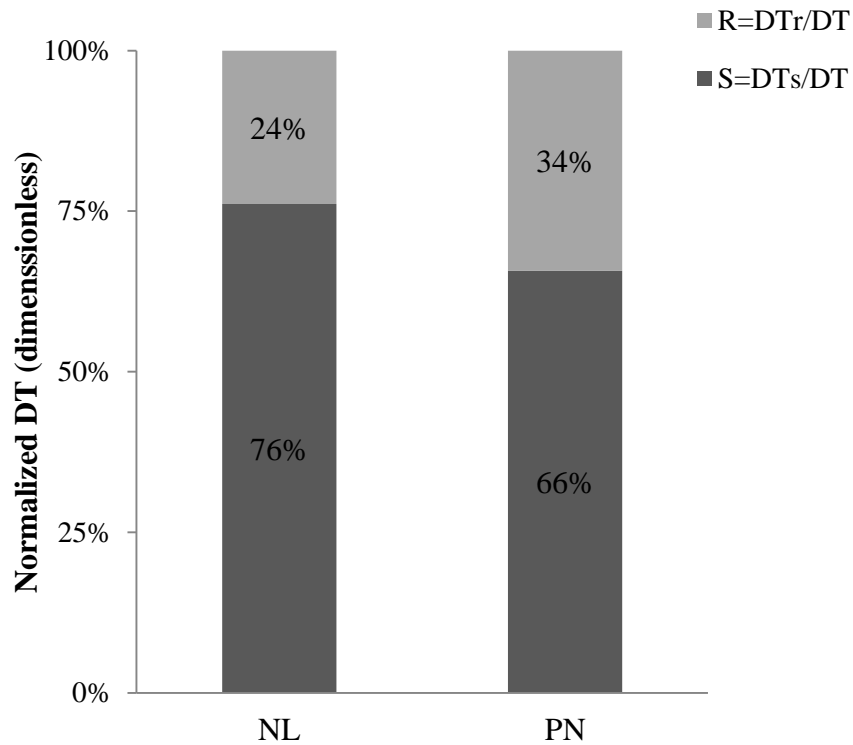
Figure 9.6 Normalized DT in NL and PN groups.
Intergroup comparison of the percentage of normalized DT due to stiffness (S) and relaxation (R). A significantly larger percentage of total DT is due relaxation in the PN group ($p<0.001$). DT, E-wave deceleration time; NL, normal filling; PN, pseudonormalized filling. See text for details.

Figure 9.7 shows receiver operator characteristic (ROC) curve for the parameter R ($=DT_r/DT$) in the unblinded study of 30 subjects. ROC analysis demonstrates the capability of parameter R (R=0.28 as a cutpoint) in differentiating PN vs. NL subjects with high sensitivity (0.93) and specificity (0.93). The area under ROC curve (AUC) is 0.98.
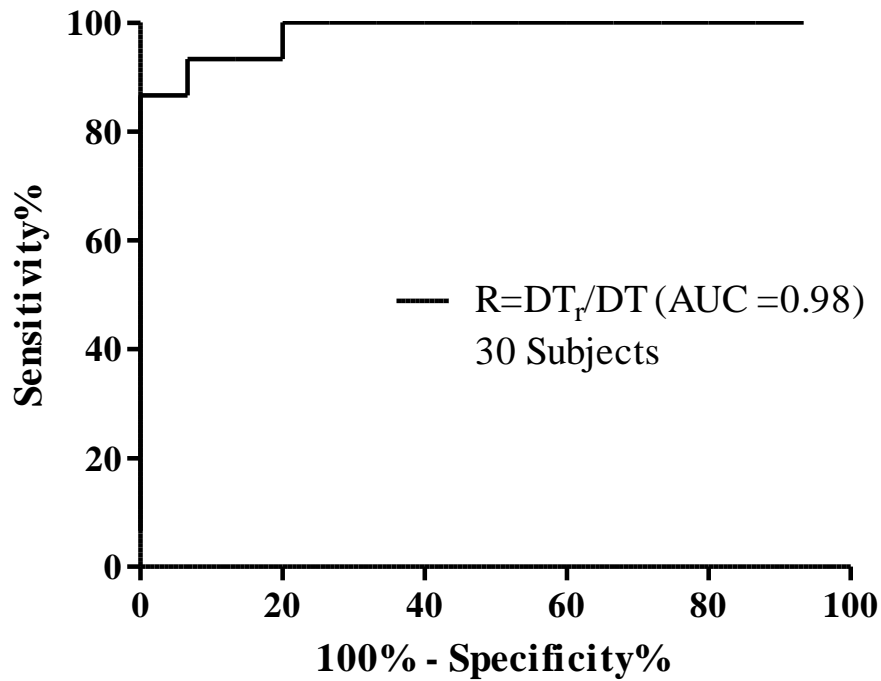
Figure 9.7 ROC curve for the percentage of normalized DT due to relaxation.

Receiver operator characteristic curve for the percentage of normalized DT due to relaxation (R= DT_r/DT) in unblinded study demonstrates the ability of parameter R (R=0.28 as a cutpoint) in differentiating PN vs. NL subjects with high sensitivity (0.93) and specificity (0.93) yielding an area under curve (AUC) of 0.98. DT, E-wave deceleration time; DT_r, relaxation component of DT; PN, pseudonormalized filling pattern; NL, normal filling pattern. See text for details.

9.4.5 Blinded Analysis

Using the cutpoint value of R=0.28 (determined in the unblinded study), the blinded observer predicted 18 subjects correctly in NL group (21 subjects) and 19 subjects in PN group (21 subjects). Hence, blinded analysis of 42 subjects demonstrates the ability of parameter R (DT_r/DT) in differentiating PN vs. NL subjects with high sensitivity (0.90) and specificity (0.86).

9.5　Discussion

9.5.1　Diastolic Function Evaluation

Echocardiography is the primary and preferred non-invasive method of DF evaluation. E-wave amplitude and shape reflects global volume accommodation, whereas E' reflects the longitudinal component of volume accommodation. E' is known to be impaired in dysfunction, and E/E′ is known to correlate with filling pressures, i.e., pulmonary capillary wedge based on established physiologic mechanisms (5, 15, 27).

9.5.2　Pseudonormal Filling

Both impaired relaxation and restrictive patterns (grade 1 and 3 of DD) can be distinguished from NL using mitral inflow pattern features (E/A ratio). Maintenance of similar atrioventricular pressure gradient in PN and NL setting generates in E-waves that are indistinguishable using conventional metrics such as E_{peak}, E_{dur},, DT, VTI, and E/A (as shown in Figures 9.2, 9.3, and 9.8). Thus, distinguishing PN filling (grade 2 of DD) from NL requires additional information such as E' or response to respiratory (strain) maneuvers. PN can be distinguished from NL by reduced E' and increased E/E'. Cardiac catheterization indicates that in the PN pattern, both LV and LA pressures are increased and are associated with stiffer chambers compared to NL. E/E′ >15 indicates elevated pulmonary capillary wedge pressure, whereas E/E′ <8 is associated with normal LA pressures (29).

9.5.3 <u>PDF Analysis of E-waves, Diastolic Function and DT Fractionation</u>

The PDF method has previously shown that the chamber relaxation parameter c was significantly higher in hypertensive compared to non-hypertensive controls (13). Furthermore, the PDF relaxation parameter c differentiated between diabetic vs. control subjects while conventional indexes such as DT, E_{peak}, and tau failed to do so (35). The peak atrioventricular pressure gradient, obtained from the PDF parameters as kx_o (2) was significantly higher in the diabetic group. The PDF formalism has also characterized mitral annular oscillations (MAO) after the E'-wave and showed that the absence of MAO indicates relaxation related diastolic dysfunction (36). The physiologic role of E' as a longitudinal volume accommodation index has been elucidated in terms of impedance (5).

An additional PDF based mechanistic advance in understanding diastolic function includes the insight that during diastasis the ventricle is in (transient) static equilibrium, such that atrial and ventricular pressures are equal (forces are balanced, but they are not zero) and transmitral flow is absent although residual vortices may be present (32, 33). Accordingly, the passive, in-vivo equilibrium volume of the (fully relaxed) LV is its volume at diastasis (40). Beat to beat variation in diastatic volume and pressure generate a locus of P, V points whose slope via linear regression, defines in-vivo passive chamber stiffness (40).

Although pioneering work by Little et al indicated that deceleration time (DT) and stiffness (18) are inversely related, subsequent PDF analysis has refined that view by showing that E-wave DT is determined jointly by stiffness and relaxation (k and c PDF parameters) rather than stiffness alone (38). Because indistinguishable E-waves having the same DT have been shown to have different chamber stiffness (dP/dV) and relaxation (tau) on simultaneous

hemodynamic recording, it follows that E-wave DT may not provide an accurate determination of LV chamber stiffness if LV relaxation remains unknown. Based on these principles we have previously derived and validated a method by which E-wave DT can be fractionated into stiffness (DT_s) and relaxation (DT_r) components (21, 22) such that $DT = DT_s + DT_r$.

Using PDF analysis and the DT fractionation method we have recently shown (21) that atrial fibrillation (AF) chambers have increased diastatic passive chamber stiffness compared to normal sinus rhythm (NSR) chambers at diastasis. Additionally, compared to NSR, a larger percentage of DT is due to stiffness than to relaxation in AF.

In the current study we analyzed E-waves via the PDF formalism and fractionated them into their stiffness and relaxation components in age matched NL and PN groups. Figure 9.8 illustrates NL and PN E-waves, showing their indistinguishability using conventional metrics (E_{peak}, E_{dur}, and E/A) while generating significantly different PDF parameters (k and c) and stiffness and relaxation components of DT (DT_s and DT_r).
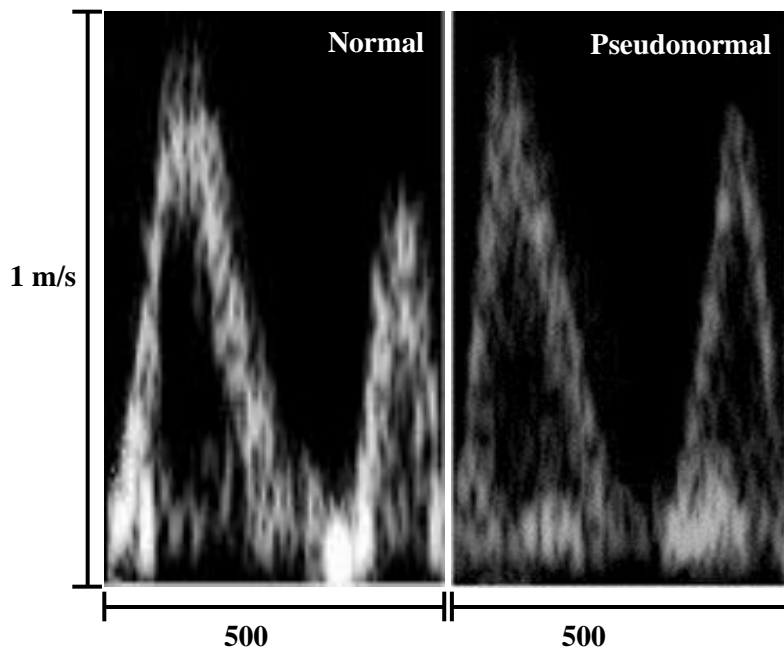

Figure 9.8 E-waves comparison in NL and PN subjects.
E-waves of two selected subjects (Normal pattern, Pseudonormal pattern) with indistinguishable E-wave duration, E_{peak} , E/A ratio but significantly different values for PDF parameters (k and c) and stiffness and relaxation components of DT (DT_s and DT_r).

The higher PDF stiffness parameter k and shorter DT_s (inversely related to stiffness) in the PN group compared to NL group (p<0.001) established the increased chamber stiffness associated with PN patterns. Similarly, higher PDF (worse) relaxation parameter c and longer DT_r observed in the PN group compared to NL group (p<0.001) established impaired relaxation compared to NL. Shorter DT_s (higher PDF stiffness parameter k) with longer DT_r (higher (worse) relaxation parameter c) in PN than in NL reveals how simultaneous increased stiffness and impaired relaxation oppose each other in generating PN E-waves that conventional analysis cannot distinguish from NL. The fraction of DT accounted for by relaxation (R) in the PN group is significantly higher than in the NL group (p<0.001). These results quantify the simultaneous increase in stiffness (that shortens DT) and impairment in relaxation (that lengthens DT) that oppose each other to generate E-waves that are indistinguishable from NL. Furthermore, PDF analysis and fractionation of DT to its stiffness and relaxation components distinguishes PN from NL without requirement for load varying respiratory maneuvers or measurement of E'. By using subjects as their own controls and trending their progress echocardiographically, the method is well suited to assess the beneficial or adverse chamber remodeling consequences of alternative pharmacologic approaches on diastolic function in all subjects. In the blinded study (no E'-wave or LVEDP information) the cutpoint selection of R=0.28 from unblinded study yielded high sensitivity (0.90) and specificity (0.86) in differentiating NL and PN groups.

9.6   Limitations

9.6.1   <u>Sample Size</u>

Although the total number of datasets subjected to blinded analysis (n=42) by an independent observer, based on the initial 30 unblinded and 12 additional blinded (for initial comparison to the 30 unblinded datasets) is modest, and may be viewed as a potential statistical limitation, the total number of E-waves analyzed (n=931) mitigates the sample size limitation to an acceptable degree. The sample size limitation is also mitigated by the demonstrated high sensitivity and specificity achieved by the blinded study in differentiating PN from NL. The unblinded (30 subjects) and blinded (42 subjects) studies had power of >90% to detect a true difference of DT_s, DT_r, R and S parameters between PN and NL group with a significance level of 0.01.

9.7   Conclusions

Diastolic function was assessed via the PDF formalism by fractionating E-wave deceleration time into its stiffness (DT_s) and relaxation (DT_r) components in age matched, PN and NL filling pattern groups in both unblinded and blinded groups. Both the PDF parameters by themselves and, DT_s, DT_r differentiated NL vs. PN groups. Based on the cutpoint value of R=0.28 from the unblinded study, the blinded study yielded excellent sensitivity (0.90) and specificity (0.86) in predicting PN vs. NL based on E-wave analysis alone. The method revealed and quantified the opposing effects of stiffness (shortens DT) vs. relaxation (lengthens DT) on total DT resulting in total DT being indistinguishable from NL. The method is well suited to assess the natural history of HFpEF and the beneficial or adverse chamber remodeling consequences of alternative pharmacologic approaches on DF in all subjects.

9.8   References

1.   **Appleton CP, Firstenberg MS, Garcia MJ, and Thomas JD**. The echo-Doppler evaluation of left ventricular diastolic function. A current perspective. *Cardiol Clin* 18: 513-546, ix, 2000.

2.   **Bauman L, Chung CS, Karamanoglu M, and Kovács SJ**. The peak atrioventricular pressure gradient to transmitral flow relation: kinematic model prediction with in vivo validation. *J Am Soc Echocardiogr* 17: 839-844, 2004.

3.   **Chung CS, Ajo DM, and Kovács SJ**. Isovolumic pressure-to-early rapid filling decay rate relation: model-based derivation and validation via simultaneous catheterization echocardiography. *J Appl Physiol (1985)* 100: 528-534, 2006.

4.   **Feigenbaum H**. *Echocardiography*. Baltimore, MD: Williams & Wilkins, 1993.

5.   **Ghosh E, and Kovács SJ**. Early left ventricular diastolic function quantitation using directional impedances. *Ann Biomed Eng* 41: 1269-1278, 2013.

6.   **Gottdiener JS, Bednarz J, Devereux R, Gardin J, Klein A, Manning WJ, Morehead A, Kitzman D, Oh J, Quinones M, Schiller NB, Stein JH, Weissman NJ, and Echocardiography ASo**. American Society of Echocardiography recommendations for use of echocardiography in clinical trials. *J Am Soc Echocardiogr* 17: 1086-1119, 2004.

7.   **Hall AF, and Kovács SJ**. Automated method for characterization of diastolic transmitral Doppler velocity contours: early rapid filling. *Ultrasound Med Biol* 20: 107-116, 1994.

8.   **Hosmer DW, and Lemeshow S**. *Applied logistic regression*. New York: Wiley, 2000, p. xii, 375 p.

9.   **Klein AL, Burstow DJ, Tajik AJ, Zachariah PK, Bailey KR, and Seward JB**. Effects of age on left ventricular dimensions and filling dynamics in 117 normal persons. *Mayo Clin Proc* 69: 212-224, 1994.

10.   **Kovács S, MD M, and CS P**. Modelling cardiac fluid dynamics and diastolic function. *Philosophical Transactions of the Royal Society (A)* 359: 1299-1314, 2001.

11.   **Kovács SJ, Barzilai B, and Pérez JE**. Evaluation of diastolic function with Doppler

echocardiography: the PDF formalism. *Am J Physiol* 252: H178-187, 1987.

12.   **Kovács SJ, Meisner JS, and Yellin EL**. Modeling of diastole. *Cardiol Clin* 18: 459-487, 2000.

13.   **Kovács SJ, Rosado J, Manson McGuire AL, and Hall AF**. Can trasmitral Doppler E-waves differentiate hypertensive hearts from normal? *Hypertension* 30: 788-795, 1997.

14.   **Kovács SJ, Setser R, and Hall AF**. Left ventricular chamber stiffness from model-based image processing of transmitral Doppler E-waves. *Coron Artery Dis* 8: 179-187, 1997.

15.   **Lisauskas J, Singh J, Courtois M, and Kovács SJ**. The relation of the peak Doppler E-wave to peak mitral annulus velocity ratio to diastolic function. *Ultrasound Med Biol* 27: 499-507, 2001.

16.   **Lisauskas JB, Singh J, Bowman AW, and Kovács SJ**. Chamber properties from transmitral flow: prediction of average and passive left ventricular diastolic stiffness. *J Appl Physiol (1985)* 91: 154-162, 2001.

17.   **Little WC, and Oh JK**. Echocardiographic evaluation of diastolic function can be used to guide clinical care. *Circulation* 120: 802-809, 2009.

18.   **Little WC, Ohno M, Kitzman DW, Thomas JD, and Cheng CP**. Determination of left ventricular chamber stiffness from the time for deceleration of early left ventricular filling. *Circulation* 92: 1933-1939, 1995.

19.   **Maeder MT, and Kaye DM**. Heart failure with normal left ventricular ejection fraction. *J Am Coll Cardiol* 53: 905-918, 2009.

20.   **Mirsky I, and Pasipoularides A**. Clinical assessment of diastolic function. *Prog Cardiovasc Dis* 32: 291-318, 1990.

21.   **Mossahebi S, and Kovács SJ**. Diastolic Function in Normal Sinus Rhythm vs. Chronic Atrial Fibrillation: Comparison by Fractionation of E-wave Deceleration Time into Stiffness and Relaxation Components. *Journal of Atrial Fibrillation* 6: 13-19, 2014.

22.   **Mossahebi S, and Kovács SJ**. Kinematic Modeling Based Decomposition of Transmitral Flow (Doppler E-wave) Deceleration Time into Stiffness and Relaxation Components. *Cardiovascular Engineering & Technology* 5: 25-34, 2014.

23. **Mossahebi S, and Kovács SJ**. Kinematic modeling-based left ventricular diastatic (passive) chamber stiffness determination with in-vivo validation. *Ann Biomed Eng* 40: 987-995, 2012.

24. **Mossahebi S, Shmuylovich L, and Kovács SJ**. The thermodynamics of diastole: kinematic modeling-based derivation of the P-V loop to transmitral flow energy relation with in vivo validation. *Am J Physiol Heart Circ Physiol* 300: H514-521, 2011.

25. **Mossahebi S, Zhu S, Chen H, Shmuylovich L, Ghosh E, and Kovács SJ**. Quantification of global diastolic function by kinematic modeling-based analysis of transmitral flow via the Parametrized Diastolic Filling formalism. *J Vis Exp (In Press)* 2014.

26. **Mossahebi S, Zhu S, Chen H, Shmuylovich L, Ghosh E, and Kovács SJ**. Quantification of global diastolic function by kinematic modeling-based analysis of transmitral flow via the Parametrized Diastolic Filling formalism. *Journal of Visualized Experiments (In Press)* 2014.

27. **Nagueh SF, Appleton CP, Gillebert TC, Marino PN, Oh JK, Smiseth OA, Waggoner AD, Flachskampf FA, Pellikka PA, and Evangelista A**. Recommendations for the evaluation of left ventricular diastolic function by echocardiography. *J Am Soc Echocardiogr* 22: 107-133, 2009.

28. **Ohno M, Cheng CP, and Little WC**. Mechanism of altered patterns of left ventricular filling during the development of congestive heart failure. *Circulation* 89: 2241-2250, 1994.

29. **Ommen SR, Nishimura RA, Appleton CP, Miller FA, Oh JK, Redfield MM, and Tajik AJ**. Clinical utility of Doppler echocardiography and tissue Doppler imaging in the estimation of left ventricular filling pressures: A comparative simultaneous Doppler-catheterization study. *Circulation* 102: 1788-1794, 2000.

30. **Pasipoularides A**. Evaluation of right and left ventricular diastolic filling. *J Cardiovasc Transl Res* 6: 623-639, 2013.

31. **Pasipoularides A**. Right and left ventricular diastolic pressure-volume relations: a comprehensive review. *J Cardiovasc Transl Res* 6: 239-252, 2013.

32. **Pasipoularides A, and ebrary Inc.** The Heart's Vortex
intracardiac blood flow phenomena. Shelton, CT.: People's Medical Publishing House USA Ltd,, 2010, p. xxv, 927 p.

33.   **Pasipoularides A, Shu M, Shah A, Womack MS, and Glower DD**. Diastolic right ventricular filling vortex in normal and volume overload states. *Am J Physiol Heart Circ Physiol* 284: H1064-1072, 2003.

34.   **Redfield MM, Jacobsen SJ, Burnett JC, Mahoney DW, Bailey KR, and Rodeheffer RJ**. Burden of systolic and diastolic ventricular dysfunction in the community: appreciating the scope of the heart failure epidemic. *JAMA* 289: 194-202, 2003.

35.   **Riordan MM, Chung CS, and Kovács SJ**. Diabetes and diastolic function: stiffness and relaxation from transmitral flow. *Ultrasound Med Biol* 31: 1589-1596, 2005.

36.   **Riordan MM, and Kovács SJ**. Quantitation of mitral annular oscillations and longitudinal "ringing" of the left ventricle: a new window into longitudinal diastolic function. *J Appl Physiol (1985)* 100: 112-119, 2006.

37.   **Sharma K, and Kass DA**. Heart failure with preserved ejection fraction: mechanisms, clinical features, and therapies. *Circ Res* 115: 79-96, 2014.

38.   **Shmuylovich L, and Kovács SJ**. E-wave deceleration time may not provide an accurate determination of LV chamber stiffness if LV relaxation/viscoelasticity is unknown. *Am J Physiol Heart Circ Physiol* 292: H2712-2720, 2007.

39.   **Sohn DW, Chai IH, Lee DJ, Kim HC, Kim HS, Oh BH, Lee MM, Park YB, Choi YS, Seo JD, and Lee YW**. Assessment of mitral annulus velocity by Doppler tissue imaging in the evaluation of left ventricular diastolic function. *J Am Coll Cardiol* 30: 474-480, 1997.

40.   **Zhang W, Chung CS, Shmuylovich L, and Kovács SJ**. Is left ventricular volume during diastasis the real equilibrium volume, and what is its relationship to diastolic suction? *J Appl Physiol (1985)* 105: 1012-1014, 2008.

41.   **Zile MR, and Brutsaert DL**. New concepts in diastolic dysfunction and diastolic heart failure: Part I: diagnosis, prognosis, and measurements of diastolic function. *Circulation* 105: 1387-1393, 2002.

APPENDIX

Listing of Published Abstracts

A1: THE THERMODYNAMICS OF DIASTOLE: DIASTOLIC FUNCTION ASSESSMENT USING E-WAVE DERIVED ENERGY, WITH IN-VIVO VALIDATION
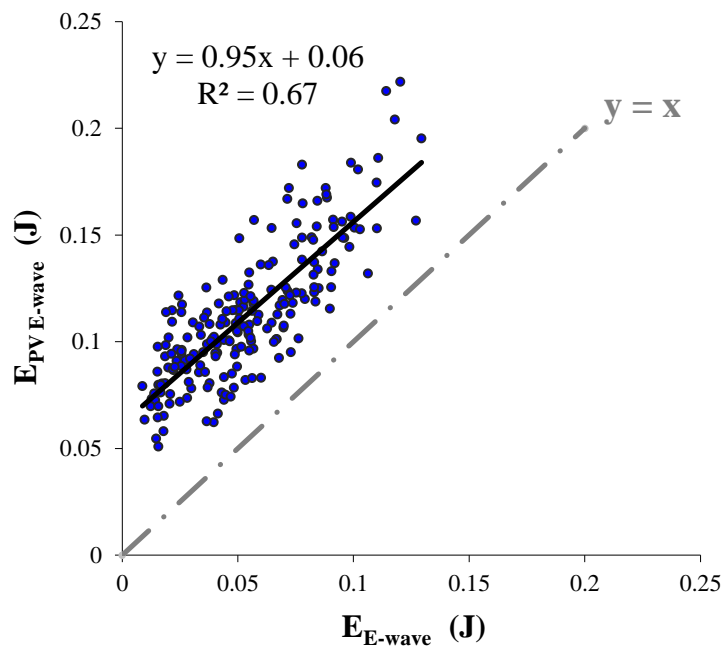
Sina Mossahebi, Leonid Shmuylovich, Sándor J. Kovács

Pressure-volume (P-V) loop based analysis facilitates thermodynamic assessment of left ventricular function in terms of work, and energy. Typically these quantities are calculated for a cardiac cycle using the entire P-V loop, rather than diastole alone. Diastolic function (DF) can be quantified non-invasively by suitable analysis of Doppler E-wave contours.

The first law of thermodynamics requires that energy E computed from the Doppler E-wave (E_{E-wave}) and the same portion of the P-V loop ($E_{PV-E-wave}$) should be correlated. No previous studies have calculated these energies or experimentally validated their predicted relationship. To test the hypothesis that $E_{PV-E-wave}$ and E_{E-wave} are equivalent we employed a validated kinematic model of filling to derive EE-wave in terms of chamber stiffness (k), relaxation/viscoelasticity (c) and load (x_o).

For validation, simultaneous invasive (Millar) P-V data and non-invasive echocadiographic data from 12 subjects (205 total cardiac cycles) with normal diastolic function were analyzed. Kinematic modeling based EE-wave for each diastole was computed and compared to $E_{PV-E-wave}$ from simultaneous P-V data. Linear regression yielded: $E_{PV-E-wave} = a\ E_{E-wave} + b$ ($R^2 = 0.67$), where a=0.95, and b=0.06.

We conclude that the E-wave derived expression for the energy for suction initiated early rapid filling is an accurate measure of filling energy obtained by simultaneous P-V measurement. This provides a novel, mechanism based index for DF assessment.


Scatter plot with axes E_{E-wave} (J) on the horizontal and $E_{PV\ E-wave}$ (J) on the vertical. Regression line labeled y = 0.95x + 0.06, R² = 0.67, with reference line y = x.

A2: ECHOCARDIOGRAPHIC DETERMINATION OF LEFT VENTRICULAR DIASTATIC CHAMBER STIFFNESS: KINEMATIC MODELING-BASED DERIVATION WITH IN-VIVO VALIDATION

Sina Mossahebi, Sándor J. Kovács

The slope of the diastatic pressure-volume relationship (D-PVR) defines passive left ventricular (LV) stiffness K. Although K is a relative measure, an absolute measurement method (cardiac catheterization) s employed to obtain it. Echocardiography is the preferred quantitative diastolic function (DF) assessment method and Doppler E-waves can only provide relative, rather than absolute, pressure information. We hypothesized that appropriate E-wave analysis can generate the D-PVR$_{E\text{-wave}}$ whose slope, $K_{E\text{-wave}}$, is the E-wave derived diastatic, passive chamber stiffness - a relative DF index. A validated kinematic model of filling and Bernoulli's equation were used to compute pressure and volume at diastasis, to generate D-PVR$_{E\text{-wave}}$, parametrized by the kinematic model's E-wave derived indexes of stiffness (k), relaxation/viscoelasticity (c) and load (x_o). For validation, simultaneous (conductance catheter) P-V and echocadiographic E-wave data from 30 subjects (444 total cardiac cycles) having normal LV ejection fraction (LVEF) and a physiologic range of LV end-diastolic pressure (LVEDP) were analyzed. For each subject, the locus of physiologically varying diastatic P-V points were fit linearly to generate D-PVR$_{CATH}$ with slope K_{CATH} as catheterization derived diastatic stiffness. For each subject (15 beats average) $K_{E\text{-wave}}$ was compared to K_{CATH} via linear regression yielding: $K_{E\text{-wave}} = \alpha K_{CATH} + b$ ($R^2 = 0.90$), where, $\alpha = 0.98$ and $b = 0.03$.

We conclude that E-wave derived diastatic stiffness $K_{E\text{-wave}}$, quantitated via kinematic modeling of filling provides an excellent estimate of simultaneous, catheterization-based, P-V defined diastatic stiffness, K_{CATH}. Hence, in chambers at diastasis, passive LV stiffness, can be accurately determined by appropriate analysis of transmitral flow (E-wave).

292
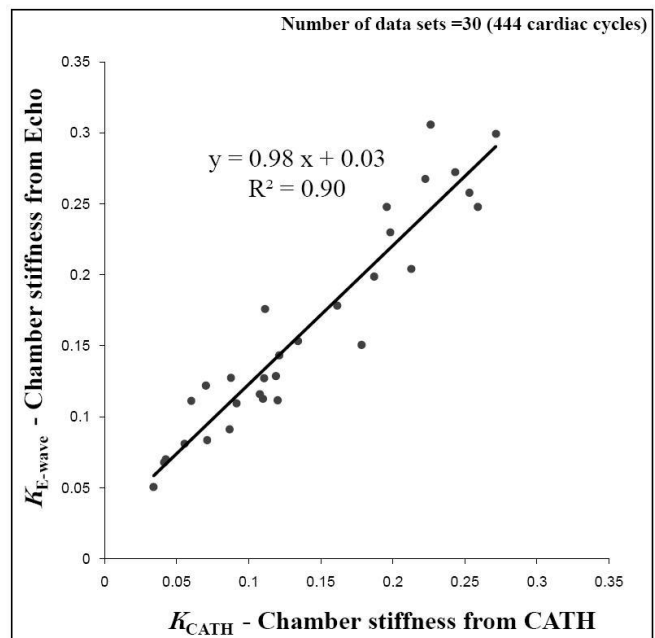
A3: ECHOCARDIOGRAPHIC ASSESSMENT OF CHAMBER STIFFNESS: CONTRASTING NORMAL SINUS RHYTHM AND CHRONIC ATRIAL FIBRILLATION

Sina Mossahebi, Leonid Shmuylovich, Sándor J. Kovács

Echocardiographic diastolic function (DF) assessment remains a challenge in atrial fibrillation (AF), because indexes such as E/A cannot be used and because chronic, rate controlled AF causes chamber remodeling. To determine if echocardiography can accurately characterize diastolic chamber properties we compared 14 AF subjects to 24 normal sinus rhythm (NSR) subjects undergoing simultaneous echocardiography-cardiac catheterization (417 beats analyzed).

Conventional DF parameters (DT, E_{peak}, AT, E_{dur}, E-VTI, E/E') and novel E-wave derived, kinematic modeling based parameter specific for chamber stiffness (*k*), were compared. For validation, chamber stiffness (*dP/dV*) was independently determined from simultaneous, multi-beat P-V loop data. Results show that neither AT, E_{peak} nor E-VTI differentiated between groups. Although DT, E_{dur} and E/E' did differentiate between groups (DT_{NSR} vs. DT_{AF} $p<0.001$, E_{durNSR} vs. E_{durAF} $p<0.005$, E/E'_{NSR} vs. E/E'_{AF} $p<0.05$), the model derived chamber stiffness parameter *k* was the only parameter specific for chamber stiffness, (k_{NSR} vs. k_{AF} $p<0.005$). The invasive gold-standard, end-diastolic stiffness in NSR was indistinguishable from end-diastolic (i.e. diastatic) stiffness in AF ($p=0.57$). Importantly, the analysis provided mechanistic insight by showing that diastatic stiffness in AF was significantly greater than diastatic stiffness in NSR ($p<0.005$).

We conclude that passive (diastatic) chamber stiffness is increased in chronic, rate controlled AF hearts relative to NSR controls and that in addition to DT, the E-wave derived, chamber stiffness specific index *k,* differentiates between AF vs. NSR groups, even when invasively determined end-diastolic chamber stiffness fails to do so.

	NSR (n=24)	AF (n=14)	p	p NSR_{ED} vs. NSR_D
Hemodynamic Parameters:				
P_{ED} (mmHg)	19±5	18±5	0.46	$p<0.0001$
V_{ED} (ml)	160±32	170±58	0.46	$p<0.0001$
P_D (mmHg)	13±3	18±5	<0.001	
V_D (ml)	122±31	170±58	<0.001	
dP/dV_{ED} (mmHg/ml)	0.14±0.09	0.16±0.09	0.57	$p<0.001$
dP/dV_D (mmHg/ml)	0.09±0.06	0.16±0.09	<0.005	
Echocardiographic Parameters				
Peak E-wave velocity (E_{peak}) (cm/s)	78±20	89±28	0.17	
E-wave acceleration time (AT) (ms)	92±10	89±16	0.53	
E-wave deceleration time (DT) (ms)	203±28	171±21	<0.001	
E-wave duration time (E_{dur}) (ms)	295±33	260±33	<0.005	
k_{PDF} ($1/s^2$)	189±31	238±66	<0.005	
E-VTI (cm)	11.8±0.04	12.8±0.04	0.45	
E/E'	4.8±1.7	6.0±1.9	<0.05	

A4: THE ISOVOLUMIC RELAXATION TO EARLY RAPID FILLING CONNECTION: MODEL PREDICTION AND IN-VIVO VALIDATION

Sina Mossahebi, Sándor J. Kovács

Although cardiac catheterization is the gold standard, Doppler echocardiography is the preferred non-invasive diastolic function (DF) characterization method. The physics and physiology of diastole requires continuity of left ventricular (LV) pressure generating forces before and after mitral valve opening (MVO). Correlations between invasive measures of isovolumic relaxation (IVR) such as tau (time-constant of IVR) and noninvasive, echocardiographic E-wave derived parameters, such as peak atrioventricular gradient, have been established. However the missing conceptual link and experimental validation establishing the end IVR force to initial suction force, initiating filling via the Doppler E-wave has remained elusive.

We hypothesize that the terminal force of IVR ($F_{t\ IVR}$) and the initial force of early rapid filling ($F_{i\ E-wave}$) after MVO must be correlated. For validation, simultaneous (conductance catheter) P-V and E-wave data from 20 subjects (mean age 57 years, 13 men) having normal LV ejection fraction (LVEF>50%) and a physiologic range of LV end-diastolic pressure were analyzed. For each cardiac cycle validated kinematic models for pressure during IVR and for the subsequent transmitral flow velocity (E-wave) provided $F_{t\ IVR}$, and $F_{i\ E-wave}$. Specifically, we derived terminal force of IVR ($F_{t\ IVR}$) from Chung's kinematic modeling of IVR [1] and the initial force of early rapid filling ($F_{i\ E-wave}$) from kinematic modeling of transmitral flow (PDF formalism [2]).

We analyzed 308 beats (~15 beats per person). When analyzed on an individual basis, a close linear relationship was found for the terminal force of IVR and the initial force of early rapid filling in accordance with the prediction ($R^2 > 0.60$). Data from one subject is shown in Figure 1. The relationship between $F_{i\ E-wave}$ and $F_{t\ IVR}$ in 20 datasets including all 308 beats is shown
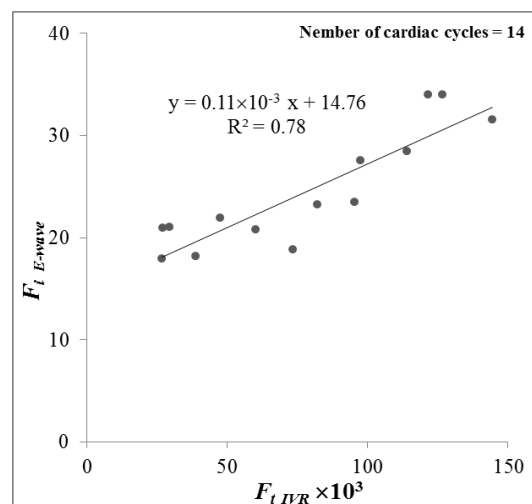

Figure 1. Correlation between initial force of early rapid filling ($F_{i\ E-wave}$) and terminal force of isovolumic relaxation ($F_{t\ IVR}$) in one subject datasets consisting of 14 cardiac cycles.

in Figure 2. It yielded an excellent linear correlation $R^2 = 0.69$.

The model-derived terminal force of IVR and the model-derived initial force of early rapid filling are highly correlated. These simultaneous measurements of pressure and flow provide novel insight into the physiologic mechanisms of isovolumic relaxation and early rapid filling by linking of the required forces.
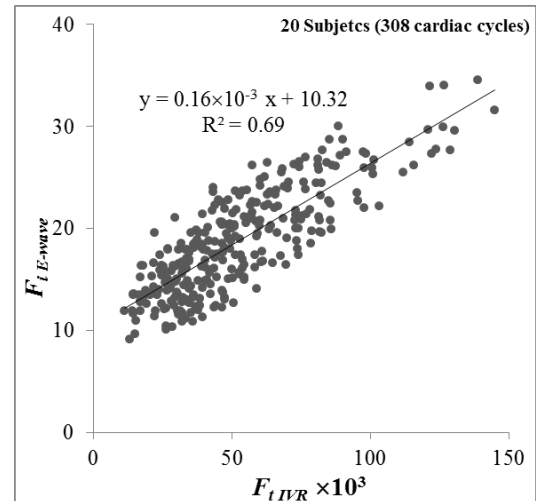

Figure 2. Correlation between initial force of early rapid filling ($F_{i\ E\text{-wave}}$) and terminal force of isovolumic relaxation ($F_{t\ IVR}$) in 20 normal DF datasets consisting of 308 cardiac cycles.

A5: DECOMPOSITION OF E-WAVE DECELERATION TIME INTO STIFFNESS AND RELAXATION COMPONENTS
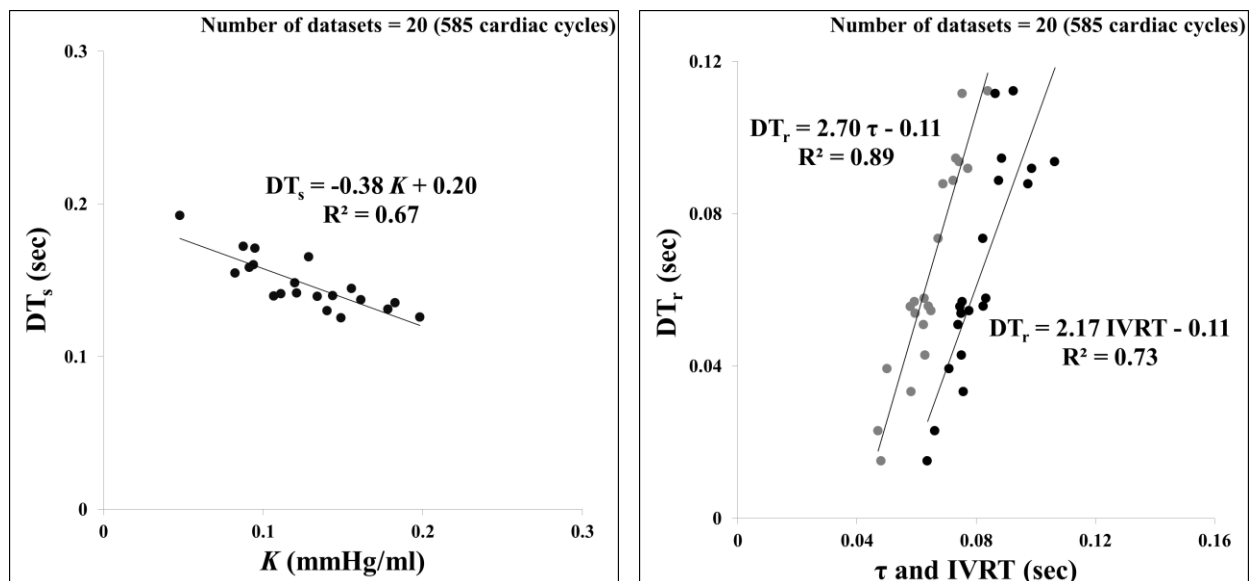
Sina Mossahebi, Sándor J. Kovács

The short deceleration time (DT) ("constrictive-restrictive") E-wave pattern is due to increased chamber stiffness, while prolonged E-wave deceleration time is due to 'delayed relaxation'. Therefore, stiffness and relaxation are DT determinants. DT has been expressed algebraically as a function of stiffness only. Subsequent analysis of E-waves via the parametrized diastolic filling (PDF) formalism revealed that DT is an algebraic function of both stiffness and relaxation.

We hypothesize that E-wave analysis via PDF permits decomposition of DT into stiffness (DT_s) and relaxation (DT_r) components ($DT = DT_s + DT_r$), reflecting diastatic chamber stiffness (K, slope of diastatic P-V relation), and relaxation (τ isovolumic time-constant) effects. For validation, simultaneous (conductance catheter) pressure-volume (P-V) and E-wave data from 12 control subjects, normal (>50%) LV ejection fraction, and 4 with delayed relaxation (DT>220 msec) were analyzed. PDF analysis of each E-wave provided DT_s and DT_r.

For all 20 subjects (29 beats/subject, 585 beats total) linear regression yielded $DT_s = \alpha K + \beta$ ($R^2 = 0.67$) where $\alpha = -0.38$ and $\beta = 0.20$, and $DT_r = m \tau + b$ ($R^2 = 0.89$) where m = 2.70 and b = -0.11.

E-wave DT consists of stiffness (DT_s) and relaxation (DT_r) components that are determined by diastatic chamber stiffness (K) and relaxation (τ) respectively.

297

A6: DIASTOLIC FUNCTION IN NORMAL SINUS RHYTHM VS. CHRONIC ATRIAL FIBRILLATION: QUANTITATIVE COMPARISON BY FRACTIONATION OF E-WAVE DECELERATION TIME INTO STIFFNESS AND RELAXATION COMPONENTS

Sina Mossahebi, Sándor J. Kovács
Circulation. 2013: 128: A10604

Atrial fibrillation (AF) is the most common pathologic cardiac arrhythmia. Although the electro-physiologic mechanism of AF has been characterized, the diastolic function (DF) consequences of AF in terms of stiffness and relaxation have not been fully elucidated. The physiologic suction-pump attribute of early diastole has been modeled in analogy to the recoil of a damped harmonic oscillator. The Parametrized Diastolic Filling (PDF) model has been extensively validated and accurately predicts clinical E-wave contours in terms of load, stiffness (k_{PDF}) and relaxation (c_{PDF}) parameters. It predicts that E-wave deceleration time (DT) is a function of both stiffness and relaxation. The fractionation method has been previously validated with DT_s and DT_r correlating with simultaneous (MILLAR) stiffness (*dP/dV*) and relaxation (tau) with r=0.82 and r=0.94 respectively. Accordingly, PDF-based E-wave analysis provides a method for fractionating total DT into stiffness (DT_s) and relaxation (DT_r) components such that $DT=DT_s+DT_r$.

We compared 15 age matched, chronic AF subjects to 15, in normal sinus rhythm (NSR) by analyzing simultaneous echo-cardiac catheterization data (599 beats). Conventional DF parameters (DT, AT, E_{peak}, E_{dur}, E-VTI, E/E') and c_{PDF}, k_{PDF}, DT_s and DT_r were compared. DT in AF was shorter than in NSR (p<0.005) and diastatic chamber stiffness, k_{PDF} in AF, was higher than in NSR (p<0.01). For NSR 75% of DT was accounted for by stiffness and 25% by relaxation whereas for AF 81% of DT is due to stiffness and 19% is due to relaxation (p<0.005).

We conclude that fractionation of DT into relaxation and stiffness components shows that AF has increased stiffness compared to NSR. In addition, a larger percentage of E-wave DT in AF is due to stiffness than to relaxation compared to NSR. This novel method allows for longitudinal assessment of impact of alternative treatment strategies on chamber stiffness and relaxation in all clinical settings.

Echocardiographic Parameters	NSR (n=15)	AF (n=15)	p
Peak E-wave velocity (E_{peak}) (cm/s)	71±15	90±28	0.03
E-wave acceleration time (AT) (msec)	89±12	87±17	0.72
E-wave deceleration time (DT) (msec)	190±19	164±24	<0.005
E-wave duration time (E_{dur}) (msec)	279±27	251±39	<0.05
k_{PDF} ($1/s^2$)	194±41	249±75	<0.01
E-VTI (cm)	10.0±0.03	11.4±0.04	0.32
E/E'	4.7±1.8	6.0±1.9	<0.05
DT_s (msec)	142±14	135±29	0.41
DT_r (msec)	48±9	32±10	<0.001
S=DT_s / DT (%)	75±3	81±6	<0.005
R=DT_r / DT (%)	25±3	19±6	<0.005

A7: DISTINGUISHING PSEUDONORMALIZED FROM NORMAL FILLING BY FRACTIONATING E-WAVE DECELERATION TIME INTO ITS STIFFNESS AND RELAXATION COMPONENTS

Sina Mossahebi, Sándor J. Kovács

Pseudonormalized (PN) filling patterns indicate diastolic dysfunction. In PN filling transmitral E-and A-waves may be indistinguishable from normal (NL), requiring classification according peak E'. E-wave analysis via the parametrized diastolic filling (PDF) formalism allows fractionation of DT into stiffness (DT_s) and relaxation (DT_r) components such that DT = $DT_s + DT_r$. Simultaneous echo-cath has previously validated the fractionation method with DT_s and DT_r correlating with cath derived (MILLAR) stiffness (dP/dV) and relaxation (tau) with r=0.82 and r=0.94, respectively. We hypothesize that PDF analysis and DT fractionation can distinguish between normal and PN groups having indistinguishable, normal LVEF and E-wave patterns.

We compared 10 age matched PN (elevated E/E') subjects to 10 NLs, by analyzing simultaneous echo-cath data (510 beats). Conventional DF parameters (DT, E_{peak}, E_{dur}, E-VTI, and E/A), and PDF relaxation (c_{PDF}) and stiffness (k_{PDF}) parameters, DT_s, DT_r were compared.

Conventional parameters (DT, E_{peak}, E_{dur}, E-VTI, E/A) did not differentiate between groups. k_{PDF} , c_{PDF} (p<0.001), and DT_s , DT_r (p<0.005) differentiated between groups. Shorter DT_s and higher k_{PDF} in PN than in NLs indicate that PN chambers are stiffer than NL.

PDF parameters, relaxation and stiffness components of DT can differentiate normal and PN filling without requiring knowledge of E', and show that PN has increased stiffness compared to normal filling.

	Normal	Pseudonormal	Significance
Number of Subjects	10	10	NA
Age (y)	60±9	60±11	0.93 (NS)
Heart Rate (bpm)	66±8	65±8	0.68 (NS)
Ejection Fraction (EF) (%)	71±8	71±9	0.99 (NS)
LVEDP (mmHg)	14±3	19±4	<0.005
Peak E-wave (E_{peak}) (cm/s)	81±6	83±11	0.69 (NS)
Peak A-wave (A_{peak}) (cm/s)	72±10	76±12	0.46 (NS)
E/A (dimensionless)	1.2±0.2	1.1±0.1	0.42 (NS)
Peak E'-wave (E'_{peak}) (cm/s)	15±4	9±2	<0.001
E/E' (dimensionless)	4.8±0.8	9.0±1.5	<0.001
E-wave deceleration time (DT) (ms)	180±10	185±14	0.37 (NS)
E-wave duration (E_{dur}) (ms)	262±10	257±21	0.58 (NS)
E-VTI (cm)	9.9±1.9	10.7±1.0	0.33 (NS)
c_{PDF} (1/s)	16.0±1.8	21.0±1.7	<0.001
k_{PDF} (1/s^2)	211±14	257±28	<0.001
DT_r (msec)	43±8	61±14	<0.005
DT_s (msec)	137±7	124±8	<0.005

NA   not applicable,   NS   not significant

Curriculum Vitae

Name: Sina Mossahebi

Personal Information: Sex: Male

Date of Birth: 09/21/1981

Place of Birth: Tehran – Iran

Citizenship: Iran

Visa Status / Type: F1

Address and Telephone Numbers:

Office: Cardiovascular Biophysics Laboratory, Washington University in St. Louis, 660 S Euclid Ave., Box 8086, St. Louis MO 63110

Phone: (314) 454-7614

Home: 5630 Pershing Ave., Unit 28, St. Louis, MO 63112

Phone: (314) 775-6717

Present Position: PhD Candidate

Education:

Undergraduate:	B.S. in Physics, University of Tehran, Iran	2004
Graduate:	M.S. in Physics, University of Tehran, Iran	2007
	M.S. in Physics, Washington University in St. Louis	2013
	Ph.D. in Physics, Washington University in St. Louis	2014 (Expected)

Academic Positions / Employment:

Cardiovascular Biophysics Laboratory, Washington University in St. Louis   2009 – Present
Graduate Research Assistant

Honors and Awards:

Teaching Assistant scholarship, Washington University in St. Louis	2009 – Present
Hughes Fellowship, Washington University in St. Louis	2008 – 2009
Honor student, UW-Milwaukee	2008
Chancellor's Golda Meir Library Scholar Awards, UW-Milwaukee	2007 – 2008
Honor student, University of Tehran, Iran	2004 – 2007

Professional Societies and Organizations:

        Member of American Physical Society (APS)

        Member of American Heart Association (AHA)

        Member of American College of Cardiology (ACC)

        Member of Biomedical Engineering Society (BMES)

Research Support :

Governmental	- None
Non-governmental	- Department of Physics, Washington University in St. Louis - Alan A. and Edith L Wolff Charitable Trust, St. Louis - Barnes-Jewish Hospital Foundation

Teaching Title and Responsibilities:

Graduate Teaching Assistant, Washington University in St. Louis

o Teaching Assistant, Physics of the Heart (3 semesters)	2011 – Present
o Lab Instructor, Fundamental Physics (6 semesters)	2009 – 2014
o Head Lab Teaching Assistant, Fundamental Physics	2013 – 2014

Graduate Teaching Assistant, University of Tehran, Iran

o Teaching Assistant, Quantum Mechanics 2	Spring 2007
o Teaching Assistant, Quantum Mechanics 1	Fall 2006

Bibliography:

Peer reviewed manuscripts
1. **Sina Mossahebi**, Sándor J. Kovács, Fractionating E-wave deceleration time into its stiffness and relaxation components distinguishes pseudonormal from normal filling, 2014 (In Review)
2. **Sina Mossahebi**, Sándor J. Kovács, Diastolic Function in Normal Sinus Rhythm vs. Chronic Atrial Fibrillation: Comparison by Fractionation of E-wave Deceleration Time into Stiffness and Relaxation Components, *J AFIB*. 2014: 6(5): 13-19
3. **Sina Mossahebi**, Simeng Zhu, Howard Chen, Leonid Shmuylovich, Erina Ghosh, Sándor J. Kovács, Quantification of global diastolic function by kinematic modeling-based analysis of transmitral flow via the Parametrized Diastolic Filling formalism, *J Vis Exp*. 2014 (*In Press*)
4. **Sina Mossahebi**, Sándor J. Kovács, The Isovolumic Relaxation to Early Rapid Filling Connection: Kinematic Model Prediction with in-vivo Validation, *Physiological Reports*. 2014: 2(3), E00258
5. **Sina Mossahebi**, Sándor J. Kovács, Decomposition of E-wave deceleration time into stiffness and relaxation components, *Cardiovasc Eng Technol*. 2014: 5(1): 25-34
6. **Sina Mossahebi**, Leonid Shmuylovich, Sándor J. Kovács, Echocardiographic assessment of chamber stiffness in chronic atrial fibrillation vs. normal sinus rhythm, *J Afib*. 2013: 6(3): 45-50
7. **Sina Mossahebi**, Sándor J. Kovács, Kinematic Modeling-based Left Ventricular Diastatic (Passive) Chamber Stiffness Determination with In-Vivo Validation, *Annals Biomed Eng*. 2012: 40(5): 987-995
8. **Sina Mossahebi**, Leonid Shmuylovich, Sándor J. Kovács, The Thermodynamics of Diastole: Kinematic Modeling based Derivation of the P-V Loop to Transmitral Flow Energy Relation, with In-Vivo Validation, *Am J Physiol Heart Circ Physiol*. 2011: 300: H514-H521

Abstracts
1. **Sina Mossahebi**, Sándor J. Kovács, Distinguishing Pseudonormalized from Normal Filling by Fractionating E-wave Deceleration Time into Its Stiffness and Relaxation Components, *J Am Coll Cardiol*. 2014: 63(12_S): A1191
2. **Sina Mossahebi**, Sándor J. Kovács, Diastolic Function in normal sinus rhythm vs. chronic atrial fibrillation: Quantitative comparison by fractionation of E-wave deceleration time into stiffness and relaxation components, *Circulation*. 2013: 128: A10604
3. **Sina Mossahebi**, Sándor J. Kovács, Decomposition of E-wave deceleration time into stiffness and relaxation components, *J Am Coll Cardiol*. 2013: 61(10): E866
4. **Sina Mossahebi**, Leonid Shmuylovich, Sándor J. Kovács, Echocardiographic assessment of chamber stiffness - contrasting normal sinus rhythm and chronic atrial fibrillation, *Circulation*. 2012: 126: A12095
5. **Sina Mossahebi**, Sándor J. Kovács, The isovolumic relaxation to early rapid filling connection: Model prediction and in-vivo validation, *BMES*. 2012-001072
6. **Sina Mossahebi**, Sándor J. Kovács, Echocardiographic Determination of Left Ventricular Diastatic Chamber Stiffness: Kinematic Modeling-Based Derivation With in-vivo Validation, *Circulation*. 2011: 124: A13595
7. **Sina Mossahebi**, Leonid Shmuylovich, Sándor J. Kovács, The Thermodynamics of Diastole: Diastolic Function Assessment Using E-wave Derived Energy, with In-Vivo Validation, *J Am Coll Cardiol*. 2011: 57(14): E660